A Two-stage Structural Optimisation and Thermal Discretisation of Non-Convective Structured Insulators

Applications in Granular-solid Structures
by Additive Manufacturing Technology

By

Bertrand D. Ngim

2008

Loughborough University

Abstract

A systematic design procedure for characterising the strength and insulation requirements of a modular unit structure from additive manufacturing has been presented. The proposed 'two-stage' method consists of structural optimisation and thermal 'discretisation', through use of the Metamorphic Development (MD) and Discretisation by Partitioning Method (DbPM), respectively. A structural layout optimisation method of a consolidated granular-solid structure for strength requirements is demonstrated. The reliability of the layout optimised design solution tested using experiments and finite element analysis (FEA) are reproduced with reasonable accuracy. Layout optimisation yielded 40% savings in build material, whilst satisfying the targeted deflection. In terms of insulation performance, it was found that the heat transfer across the differentially heated and cooled structures could be controlled and optimally discretised through use of the proposed DbPM. The attributes of the approach have been demonstrated through 88% reduction in heat transfer rate, for an idealised enclosure model, and 40% for the investigated design optimisation study. The reliability of the thermally discretised design solutions have been validated through a devised validation procedure.

The research demonstrated that the attributes of layout and configuration/sizing optimisation methods could be used as a 'two-stage' method, to produce conceptual design solutions to address engineering design problems encompassing more than one physics 'domain'. It was also demonstrated that strength and insulation requirements could be achieved through use of single material, by means of varying geometry to achieve the required functionalities. The current research introduced the notion of design optimisation for additive manufacturing, which have not previously been considered for load bearing thermal insulative granular-solid structures.

Acknowledgement

I would like to extend my utmost gratitude to my supervisors, Dr. Rupert Soar and Dr. Jing-sheng Liu, for their guidance throughout this research.

I would also like to thank my immediate colleagues and members of technical staff within the Wolfson School of Mechanical and Manufacturing Engineering Department of Loughborough University, who have helped me in one way or another towards the accomplishment of this research.

Above all, I would like to thank my parents, for their undying dedication to my personal well-being, and to my wife, for her understanding support, who deserves my utmost gratitude.

Publications

[1] Ngim, D.B., Liu, J.-S., Soar, R.C., 2007. Design optimisation for manufacturability of axisymmetric continuum structures using metamorphic development. International Journal of Solid and Structures 44, 685-704. ISSN 0020-7683 doi:10.1016/j.ijsolstr.2006 05.016

[2] Ngim, D.B , Liu, J.-S., Soar, R.C., 2009. Design optimisation of consolidated granular-solid prismatic beam using metamorphic development. International Journal of Solids and Structures 46, 726-740. ISSN 0020-7683 doi:10.1016/j.ijsolstr.2008.09.031

"Whether you think you can or whether you think you can't, you're right."

Henry Ford (1863 – 1947)

Table of Contents

Abbreviations

2D	Two-dimensional
3D	Three-dimensional
3PB	Three-point bending
AiC	Automation in construction
AMT	Additive manufacturing technology
CAD	Computer aided design
CC	Contour Crafting
CFD	Computational fluid dynamics
DbPM	Discretisation by partitioning method
DEM	Discrete element method
D-P	Drucker-Prager
ESO	Evolutionary structural optimisation
FC	Freeform Construction
FEA	Finite element analysis
GA	Genetic algorithm
ISO	International Standards Organisation
MD	Metamorphic development
M-C	Mohr-Coulomb
PC	Precast concrete
PSO	Particle swarm optimisation
RM	Rapid manufacturing
RP	Rapid prototyping
SA	Simulated annealing
SBG	Simulated biological growth
SFC	Solid freeform construction
SFF	Solid freeform fabrication
SLS	Selective laser sintering
TBL	Thermal boundary layer

Nomenclature

a	DbPM validation procedure constant
A	Area (m^2)
b	Real constant thickness (m)
c	Cohesion coefficient (MPa) or specific heat capacity (J kg^{-1} K^{-1})
E	Young's modulus (GPa)
F	Force (N)
F_τ	Frictional force (N)
F_σ	Normal force (N)
M	Bending moment (Nm)
L, l	Length (external, internal) (m)
H, h	Height (external, internal) (m)
I	Invariant of stress tensor (Pa)
$\imath$	i-th local cell
J	Invariant of deviatoric stress tensor (Pa)
k	Pure shear yield stress or thermal conductivity (MPa)
m	Parameter in Mohr-Coulomb criteria or mass (kg)
$n_\imath$	Number of iterations
N	Number of partitions
N_o	Number of optimum partitions
T	Temperature (K)
t	Member section thickness (m)
g	Gravitational acceleration (ms^{-2})
S	Section modulus (MPa)
s	Subenclosure aspect ratio
V	Shear force (N) or volume (kgm^{-3})
w	Width (m)
v	Velocity (vertical component) (ms^{-1})
u	Velocity (horizontal component) (ms^{-1})
U	Strain energy (J)
p	Normal pressure (Pa)
q	Heat flux (Wm^{-2})
Q	Heat transfer rate (W)
Ra	Rayleigh number
Nu	Nusselt number
Pr	Prandtl number

Greek letters

α	Angle of dilatancy (deg)
β	Coefficient of thermal expansion ($1/T$)
η	Efficiency (%)
φ	Solid/fluid volume fraction or porosity (%)
φ_μ	Angle of intergranular friction (deg)
ρ	Density (kgm^{-3}) or deviatoric length (MPa)
ξ	hydrostatic length (MPa)
σ	Stress (MPa)
σ_y	Yield stress (MPa)
σ_t	Yield stress (tensile) (MPa)
σ_c	Yield stress (compression) (MPa)
σ_{eqv}	Equivalent stress (MPa)
τ	Shear stress (MPa)
υ	Poison's ratio or fluid velocity (ms^{-1})
δ	Displacement/deflection (mm)
μ	Dynamic fluid viscosity ($kgm^{-1}s^{-1}$)
θ	Angle (deg) or dimensionless temperature
Θ	Continuum truss member (deg)
ψ	Stream function (m^2s^{-1})
ω	Vorticity (ms^{-1})
γ	Angle of repose (deg)
ν	Dilatancy coefficient or kinematic viscosity (m^2s^{-1})
ε	Strain (%)
χ	Rate of suppression of heat transfer (%)

List of Figures

List of Tables

1

Introduction

1.1 Introduction

The goal of structural engineers is to design structural systems according to design requirements set by industry standards and building codes. In today's highly competitive engineering industry, a design that performs a required task satisfactorily is no longer sufficient. Designs require optimal solutions based on specified requirements. More so, sustainable engineering and development is of utmost importance. Designs not only have to achieve optimal performance, but also efficiency. Optimal designs should be cost effective, from the design stages through to manufacturing. It should take into consideration minimal material usage and facilitate the reuse of build materials at the end of service life. In addition, structural systems should ideally be designed to meet more than one function, utilising the minimal possible space and material. Conventional design approaches require different materials to deliver a required functionality. In buildings, these could be thermal, acoustics, structural, aesthetics, etc. An emerging approach is the use of geometry (or layout) towards achieving certain functionalities, whilst retaining a single material build. Recently, methods for design optimisation of structures have been developed to support the design of such complex systems. As engineering computational capabilities increase, the scope for modelling and optimisation increased, enabling the undertakings of larger design problems (Kim *et al.*, 2002). Modelling and optimisation enables improvements in the efficiency of the design process. However, engineers are often faced with the problem on how optimised designs could be efficiently manufactured and put into application. With the advent of Additive Manufacturing Technologies

(AMT's), the attributes of structural layout optimisations methods as an engineering design tool could potentially be enhanced.

Nowadays, there is a clear trend in industry towards products spanning over several engineering domains. Simultaneously, there is pressure to develop products faster, at competitive prices and to high quality standards. Similar challenges are faced by the construction industry on how the design of building structures could be optimised to facilitate modern methods of construction. The application of design optimisation is not new in this field. However, most of the applications are focussed on civil structures and design optimisation is not widespread in mass construction applications. In light of that, engineers are faced with challenges to develop design methods which consider optimisation at the design stages, to justify its potential gains over conventional 'trial and error' methods.

Most building structures such as walls, floors, columns, beams, etc., not only function as structural elements, but to some extent act as thermal barriers to minimise heat loss. Conventional designs address this problem through use of materials with different properties, to solve the design problems which involve satisfying both strength and insulation requirements. However, this is not the case when the volume of the design space becomes a design constraint. An alternative approach is the 'generalised layout' methods. Research on layout optimisation has shown that alternative solutions, which otherwise may not have been obtained from analytical methods, is feasible. In addition, such design tools aid the creativity, efficiency and quality. Its relevance in modern day structural engineering could not be stressed more. Although much of the work is still centred on research, interest is gradually shifting towards the focus on manufacturability of optimal design solutions.

One potential application of layout optimisation is the integration of functionalities. The reduction of overall material usage, integration of 'form' and 'function', whilst maintaining single material build are just some of the potential benefits. When coupled with AMT's, it forms an attractive 'package'. Hence, the application of both AMT's and design optimisation methods may be seen as complementary, with AMT's as the manufacturing forefront. In construction applications, functional geometry layouts

could be integrated into building structures, potentially enabling more functions to be 'squeezed' into a limited build space. Value added functionalities, obtained through layout optimisation, could deliver a competitive advantage over conventional designs. This would pave the way for the integration of 'passive' functional layouts that do not require external energy, moving one step closer towards self sufficient buildings.

Nature, as in the case of termite mounds, has demonstrated the characteristics of a 'smart structure' using single material to harness renewable energy sources. Termites are able to do this by forming complex ducts and channels which not only resemble a respiratory system, but functions effectively just as well. Hence, it is hoped that the new generation of building structures could employ a similar design approach. However, the transfer of 'knowledge' from nature to engineering may not be straightforward. In building structures, a clear distinction lies between 'form' and 'function'. Form dictates how structures are shaped based on human-building ergonomics. In convectional designs, functional elements (i.e. insulation, structural, etc.) which the occupants do not interact directly, form a 'cladding' where no link exists between the two. This is the distinct feature which separates human-engineered structures to that of nature's and hence drives the challenge on how a design approach could be developed.

This research addresses the design optimisation problem in which a unit cell structure has to satisfy two requirements, mechanical strength and thermal insulation. This work attempts to uncover the layout optimisation of granular-solid structures and the nature of heat transfer in enclosures with varying partitioning layouts. A 'two-stage' layout optimisation and discretisation is devised to identify the cross-sectional layout optimised for strength and insulation requirements. In the first stage, layout optimisation is performed to yield a mass minima structure, subjected to stress and deflection constraints. In the second stage, the internal airspaces are discretised to reduce the global heat transfer. The current work draws the attention to an emerging class of structural-thermal design problems, in which the design of a structure is derived from a combination of heat transfer and mechanical strength considerations, respectively.

1.2 Overview of dissertation

This thesis presents a design approach for an optimised granular-solid modular unit cell structure considering the strength and insulation requirements. It presents the results and findings of the academic research undertaken to arrive at a suitable solution, organised into ten chapters. Below is a brief description of the flow of this research.

Chapter 2 reviews the technologies of additive manufacturing in construction. It gives a view into the possible future of the manufacturing of building structures using 'assembly' and 'material distribution' approach. It explores the factors which spur the development and application of modern methods of construction, particularly Automation in Construction (AiC) and Freeform Construction (FC) methods.

Chapter 3 reviews the state of art of the layout or topology optimisation methods for structural optimisation. This is followed by the introduction to the concept of optimal design and a review of the well known layout optimisation methods Also covered are the design approaches to modify the heat transfer of structures, by means of the layout approach using single material. Finally, the notion of design methods for problems with structural and thermal requirements is presented.

Chapter 4 covers the background theory to the mechanics of granular materials. The notion of the 'continuum theory' used to idealise a non-continuum medium is given. In relation to the interest of this research, more emphasis will be given to the frictional behaviour of 'granular-solid' materials. Also covered are the failure criteria for such materials. The understanding of the mechanics of granular material is essential, considering that a granular material from AMT's is to be used as a substitute for concrete materials.

In Chapter 5, a method for layout optimisation of consolidated granular-solid structures is presented. The chapter covers the selection of a suitable granular-solid material by AMT's, over the commonly used concrete material. This is followed by the calibration of the failure criterion of the chosen material, in which is SLS (selective laser sintering) Nylon-12. A layout optimisation study was performed using the metamorphic

development (MD) method on a prismatic beam. Also presented are methods involved in the post-processing and manufacturing of the test specimens of the optimised structure. Finally, the results from the analyses and layout optimisation are presented and discussed.

Chapter 6 presents the initial investigations on the effects of thermal resistance (or *R*-value) of single material fully divided granular-solid structures. At this stage, no optimisation is performed. The work concerns only the analysis to uncover the nature of heat transfer in enclosures due to the presence of 'fully dividing' thin solid partitions of the same material as the main enclosure. Also covered are procedures involved in the post-processing and manufacturing of the test specimens of the fully divided structures.

Chapter 7 presents 'Stage-1' of the two-stage design approach. The work determines an optimal cross-sectional layout for an idealised modular unit granular-solid structure. The findings of Chapter 5 form the basis which paves the way for the investigations to address the structural requirements of a structured insulator enclosure. In all, two different load cases were considered. The first load case considers only mechanical loads and the second takes into consideration the effect of the thermal loads. The attributes of the proposed design solutions are then compared and discussed.

In Chapter 8, 'Stage-2' of design approach which involves the application of the discretisation by partitioning method (DbPM) is presented. The current work focuses on the optimal discretisation of a structurally optimised enclosure obtained from the previous chapter. The concept to discretise uniformly shaped structures, with the aim to minimise the global heat transfer is presented. In the second part, the DbPM is modified and extended to cover structures with multiply arbitrarily shaped openings. In addition, a validation procedure was devised and performed to test the consistency of the DbPM.

Finally, the summary and conclusions drawn from this thesis study are given in Chapter 9. The chapter summarises the key findings of this research along with the recommendations of further works.

A breakdown of the flow of the chapters of this thesis and aforementioned method of approach is shown in Fig. 1.1.

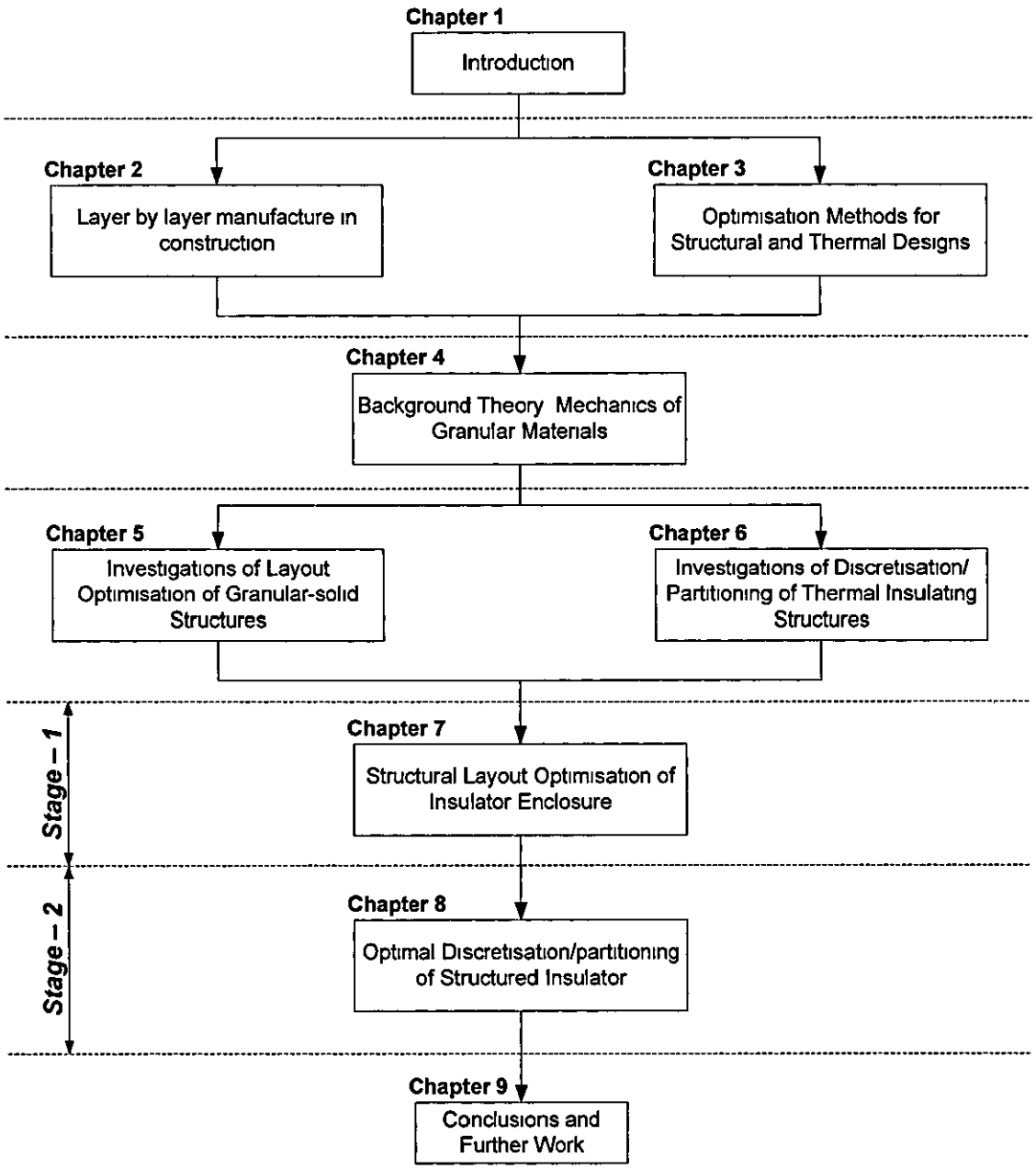

Fig 1 1 Breakdown of thesis and the method of approach highlighting the proposed 'two-stage' structural optimisation and thermal discretisation design approach

2

Layer by Layer Manufacturing in Construction

2.1 Integrated functionality and optimisation

Adding functionalities to products or structures at 'no extra' manufacturing cost increases the process viability of Freeform Construction (FC). In construction, examples of functional elements commonly found in buildings are load bearing structures, thermal barriers, structural joints, interface, etc. For example, a typical wall structure has to support a given load, and act as a thermal barrier. Due to their differences in functionality, both structural and insulating elements are manufactured from materials with properties fit for their intended purposes, as Fig. 2.1(a) shows. In most cases, structural elements typically exhibit high strength, density and thermal conductivity, compared to low strength thermal insulating elements.

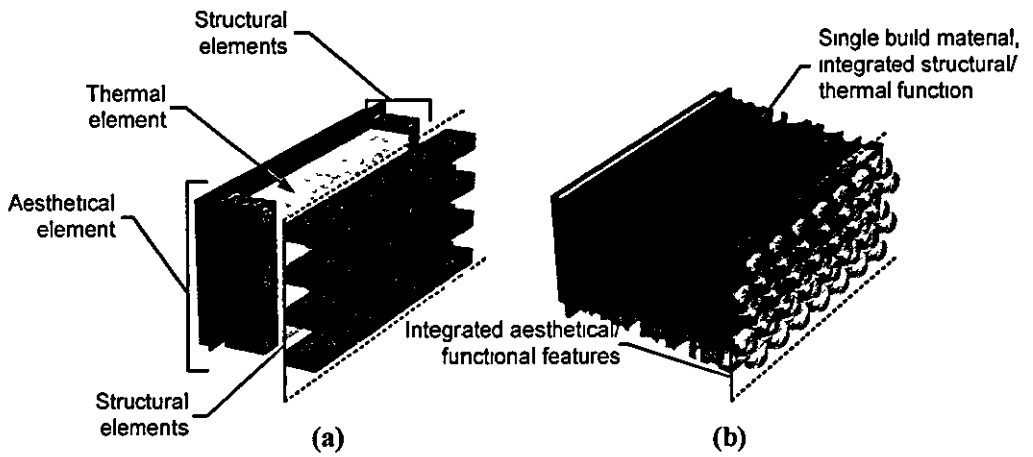

Fig 2 1 Concept design of wall structure with integrated functionalities (a) conventional wall structure, (b) concept design optimised wall structure (Soar, 2006)

In terms of design, the integration of functionality could be realised, with the aid of design optimisation methods. This approach enables structures with 'functional

elements' to be 'generated', using a single material. Unlike conventional designs which rely on various materials, the use of a single material could be potentially beneficial, as hightlighted by Soar (2006) and Khosenevis (2004). Functional elements may be integrated to structures by means of controlling geometry layout through use of a material distribution optimisation approach, as Fig. 2.1(b) shows. The general idea is to try and 'squeeze' different functional elements into the least possible design space.

Design solutions generated with the aid of layout optimisation often exhibit geometric complexity. Ngim *et al.* (2007) and Chang and Tang (2001) showed that it is almost impossible to manufacture such structures efficiently with conventional methods. In terms of manufacturing, AMT could potentially be seen as the most viable approach.

In construction, similar processes are immerging. The question lies in the fact whether current AMT's could be scaled up or that new system may have to be developed to suit the needs for large scale structures.

2.2 Introduction to Additive Manufacturing Technologies

Additive Manufacturing Technologies (AMT's), Rapid Manufacturing (RM), Rapid Prototyping (RP) and Solid Freeform Fabrication (SFF) all refer to the same family of processes. In this thesis, these terms are used interchangeably. Processes in AMT's build solid objects by producing and bonding cross-sections of a part, in small organised increments, one layer on top of the other to controlled thicknesses (Cooper, 2001). These processes contrast the traditional subtractive and formative methods.

An example of AMT, the 3D printing process, is shown in Fig. 2.2. In general, most commercial AMT's operate on a similar fundamental approach. Initially, a 3D solid model is created in a CAD system. This is later converted into .STL format, a standard which can be read by most current RP systems. The solid surfaces are then described using standard triangulation then 'sliced' into 2D cross-sectional layers to be constructed sequentially.

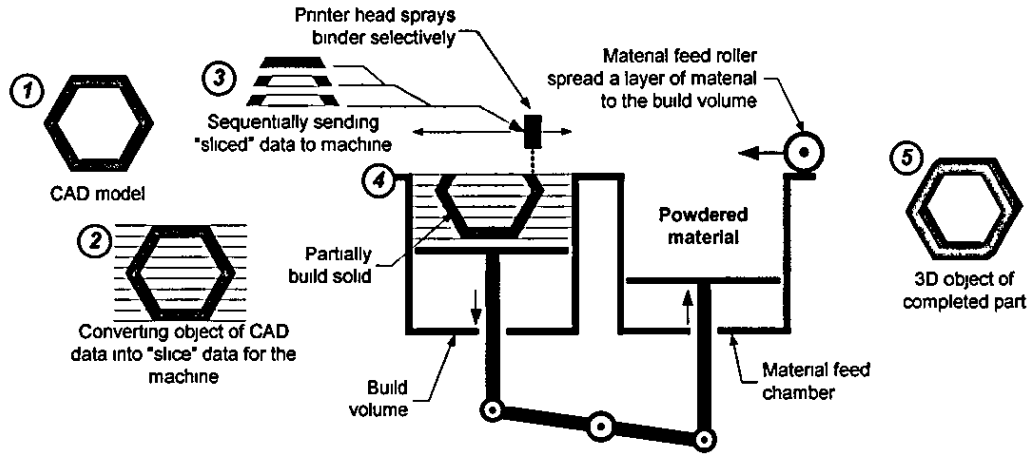

Fig 2 2 Schematic representation of a 3D printing AMT process

The layer by layer approach essentially simplifies the building of parts with complex geometries which otherwise is impossible to machine. Depending on the typr of processes, AMT's offer almost unlimited geometric build freedom. This feature is beneficial as it provide means for the integration of value added features. The integration of 'functionality', through use of optimised geometries is seen as one of the main attributes of AMT's. In addition, AMT's could be seen as the enabling technology in the realisation of optimised structures (Ngim *et al.*, 2007).

AMT's have advanced from prototyping to 'end-use' parts, largely down to the research in build materials (Wohlers, 2004). Materials and process development play a key role. Currently, end-used parts by most AMT's are not suitable for extreme loading applications. However, for parts which operate in less extreme conditions, such as those found in buildings, current AMT's could potentially be applied. The question lies in whether existing AMT's could simply be 'scaled-up' or whether specific processes will be required for construction applications (Soar, 2006). If scaling-up were to be considered, systems utilising mineral-based granular materials have greater potential because granular materials are more durable under compression. This makes them ideally suitable for building structures.

2.3 AMT's in construction

There have been a few applications of AMT's in construction. A special issue of Automation in Construction (Volume 11, Issue 3, pp265-349, 2002) covers this. Most

of the topics concerned the fabrication of physical models for architectural visualisation (Ryder *et al.*, 2002), to the production of large objects (Broek *et al.*, 2002). In spite of these advancements, applications of AMT's in load bearing structures were scarce.

2.3.1 Solid Freeform Construction (SFC)

Through an exploratory investigation of SFC, Pegna (1997) demonstrated a technique for the fabrication of large scale components of > 1 m^3. Through experiments performed in a controlled lab environment, samples of cement-sand masonry were produced using SFC on geometries which could not be obtained by conventional casting methods. Sample structures were manufactured by an incremental blanketed sand deposition, followed by selective deposition of Portland cement through a mask, where pressurised steam was used as the binding agent. SFC was initially designed to be automated, as the process flow in Fig. 2.3(a) shows. However, due to the lack of funds, slight modifications were made and the process was manually implemented, as Fig. 2.3(b) shows.

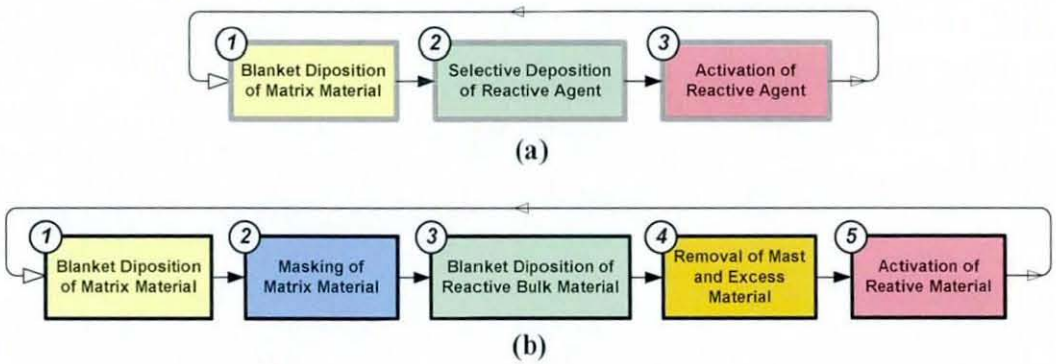

Fig. 2.3 Process flow of selective deposition process by SFC (Pegna, 1997): (a) actual automated fabrication process; (b) manually implemented fabrication process.

Pegna noted that the most likely route to AMT's for large parts, while retaining some material flexibility was selective aggregation. For any AMT to match existing construction rates, aggregation processes such as ink-jet or laser sintering would not meet the required deposition rates. In order to assess the potential of SFC, an estimated calculation was given by Pegna (Table 2.1).

Table 2.1

Estimated build time of SFC (Pegna, 1997)

Building Height	Building base area	Number of floors	Required volumetric flow rate	Estimated construction time
7.5m	$200m^2$	2	$1.04m^3$ per hour	1440 hours

Based on the selective aggregation process, SFC yielded structures of reasonable material properties. Potential savings were also highlighted by reusing unused material. The work was promising and demonstrated that the principles of AMT's could be applied to construction materials.

Through SFC, Pegna introduced a concept which was a departure from current assembly techniques. SFC is a process based on the 'wet' construction technique. However, the current emphasis is towards promoting 'dry' and eliminating 'wet' construction methods. SFC introduced the notion of a computer controlled process for the preparation, delivery, and deposition of matrix and binder materials in a 'wet' form. This hybrid of 'wet' and 'dry' technique could be seen a pioneering method of FC, in which a new and emerging research field, is currently under active research.

2.3.2 Contour Crafting (CC)

Developed by Khoshnevis (2004), CC is a layer by layer extrusion process for fabricating structures at a range of scales. Some of the important features of CC were its high deposition rates and the ability to use a wide choice of build materials. Using thixotropic materials with rapid curing properties and low shrinkage characteristics, consecutive layers of wall structures can be built by an incremental fashion of controlled thickness, as Fig. 2.4 shows.

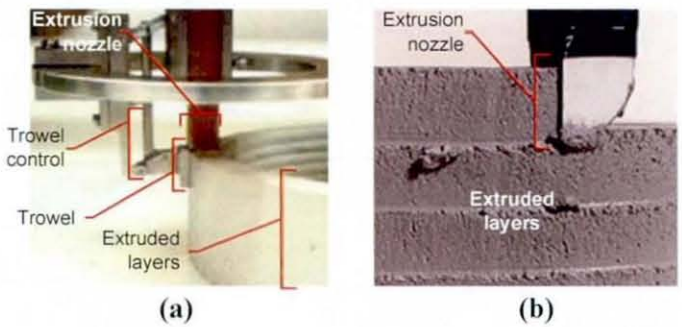

(a) (b)

Fig. 2.4 CC extrusion process: (a) extrusion nozzle with active side trowel; (b) extrusion nozzle with integrated trowel (Khoshnevis, 2004).

In CC, the deposition of build materials was carried out in two stages. In order to improve the finish of the visible surfaces, extruded materials at the shutter of the nozzle is shaped and smoothed by a secondary manipulator (trowel) as it is extruded. The combination of these processes was a system which can deposit relatively large quantities of build material, while maintaining a high quality surface finish. CC is a hybrid method, where the extrusion process for forming object surfaces and filling the object core is combined. The CC process and the components of extrusion nozzle are depicted in Fig. 2.5. CC successfully demonstrated the fabrication of a prototype full scale straight wall, using concrete material, is shown in Fig. 2.6 (Khoshnevis, 2005). Other features which could be integrated with CC included automated assembly and placement of integrated service components (Khoshnevis, 2004).

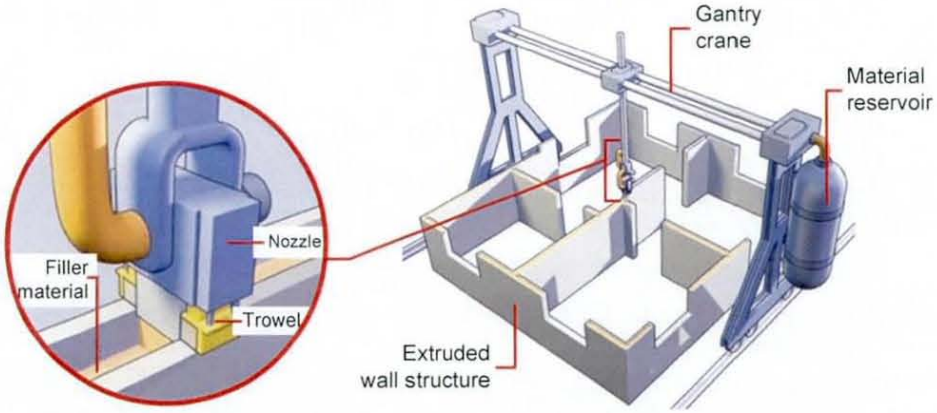

Fig. 2.5 Construction of buildings by CC: (a) extrusion nozzle extruding wall surfaces and filling core material; (b) CC system on an automated gantry.

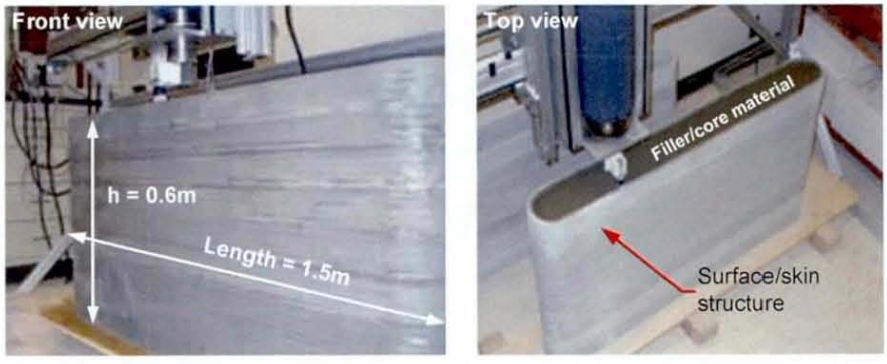

Fig. 2.6 Prototype wall by CC: (a) Full scale concrete straight wall section; (b) filler/core material within a surface skin structure (Khoshnevis, 2005).

CC is geared towards automating the 'wet' construction technique, with combined the advantages of both FC and automated assembly. CC may have the potential to construct architectural designs of complex 2D cross-sectional geometries which are expensive to build using manual approaches. Developments are underway to explore the use of in-situ materials for application in low income housing and emergency shelters. CC is currently leading the field in a new approach to automated construction.

CC represents a process for constructing large scale structures based on the principles of AMT's, which is envisaged to offer better geometrical build freedom (Khoshnevis, 2004). The perceive benefits of this feature are that value added functionality could be integrated to structures build, by means of controlling and optimising geometries of solid objects. Other benefits include the reduction of solid waste and potential material savings.

2.4 Problems facing construction

The construction industry has been going through an evolutionary period similar to that undergone by the manufacturing-based industries. At present, the fundamental principles used in construction have remained relatively unchanged. Recent developments of production methods were focussed on the shift of onsite manual assembly to offsite automation (Balaguer *et al.*, 2002). Although some of these issues have been addressed by 'standardisation' and 'pre-assembly' (Wing and Atkin, 2001), there is a need for more radical solutions. Such was demonstrated by the FutureHome project through the development of the integrated construction automation (ICA) concept, intended to bridge the gap between construction and factory-based manufacturing. In view of that, future methods for construction must be able to respond to new challenges and to address environmental issues with new materials and solutions for buildings at end of life applications (Buswell *et al.* 2006).

This review gives the reader an appreciation of modern methods of rapid construction and covers the background of recent advancement in construction methods, specifically

Automation in Construction (AiC) by the 'layer by layer' assembly and 'material distribution' techniques.

2.5 Background to 'assembly' methods in construction

2.5.1 Factors of development

The origins of the developments and applications of AiC's, at a commercialised scale, can be traced back to Japan. Since the uptake of robotics and automation, factory based manufacturing industry had gained the advantage over the construction industry, in terms of increased productivity and reduced labour (Cosineau and Nobuyasu, 1998; Wakisaka *et al.*, 2000). From the onset of the early 1980's, Japan's manufacturing industry had consistently achieved higher profits over the construction industry. In contrast, the construction industry, with much of its processes being performed manually, was lagging behind. One of the key drivers which motivated the development of early AiC's were primarily due to the shortage of skilled manual labours. The factors of development were;

- Direct human manual labour replacement
- Increased build finishing quality
- Improved working environment for human workforce
- Increased build productivity
- Greater control over the build process
- Supplement to the shortage of skilled labour

2.6 Commercialised 'assembling' AiC Systems

AiC's covered in this section are systems which employ a layer by layer 'assembly' technique. These systems are based on the principles stemming from the industrial sector, where the building is essentially regarded as a 'product'. Based on Howe's (2000) classification, AiC's which employ an assembling technique can be classified into two of the categories.

i) Top layer down – Systems which formed a systematic factory, fixed in the context of the building/work site.

ii) Bottom layer up – Systems which formed a systematic factory with limited translation within the building/work site.

The two fundamental methods of AiC's (from an AMT's perspective) are the 'top layer down' and the 'bottom layer up' approach, as figure Fig. 2.7 shows.

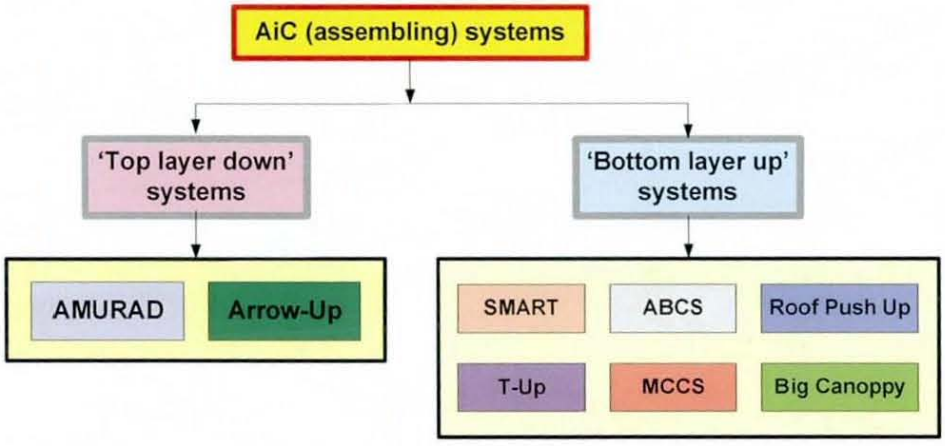

Fig. 2.7 Classification of AiC systems which employ an assembling technique

Japanese AiC's are analogous to the more familiar processes such as aircraft and ship building. They are essentially assembling processes of individual components, manufactured using a combination of formative and subtractive techniques. These systems promote the 'dry construction' method, contrasting traditional techniques which tend to create unorganised work environments, known as 'wet construction' methods (Soar, 2006).

2.7 'Top layer down' systems

Within this category are robotic systems which form a systematic factory, fixed in the context of the worksite. In this category are two systems which employ the 'top layer down' approach. These systems could only construct buildings of restricted height of ~ 12 floors maximum, with aspect ratio of ~ 3:1 due to cost and technical reasons.

Two construction firms developed and applied these systems. The system by Kajima Corp. and Fujita Corp., were known as the 'Automated Up-rising Construction by Advanced Technique' (AMURAD), and the 'Arrow-Up system', respectively (Fig. 2.8). Both had similar build techniques, where an aggregate of completed floors were 'extruded' upwards by a series of hydraulic jacks from the ground factory below. Analogous to AMT's 'top layer down' techniques such as EnvisionTec's Perfactory system (Wholers, 2004), both AMURAD and Arrow-Up consist of a purpose built onsite fixed factory at ground level. Building materials, as well as modular units, in AMURAD's case, could be fed through the ground factory (Kajima, 1997). Once the bottom last floor is completed, the ground factory is disassembled and the building completed (Howe, 2000).

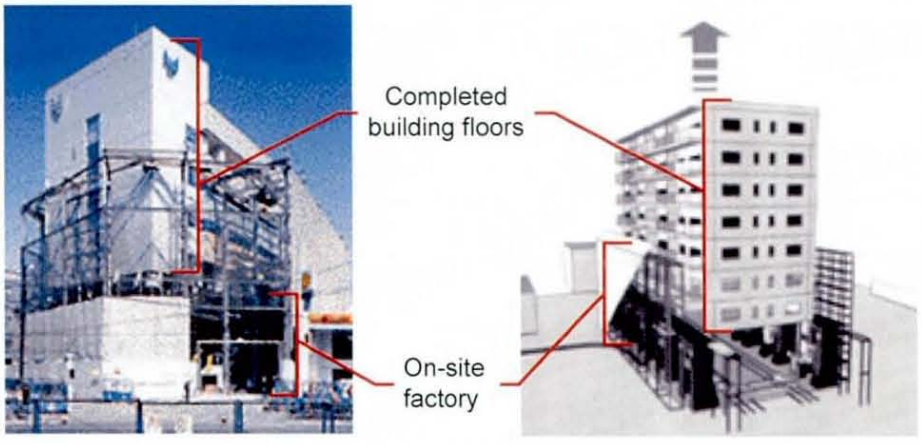

Fig. 2.8 AMURAD system of Kajima Corp.: (a) on site factory fixed at building ground level; (b) completed floors are raised from ground factory.

2.8 'Bottom layer up' systems

Within this category are systems with an 'onsite factory' capable of 'moving' itself vertically along the height of the building. Fig. 2.9 shows an example of this system, namely the Big Canopy system. In general, systems of this category are typically used to construct buildings of more than 10 floors, in order to be cost effective. During their peak, from the 1980's till the late 90's, there were seven Japanese construction firms which developed and applied such systems (Cousineau and Nobuyasu, 1998).

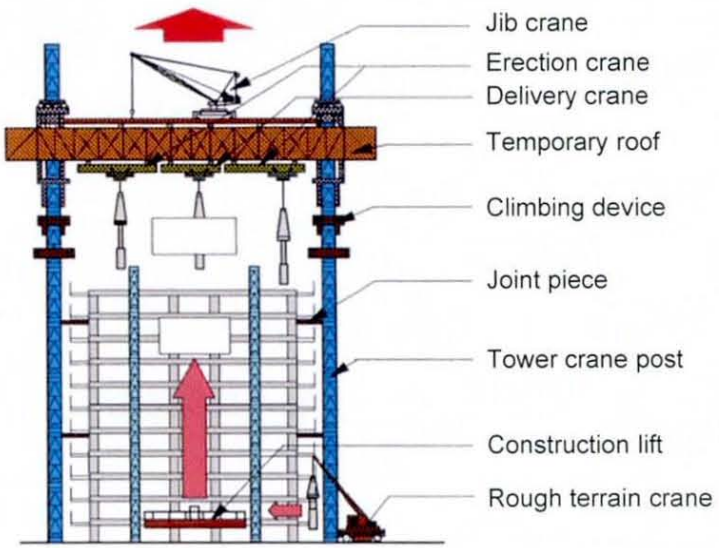

Fig. 2.9 Moving factory AiC's – The Big canopy system (Wakisaka *et al.*, 2000)

Instead of assembling and 'extruding' upwards an aggregation of completed floors, the factory modules of moving systems would always remain on top of the building. They are designed to have vertical movements to 'climb' up support posts, rather than being fixed at ground level. These systems progressively build by adding layers to the top of the building structure in a 'bottom layer up' fashion. In general, their built approach is synonymous to the 'bottom layer up' methods used by most of the current AMT's. Within systems of this category, the term 'sky factory' and 'ground factory' is referred to the moving and ground level factory respectively (Tanijiri *et al.*, 1997).

2.8.1 ABCS

Obayashi Corp.'s ABCS (Automated Building Construction System) was the first AiC system to be commercially applied to construction projects (Cousineau and Nobuyasu, 1998). The system operates based on a combination of automated and conventional methods. ABCS consist of a Super Construction Factory (SCF) (Fig. 2.10), integrated to the overhanging travelling cranes, jacking/climbing systems and a control room (Fig. 2.11a). During the build process, the SCF is raised one story at a time using an alternating approach as each floor progressed (Fig. 2.11b). Work environment is improved by an 'all-weather' shield which ensured that work is uninterrupted. Issues of safety and material handling were also reduced with the presence of high levels of automation which relied on less direct labour (Yamazaki and Maeda, 1998).

Fig. 2.10 Components of the ABCS by Obayashi Corp. (Obayashi, 1998)

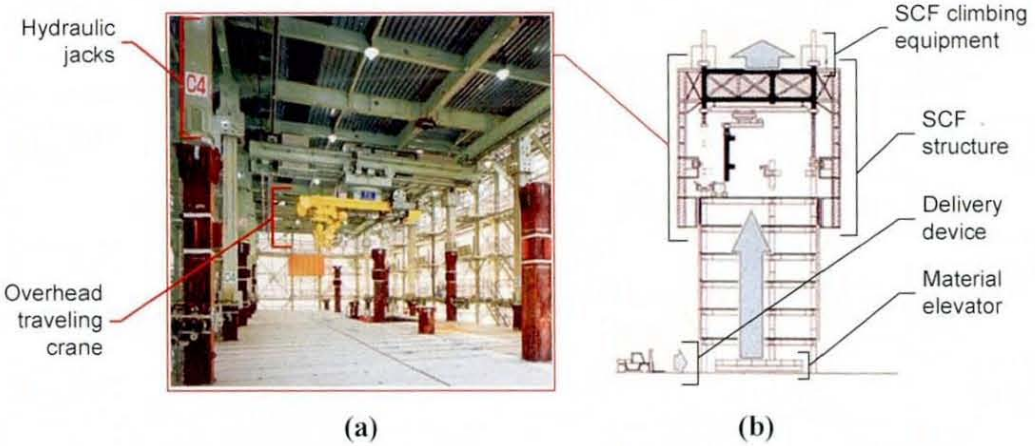

Fig. 2.11 Jacking and lifting mechanism of ABCS (Obayashi, 2004): (a) internal factory floor of ABCS system; (b) method of erection and factory floor.

2.8.2 Roof Push-up

The 'Roof Push-Up' system was developed and applied by Takenaka from the late 1980's to the mid 1990's. The 'top floor' or the 'roof' is constructed and pushed up one floor at a time as the building progressed (see Fig. 2.13). By initially constructing the top floor of the building, work can be carried out under it without being hindered by weathering elements. Setting up the Push-Up system does not require large amounts of worksite space as claimed by Takenaka Corp., in which is often limited in sky scraper construction (i.e. construction in between existing buildings), as Fig. 2.12 shows. The Push-Up could also be utilised near airports and railways or immediately below power lines, where the use of a crane is seen to be impossible (Takenaka, 2000).

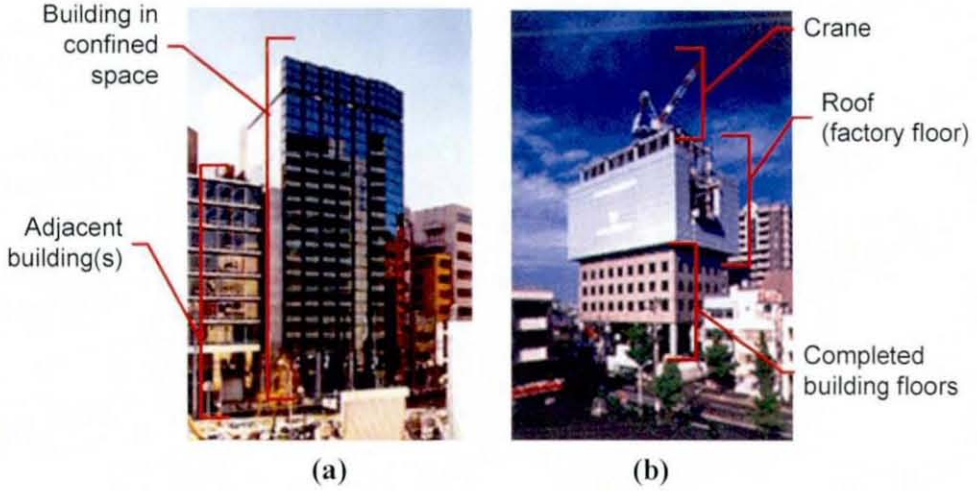

Fig. 2.12 Roof Push-Up system by Takenaka Corp.: (a) Construction in between buildings; (b) system components (Takenaka, 2000).

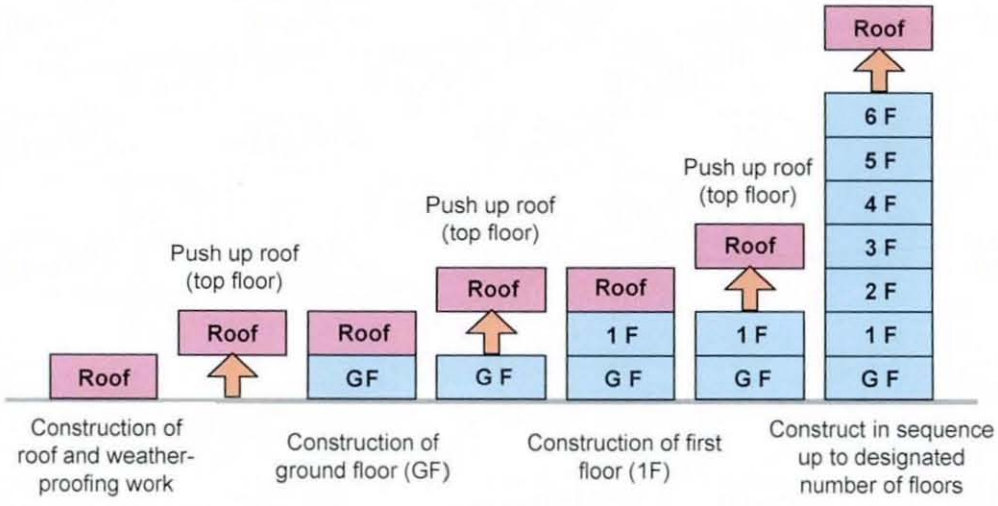

Fig. 2.13 Method of construction of the Roof Push-Up method (Takenaka, 2000)

2.8.3 MCCS

The MCCS (Mast Climbing Construction System) was developed and applied by Maeda Corp. This system, while still being widely applied in Japan, is most economical for low rise buildings with short spans, as Fig. 2.14 shows. The level of automation of the MCCS is considered to be higher than most Japanese systems. The interior work floor is clear of machinery and contains only the jacking systems supported by exterior columns. The conveying systems consisted of overhead cranes and sliding lifts controlled by a central computer. The overhead cranes are used to pick up heavy materials at ground level and automatically position them at their predetermined location. Lighter materials are picked up by the sliding lifts at ground level to be unloaded at predetermined floors using a slide table. Cited benefits were a reduction in manpower, with fewer skilled labour required, due to the level of automated tasks and prefabricated components (Cousineau and Nobuyasu, 1998).

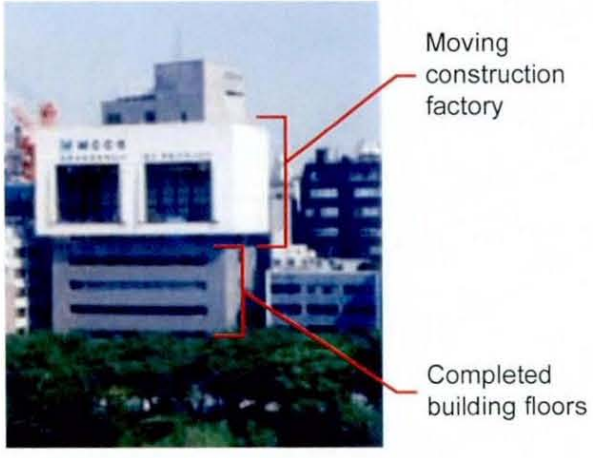

Fig. 2.14 MCCS System by Maeda Corp. during of the Sekai Bunka Sha Building in Tokyo, Japan (Maeda, 1998)

2.8.4 T-Up

Taisei's T-Up system was quite different from the rest. Its 'sky factory' is constructed on the building's structural core which would eventually become the top floor (see Fig. 2.15). The work platform is supported by the building's core and not by external steel columns. The framework and jacking systems is supported by the building's core which is designed to be earthquake resistant. Construction processes starts with the building's foundation work, erection of the central core, followed by the erection of crane platform which utilises the top part of the building as the work space. The roof section is assembled to provide a weatherproof work environment. The lower floors are

constructed from the factory floor. The factory floor and the 'hat' are raised along the building's core as construction progresses. Fig. 2.16(a) to (b) shows the schematic diagram of the assembly process of the T-Up systems (Taisei, 1995).

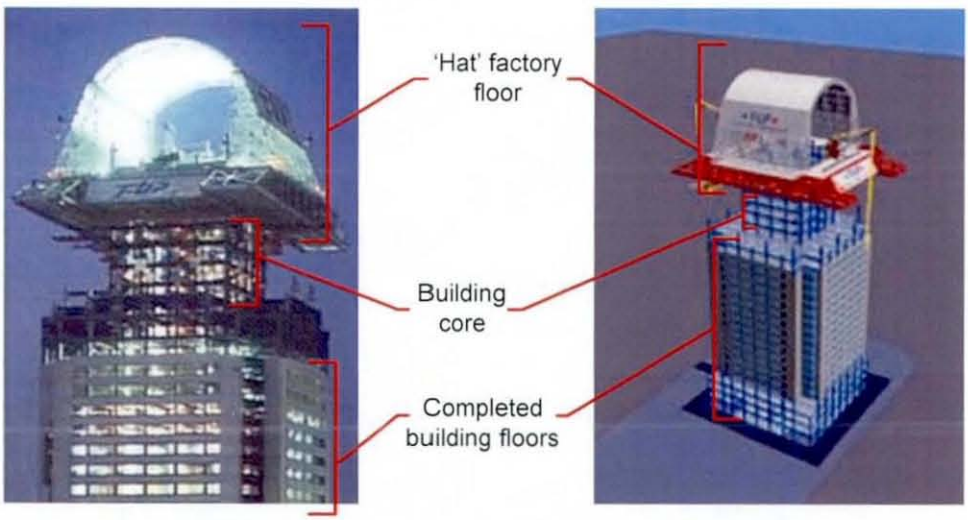

Fig. 2.15 Taisei Corp.'s T-Up system with Sky factory on the building (Taisei, 1995)

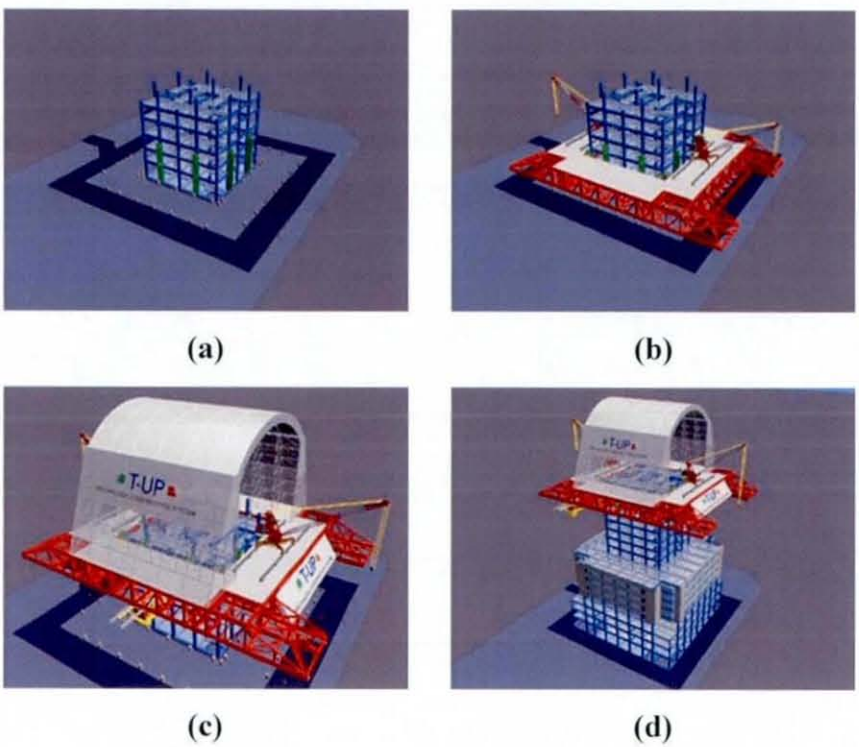

Fig. 2.16 T-Up build process: (a) erection of building core; (b) erection of crane platform; (c) crane platform raised and 'hat' assembled; (d) 'hat' raised and building assembled from below (Taisei, 1995).

2.8.5 SMART

The SMART (Shimizu Manufacturing system by Advanced Robotic Technology) consists of a moving factory supported by four steel columns, as Fig. 2.17(a) and (b) show. Tower cranes on top are use for material delivering and erecting of structural steel structures. The tower SMART, shown in Fig. 2.17(c), is an adaptation of the system for the construction of building or towers with high aspect ratio. SMART consisted of an automated lift-up, material transport, steel assembly and welding systems and a computerised management system. Building materials are bar-coded for identification which is transported to their designated location by an automated transport system. Steel columns are assembled with the aid of human operators before being welded together by automated welding robots. Upon completion of each floor, the entire factory is raised by hydraulic jacks for work to be carried out on the subsequent floors. The steel columns and factory are designed to be re-used and dismantled once construction is completed (Yamazaki and Maeda, 1998).

Fig. 2.17 Shimizu Corp.'s SMART System: (a) construction of residential tower in Chiba, (b) Construction of the Joroku Bank building in Nagoya, Japan, (c) Tower SMART.

2.8.6 Big Canopy

The Big Canopy system by Obayashi Corporation consists of a weather proof overhanging roof supported by four steel columns at the building's outer perimeter. The system was the only automated assembling system for pre-cast concrete (PC) buildings. The Big Canopy system, as shown in Fig. 2.18(a), generally shares similar operating principles to the ABCS. However, several differences exist. As Big Canopy primnarilly deals with PC, raising the level of automation is difficult. More manual work is required to connect and disassemble the temporary construction shoring. Because concrete requires time to set, it is seen to be technically difficult to provide a sufficient all-weather assembly plant. Higher payload is required as PC members are heavier than steel columns used. Big Canopy was mainly applied to buildings of at least twenty stories to remain cost effective. The shortcoming of this system was the requirement of sufficient space for the erection of the temporary posts and the unloading of the delivered materials. During the 1990's, Big Canopy is the only system to be used outside Japan (Wakisaka *et al.*, 2000).

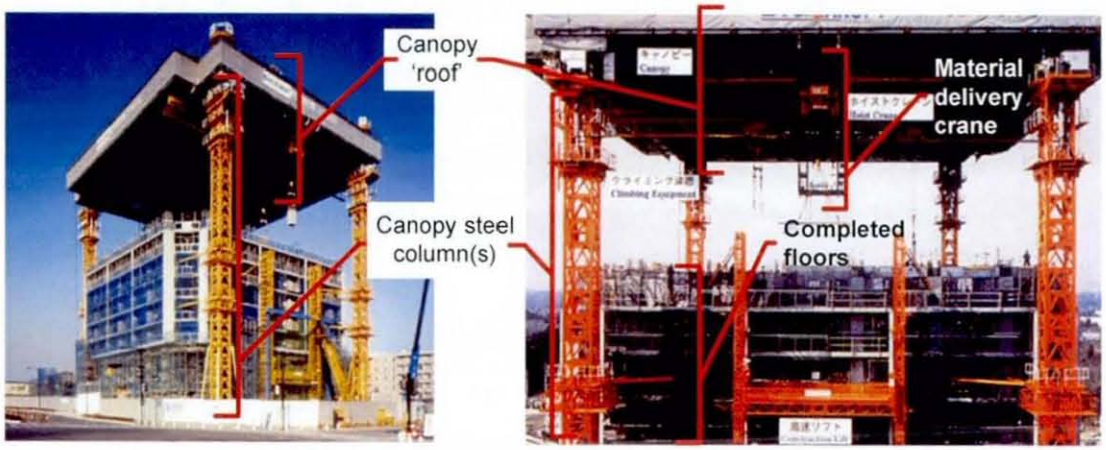

Fig. 2.18 Obayashi Corp.'s Big Canopy system: (a) Assembling of precast concrete (PC) building; (b) factory floor (Obayashi, 2004).

2.9 Summary of 'assembling' AiC systems

Table 2.2

Evaluation of the features and development goals of various assembling Japanese AiC systems

AiC Systems	Features	Development goals	Evaluation
 Big Canopy (Obayashi Corp.)	• 'All weather' temporary roof. • 3 Hoist exchange overhead cranes. • 4 oil-hydraulic climbing units. • 4 posts of tower cranes. • 1 construction elevator.	• Improved overall productivity. • Improvement of construction environment. • Reduce construction period. • Improve work environment. • Reduce labour. • Improve quality.	The only pre-cast concrete system. Least automated of all systems. 60-80% savings in manpower. Minimised materials cost. Construction of 28-floor PWC Building in Singapore took only 26 months with 25 workers. Canopy roof improved working environment.
 ABCS (Obayashi Corp.)	• A Super Construction Factory (SCF) • An automated storage system. • Automated material delivery system. • Hydraulic jacks are at top of SCF.	• Shorten construction time. • Reduce labour. • Improve productivity. • Improve quality. • Increase safety. • Improve work environment.	30% reduction in manpower. But 31% increase in labour for welding at areas inaccessible to welding robots. Ground floor material handling demanded 18% of total manpower. Acceptable noise of 60dB but unacceptable measurement of 70dB at factory floor.
 SMART (Shimizu Corp.)	• Automated lift-up system. • Automated transport system. • Automated steel assembly system. • Automated welding system. • Computerised information management system.	• Provide all-weather work environment. • Provide safe working conditions. • Reduce labour and management hours. • Shorten construction time. • Reduce material waste.	Work scheduling was more predictable due to all-weather sheeting. Man hours were reduced due to computerised control systems, prefabrication and material handling. 50% labour savings which translates to 30% of overall cost savings. Waste reduction of over 70% was realized.

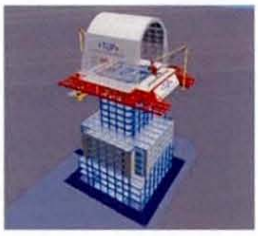 T-Up (Taisei Corp.)	• Earthquake proof building core. • A gigantic robot system consisting of 4 arms. • Automated jacking system. • AGVs for material transport.	• Improve construction time by 30%. • Provide cleaner, safer, and quieter working environment. • Reduce dangerous and disorganised work. • Improve construction quality.	Over 40% of material delivered by AGVs. Better sensory technology to provide potential to work all night delivering materials to appropriate floors awaiting assembly by human and robot operators in the morning.
 AMURAD (Kajima Corp.)	• System with ground level factory. • Ground level lifting systems. • Each floor is assembled at ground level and completed floors are jacked up. • Handles modular units.	• Reduce construction time. • Improve work environment. • Reduce material waste. • Reduce manpower. • Improve safety. • Reduce material handling time.	30% reduction in construction time. 50% reduction in manpower. 50% reduction in construction waste. Overall cost is estimated to be the same as conventional method. Building height restricted to 12 to 15 floors. In terms of market, most construction project in Japan fall in this category.
 Push-Up (Takenaka Corp.)	• Weather proof working environment. • Protected work environment. Less fear of flying objects. • Uses less mechanical equipments, therefore, coast is similar to conventional construction methods. • Optional overhanging crane.	• Improve productivity. • Improve work environment. • Improved safety. • Reduced operating cost (after improvements were introduced). • More predictable work schedule.	Construction is first carried out starting from top floor of the building and pushed up one floor at a time, building from the floor below. This method can be utilised in construction near airports and railways and immediately below microwaves, where cranes cannot be installed on the top floor of buildings.
 MCCS (Maeda Corp.)	• Jacking system supported by exterior columns. • Clear working interior for easier construction. • Overhead cranes for picking and positioning structural columns. • Sliding cranes for lifting lighter finishing material.	• Improve work environment. • Reduce construction time. • Reduce labour through automation and mechanization. • Improve productivity. • Consistent and improve workmanship.	Most economic for low rise, short span buildings. 20 – 30% reduction in manpower with introduction of multi-disciplinary labour. Significant waste reduction was achieved through prefabrication. With improvements to the system, cycle time was reduced from nine to seven days per floor.

2.10 Limitations of 'assembling' AiC systems

In general, the Japanese AiC's attempted to bring onsite construction towards factory-based manufacturing. Although being developed independently, they share many common fundamental operating features. Despite the introduction of a greater level of automation, several key limitations exist. Current AiC's rely heavily on onsite and offsite manufactured and 'pre-fabricated' building components. Although benefits were gained through their implementation, most of the Japanese AiC's are not widely used today. Shigehiko Tanabe of Shimizu Corp., when interviewed by Rupert Soar, highlighted these issues;

i) The lack of construction space for the onsite factory

ii) Limited build geometry

iii) Asia Pacific economic downturn in the late 1990's

The first reason was related to the 'workspace' constraints for the onsite factory. One limitation of moving factory systems was the requirement of ample site space, the only exception being the Roof Push-Up system. These systems were more suitable for applications where space is not an issue. Lack of workspace may also hamper the conveying construction materials. In addition, the source of construction materials supply is required to be within close proximity, to maintain process efficiency.

The second reason was related to the form of buildings Japanese AiC's could produce. The review showed that all buildings assembled by both the 'moving factory' and 'fixed factory' systems all fall into the cubic design category, mainly due to the supports and position of the elevating columns. Form is also reflected by the geometry of the pre-fabricated components used. In principle, the assembly of non-cubic buildings are possible. This could be achieved by increasing types of prefabricated components to cover a wide range of geometry However, having an increased range of prefabricated building components just to produce non-cubic buildings would not justify cost outcomes. This would also increase the process variables, as robot manipulators needed to be reprogrammed to handle them. Interestingly, none of the AiC's adopted this approach. This could probably suggest, in order economically sound, the range of prefabricated components and process variables had to be kept

minimal. Although the AiC systems are currently not in use, this condition should be temporary and is expected to pick up in the near future (Howe, 2005).

Japanese AiC's are complex integration of many processes elements. Though termed as 'rapid construction', they are complex because of the variety of prefabricated components needed to be positioned accurately. The next section covers some of the groundbreaking approaches in construction by a 'material distribution' technique, analogous to the 'layer by layer' methods employed by current AMT's.

2.11 Summary and concluding remarks

The review covers the current state of art of modern methods of construction, from 'assembling' and material 'distribution' approaches, on their impact on the construction industry. The notion to the integration of functionality through design optimisation which could potentially be achieved using single bulk material was introduced.

Although the Japanese AiC's 'transferred' the factory-based assembling approach to construction, the fabrication of layout optimised structures with a certain degree of functionality would requir a new approach. What the current construction industry may be lacking is the change in fundamental techniques on how buildings could be constructed.

Traditional methods, to a certain degree, were seen to be largely based on the 'assembling' approach utilising multiple material. The fundamentally different SFC and CC presented the notion of an alternative method to current construction practices. With the latter adopting the AMT approach, they are a departure from traditional methods. Coupled with the advancements of Computer Aided Design (CAD) packages, these form the forefront to address the manufacturing requirements of layout optimised structures. When used in conjunction with layout optimisation methods, they compliment each other by forming an attractive package.

3

Layout Optimisation Methods for Structural and Thermal Design Problems

3.1 Introduction

Design optimisation methods are seen as enabling technologies which could offer a systematic approach to the design process. Originally, they are employed mainly in the aerospace industry for weight reduction of structures, without compromising performance. Over the years, it has gained considerable research interest and found applications in a vast range of engineering problems. Conputing power and the increasing requirement to handle massive calculations have gone hand in hand, resulting in ever more complex calculations to be performed. Its development was further spurred by the advent of improved processing power and engineering computational or numerical methods the likes of finite element analysis (FEA) and computational fluid dynamics (CFD) in engineering analyses.

3.2 Concept of optimal design

Optimisation is concerned with achieving the best possible solution to an objective, while satisfying all specified requirements. Its application is infinite and can be employed to find the best solution to all quantifiable problems including engineering design problems (Kim *et al.*, 2002). An almost infinite number of quantifiable parameters may be identified (i.e. cost, performance, weight, etc.). Design optimisation, is a process where user needs are transformed into a detailed specification of a system, or object which physical form and function is consistent to the needs of the

user (Liu, 1996). In general, the formulation of optimal design problems involves the identification of *design variables*, *objective function*, and *design constraints*.

A *design variable* is a numerical value which can be controlled. Design variables may be 'continuous' or 'discrete'. Continuous design parameters have a range of values, and can take on any value in a given range, such as the length of a beam. Discrete design parameters can only take on isolated values, usually from pre-specified selections (i.e. number of reinforcement ribs). Design variables are often bounded by a maximum or minimum value.

A *constraint* is a condition that must be satisfied in order for the design to be feasible. For instance, the strength of a beam must be able to sustain its own weight. In addition to physical laws, constraints can reflect resource limitations, user requirements or bounds on the validity of the analysis models. Constraints which imposed a lower or upper limit on certain quantities are called inequality constraints. In some design problems, equality constraints are required (i.e. the required length of a beam). A design constraint could sometimes be specified as a design requirement or design criterion.

An *objective function* is a numerical value which is to be maximised or minimised. It provides means for different designs to be compared and distinguished one from another as being better. For example, it is common that weight of structures are minimised to maximise profit, or stress is minimised to increase strength and fatigue resistance. Many optimisation methods work only with single objectives. When these methods are used, the various objectives are weighed, and summed to form a single objective. All objective functions are influenced by the design parameters. For cases with two or more objectives, the problem is a 'multiobjective' or 'multicriterion' optimisation problem. For such cases, additional steps must be taken to solve such problems. Once the above quantities have been identified, the design problem is then reduced to a numerical problem.

3.2.1 Description of optimisation problems

In formulating an optimisation problem, certain quantities are fixed at the outset, known as pre-assigned parameters. All quantities which were not pre-assigned are called design variables. Mathematically, an optimisation problem could be stated as:

Find the set of design variables $\boldsymbol{X} = (x_1, x_2, \ldots, x_n)$ that will minimise (or maximise) the performance parameter

$F(\boldsymbol{X})$ *(objective function)*

Subject to,

$G_j(\boldsymbol{X}) \leq 0, \quad j = 1, 2, \ldots, p_j$ *(inequality constraints)*

$H_i(\boldsymbol{X}) = 0, \quad i = 1, 2, \ldots, q_i$ *(equality constraints)*

$x_i^l \leq x_i \leq x_i^u, \quad i = 1, 2, \ldots, n_i$ *(side constraints)*

where n is the number of design variables, p is the number of inequality constraints, and q is the number of equality constraints. x_i^l and x_i^u denotes the lower and upper bounds of the design variable x_i. For example, lower bounds are commonly used to define a minimum cross-sectional area of a structural member and to prevent it from going below zero. It would be of no practical sense for structural members to have negative cross-sectional area or volume (Hansen and Vanderplaats, 1988).

Typically, optimisation problems are nonlinear. A recurring iterative process is often required before a solution could be obtained. The optimisation problem is solved by a combined analysis/optimisation procedure which involves analyses and redesign. Most design optimisation methods operate in conjunction with a numerical solver, with a purpose to assess the performance of a design. The analysis required depends on the nature of the physics of the design problem. The current research will consider FEA for structural optimisation and CFD for thermal optimisation. In general, five fundamental steps were involved. They are;

i) Development of an initial design
ii) Numerical analysis of the design
iii) Sensitivity analysis
iv) Redesign
v) Assessment of design performance

In step i), depending on the type of method used and the design problem, the choice of the initial design may have significant influence on the final optimal design. The number of iterative cycles required for convergence may also be affected by the choice of the initial design. Therefore, the chosen initial design should be realistic and appropriate with respect to a given problem, even for methods where the final solution is not affected by the chosen initial design. Grooms *et al.* (1990) noted that with the selection of some initial designs, an optimisation may fail to converge.

In step ii), numerical analysis forms an important part of the design process because it verifies the feasibility of the designs, so that no constraints are violated. For structural optimisation, this is often performed using FEA. For thermal optimisation, this may be performed by FEA or CFD.

Step iii) involves the evaluation of the objective functions, constraint functions, objective derivatives and/or constraint function derivatives with respect to design variables. The efficiency of the evaluation of objective functions depends on computing power. This could pose as a barrier in some design problems which involves calculations of many design variables, for instance > 1000 variables (Liu, 1996).

Step iv) involves the optimisation process to synthesise a better design, one which improve the system's objective function. In layout methods, this could be the addition or removal of materials. In shape methods, the shape of the structure is varied and accompanied by the remeshing of the optimisation model. In sizing methods, the dimensions of a structure or a member is varied.

Steps ii) to iv) are repeated until the design satisfies a chosen 'convergence criteria', when a design is chosen not to be improved further. These steps can either be performed manually or automatically. Efficiency is usually higher with automated approaches. With either approach, the fundamentals of an optimisation process remained unchanged.

Step v) is the final step in the iterative process where the convergence of the designs is assessed. The convergence criteria may be changes in objective function gradients, changes in design variables, or simply the limit on the number of iteration cycles (Liu, 1996). For structural optimisation, this could be stress, deflection or mass constraints. For thermal problems, this could be temperature or heat flux constraints.

3.3 Types of structural optimisation problems

Design optimisation problems can be classed as sizing, shape, and layout/topology methods. Sizing optimisation is typically applied to truss member type structures. Design variables can be the member thicknesses of a beam member. It is relatively straight forward and does not require changes in the FE model when the structure is modified. Shape optimisation however, determines an optimal boundary of a structure for a given topology. The design variables are typically spline control points defining the shape of a structure in 2D or 3D. Unlike sizing methods, shape optimisation changes the FE model and hence adds difficulties in having to integrate the mesh generation Sizing and shape methods however, suffer from the dependency of the initial structure (Kim *et al.*, 2002). Solutions obtained by sizing and shape methods maintain relatively similar topology as the chosen initial design. More often than not, these solutions may be far from optimal because other competing topologies cannot be explored (Liu *et al.*, 2000). Topology or layout optimisation is therefore developed to overcome this deficiency. To a certain degree, it is capable of simultaneously addressing layout and shape optimisation problems, in which solution is independent of the chosen initial design (Liu *et al.*, 2000).

3.4 Review of layout optimisation methods

Methods for optimal structural designs were developed to solve a class of problems which involves the design of elastic structures. In general, these problems are mainly concerned with finding optimal design layouts in which the compliance and weight is minimised subjected to design constraints. The review covers the 'deterministic' generalised layout methods and 'non-deterministic' (stochastic) optimisation methods used in engineering design problems.

i) Homogenisation Method

ii) Evolutionary Structural Optimisation (ESO)

iii) Metamorphic Development (MD)

iv) Simulated Biological Growth (SBG)

v) Genetic Algorithm (GA)

vi) Simulated Annealing (SA)

vii) Particle swarm optimisation (PSO)

In this review, more attention will be given to the generalised layout techniques as it forms the basis the method used to address the investigated design problems.

3.4.1 Homogenisation method

The homogenisation method by Bendsøe and Kikuchi (1988) is a technique developed to solve a class of shape optimisation problems which involved varying topology, known as 'generalised layout' problems. It is one of the earliest methods of this class. It enables optimal topologies of structures to be generated in a predefined design domain, using a stiffness-density relation obtained by the homogenisation of cellular microstructure. Admissible structural material is introduced in the form of composites with perforated microstructures of varied densities and orientation. Homogenisation is an alternative approach to shape optimisation. Shapes of structures were represented without the use of shape functions, which was found to exhibit difficulties when geometries of structures are design variables (Suzuki and Kikuchi, 1991). Homogenisation seeks to transform a shape optimisation problem to a material distribution problem using composite materials. Two material constituents, substance (or solid) and void were considered. The initial design is a solid space with material to be removed. The use of a fixed design domain simplifies the construction of a FE approximation, and remeshing was avoided. The method allows optimal topologies of structural members to be 'predicted', in the form of a non-smooth estimated boundary. Fig. 3.1 depicts a homogenisation solution of a rigidly fixed, plane stress cantilever. Black and white areas indicate solid and voids respectively and greyscales indicate intermediate densities (Kim *et al.*, 2002).

Fig 3.1 Typical optimisation solution of a plane stress thick cantilever by homogenisation (a) Initial design in a bounded design domain, (b) optimised layout with varying density

The application of homogenisation to solve structural optimisation problems was reported in Chirehdast and Papalambros (1992), Tenek and Hagiwara (1994), Jacobsen *et al.* (1998), Fernandes *et al.* (1999), Nishiwaki *et al.* (2001), Ansola *et al.* (2002) and Liu *et al.* (2006). The method is also extended to cover generalised layout design of vibrating structures. These include, static and vibrational shape and topology optimisation using homogenisation and mathematical programming (Tenek and Hagiwara, 1993), topological design for vibrating structures (Ma *et al.*, 1995), unified topology design of static and vibrating structures using multi-objective optimisation (Min *et al.*, 2000) and optimum topology and reinforcement design of vibrating disk and plate (Krog and Olhoff, 1999). Homogenisation is also used in the optimisation of composite structures. These include homogenisation-based design of composites (Swan and Kosaka, 1997), design of functionally graded composite structures (Lipton, 2002) and the design of two-phase isotropic composites (Sigmund, 2000). Homogenisation was also applied in the design of biomechanical structures. A good review is given by Machado and Trabucho (2004) and Hoppe and Petrova (2004).

Despite the use of homogenisation in the aforementioned design problems, several drawbacks were highlighted. Homogenisation could not be used in design problems where the size of the design space is not known a priory. Designs could only be carried out in bounded design domains. Therefore, other possible optimal solutions which lie beyond could not be explored. The optimised solution is dependent on the ground mesh from which density is degraded. No mechanism is present to reinstate degraded densities if the existence of a particular unit cell element is later found to be desirable. Due to the nature of the method, optimised structures are highly perforated and contain

'microvoids'. Intermediate densities within structures are represented by blurred greyscales structures. From a practical standpoint, this is undesirable since the primary goal is to find a real shape. In engineering designs, the grey level image should be converted to a binary image. The second stage of the optimisation involved post-processing, through a procedure called 'lumping'. Each element of the structure is converted to 'solid' or 'void', based on a microscopic scale (Bendsøe and Kikuchi, 1988). Allaire (2004) introduced a technique, known as 'density penalisation'; a method which forces intermediate densities to take on values of 1 and 0. A general idea of the method is shown in Fig. 3.2.

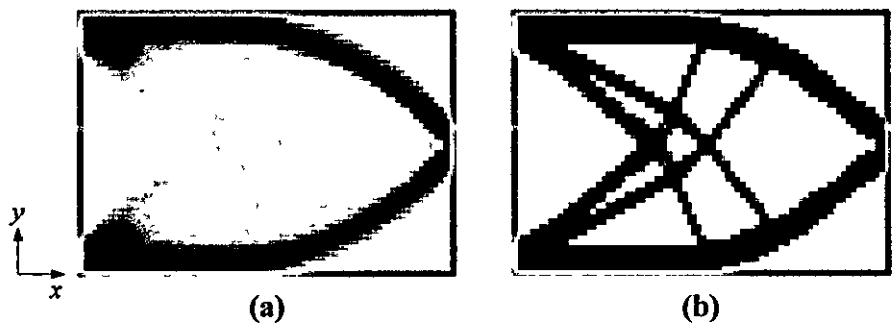

Fig 3 2 'Density penalisation' of an optimised layout by the homogenisation (a) Composite design with intermediate densities, (b) density penalised design (Allaire, 2004)

3.4.2 Evolutionary Structural Optimisation (ESO)

ESO is one of the earliest generalised topology optimisation method developed based on a binary material distribution approach (Xie and Steven, 1993). Its concept is based on the notion that 'by slowly removing inefficient material from a structure, the shape or topology of the structure evolves towards an optimum' (Xie and Steven, 1997). The efficiency or relevance of materials used in structural components could be determined by their stress levels. The use of material is considered to be inefficient or under-utilised, if their stresses are relatively low, compared to the safe operating stress. Hence, under-stressed materials which do not contribute to the overall integrity are identified and removed, reducing the total volume in the form of discrete design variables of FE's. The ESO design cycle consists of analysis, calculation of sensitivity numbers and element (or material) removal. An example procedure shown in Fig. 3.3 involved the following steps:

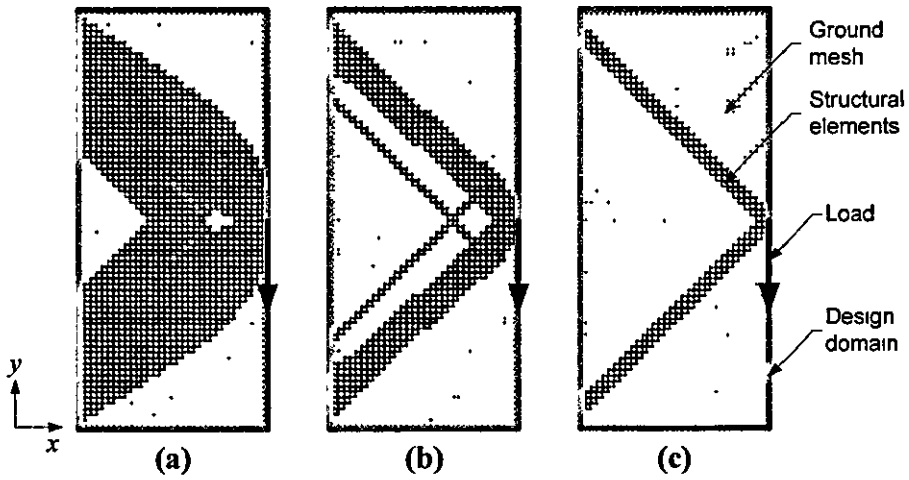

Fig 3 3 Evolutionary history of topology optimisation of a deep cantilever beam (a) Iteration-50, (b) iteration-150, (c) optimal topology (Liang *et al*, 1999)

i) The design domain, an area or volume large enough cover the final design is discretised into fine mesh of quadrilateral FE's of uniform size.

ii) The structure is analysed using FEA for the given kinematic boundary constraints, boundary conditions and loads.

iii) Sensitivity numbers for element removal are calculated. This procedure involves the evaluation of an element removal criterion or rejection ratio (RR), and an element removal ratio (ERR).

iv) Elements which satisfy the sensitivity numbers calculated in step iii) are removed from the structure.

v) Steps iii) and iv) are repeated iteratively until a steady state is reached.

The application of ESO as a generalised method to solve topology optimisation problems was reported in Chu *et al*, (1996), Li *et al.* (2001), Rong *et al.* (2001), Guan *et al.* (2003), Kwak and Noh (2006), Li *et al.* (2000), Steven *et al.* (2002), Das *et al.* (2005), Xie *et al.* (2005) and Yang *et al.* (2005). ESO was also applied to find optimal design of continuum frame structures, presented in Steven *et al.* (2000), Li *et al.* (2003) and Manickarajah *et al.* (2000). ESO was also applied to optimise dynamically loaded structures, reported in Xie and Steven (1995) and Haiba *et al.* (2005). Since its development, several variants of ESO emerged. These are additive evolutionary structural optimisation (AESO) and the bi-directional evolutionary structural optimisation (BESO) (Querin *et al.*, 2000a, 1998). In AESO, elements are introduced

to areas of the structure where they were needed, with a similar evolutionary procedure to the classic ESO. In this approach, the design is started from a severely 'under-designed' model consisted of minimal amount of elements, instead of an 'over-designed' structure in the form of a ground mesh. However, several drawbacks were identified. In AESO, materials could only be added to a structure to distribute high stresses. No mechanism for removal of under-stressed materials was present. The presence of under-stressed or inefficient materials resulted designs with topologies which were far from optimal, in terms of a fully stressed structure of minimum weight (Querin *et al.*, 2000a). These drawbacks have been addressed by BESO, an optimisation method which combines both the element additive and removal attributes of AESO and ESO (Querin *et al* , 1998, 2000b). In BESO, the elements of a structure could either be removed or added. The technique for addition and removal of elements are based on the basic principles of ESO and AESO, in which both methods were combined to work together.

Despite the advancements of the ESO methods, one fundamental drawback was the dependence of the solution on the ground mesh from which it evolved and on the sequence of element removal. Once a certain under-stressed element is removed, ESO is unable to reintroduce, if at a later stage its presence is found to be desirable. For continuum layout designs, the dependence of ground mesh could lead to lengthy solution time because more elements are required to be removed than retained. Although the capability to add and re-introduce elements was added to ESO through BESO, designs were still restricted to the positions of previous elements to an area (or volume) predefined by the ground mesh (Liu *et al.*, 2000). Designs are limited to a pre-specified bounded design domain. Despite the notion 'evolutionary', the ESO methods do not resemble biological inspired steps, based on the Darwinian theory of 'evolution', and should not be confused with evolution strategies of genetic algorithms (Baumann and Kost, 2005).

3.4.3 Metamorphic Development (MD)

Metamorphic development (MD) is a layout optimisation method to find optimal structural shapes and topologies through minimisation of structural mass and compliance, subjected to stress and deflection constraints (Liu *et al.*, 2000). A ground

mesh or bounded design domain is not required. Design optimisation could also start from any degree of development, between an under-designed and over-designed structure. Good examples of these could be found in Liu *et al.* (2001) and Ngim *et al.* (2009), respectively. The method is aimed at producing 'mass minima' design solutions. In contrast to existing layout methods, MD is one of the latest techniques developed.

Optimal designs of structures are developed through MD's simultaneous growth and degenerative approach, with the aim to ensure satisfactory or improved overall performance. Growth and degeneration is represented by the addition and removal of nodes from an optimisation model under development. MD has the mechanisms to introduce and re-introduce new nodes and elements (i.e. nodes which had been removed in previous iterations) For instance, element E_a might render element E_b to be inefficient, thus E_b is removed. When E_a is removed at a later iteration, this might render E_b desirable. This feature enables the topology of a design space to be more robustly explored. Elements which do not contribute effectively to strength and stiffness are systematically identified and removed. New elements are added to the structure at localities where they are most needed, to distribute or disperse load, and to form new 'load paths'. The use of a design domain is optional. If specified, a design domain may contain a number of sub-domains which could be finite or infinite in size.

Substantial computational savings may be gained through MD (Liu *et al.*, 2000). Layout methods which employ a degenerative only approach would eventually have most of its ground mesh removed, leading to prolonged solutions. A drawback of ground mesh methods is the dependence of the final solution on the starting ground mesh. However, this is not the case with MD. The method has been tested to give consistent results, independent of the chosen initial design (Liu *et al.*, 2000) Optimisation methods by the degenerative approaches must start from a bounded design domain. In certain cases, the best size initial ground mesh may not be known *a priori.* An example is shown in Fig. 3.4. The task is to find an optimal shape which minimises the average strain energy of a centrally loaded suspended object under gravitational load. Without the use of a bonded domain, the optimal shape resembles a 2D cross-section of an apple (Liu *et al.*, 2005).

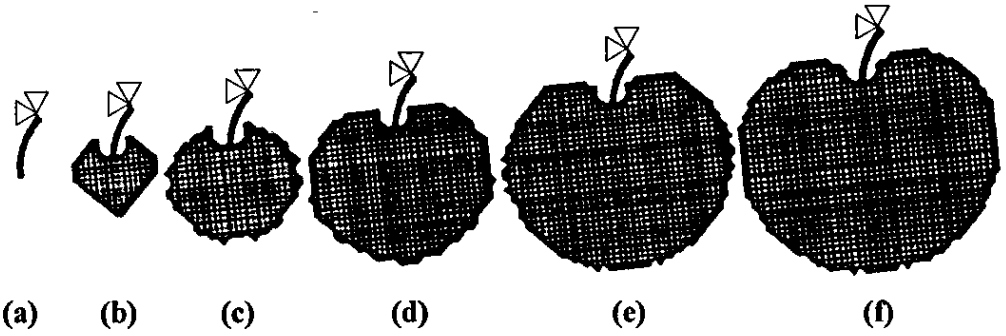

Fig 3 4 Optimal shape for a 2D suspended structure by MD (a) Initial design, a 'stalk', (b) iteration-10, (c) iteration-20, (d) iteration-40, (e) iteration-60, (f) iteration-76 (Liu *et al*, 2005)

Applications of MD to solve layout optimisation problems have been reported. Liu *et al.* (1999) presented examples of design optimisation case studies of a fixed-end beam structure and C-spanner Liu *et al.* (2000) demonstrated several benchmark studies of MD to optimise a 'Michell structure' (Michell, 1904) and a fixed-end cantilever. Optimised solutions by MD were consistent with those produced by existing topology optimisation methods and were found to be slightly lighter and require less recurring iteration. Liu and Lu (2001) applied MD to optimise the design of micro-fibre holder clips. MD was extended to cover the design optimisation of axisymmetric structures. These include the shape optimisation of cylindrical nozzles in spherical pressure vessel (Liu *et al.*, 2001), optimisation case studies of generic axisymmetric structures (Liu *et al.*, 2005), and the design optimisation for manufacturability (Ngim *et al.*, 2007).

MD contrasts other existing layout methods. The features not found in existing topology optimisation methods are;

i) For 2D design problems, two different element types (quadrilateral and triangular) are simultaneous used to build up a structure.

ii) The Dynamic Growth Factor (DGF) is an adaptive function.

iii) Both continuum (i.e. shell and solid) and line (beam) elements may be used.

iv) A bounded design domain is optional. Design domains may either be finite or infinite.

The potential of MD as a systematic design tool to investigate optimal topologies and innovative solutions to structural designs have been presented. Although further developments may be required, the unique features highlighted offer the possibility that

the MD method would be able to solve large-scale engineering structural design problems which may be impractical for ground mesh based methods. In this research, the MD method forms the basis of the layout optimisation. This forms Stage-1 of the proposed two-stage method.

3.4.4 Simulated Biological Growth (SBG)

Biological structures, through natural selection have developed mechanisms to produce load bearing structures optimally adapted to a given load. Natural selection offers two different strategies. First, the trial and error strategy which better designs were created by 'mutation', with slow stochastic success. The second strategy is 'adaptive growth' Structures such as trees and bones adapt flexibly to changes in loading conditions so that a design of high reliability with minimum material consumption and energy would emerge. The principle of low weight and fatigue resistance could be found in all load bearing biological structures, often achieved by uniform stress distribution, or axiom of uniform stress on the surfaces of structures. The axiom of uniform stress is identified as a basic rule for biological load carriers. From these concepts, Mattheck and Burkhardt (1990) developed the Simulated Biological Growth (SBG) optimisation methods for structural engineering applications known as;

i) The Computer Aided Optimisation (CAO)

ii) The Soft Kill Option (SKO)

iii) Computer Aided Internal Optimisation (CAIO)

The reader may refer to Mattheck *et al.* (1993) and Mattheck (1998) for a comprehensive review of which the relevant topics are summarised.

3.4.4.1 Computer Aided Optimisation (CAO)

Concentrations of local stress on surfaces, caused by notches or abrupt changes in geometry are causes of fatigue failure (Mattheck, 2006). The prevention of stress raising effects is of great importance in biological structures as it is in engineering design. CAO is a shape optimisation technique based on the basic growth mechanism and self optimisation of tree cambiums, which satisfy a 'near constant' stress. Artificial growth is selectively guided to reinforce overloaded surfaces In CAO, optimisation only takes place on existing surfaces. CAO is not limited to the domain of biological

structures and can be extended to engineering design problems. Case studies of the applications of CAO in engineering components have been reported. These include the design optimisation of a tensile plate (Bethge and Mattheck, 1990), rubber bearings subjected to large deformations (Mattheck and Erb, 1991), a cylindrical cantilever beam (Mattheck *et al.*, 1993), beam shoulders (Mattheck, 1998) and orthopaedic screw thread designs (Mattheck, 1998). Through experiments, Mattheck (1998) noted that surface shape optimised components is found to be superior compared to non-optimised designs. Fig. 3.5 shows the shape optimisation of an orthopaedic screw thread profile by CAO. The screw withstood twenty times as many load cycles as the non-optimised screw and reduced the danger of implant factures to an absolute minimum (Mattheck, 1998).

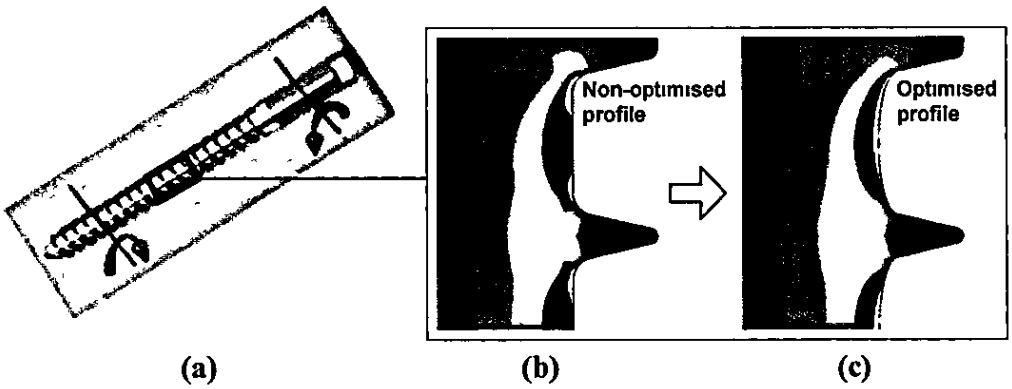

Fig 3 5 Orthopaedic screw optimisation by CAO (a) Orthopaedic screw, (b) original thread design, (c) optimised thread design (Mattheck, 1998)

3.4.4.2 Soft Kill Option

Bones are biological load carriers designed to endure enormous number of load cycles under service conditions. They are able to react to natural loading changes not only by modifying its shape and adaptive remodelling mechanisms, but also by adaptive mineralisation (Baumgartner *et al.*, 1992). The SKO developed based on this analogy, is a layout optimisation technique which the basic mechanisms of the adaptive mineralisation bone structures were simulated using FEA (Baumgartner *et al.*, 1992). Stress distributions are calculated for loading conditions which correspond to those of the component in service, in an initial design area large enough to cover the final design. The Young's modulus is increased in areas subjected to high loads and reduced (or softened) and finally discarded or 'killed' in unloaded areas (Baumgartner *et al.*,

1992; Mattheck *et al.*, 1993). SKO is an efficient design tool for developing lightweight constructions based on natural laws. Case studies on the applications of SKO have been reported. Mattheck *et al.* (1997) used a modified SKO to predict root growth and morphologies of trees for different loading and solid conditions. Similarly, SKO is not limited to biological structures. It has been extended to engineering design problems such as cantilever beams and reinforcement of shell structures (Baumgartner *et al.*, 1992; Mattheck *et al.*, 1993). A framework structure developed by SKO is shown in Fig. 3.6. The design area was internally restricted by access for bolts which have to remain circular. The result is a mass minima design which approached optimum. The combined application of SKO and CAO provided a fatigue resistance lightweight design (Mattheck *et al.*, 1993). In a way, the SKO method resembles ESO.

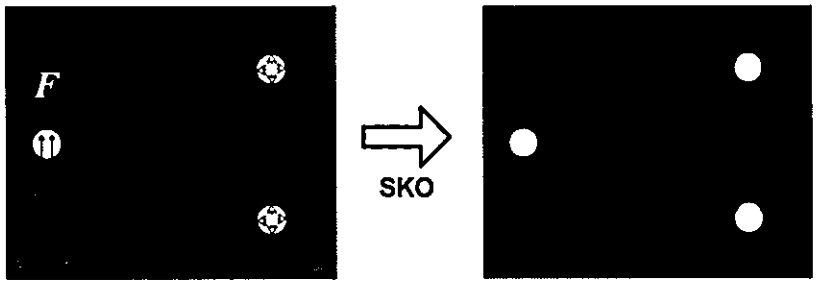

Fig 3 6 SKO design of framework structure (a) Initial design area with service loads, boundary conditions and design constraints, (b) optimised design (Mattheck, 1998)

3.4.5 Genetic Algorithms (GA's)

Genetic algorithms (GA's) are stochastic search methods inspired by the basic mechanisms of natural selection, based on the theory of biological evolution and adaptation (Goldberg, 1989). GA's are global search algorithms where the iterative histories of structural optimisation problems were simulated by artificial evolution and adaptation. The Darwinian concept is employed to yield the best or better characteristics among a population, where random information exchange is performed to create superior offspring. In the last decade, GA's have been used in the field of optimisation for engineering structures, particularly for finding optimal layouts of truss structures (Jenkins, 1991; Oshaki, 1995).

Chapman *et al.* (1994) extended the application of GA's to layout optimisation of continuum structures. GA-based layout optimisation is different to the material

distribution approach employed in FE-based methods. In GA's, a population of potential solutions are considered, where the search for optimum solutions are done by extensively sampling of the design space. This technique contrasts FE-based methods, where designs are often concentrated on the development and refinement of one solution. In GA's, design variables are coded as bit strings of 'chromosomes'. Shapes of structures are represented by chromosomes consisting of strings of binary digits. The number of digits, or genes in each chromosome is equal to the number of elements, and corresponds to a particular element in the design domain. Fig. 3.7 shows an example of the many possible layout of a structure represented by a binary string chromosome mapped on a design domain.

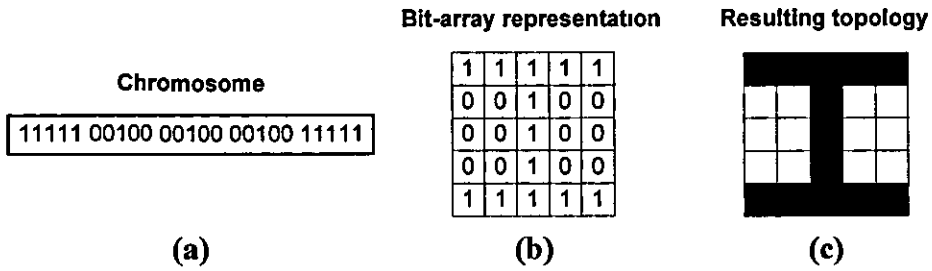

Fig 3 7 Mapping of chromosome into a design domain (a) Binary string chromosome, (b) bit-array representation, (c) resulting topology (Chapman *et al* 1994)

Although GA's have been widely applied in the optimisation of truss layouts, in the last decade it has started to gain attention in generalised layout optimisation. One of the earliest applications in layout optimisation for structures with weight and displacement constraints was presented by Kane and Schoenauer (1996). Jakiela *et al.* (2000) demonstrated an optimisation approach for short cantilever designs. Chen and Lin (2000) applied GA's to determine optimal boundaries of design space for layout problems. Hansel *et al.* (2002) demonstrated the use of GA's as an approach for realising weight-minimal multilayered laminate composite by topology optimisation. Capello and Mancuso (2003) presented a GA-based combined shape and layout optimisation approach for cantilever and plate structures Wang and Tai (2004) proposed a graphical representation for structural layout optimisation using GA's to find designs with minimum compliance and weight. Woon *et al.* (2005) presented an optimisation technique for continuum layouts through a multi-GA system. Madeira *et al.* (2005) developed a multi-objective optimisation of structural layout by GA's and tested it on a short cantilever subjected to two loading cases. Wang and Tai (2005)

implemented a bit-array representation method for structural layout optimisation using GA's which emphasised on the connectivity of designed structures.

Despite the successful application of GA's, a few drawbacks were identified. GA's often require large numbers of function evaluations. In some cases, this leads to computationally expensive solutions. For relatively small problems, GA-based solutions still require an arguably 'impractical' amount of computation (Jakiela *et al.*, 2000). Because analysis is computationally expensive for large scale problems, structures subjected to GA-based topology optimisation must be limited in size and complexity (Chapman *et al.*, 1994). Design solutions consist of jagged boundaries and additional post-processing is required. Furthermore, GA's must work in a bounded design space and could not be applied to problems where the size of the design domain is not known *a priori*, as all design parameters must be coded in the form of chromosomes of finite length. A method to reduce the prohibitively high amount of computational time for large topology optimisation was proposed by Adeli and Kamal (1992). The proposed method uses a parallel and vector algorithm on a shared memory parallel machine and distributed GA's for optimisation on a cluster of workstations connected via a local area network (LAN). To minimise the overall computational effort for large-scale design optimisation problems, alternate approximation concepts were necessary to ensure the efficiency of GA's.

3.4.6 Simulated Annealing (SA)

Simulated annealing (SA) is a stochastic search procedure for finding the minimum of a function, inspired by the physical annealing and cooling process of metals (Kirkpatrick *et al.*, 1983). Annealing denotes a physical process in which solid metal is melted at high temperatures until all particles can move freely with respect to one another. This is then followed by cooling until thermal mobility is lost. If molten metals at high temperatures are allowed to cool to a solid state for a sufficiently long time, metal particles could move freely during this cooling process, and will end up in a structure with minimum energy. From an optimisation point of view, the global minimum (or optimum) of the problem can be represented by this minimum energy state. The optimum metallic grain configuration is one where all particles are aligned in a low level lattice. Conversely, if the annealing process is not given sufficient time to

complete the cooling process, the molten metal would still solidify, but with higher energy. Metal particles would line up with their neighbours, but different regions may point in different direction. This energy state indicates a local minimum. In such cases, whole regions of metal particles have to be reversed in order to escape the local optima, as Fig. 3.8 shows.

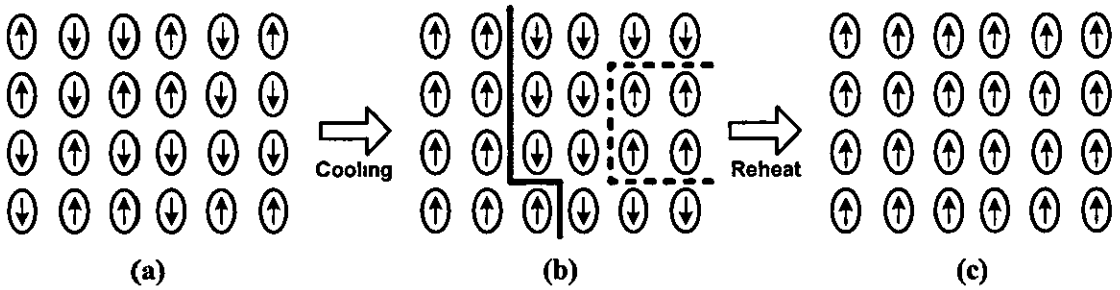

Fig 3 8 Concept of Simulate Annealing (SA) optimisation· (a) High temperatures, random crystal alignments, (b) low temperatures, formation of localised crystals; (c) reheat, particles reorientate (Leite and Topping, 1999)

In contrast to GA's, SA is point-based, instead of population-based. In an optimisation procedure, GA's evolve a number of complex systems concurrently, while SA develops and refine. SA was first used for structural optimisation in the late 1980's. Elperin (1988) described the basic ideas of the SA algorithm for structural optimisation where discrete design variables are used. Salama *et al.* (1990) presented an optimal placement of actuators for large flexible space structures. Most of the applications of SA were in the optimum design of truss and skeleton structures. Balling (1991) applied SA to the discrete optimisation of 3D steel frames. Lee and Lee (1992) applied SA to the minimum weight design of trusses with discrete variables. Bennage and Dhingra (1995) applied SA to single and multi-objective optimal designs of truss structures with discrete and continuous variables. Manoharan and Shanmuganathan (1999) used SA to optimise truss structures and compared the applicability of the method to other optimisation methods. Hasançebi and Erbatur (2002) used SA to optimise the layout of trusses. Recently, Baumann and Kost (2005) demonstrated a SA optimisation approach to build-up truss and grillage structures from simple initial configurations.

Despite the wide use of SA for trusses and space frame designs, their application in generalised layout problems were scarce. Anagnostou *et al.* (1992) proposed a SA-based layout optimisation approach as a combinatorial procedure for a part design

which combines the processes of conceptual, geometry, mesh generation, analysis and optimisation. Shim and Manoochehri (1997) presented a combinatorial optimisation procedure based on the SA approach for generation of optimal configuration of structural members. Of late, Shalaby and Saitou (2004) proposed a topology optimisation design approach of structural supports for micro-electro mechanical systems (MEMS) switch using Hybrid Discrete Simulated Annealing (HDSA). Fig. 3.9 shows the sub-optimum topology obtained by HDSA from an optimisation run.

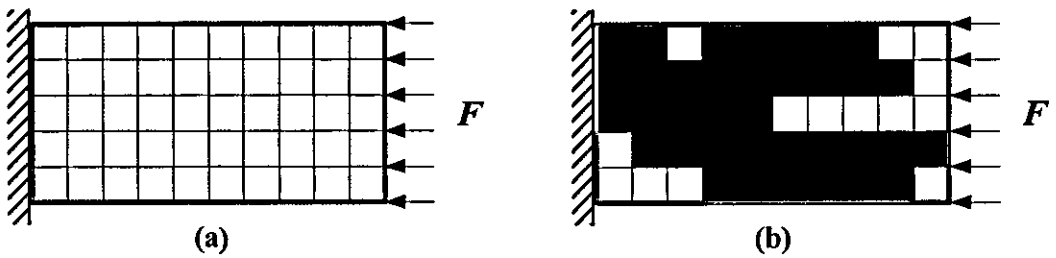

Fig. 3 9 Optimisation of a MEMS switch subjected to horizontal loads by HDSA (a) Design domain, (b) proposed sub-optimal topology (Shalaby and Saitou, 2004)

Although SA has been extended to generalised layout problems, several drawbacks were highlighted. In SA, structures are represented by course binary elements with abrupt surface changes. The sizes of optimisation models were somewhat limited and design domains are bounded (Anagnostou *et al.*, 1992). Smooth profiles could not be approximated and could result in the loss geometrical details. Hence, design solutions obtained are sub-optimal and require post-optimisation. SA optimisation is computationally expensive, where a high number of functions evaluations are required. For reducing the prohibitively large amount of computations, modifications are made to SA and computing hardware setup in order to overcome this problem. Park and Sung (2002) used a two-phase SA which computations were distributed over a cluster of ten remotely distributed personal computers. Leite and Topping (1998) experimented with various network configurations to maximise computing power. Chen and Su (2002) used SA to optimise the designs a stepped cantilever and cantilever plate and noted that SA required more computational time than other traditional mathematical programming methods. In these cases, solutions obtained were sub-optimal. With respect to the amount of computations required for sizing optimisation, the efficiency of SA is questionable, particularly in generalised layout design problems. In context to this thesis, the size of the optimisation models is considerably larger than

the layout optimisation problems presented by Shalaby and Saitou (2004). Therefore, the use of SA may not be appropriate.

3.4.7 Particle Swarm Optimisation (PSO)

Particle Swarm optimisation (PSO) is a recent addition to a growing collection of population based probabilistic search algorithms. Many search algorithms are based on some natural phenomena and PSO is no exception. It is developed based on the simplified concept of the social behaviour reflected in flock of birds, bees, and fish that adjust to their physical movements to avoid predators, and seek the best food sources (Kennedy and Eberhart, 1995; Eberhart and Kennedy, 1995). A physical analogy might be a shoal of fish adapting to its environment. In this analogy, each fish makes use of its own memory, as well as the knowledge gained by the shoal to adapt efficiently. The method is based on the premise that social sharing of information among members of a species offers an evolutionary advantage or 'collective intelligence'. Every swarm agent of PSO explores a possible solution. It adjusts its movement according to its own and its companion's movement experience. The individual's best position is the best solution found by one particle in the course of a movement. Conversely, the best position of the whole swarm is a global best solution. Every swarm continuously updates itself through the above mentioned best solutions. Therefore, a new generation of community would come into being, which has moved closer towards a better solution, ultimately converging onto the optimal solution.

Over the years, applications of PSO in the area of structural optimisation have started to gain attention. Fourie and Groenwold (2002) applied the PSO algorithm in size and shape optimisation. The authors tested the method on optimisation problems such as bar truss layouts, plane and space frame layouts, and a torque arm. A similar study was presented by Schutte and Groenwold (2003). Venter and Sobieszczanski-Sobieski (2004) presented a multidisciplinary optimisation of a transport aircraft wing. The authors investigated the basic PSO algorithm and applied it to the minimum weight design of a wing structure. Bochenek and Foryś (2006) developed an optimisation algorithm based on the PSO concept and applied it in the structural optimisation problem to solve post-buckling behaviour of a Koiter frame. Kitayama *et al.* (2006) suggested a penalty function approach for mixed discrete nonlinear problems by PSO.

The authors presented a design optimisation study to find the optimal length and thickness of a pressure vessel. Perez and Behdinan (2007) presented the background and implementation of a PSO algorithm for constraint structural optimisation tasks for truss and frame structures. Omkar *et al.* (2008) presented a vector evaluated PSO method for the design optimisation of composite structures. The authors considered the minimisation of weight of the composite components and the minimisation of cost, by varying the number of layers, lamina thickness and stacking sequence. Good examples in the design optimisation of composite box-beams are given by Kathiravan and Ganguli (2007) and Rao *et al.* (2007). Li *et al.* (2007) presented a heuristic PSO for optimum design of a pin connected structure. Jármai *et al.* (2006) investigated the optimal design of a cylindrical orthogonally stiffened shell member using the PSO.

Since its development, PSO have found many applications in engineering design problems. Publications on PSO are voluminous ranging from operational scheduling, forecasting, process flow, control systems to the development of artificial intelligence systems. On the contrary, applications in the field of structural optimisation are largely focused on investigations of design studies which involved configuration and sizing. The nature of the goals of these investigations was somewhat similar to those addressed by GA's and SA methods. In all, the application of PSO in the field of generalised layout design optimisation problems of structures is not as common as the other methods. As previously covered, the approach which stochastic methods handle generalised layout design problems would require large number of function evaluations. This contrasts the generalised layout methods where the optimisation is focused on the development and refinement of one model. Despite its simplicity and robustness, computational cost is always a concern when using stochastic based search algorithms. As an example, Venter and Sobieszczanski-Sobieski (2004) highlighted that an average optimisation run would require an average of 9660 analyses to converge, for that of a three discrete design variable design problem. In contrast, the discrete combination of some layout optimisation problems may be several orders of magnitudes more, hence making the method computationally expensive in dealing with discrete FE variables.

3.5 Summary of layout optimisation methods

The review shows stark contrast between the FE-based and stochastic methods. Although the latter are generally known to be more flexible, it could be seen that generalised layout problems solved using stochastic methods are greatly limited by size. The use of such methods for complex design problems is scarce, in comparison to FE-based methods. The cited barriers are often due to the amount of design variables they could efficiently handle. In contrast to FE-based methods, stochastic methods are computationally intensive and the search for an optimal solution is often limited by the size of the model. For this research, in terms of practicability, FE-based methods hold the advantage when it comes to the overall efficiency in obtaining a layout solution.

3.6 Methods for thermal design problems

The methods reviewed are concerned with the optimisation of structures under mechanical loads only. A review of the design methods for optimal thermal performance of structures is given in this section. The amount of published literature in this field is voluminous. The literature survey revealed that most of the work concentrated on techniques to enhance heat transfer. Good examples include heat sinks (Ledezma and Bejan, 1996), arrangement of staggered plates (Fowler *et al*, 1997), disc-shaped cooling structures (Rocha *et al.*, 2002), dendritic heat exchangers (Bejan, 2002), dendritic disc structures (Wechsatol *et al.*, 2003) and multi-scale structures for maximal heat transfer (da Silva *et al.*, 2006). In contrast, research on the optimal thermal design aimed at suppressing heat transfer has received little attention, in spite of their significance in many engineering applications.

In this thesis, methods for optimal thermal designs are classified into two groups:

i) Layout and shape optimisation

ii) Partitioning or discretisation method

In view of the interests of this research, more attention will be given to the background of existing techniques which focus on the use of single material and the control of geometry to optimise structures for maximum thermal resistance.

3.7 Layout methods

Researches in shape and layout optimisation are mostly focussed on elasticity problems. In spite of its significance, layout optimisation of heat transfer of solids has received less attention. One of the most common thermal design problems is the search of an optimum shape or size to achieve specific heat transfer objectives (Lan *et al.*, 2001). Cooling fins, thermal diffusers, moulding dies are some examples of shape and layout optimisation (Lee, 1993). Kwak (1994) suggested that early research is concentrated on the shape design sensitivity analysis (SDSA) method. Haftka (1981) presented a FE-based technique for computing the sensitivity of temperature changes with respect to the changes in design variables. Park and Yoo (1988) developed a boundary element-based algorithm for shape optimisation of various heat transfer problems of 2D continuum structures. Tortorelli *et al.* (1989) derived the sensitivity formulations for thermal systems by the Lagrangian multiplier technique. Meric (1988) presented the SDSA expressions for optimisation of heat conducting solid bodies. Cheng and Wu (2000) computational method for shape design of heat conduction problems with the use of a combined body-fitted grid generation scheme and conjugate gradient optimisation method. Lan *et al.* (2001) presented design problems of shape profiles of a conductive medium to achieve a uniform temperature distribution.

In the above approaches, the shapes of structures were optimised by varying the nodal coordinates. SDSA-based methods attempt to represent the geometry of a complex model in an efficient manner. However, the shapes of boundaries are restricted by design variables and boundary functions. Sophisticated remeshing process is often required for each iterative design. Although SDSA are of great theoretical significance, several limitations exist when it comes to practical applications. The mathematical complexity of SDSA results in high computational cost, which could become prohibitive in practical design problems. Also, optimal designs are restricted by the chosen initial shape, and there is less probability to find alternative solutions.

Significant progress in optimal design methods for structural problems which avoids remeshing and change of nodal positions had been extended to heat transfer problems of continuum solids. The idea of this approach is to systematically locate unnecessary or inefficient material in a structure which do not contribute to heat transfer, and

eliminate them from the FEA model. For layout-based heat transfer design problems, a region is expected to seek 'as-close-to-an-even' distribution of temperature or heat flux as possible, within the design domain. To extend the well-established topology algorithm from elastic to thermal problems, Li *et al.* (1999; 2000) presented a generalised non-gradient procedure to both shape and layout optimisation for heat conduction problems, in which a uniform efficiency of material usage in terms of local heat flux was achieved. An example of the optimisation procedure is illustrated in Fig. 3.10.

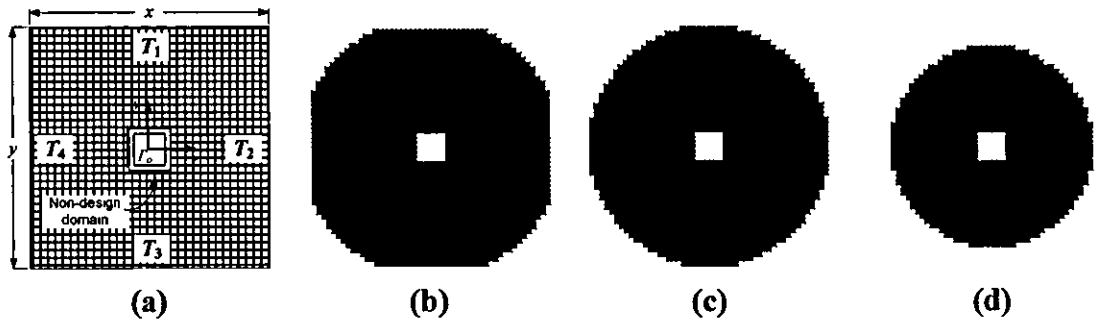

Fig 3 10 Evolution history of shape optimisation by ESO (a) Initial FEA model for a hollow solid, (b) iteration-8, (c) iteration-10, (c) iteration-12 (Li *et al*, 1999)

Such flux-based topology optimisation procedures are later extended to other physical situations to cover a range of practical examples in torsional, conductive, electrical and magnetic field problems (Steven, 2000). Recently, Li *et al.* (2004) extended ESO to material layout design of thermal conduction problems to minimise the temperature at specific nodes, by both layout (conducting solid or void) and bi-material designs (conductor and insulator). An example of the design is shown in Fig. 3.11.

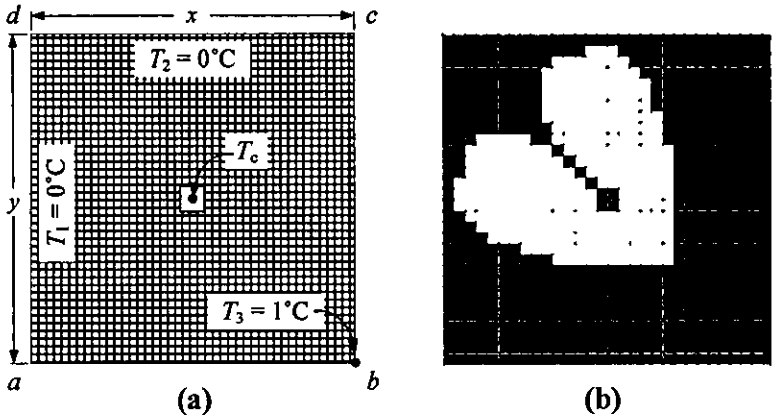

Fig 3 11 Optimal design of a heat conductive field by ESO (a) Initial FEA model, (b) optimum topology (Li *et al*, 2004)

In a different study, Zhuang *et al.* (2007) presented a level set method for topology optimisation of heat conduction problems under multiple thermal load cases. Examples of topology optimisation of heat conduction problems for single and multiple thermal load cases were given.

Despite the use of layout methods in some design problems, several potential drawbacks were highlighted. Due to the nature of approach, they could not be readily extended to solve thermal optimisation problems which involve multiple modes of heat transfer. The reason being, the meshing strategy for field quantities in stress analysis is not readily extendable to that of a thermal analysis. More importantly, for plane problems, optimisation models for both structural and conductive thermal problems could be approximated using a uniform mesh, without the accuracy of the solutions being compromised. However, in many in practical situation, especially those concerned with the design of thermal insulation, the effects of multiple modes of heat transfer, which lead to conjugate problems, cannot be neglected. Although certain FEA packages could be used to compute the velocity potential function of a flow system in an enclosed airspace with the use of a 'coupled field' analysis (ANSYS, 2004), differences in meshing requirements for solid and fluid regions pose a challenge. For fluid analysis, it is common that a finer mesh is used to discretise the boundary layers of fluid regions, and courser mesh for expected freestream regions. The presence of a non-uniform mesh could pose a challenge to current layout methods. Another mesh related drawback was that the use of uniform size quadrilateral elements alone would result in jagged boundaries and a loss in the fluid flow detail for structures with curvilinear profiles. At present, layout-based approaches can only be applied to design optimisation of conductive thermal problems. Although optimisation for reduced heat conducting fields, by means of varying topology has been proposed (Li *et al.*, 2004), the design approach in which thermal conductivity of a solid structure is taken as the design variable is of little significance to practical applications.

This drawback suggests that the design optimisation of structures subjected to conjugate heat transfer in solids and fluid regions requires a different strategy. In the next section, a review on the optimal design methodologies which considers the effects

conjugate problems is presented. This research is focussed on the optimal design of structures to increase thermal resistance. Emphasis is given to the design of fluid-filled enclosures, which are found to be more effective. The review covers how thermal insulation of enclosures could be improved when bounded airspaces are 'discretised' or 'partitioned' to form partitioned solid-fluid composites.

3.8 Classification of discretisation/partitioning methods

Over the last two decades, research on heat transfer in enclosures is a topic of considerable engineering interest. Due to its inherent reliability and simplicity, applications range from thermal designs of buildings to cryogenic storage, and cooling of electronic components. Reviews are presented by Biserni *et al.* (2004), Augusto *et al.* (2006) and Ledezma and Bejan (1996). In the 1980's, interest was given to problems which consider natural convection-conduction in partially and fully divided enclosures, due to its fundamental importance in connection with various technological applications. A review on the classification of discretisation or partitioning methods, in existing literatures, suggest that most of the work in this particular field was primarily focussed on three types of enclosures, classified as;

i) undivided
ii) partially divided
iii) fully divided

3.8.1 Undivided cavities

Fig. 3.12 depicts the schematic diagram of a fluid-filled undivided cavity. Bejan (1985) analysed the flow and temperature concentrations fields in the boundary layer flow and determined the heat and mass transport characteristics of a vertically orientated rectangle cavity. Chang and Tsai (1997) analysed natural convection in a square cavity with a cold source. Corcione (2003) investigated the natural convection in rectangular cavities simultaneously heated from below and cooled from above. Cianfrini *et al.* (2005) analysed the behaviour of tilted square cavity with differentially heated opposite walls, for Rayleigh (Ra) number $10^4 \leq Ra \leq 10^6$. In the aforementioned studies, shapes and sizes of cavities were fixed, thus neglecting the relationship of natural convection with cavity aspect ratios, in which is an important aspect in the design optimisation for pure thermal problems.

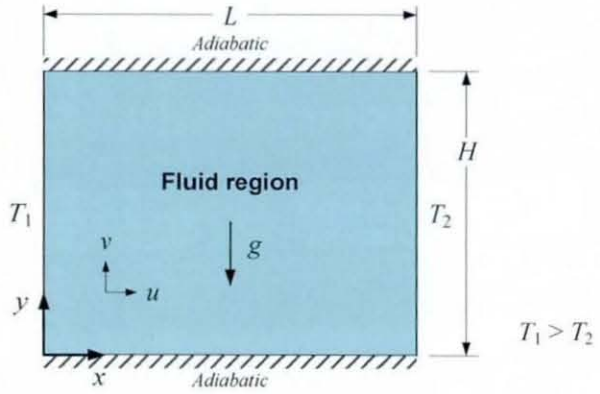

Fig. 3.12 Schematic diagram of an unbounded undivided cavity

Studies presented by Ganzarolli and Milanez (1995) and Frederick (1999) considered the height and length (or width) aspect ratio (S) of differentially heated shallow and tall cavities as design variables. From these studies, it was observed that the average Nusselt number (Nu) is a function of cavity the aspect ratios (see Fig. 3.13). With reference to Fig. 3.13(b), thermal performance could be gained significantly when cavity aspect ratio is increased. Conversely, this was not the case for shallow cavities (see Fig. 3.13a). Although optimisation was not implemented in these studies, the authors presented the notion and proved the concept that heat transfer in cavities could be controlled by varying geometry.

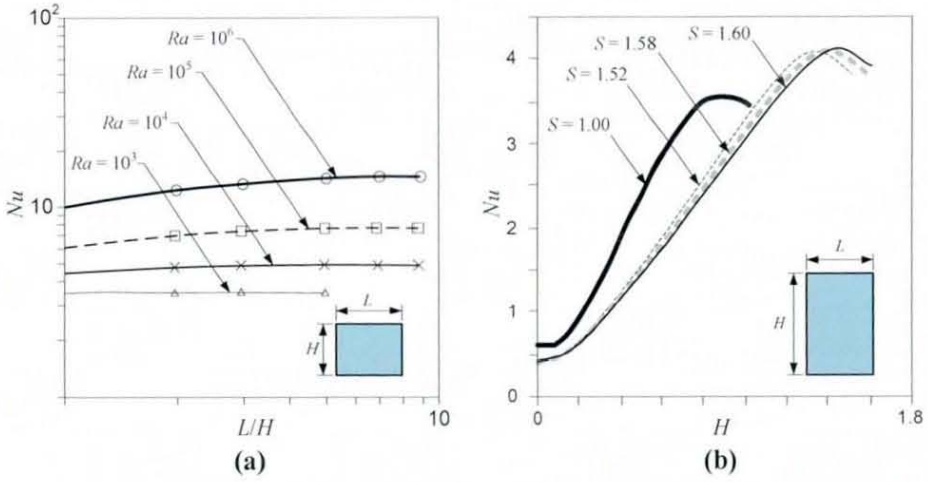

Fig. 3.13 Average Nusselt number (Nu) as a function of cavity aspect ratio: (a) Shallow cavity ($S = L/H$) (Ganzarolli and Milanez, 1995); (b) tall cavity (Frederick, 1999).

The studies dealt only with heat transfer in cavities modelled as fictitious enclosed fluid regions where the presence of conducting medium was neglected. However, many practical situations, especially those concerned with the design of thermal insulation, conduction in solids could have important effects on the natural convection flow in the enclosure, leading to conjugate problems, shown in Fig. 3.14.

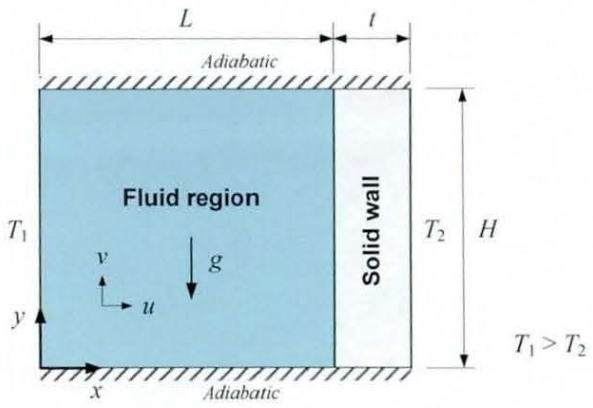

Fig. 3.14 Schematic diagram of a conjugate problem of a single partially bounded cavity.

A cavity adjacent to a conducting solid wall is a widely studied design problem. Kaminskin and Prakash (1986) numerically analysed the conjugate natural convection in a square cavity considering the effects of conduction on a vertical wall. Du and Bilgen (1992) studied the coupling of wall conduction with natural convection in a rectangular cavity. Misra and Sarkar (1997) used FEA to analyse the conjugate natural convection in a square cavity with a conduction vertical wall. These studies showed that conduction of solids adjacent to fluid is important and its effects could not be

neglected. In order for these studies to have any significant applications in practical design problems, fluid-filled cavities had to be fully bounded by solid walls, hence the term 'enclosures' or 'enclosed structures', as depicted in Fig. 3.15. Such a study was conducted by Liaqat and Baytas (2001), results showed a significant change in the thermo buoyant flow parameters, compared to non-conjugate type investigations.

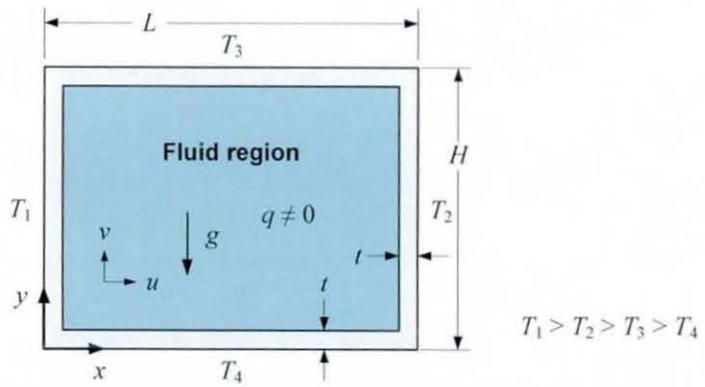

Fig. 3.15 Schematic diagram of an undivided enclosure with conducting walls (grey region) of finite thickness and thermal conductivity (Liaqat and Baytas, 2001).

Although researches on undivided single enclosures have found many thermal engineering applications, their efficiency as thermal insulators is questioned, particularly if they were to be used as a primary form of thermal insulator. The heat flow rate which could be suppressed by single enclosure does not produce an effect which is significant enough. In the next section, a review on the suppression of heat transfer by partially divided enclosures is given. Emphasis is given to design methods on how dividers and baffles fitted to fluid-filled enclosures could provide any further suppression of heat transfer across fluid filled enclosures.

3.8.2 Partially divided cavities

Fig. 3.16 shows a schematic diagram of a partially divided enclosure with protruding solid baffles. Lin and Bejan (1983) presented an experimental study of buoyancy driven convection in a rectangular enclosure fitted with a vertical adiabatic partition. Nansteel and Greif (1984) studied the natural convection in enclosures with 2D and 3D partitions. In these studies, the end walls and partitions were assumed to be adiabatic. Chang *et al.* (1982) and Bajorek and Lloyd (1982) noted that experimentally determined Nusselt numbers were significantly higher than values predicted from enclosures with adiabatic walls. To obtain realistic predictions, the end walls are assumed to be perfectly conducting and the partitions were assumed to have finite thermal conductivity. Zimmerman and Acharya (1987) numerically studied the natural convection in an enclosure with perfectly conducting horizontal walls with conducting baffles of finite conductivity. Archarya and Jetli (1990) presented a numerical study on the heat transfer and flow patterns in a partially divided square box with different baffle locations and geometries. Chen and Ko (1991) presented a numerical study on the natural convection in a 2D partially divided rectangular enclosure with different baffle opening ratios. Archarya and Mehrotra (1991) experimentally studied the natural convection of smooth and ribbed vertical channels. Viswatmula and Amin (1995) numerically studied the effects of multiple obstructions on natural convection in vertical channels. Sun and Emery (1997) examined the natural convection in a 2D enclosure with discrete internal heat sources and an internal baffle. Dagtekin and Oztop (2001) numerically analysed the natural convection of two heated partitions within an enclosure.

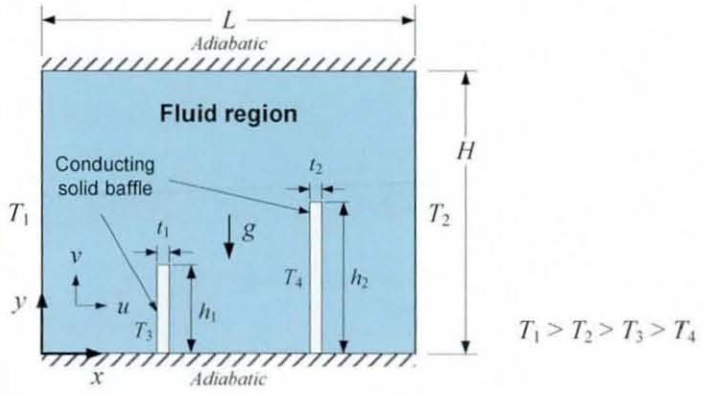

Fig. 3.16 Schematic diagram of a single partially divided cavity

The above studies highlighted the influence of heat transfer due to the presence of dividers and baffles. The *Nu* for partially obstructed enclosures was less than those of smooth enclosures. For enclosures with single divider, the geometry of divider was found to have greater effect than its position. The decrease in *Nu* number was observed when the number of dividers was increased. These findings suggested that heat transfer could be modified when dividers and baffles are introduced. The effects of dividers on heat transfer were found to be most significant at higher *Ra*, with a maximum reduction of approximately 31% being reported (Viswatmula and Amin, 1995).

Although not explicitly highlighted, these findings presented the notion of a design approach which could be use to solve design problems of structures with thermal requirements. In terms of insulation, enclosures with undivided airspaces offer the least thermal resistance, despite the fact that atmospheric air is a good thermal insulator. Even with the addition of dividers and baffles, the rate of suppression did not produce any significant reduction. Further research has shown that the insulation of fully divided enclosures, by partitioning was superior to partially divided ones.

3.8.3 Fully divided cavities

Although heat transfer in enclosures with various geometries and divider configurations had been studied, research on enclosures with fully divided subenclosures is scarce. Fig. 3.17 shows a schematic diagram of a fully divided enclosure with multiple impermeable solid conducting partitions.

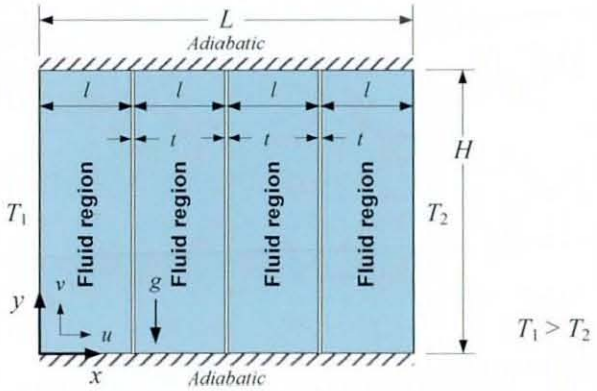

Fig. 3.17 Schematic diagram of an enclosure with fully divided sub-enclosures

A pioneering study was presented by Anderson and Bejan (1981), where both experimental and numerical investigation was performed on the heat transfer of

differentially heated single and double vertical walls at high *Ra*. Tong and Gerner (1986) studied the effects of a vertical partition on the steady-state natural convection of an air filled rectangular enclosure. Ho and Yih (1987) numerically studied the natural convection of air-filled enclosures with different aspect ratios. Nishimura *et al.* (1987) presented an experimental study of natural convection in enclosures with an off-centre partition. In an extended study, Nishimura *et al.* (1988) conducted an experimental and numerical study on the natural convection in rectangular enclosures divided by multiple vertical partitions. Nishimura *et al.* (1989) presented an experiment study of the natural convection in horizontal enclosures with multiple partitions at a wide range of Raleigh numbers. Kangni *et al.* (1991) demonstrated a theoretical study on laminar natural convection and conduction in enclosures with multiple partitions of finite thickness and conductivity. Karayiannis *et al.* (1992) numerically investigated the natural convection in a single and two zone rectangular enclosures with varying aspect ratios. Ho and Chang (1993) presented a numerical study on the conjugate heat transfer across a vertical rectangular fluid-filled enclosure divided by multiple horizontal partitions.

These studies indicated that the net heat transfer in differentially heated fully divided enclosures decrease as more partitions are inserted, or when the structure is discretised into more cells (or subenclosures). The placement of partitions at certain locations could lead to substantial reductions in *Nu*, where a certain optimal threshold limit exists. In contrast, heat transfer in enclosures could be significantly suppressed with multiple dividers, compared with partially divided ones. The studies also indicated that the increase in height to width ratio of subenclosures could lead to a decrease in *Nu*. The reduction was found to be more significant with increased *Ra*.

For subenclosures with aspect ratios between $S = 5$ and $S = 15$, heat transfer was estimated to be reduced by over 50%, when a single partition is placed midway between the heated walls (Tong and Gerner, 1986). An approximated reduction of 61% could be realised at with $S = 10$ (Ho and Yih, 1987). Nishimura *et al.* (1988) reported that partitions have the effect to reduce net heat transfer by 55% at high *Ra*. Fig. 3.18 shows the relation for the reductions of heat transfer with respect to the number of partitions by Nishimura *et al.* (1988) and Kangni *et al.* (1991). The efficiency (η)

increases with the number of *N*-partitions. Both these studies reported the same trend, where the rate of increase is not proportional, and was observed to decrease gradually with the increase of number of partitions.

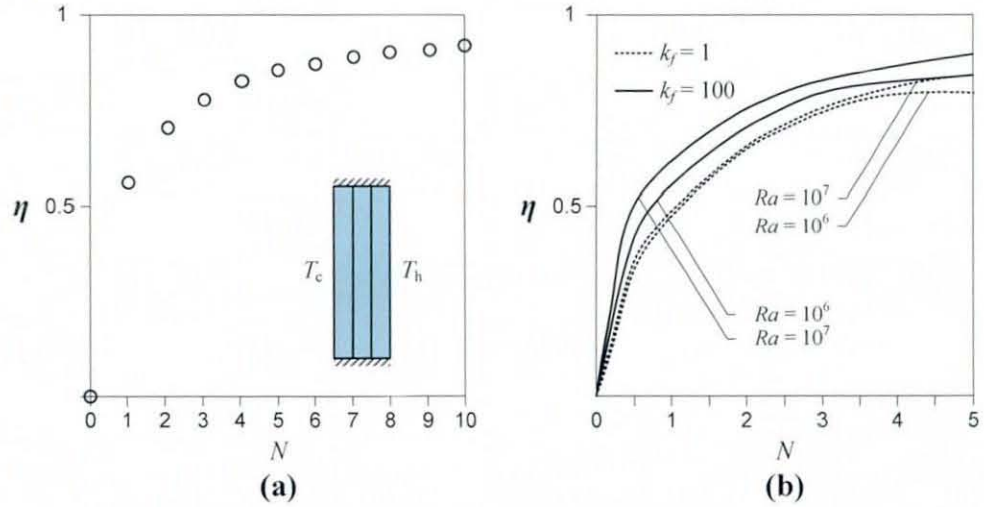

Fig. 3.18 Efficiency of partitions as a function of partition numbers: (a) Heat transfer reduction (Nishimura *et al.*, 1998); (b) efficiency of partitions at various conductivity ratios and Rayleigh numbers (Kangni *et al.*, 1991)

In contrast to undivided and partially divided enclosures, fully divided enclosures with multiple partitions could be seen as the more viable solution as an alternative form of thermal insulators. However, the discretisation of enclosures, using partitions is not analogous to the filling enclosures with insulation materials (i.e. mineral wool, glass fibres, etc.). In fact, discretisation can be viewed as a form of optimisation while filling cavities and voids with insulation material is not. While convection is suppressed by the resistance of the solid matrix, fluid flow is suppressed when the aspect ratio of a subenclosure is increased (Tong and Gerner, 1986). Although it has not been determined, a certain optimal threshold exists for thermally discretised structures. Tong and Gerner (1986) noted that filling up a cavity with insulation material, or discretising the airspace beyond a threshold point would not result in further suppression. In the light of this, an optimum threshold to which heat transfer is optimally suppressed could be attained through discretisation by partitioning. Performance wise, discretised structures were found to be comparable to conventional designs, if not, superior when the discretised layout is optimised.

3.9 Research in combined structural-thermal optimisation

In the aforementioned methods, design optimisations of structural and thermal problems were considered separately. However, in practical applications, structures are rarely subjected to loads of a single field quantity. For instance, structures may operate under simultaneous mechanical and thermal loads. Hence, it is evident that such design problems be considered as multiobjective or multidisciplinary, often with conflicting and non-measurable criteria which single field approaches can not address. Although design optimisation of structural and thermal problems has been extensively researched, focus is limited to their respective fields. Many researchers addressed structural and thermal optimisation independently, but not as a global problem. A review of existing literature suggests that few improvements have been made to current methodologies for optimal structural and thermal designs, to form a combined approach.

Research on methodologies for combined structural-thermal optimisation is relatively unknown, in spite of the significance in engineering problems. Three relevant studies have been identified. Gu *et al.* (2001) presented a 'two-stage' design optimisation method for a sandwiched 2D cellular structure for combined heat dissipation and structural load capacity. The author attempted to uncover the nature of heat transfer in lightweight cellular structures of varying cell arrangements. The objective of their study was to discover cell shapes and arrangements simultaneously optimised for structural and thermal performance with minimum weight. A range of different honeycomb structures were analysed. The findings show that 'six-connected' triangular cells provided the best overall structural and thermal performance, as Fig. 3.19 shows.

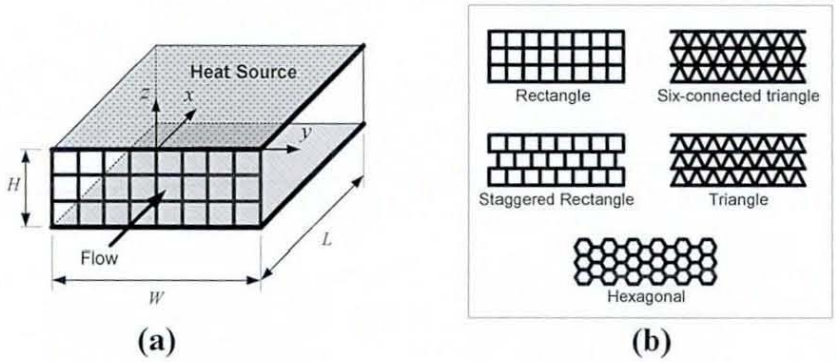

Fig. 3.19 Optimisation for combined heat dissipation and structural load capacity: (a) Design of sandwiched cellular structure for cooling a heated module; (b) types of two dimensional honeycombs analysed (Gu *et al.*, 2001).

Importantly, the work presented the notion of a new field of design optimisation for a two-field quantity problems not considered by traditional approaches.

In a related study, Lorente and Bejan (2002) presented a combined 'flow and strength' geometric optimisation of an internal structure in a vertical insulated wall with multiple air cavities, as Fig. 3.20 shows.

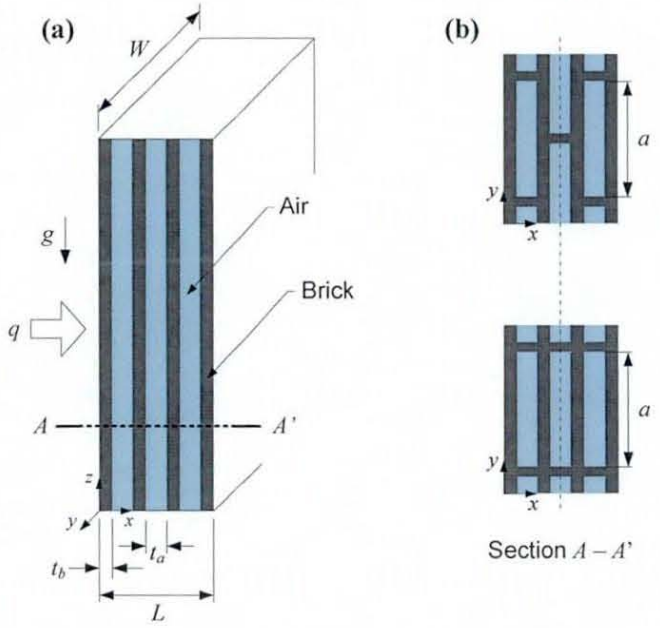

Fig. 3.20 Combined 'flow and strength' geometric optimisation of a vertical insulating wall with alternating layers of solid and air (Lorente and Bejan, 2002).

The study addresses the fundamental problem of optimising an internal structure with a vertical wall that must meet two requirements, thermal insulation and structural integrity. The objective of the optimisation was to seek optimal internal wall geometry where both thermal resistance and strength are maximised with the use of a sizing optimisation approach. This was one of the pioneering studies which highlighted the issues of conflicting objective functions for a two-field optimisation problem. It was also one of the earliest studies which dealt with optimisation to maximise thermal resistance and structural integrity. The combination of two functions, structural and thermal, was a new optimisation approach at a simple fundamental level. Importantly, the author drew attention to a new class of thermal design problems, in which the system architecture was derived from a combination of heat transfer and mechanical strength considerations.

Recently, Gosselin *et al.* (2004) presented a study on the combined heat flow and strength optimisation for geometry of mechanical structures to resist thermal attack. Unlike the two previous studies, heat dissipation and insulation was not the focus. Instead, it outlined a multidisciplinary approach in the conceptual design of structures that have two functions, structural integrity and resistance to sudden thermal attack. These two functions are considered simultaneously, from the start of the conceptual design. The proposed approach was demonstrated on the design optimisation of a beam structure. The author highlighted that the optimal architecture of a multiobjective system was a consequence of the competition between objective functions. Although the work was exploratory, its principal objective was to show that the combined heat flow and strength could be applied to a wide domain of design problems. Other design models could be combined with the proposed method in the pursuit of optimal structures which serve more than one objective. The author also noted that structures of greater complexity, such as buildings, could potentially benefit from the multidisciplinary optimisation approach.

3.10 Evaluation of methods for combined optimisation

In terms of structural optimisation, it can be seen that most recent developments are focussed on 'layout methods'. Topology optimisation has matured as a technique for conceptual designs to an efficient and versatile design tool for innovative solutions. Although methods for optimal thermal designs have found many applications, studies relating to design optimisation are scarce, particularly for load bearing insulating structures. Despite the advancements of layout methods in structural optimisation, they could not be readily extended to solve pure thermal design optimisation problems. This was mainly due to the complex nature of heat transfer analyses which require different meshing strategies. Previous studies have shown the discretisation method to be a more viable approach for conjugate thermal problems. Several studies highlight discretised structures, in the form of ordered closed cells, could potentially offer thermal performance superior to those produced by conventional methods (Wong and Gerner, 1986; Ho and Yih, 1987; Nishimura *et al.*, 1988). Although methodologies for both structural and thermal design problems had been progressively studied, research on

optimisation for combined structural-thermal considerations are relatively unknown, in spite of their significance in engineering applications. However few, the cited studies highlighted the importance and presented the notion of a combined optimisation approach for multidisciplinary problems (Gu *et al.*, 2001; Lorente and Bejan, 2002; Gosselin *et al.*, 2004). Such an approach is an attractive optimisation method for structural and thermal problems, despite these few shortcomings;

i) Structures are optimised for mechanical strength alone, or for thermal requirements alone.

ii) More emphasis is placed on the development of theoretical framework rather than on aspects of practical applications.

iii) Little success has been achieved in topology optimisation, in particular, problems with combined strength and heat transfer considerations.

iv) Previous studies only focus on optimal design solution; manufacturing consideration of such designs was neglected.

To achieve a more practical solution for combined structural-thermal optimisation problems requires large numbers of design variables and must contain elastic, thermoelastic and flux objectives. Traditional mathematical programming approaches fall short in several aspects (Li *et al.*, 2000).

i) Structural topologies are usually represented in terms of discrete design variables, where structural material is indicated as either solid or void.

ii) Various objective functions for different disciplinary are often inconsistent and may even conflict each other (Hajela, 1999).

iii) Engineering design optimisation favours methods requiring minimum preparation and little interference.

These conditions prompt the need for non-traditional optimisation approaches. In this research, a 'two-stage' optimisation approach is proposed. The method consists of a combination of the MD method and the Discretisation by Partitioning Method (DbPM) to solve design problems with mechanical strength and insulation considerations. Theoretically, MD could accommodate the above restrictions and form a basis of structural optimisation tool. MD is characterised as a discrete variable approach, requiring little work in implementing optimisation problems, and does not rely on the

features of the design space, commonly required by mathematical programming algorithms (Liu *et al.*, 2000). Alternatively, other layout methods could be used. With respect to the thesis objectives, Table 3.1 compares the attributes of the MD method against the other optimisation methods.

Table 3.1

Comparison of various methods used in the generalised layout optimisation problems.

Stochastic Search/optimisation Methods
- Search is population based and not limited to one model.
- Multiple optimal solutions could be obtained.
- Design not limited to local optimal.
- Application is not limited to structural optimisation.
- May be computationally expensive for large models.
Other Layout/topology Optimisation Methods
- Optimisation is focused on the development of one model.
- In most cases, only one design solution is given
- Designs are often local optima.
- Limited to structural optimisation only. Require less computing resources
The Metamorphic Development Method
- Optimisation is focused on the development of one model.
- Depending on design problem multiple optimal solutions could be obtained
- For certain problems, designs not limited to local optima.
- Limited to structural optimisation only.
- Computationally inexpensive.

On the other hand, the DbPM forms the basis of the design optimisation for pure thermal design problems. The DbPM can be seen as an effective discretisation design technique for heat insulating structures, by discretisation of internal viods. Previous approaches for combined structural-thermal optimisation were based on shape and sizing techniques. The proposed 'two-stage' optimisation approach attempts to incorporate the generalised layout method with configuration layout design methods to solve the design problem of a granular-solid structure with structural integrity and thermal insulation requirements.

4

Theory of the Mechanics of Granular Materials

4.1 Introduction

For this research, a granular RP material was chosen to reflect how common construction materials behave as a granular material. Current RP systems do not offer layer by layer manufacturing of concrete-based material structures. SLS (Selective Laser Sintering) Nylon-12 falls into the category of a granular material, in the same way plain concrete does, with the intention that the research findings could be correlated to Freeform Construction (FC) applications. This particular manufacturing process is seen as the best substitute for a scaled down FC process. As will be shown, the behaviour of existing construction materials (i.e. concrete, sand, rock, etc.) do not differ significantly from SLS Nylon-12, or other granular AMT-based components. SLS with Nylon-12 is one of the few processes which offer layer by layer manufacturing of non-metallic granular structures, where the mechanics of the manufactured structures closely resembles those of common construction materials, namely plain concretes. Hence, the basic understanding of the mechanics of granular materials in crucial, in which is the focus of this chapter.

4.2 General characteristics

Granular materials exhibit properties of both solids and fluids. In a cohesionless state, they take up the shape of a vessel containing them, exhibiting fluidlike characteristics. In a cohesive state, they can be heaped, behaving like solids (Feda, 1982). Some examples of granular materials are rock filled structures and compacted submicronic powders. In principle, these materials are different from each other. However, they have common features due to their granular structure, in which their mechanical

properties are greatly dependant on the mean or hydrostatic stress (Hicher, 1998). Under low mean stresses, shear stress is low and a granular material can flow, almost like a liquid. Conversely, when subjected to high mean stresses, granular materials are able to bear high loads, such as the case of civil engineering structures (Hicher, 1998). In this research, emphasis is given to the fundamental concepts which dealt with the quasi-static behaviour of granular materials, in which inertial effects have little or no effects. Rapid flow of granular materials, in which inertial effects are imminent (i.e. flow of granular materials), do not fall into the scope of this research and will not be covered.

The characteristics of the solid particles that constitute a bulk solid granular material are of major importance in influencing mechanical behaviour. The concept of a granular structure is characterised by four components; nature, arrangement, bonds and internal stress (Feda, 1982). Some of the primary properties which could result in very different behaviour are particulate size, shape, hardness, density and surface roughness. Secondary factors include moisture, degree of compaction and ambient temperature (Massoudi, 2004). The shape, size and the constituents of the grains can be very diverse, and the range of grain sizes can be very large, from μm's to m's (Hicher, 1998). However, the constituents of a granular material must be large enough, such that they are not subjected to thermal motion fluctuations. Thus, the lower size of the constituents in a granular material is approximately 1 μm. Granular materials cover a combined range of granular powders and granular solids with structural units ranging from 10 μm to 3 mm. A powder is composed of particles up to 100 μm (diameter), while granular solids consist of particles ranging from about 100 to 3000 μm (Massoudi, 2004). Brown and Richards (1970) define a bulk solid as "*an assembly of discrete solid components dispersed in a fluid such that the constituents are substantially in contact with near neighbours.*"

Fig. 4.1 depicts a two-phase granular material with a skeleton formed by structural units, and pores filled with liquid or gaseous phases. Granular materials can be defined phenomenologically or structurally (Feda, 1982). From a phenomenological viewpoint, they are materials which exhibit dilatancy, contractancy, and sensitivity to hydrostatic

stress. From a structural viewpoint, they are substances composing of mutually contacting solid particles, or structural units, within a liquid and/or gaseous phase.

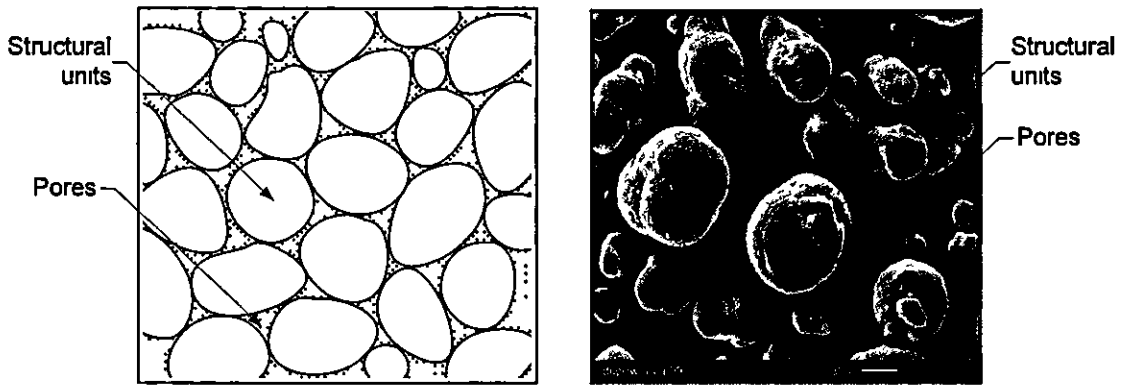

Fig. 4.1 (a) Schematic representation of an idealised granular material consisting of an assembly of structural units in mutual contact and gaseous/liquid filled pores (Feda, 1982); (b) Micrograph of sparsely packed granular powder particles of unsintered Nylon-12 (Tontowi and Childs, 2001).

The existence of mutual contacts restricts the freedom of motion of the individual structural units, and thus conditions strength and rigidity. Mechanical behaviour is a complex reflection of their structure, characterised by the freedom of motion of their structural units. One significant behaviour is deformation by mutual sliding of the structural units (intergranular deformations), in contrast to deformation of the individual structural units (intragranular deformation), typical of a continuous medium. Depending on the type of bonds the contacting solid particles are held, they can be classified as cohesionless and cohesive media.

4.3 Structural characteristics

The structural characteristic of granular materials is closely associated with the contact bonds between and inside the structural units (Feda, 1982). Generally, two types of bonds can be distinguished. Bonds produced by the effects of external loads are termed as 'friction bonds'. Bonds produced by the action of internal forces known as 'cohesive bonds'. Friction bonds are typical of all cohesionless granular materials, while cohesive bonds are found in granular materials whose structure is a result of compaction or consolidation (Feda, 1982).

4.3.1 Cohesionless and cohesive types

A slope produced by granular particulates would remain in place due to shearing stresses. Conversely, if a hole is dug, materials at the sides of the hole would slide towards the bottom. This behaviour indicates a complete absence of a bond between individual sliding particles. Sliding is continued until the angle of inclination of the slopes become equal to a certain angle, known as the angle of repose (γ) or angle of internal friction (φ). According to the theory of friction, the slope of a pile of particulates cannot be steeper than φ (where $\varphi \leq \gamma$). φ is also related to the amount of cohesion present in a granular material (Massoudi, 2004). In simple terms, the bond between particulates, known as cohesion, is influenced by a variety of forces, which include Van der Walls', Coulomb, and capillary forces. For a granular material with cohesion, a definite angle of repose cannot be assigned, since the steepest angle at which such a material can stand decreases with increasing height of the slope. When cohesion is absent, the granular material is termed as cohesionless. One which internal friction is absent is termed as an ideally cohesive medium.

4.3.2 Friction bonds

Granular materials are an assemblage of discrete particles, where interparticle forces are transmitted through contact points. With the absence of friction at contact points, a material cannot sustain applied shear forces. Friction at contact points plays the dominant role which governs the macro-deformation and strength behaviours (Tobita and Oda, 1999). A simple friction bond between two structural units is produced by the effect of contact stress and the angle of intergranular friction (φ_μ) (Feda, 1982). The strength of a friction contact is equal to the shear (adhesive) strength on the area of a real contact, which is the sum of the strength of the contact junctions. The size of these areas is a function of the contact stress and the coefficient of friction (tan φ_μ), which is equal to the ratio between the shear resistance and the compressive strength of the contact junctions. When the normal contact stress is zero, a friction bond losses its strength. If contact stresses are other than zero, friction bonding is effective for any amount of sliding of the surfaces in contact and originates immediately at any newly created contacts. Friction bonds are commonly found in all cohesion materials (i.e. dry sand, dry unsintered Nylon-12, etc.).

4.3.3 Cohesive bonds

Cohesive bonds are produced by the action of internal forces. They continue to exist even when a granular material is in an unloaded state. Two types of cohesive bonds can be distinguished, brittle and ductile bonds (Feda, 1982). In this research, only the characteristics of brittle bonds are covered. Ductile bonds will not be covered because it does not resemble the behaviour of the candidate material used in this research.

Brittle cohesive bonds are analogous to a joint between the structural units of crystalline 'cement' produced essentially be means of interaction forces between atoms (i.e. the ions or molecules of crystal lattices of continuous solids). Unlike friction bonds, the resisting area of the cement is independent of the magnitude of the contact or externally applied stress. The contact cement between two particles can be either of foreign material, or of the material of the solid particles, as in the case of sintering of compact powders, in precipitation of a material dissolved in the vicinity of high stresses contacts (Feda, 1982). A contact between two particles produced in this way is essentially similar to the lattice bonds of atoms, ions, molecules inside a structural unit. Consolidation of two particles makes the geometric area of their contacts identical with the effective contact area ($A_1 \approx A_2$). Fig. 4.2 depicts the failure of a brittle bond between particles 1 and 2.

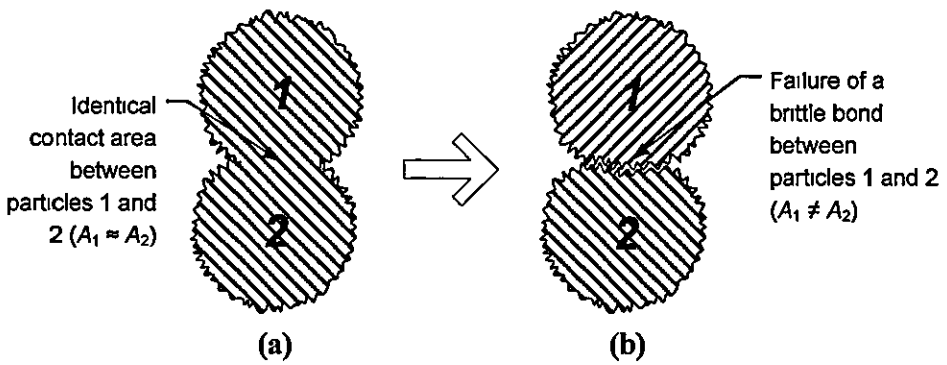

Fig 4 2 Change of a brittle bond initiated by failure to a friction bond, (a) Brittle bond in 'undisturbed' state, (b) failure initiated broken brittle bond to a friction bond (Feda, 1982)

In failure, the actual area of contact becomes smaller ($A_1 \neq A_2$), the brittle bond changes to a weaker friction bond. The change from a brittle to a friction bond causes the solid particles to move apart, whereby the volume of substance under failure grows larger. This behaviour is known as 'dilatancy', an increase of volume produced by the effect to

shear stress, which is an attendant phenomenon of brittle behaviour. Once a brittle cohesive bond has failed, it is incapable of restoring itself, during the comparatively short deformation process, hence it is irreversible. Due to the effects of cohesive bonds, granular materials exhibit shear strength even under zero normal load. For this reason, materials having such bonds are termed cohesive.

4.3.4 Consolidated (enhanced adhesion forces)

Fig. 4.3 shows a schematic diagram of the binding mechanism of enhanced cohesion joining two grains together.

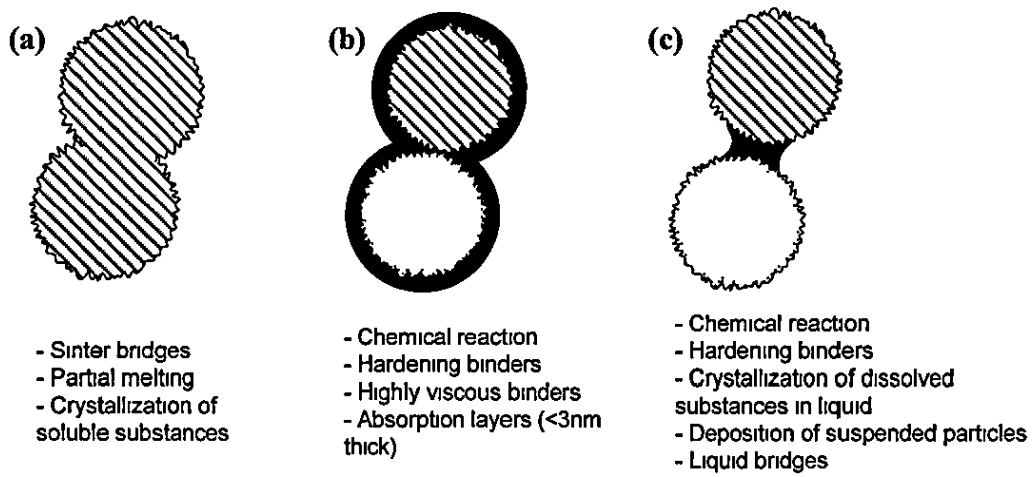

Fig. 4 3 (a) Solid bridge and particles are composed of same material, (b) particles and bridge have different composition; (c) agglomeration of particles by the formation of binder bridges (Simons and Pagliai, 2004).

Granular materials can also be classed as consolidated materials, with solid substances produced by joining (bonding, consolidation, etc.) of the structural units (Feda, 1982). The term consolidation covers various kinds of processing methods (i.e. compacting, pressing, sintering, etc.) at elevated temperatures. Under these conditions, particles of cohesionless materials are bonded by mechanisms of adhesion and cohesion. The term adhesion refers to the force with which particles are held together, which exhibit cohesive behaviour (Simons and Pagliai, 2004). Adhesion forces between particles depend on the existence of a material bridge between them. Forces from bonds developed without material bridges (i.e. Van der Walls or electrostatic effects) are much lower in magnitude than the enhanced adhesion forces provided by material bridges that bond the particles together. These bridges are formed either by the addition

of a liquid binder, which dries to form solid bridges or by structural or chemical changes at particle surfaces through sintering, crystallisation or plastic deformation.

4.4 Correlation of granular materials

Granular materials exhibit both properties of solids and fluids due to their;

i) two-phase mixtures of solid and fluid

ii) discontinuous body at the microscopic scale

iii) inhomogeneous and exhibit geometrical and mechanical anisotropy

Hence, relevant theories are required to analyse their behaviour. Cambou (1999) and Feda (1982) proposed two approaches on how the mechanical behaviour of a granular medium can be theoretically treated. The first is a macroscopic approach, based on the application of continuum mechanics, to a supposedly continuous granular sample, whose dimensions greatly exceed those of their constitutive structural units. The second involves a microscopic approach, where a complete discrete structure based on the assembly of grains of a continuous media is considered. This approach is known as the discrete element method (DEM). The applications of the two types of approach are complementary and have their own role in the modelling of granular behaviour. To date, research has developed empirical correlations that offer some links between physical parameters of discontinuous media and numerical parameters of simple constitutive equations to model the behaviour of an equivalent continuous medium (Hicher, 1998). The mechanical properties of real granular materials are complex, in which rigorous mathematical analysis of their behaviour seems impossible. Therefore, many branches of applied mechanics have to deal exclusively with the behaviour of idealised granular materials ranging from cohesionless to cohesive materials (Massoudi, 2004). However, it is fair to say that no unified theory has been proposed and that the framework of the mechanics of granular materials had not been firmly established (Feda, 1982; Oda and Iwashita, 1999; Massoudi, 2004).

4.4.1 Continuum theory

Continuum theories such as elasticity and plasticity have been extended and applied to analyse the behaviour of soils in the engineering length scale (Oka and Tamura, 1999).

The main components of continuum mechanics are the governing equilibrium equations[1], the boundary conditions[2], and the constitutive equations[3]. Over the last two decades, this approach had been successfully implemented to the FE method to solve structural problems. One of the major assumptions of continuum mechanics is that the material properties can be scaled from small laboratory samples to large material masses using constitutive relations (Bardet, 1998).

The macroscopic properties of granular materials are related to the basic structure and properties of their constituents, as well as their interactions. In order to model the macro behaviour of granular solids, constitutive equations of a material are derived from the knowledge of the local behaviour of structural units. In continuum analysis, the determination of a constitutive model[4], where material constants are involved, is often the most difficult process. Material constants are determined through physical experiments which depend on the assembly of grains of a granular medium. Researchers have produced a myriad of constitutive relations for various types of engineering materials where many of the constitutive models are clever fittings based on laboratory experimental results (Bardet, 1998). However, the application of the continuum approach alone was found to exhibit problems. Especially of those associated with the loss of uniqueness, mainly resulting from local material instability and the limitations of the constitutive equations (Bardet, 1998). These findings point to the need to seek a fundamental understanding towards the behaviour of granular materials.

4.4.2 Discrete Element Method (DEM)

As a complementary approach, DEM can be seen as an aid to continuum mechanics for not only the development of constitutive models based on physics, but also for understanding the physical origins of material instability and the limitations of continuum mechanics (Bardet, 1998). With DEM, the analysis of granular material can be done in a more realistic way, where the particle arrangements could be modelled explicitly (Kishino and Thornton, 1999). Difficulties lie in the process of simulating

1 Partial differential equations translating basic physical balances, such as stress equilibrium
2 Prescribed values of unknown quantities, or derivatives on external surfaces
3 Generalized relation between stress and strain or their respective rates

real granular materials, where a theorectically infinite number of particles with various shapes are assembled. It is inevitable that granular materials are modelled as idealised assembly of particles, since the degree of freedom (DOF) of contact forces and moments at grain level is tremendously large. Even with idealised models, the sheer numbers of individual particles, especially for smaller particles (i.e. powders) prohibit the simulation of their overall response, even with the most advanced computers (Bardet, 1998). For example, 1 cm^3 of SLS grade Nylon-12 may be consisted of as many as 5×10^6 powder particles (assuming the particles are well graded, having near spherical shape, with average diameter of 58×10 μm). Even with the most powerful computers of today, handling the computations of 1 cm^3 of Nylon-12, which corresponds to 5×10^6 particles, and their number of contacts is not computationally feasible. In view of this, it is more feasible that the attributes of DEM and continuum mechanics are combined. Hence, DEM and continuum mechanics should be perceived as complementary, not adversarial towards the understanding of the mechanics and physics of granular materials (Bardet, 1998).

4.4.3 Approximation of discontinuous to continuous media

Feda (1982), Hicher (1998), Oka and Tamura (1999) and Massoudi (2004) suggested that the mechanical behaviour of a supposedly discontinuous granular material can be modelled with reasonable accuracy, using continuum mechanics based on a constituent model. This approach is known as the phenomenological approach where real substances are replaced by mathematical models of 'structureless' continua. The application of methods of continuum theory depends on the size of the granular medium, with respect to the size of the constituent particles. Further consideration of the limits and assumptions are required, presuming that the granular material under consideration is to be modelled as a continuous medium. For force and displacement samples, the granular medium should be of sufficient size compared with the particles. This is to ensure that the actual forces and displacements can be related with reasonable accuracy, to the stress and strain of fictitious continuum medium, as Fig. 4.4 shows.

4 Constitutive, or stress-strain laws, represent mathematical models that describe the macroscopic behaviour that results from the internal constitution of a material

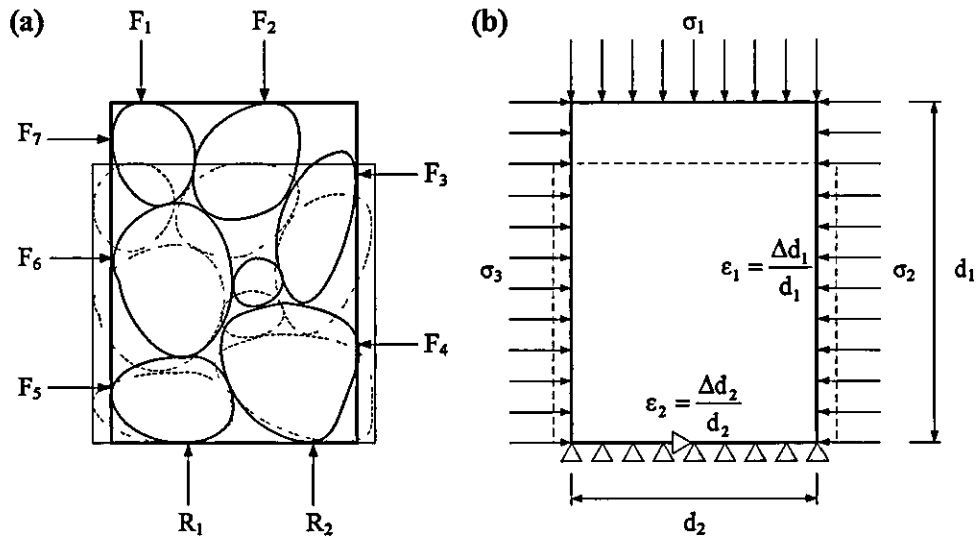

Fig 4 4 Discontinuous to continuous medium (a) 'Real' discontinuous medium, (b) idealisation of continuous medium (Hicher, 1998)

Hicher (1998) noted a lower limit of the size of grains, compared with the size of the granular medium. From a resultant force measurement experiment it was found out that in practice, the sample dimensions of a granular solid in a test apparatus had to be at least ten times larger than the largest particles (Hicher, 1998). For samples in which strength and compressibility are measured, the size of the samples had to be ten to fifteen times larger than the maximum diameter of grains (Feda, 1982). In a continuum approach, mathematical models are limited by a macro volume limit which usually has, for instance, continuous solids, a minimum characteristic dimension of 1cm in every direction. For fine grain cohesionless materials, this dimension may be 1 cm, for rock debris 10 m, and ten times more for rock massives (Feda, 1982). Displacement should be measured over a length that is large compared with the size of the structural units (Hicher, 1998). When particle size is relatively large compared to the sample size of the bulk solid, the notion of classic continua in no longer adequate to represent the granular system (Oda and Iwashita, 1999). In addition, pneumatic effects are neglected. Substances contained in voids are fluids that do not interact with the structural units (Massoudi, 2004).

4.5 Frictional behaviour

Granular material consists of an assemblage of discrete particles, in which interparticle forces are transmitted through mutual contact points. If friction is absent at contact points, the material cannot sustain applied shear forces. Some overall resistance to the applied force is generated by the interlocking effects of particles (Scott, 1963). However, this structurally induced resistance occurs only if friction is effective at contact points. Thus, friction at contact points plays a dominant role which governs the macro-deformation and strength behaviours of granular materials. In order to model the macro behaviour of granular materials, they are sometimes idealised as an assembly of rigid particles. The relative movement of rigid particles, which lead to macro-deformation, takes place as a result of sliding and rolling at contact points. This idealisation is accepted here and formed simplicity to review the development of a friction based deformation and strength behaviour model (Tobita and Oda, 1999).

4.5.1 Frictional-based deformation and strength characteristics

The mechanics of friction bonds can be described using the Coulomb's friction law. The relation between the frictional force (F_τ) and the normal force (F_σ) is given by

$$F_\tau = \mu F_\sigma = F_\sigma \tan \varphi_\mu \tag{1}$$

where μ (friction coefficient) and φ_μ (interparticle friction angle) are physical constants, respectively. Equation (1) can be rewritten in the form of

$$\tau_f = \sigma_n \tan \varphi_\mu \tag{2}$$

where $\tau_f = F_\tau/A$ (shear stress) and $\sigma_n = F_\sigma/A$ (effective normal stress) respectively, acting on a sliding plane with a contact area A. With reference to an idealised model shown in Fig. 4.5, the maximum shear resistance τ_f for shearing a granular material can also be expressed by substituting φ (angle of internal friction) for φ_μ in (2).

$$\tau_f = \sigma_n \tan \varphi \tag{3}$$

In spite of the similarity of (2) and (3), their physical meanings are quite different. φ is not a physical constant, but strongly depends on void ratio and stress state. This suggests that a granular assembly is more than just a frictional material.

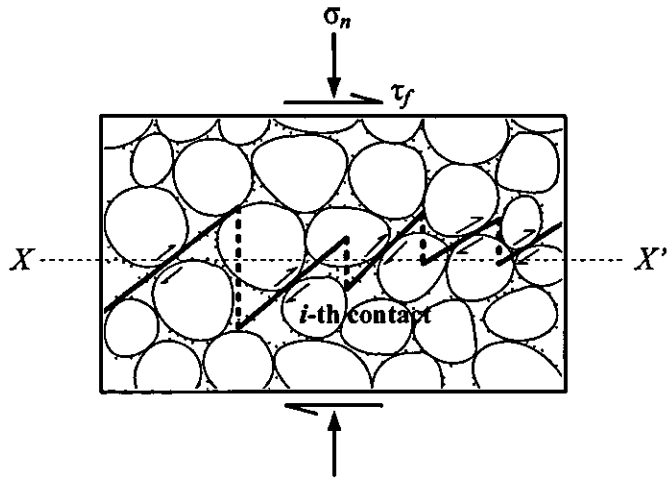

Fig. 4 5 Schematic diagram of an idealised shearing model of a granular material (Tobita and Oda, 1999)

As stated, dilatancy and contractancy are dominant features of the mechanical behaviour of granular materials, which is the ability to undergo volume changes under the action of shear stresses (Feda, 1982). The concept of dilatancy is generally taken to be the expansion of the voids which occurred in tightly packed granular arrangement, when it is subjected to deformation (Massoudi, 2004). The angle of dilatancy (α) is a parameter which characterised the strain of a medium that is no longer regarded as incompressible (Feda, 1982). A dense granular material dilates during shear, while a loose material compresses (contractancy or negative dilatancy). This meant that the mobilisation of φ consists of various components and not just the frictional component (i.e. φ_μ). Taylor (1948) and Bishop (1954) separated the shear resistance of granular soils into two components:

i) The internal frictional components between particles, which is a combination of rolling and sliding friction, and

ii) Components arising from shearing against interlocked particles.

In order to evaluate quantitatively the second component, Taylor (1948) considered that the part of the τ_f is used to provide the energy required to expand the assembly against the normal (confining) effective stress (σ_n). By assuming that the total energy applied to overcome shear resistance is given by $\tau_f \, d\gamma$. The dissipated energy, on the other

hand, is considered to be the sum of two terms, the frictionally dissipated work ($\tau_{eff} d\gamma = \sigma_n \tan\varphi'_\mu d\gamma$) and the work done against the normal stress during volume change ($-\sigma_n d\varepsilon_v$). Equating the applied energy to the dissipated energy gives

$$\tau_f d\gamma = \left(\sigma_n \tan\varphi'_\mu d\gamma\right) + \left(-\sigma_n d\varepsilon_v\right) \tag{4}$$

Rearranging (4) gives

$$\tau_f = \sigma_n \left(\tan\varphi'_\mu + \tan v\right) \tag{5}$$

where the notation of $\tan v = -d\varepsilon_v/d\gamma$ is used. The term φ'_μ is a physical angle related to both rolling and sliding angles. The dilatancy coefficient is denoted by v, which is the rate of dilatancy associated with shear deformation.

The model shown in Fig. 4.5 basically relies on the assumption that shearing of granular materials is analogous frictional sliding between two rigid bodies. The only difference was that sliding takes place on many contact surfaces. The sliding direction (θ^i) changes from contact to contact, from the general sliding direction X-X'.

Fig. 4.6(a) shows an idealised friction model based on that of Fig. 4.5.

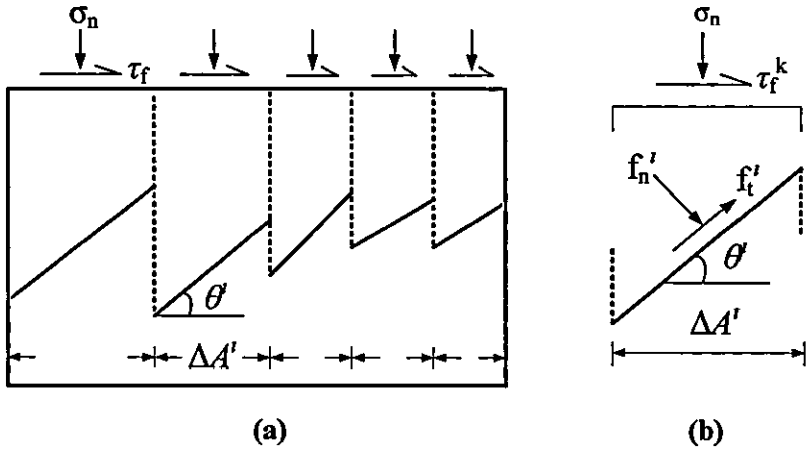

Fig. 4 6 (a) Idealised sliding model based on the contact points of Fig. 4 5 (b) sliding surface of *i-th* contact (Tobita and Oda, 1999)

By taking a single sliding surface denoted by i, shown in Fig. 4.6(b), the force components parallel and normal to the *i-th* surface in terms of shear (τ_f) and normal stresses (σ_n), acting on the X-X' shear place can be written as

$$\frac{\tau_f \Delta A^i \cos\theta^i - \sigma_n \Delta A^i \sin\theta^i}{\tau_f \Delta A^i \sin\theta^i + \sigma_n \Delta A^i \cos\theta^i} = \tan\varphi_\mu \tag{6}$$

where ΔA^i is the contact area of the *i-th* sliding surfaces projected on the general shear plane

$$\left(\sum_{(i)} \Delta A^i = A\right)$$

So that $\sigma_n \Delta A^i$ is equal to the forces acting on the *i-th* surface in the vertical direction. Rearranging (6) gives

$$\tau_f = \frac{\sigma_n\left(\tan\varphi_\mu + \tan\theta^i\right)}{1 + \tan\varphi_\mu \tan\theta^i} = \sigma_n \tan\left(\varphi_\mu + \theta^i\right) \tag{7}$$

As denoted in Fig. 4.5 and Fig. 4.6, θ^i changes from contact to contact. For simplicity, all contacts are idealised to slide at a mean sliding angle ($\bar{\theta}$). Hence, in Equation (7) $\bar{\theta}$ can be substituted for θ^i.

$$\tau_f = \frac{\sigma_n\left(\tan\varphi_\mu + \tan\bar{\theta}\right)}{1 + \tan\varphi_\mu \tan\bar{\theta}} = \sigma_n \tan\left(\varphi_\mu + \bar{\theta}\right) \tag{8}$$

Considering the kinematics at *i-th* sliding surface, the horizontal displacement dx takes place along with the volumetric expansion dy. Noting that dx/t = dγ and –dy/t = dε_v, with reference to (5) for the definition of v, we have

$$\frac{dy}{dx} = -\frac{d\varepsilon_v}{d\gamma} = \tan\bar{\theta} = \tan v \tag{9}$$

The term $\frac{d\varepsilon_v}{d\gamma}$ is defined as the angle of dilatancy (α), by means of the relation

$$\sin\alpha = \frac{d\varepsilon_v}{d\gamma}$$

Finally, (8) can be rewritten as

$$\tau_f = \sigma_n \tan\left(\varphi_\mu + v\right) \tag{10}$$

It should be noted that equation (10) differs from equation (3), which was derived from the energy consideration. According to Rowe *et al.* (1964), the additional term v in equation (10) represents two resistance sources, the external work required to make the mass expand against the normal stress σ_n plus the addition energy absorbed in friction when mass dilated.

Equation (2) can be written in terms of the major and minor effective principal stresses, σ_1 and σ_3, under the assumption that the general shear place accords with the maximum obliquity plane on which stress ratio (τ/σ_n) is maximum.

$$\frac{(\sigma_1 - \sigma_3)_f}{2} = \frac{(\sigma_1 + \sigma_3)_f}{2} \sin\varphi \tag{11}$$

where subscript *f* denotes failure or yield.

4.6 Failure criterion

The elastic limit of a material under combined state of stress is defined by its yield criterion. Failure of a material is usually defined by its load carrying capacity, where yielding itself implies failure. Hence, the yield stress is also the limit of stress. Yielding of most ductile metals is hydrostatic pressure independent. However, the behaviour of many non-metallic materials (i.e. geomaterials, etc.) are characterised by their hydrostatic dependence. Therefore, the stress invariant I_1 and ξ, which characterised this dependence should not be omitted. In the next section, two failure criteria are reviewed; the Mohr-Coulomb and the Drucker-Prager criterion, commonly used to describe the failure of hydrostatic pressure dependent materials.

4.6.1 Mohr-Coulomb criteria

The Mohr-Coulomb (M-C) criterion is a generalised version of the Tresca criterion which considered the limiting shear stress (τ_f) in a plane to be a function of the normal stress (σ_n), in the same plane at a point (Chen and Han, 1988). In contrast to the Tresca criterion, the M-C criterion allows for the effects of mean stress or hydrostatic stress. The simplest form of the Mohr envelope is a straight line, as Fig. 4.7 shows. The equation for the straight line envelope is known as the Coulomb's equation.

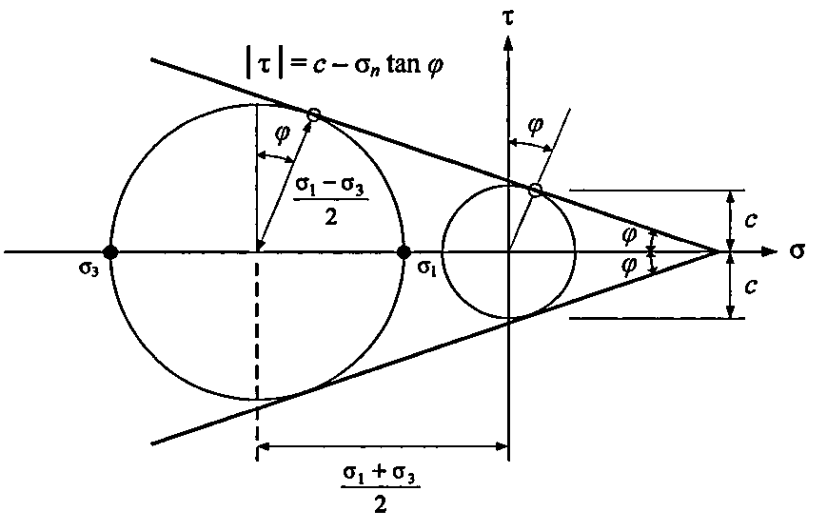

Fig 4 7 Failure envelope of Mohr-Coulomb criterion (Chen and Han, 1988)

For more general cases, in particular under high normal stress, equation (2) must be replaced by a non-linear relationship, such as a curved envelope (Tobita and Oda, 1999). For most stability analyses in soil mechanics, such a curved envelope is linearised piecewise as

$$\tau_f = c - \sigma_n \tan\varphi \tag{12}$$

where c is known as the cohesion constant. Equation (12) is known as the M-C failure criterion. The term c in equation (12) is not a representation of the true cohesion stemming from a physico-chemical process, but rather a consequence of linear approximation (Oda and Iwashita, 1999). In the case of a frictionless material ($\varphi = 0$), equation (12) is reduced to the Tresca criterion ($\tau_f = c$), and cohesion becomes equal to the yield stress in pure shear ($c = k$), where k is also known as yield stress (σ_y) written as

$$k = \sigma_y = \frac{6c\cos\varphi}{\sqrt{3}(3-\sin\varphi)} \tag{13}$$

For dry, coarse materials (i.e. non powders), c can be neglected. However, c is usually much higher where a material undergoes physico-chemical process, due to enhanced cohesion, in contrast to cohesive cohesionless materials (Feda, 1988). Both c and φ are material constants which can be calibrated from a uniaxial tension and uniaxial compression test. The yield stress in a uniaxial tension (σ_t) and uniaxial compression (σ_c), in relation to both c and φ is written as

$$\sigma_t = \frac{2c\cos\varphi}{1+\sin\varphi}, \qquad \sigma_c = \frac{2c\cos\varphi}{1-\sin\varphi} \tag{14}$$

The ratio of σ_c and σ_t is defined as

$$\mathrm{m} = \frac{\sigma_c}{\sigma_t} = \frac{1+\sin\varphi}{1-\sin\varphi} \tag{15}$$

The relationship between σ_c, c and m can be written as

$$c = \frac{\sigma_c}{2\sqrt{\mathrm{m}}} \tag{16}$$

In terms of m and φ, we have

$$\sin\varphi = \frac{\mathrm{m}-1}{\mathrm{m}+1}, \qquad \cos\varphi = \frac{2\sqrt{\mathrm{m}}}{\mathrm{m}+1} \tag{17}$$

with to $0 \le \varphi \le \frac{\pi}{2}$.

The general expression or the 3D failure surface of the M-C criterion is

$$f(I_1, J_2, \theta) = \frac{1}{3} I_1 \sin\varphi + \sqrt{J_2}\sin\left(\theta + \frac{\pi}{3}\right) + \sqrt{\frac{J_2}{3}}\cos\left(\theta + \frac{\pi}{3}\right)\sin\varphi - c\cos\varphi = 0 \tag{18}$$

Identically, equation (18) can be written in terms of variables ξ, ρ and θ as

$$f(\xi, \rho, \theta) = \sqrt{2}\xi\sin\varphi + \sqrt{3}\rho\sin\left(\theta + \frac{\pi}{3}\right) + \rho\cos\left(\theta + \frac{\pi}{3}\right)\sin\varphi - \sqrt{6}c\cos\varphi = 0 \tag{19}$$

with $0 \le \theta \le \frac{\pi}{3}$. The graphical representation of the M-C criterion is shown in Fig. 4.8.

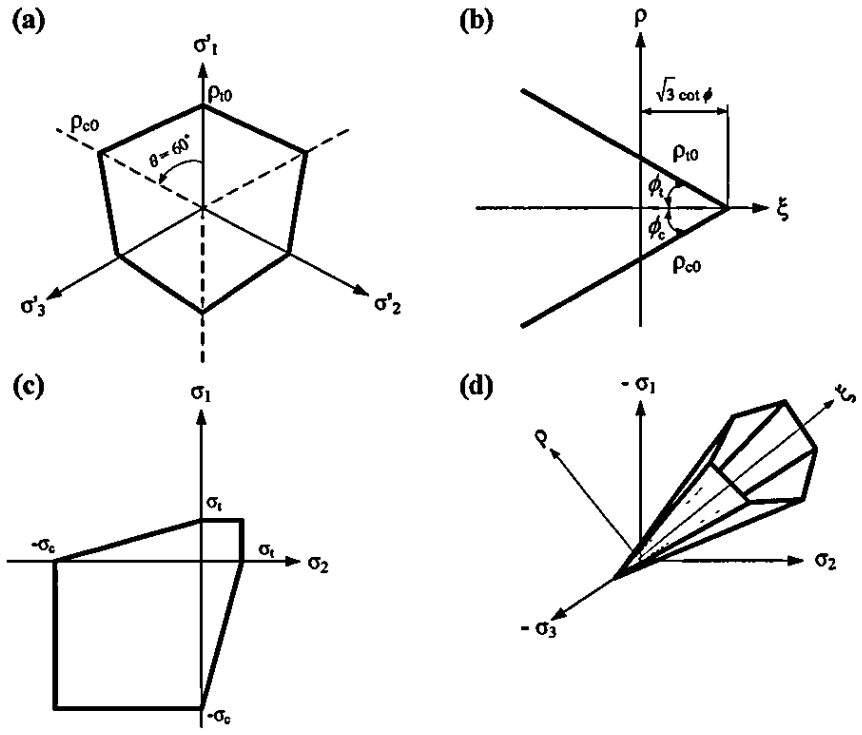

Fig. 4.8 Graphical representation of Mohr-Coulomb criterion: (a) Deviatoric π-plane; (b) meridian planes, (c) $\sigma_1 - \sigma_2$ space, (d) yield surface (Chen and Zhang, 1991)

On the deviatoric (π) plane, the cross-section of the surface is an irregular hexagon (Fig. 4.8a). The meridians of the surface are straight lines which intersect with the ξ axis at the point $\xi_0 = 2\sqrt{3}c/\tan\varphi$ (Fig. 4.8b). The two characteristics lengths of the surface on the deviatoric and meridian planes are

$$\rho_t = \frac{2\sqrt{6}c\cos\varphi - 2\sqrt{2}\xi\sin\varphi}{3+\sin\varphi}, \qquad \rho_c = \frac{2\sqrt{6}c\cos\varphi - 2\sqrt{2}\xi\sin\varphi}{3-\sin\varphi} \tag{20}$$

from which, we have

$$\frac{\rho_t}{\rho_c} = \frac{3-\sin\varphi}{3+\sin\varphi} \tag{21}$$

On the $\sigma_1 - \sigma_2$ plane, with $\sigma_1 = 0$, the surface is an irregular hexagon (Fig. 4.8c). In the quarter plane ($\sigma_1 \geq 0$, $\sigma_2 \leq 0$), the criterion, in the slope-intercept form is

$$m\sigma_1 - \sigma_2 = \sigma_c \tag{22}$$

In the principal stress space, the yield surface resembled an irregular hexagonal pyramid (Fig. 4.8d). For granular materials which $\sigma_t = \sigma_c$, (or equivalently, when $\varphi = 0$, or m = 1), it should be noted that the irregular hexagonal surface become a regular hexagon, in which the M-C failure criterion is reduced to the Tresca criterion.

4.6.2 Drucker-Prager criteria

The Drucker-Prager (D-P) criterion is a modification of the von-Mises criterion, where the influence of hydrostatic stress component on failure is introduced by inclusion of an additional term (I_1) in the von-Mises expression to give

$$f(I_1, J_2) = \alpha I_1 + \sqrt{J_2} - k = 0 \tag{23}$$

In terms of variables ξ and ρ, equation (23) can be written as

$$f(\xi, \rho) = \sqrt{6}\alpha\xi + \rho - \sqrt{2}k = 0 \tag{24}$$

where α and k are D-P material constants. When $\alpha = 0$, equation (23) is reduced to the von-Mises criterion. From a uniaxial tension and uniaxial compression test, we obtain

$$\sigma_t = \frac{\sqrt{3}k}{1+\sqrt{3}\alpha}, \qquad \sigma_c = \frac{\sqrt{3}k}{1-\sqrt{3}\alpha} \tag{25}$$

With the use of the ratio $m = \sigma_c/\sigma_t$, parameters α and k is expressed as

$$\alpha = \frac{m-1}{\sqrt{3}(m+1)}, \qquad k = \frac{2\sigma_c}{\sqrt{3}(m+1)} \tag{26}$$

On the π plane, the cross-section of the failure surface is a circle with a radius ρ (Fig. 4.9a). On the meridian planes, the surfaces are straight lines which intersect with the ξ axis at point $\xi_0 = k/\sqrt{3}\alpha$ (Fig. 4.9b). In the $\sigma_1 - \sigma_2$ plane, with $\sigma_3 = 0$, the criterion is an ellipse (Fig. 4.9c), with

$$\left(\frac{x + \frac{6\sqrt{2}k\alpha}{1-12\alpha^2}}{\frac{\sqrt{6}k}{1-12\alpha^2}} \right)^2 + \left(\frac{\frac{y}{\sqrt{2}k}}{\sqrt{1-12\alpha^2}} \right)^2 = 1$$

where

$$x = \frac{1}{\sqrt{2}}(\sigma_1 + \sigma_2), \qquad y = \frac{1}{\sqrt{2}}(\sigma_2 - \sigma_1)$$

In the principal stress space, the failure surface is a right-circular cone (Fig. 4.9d).

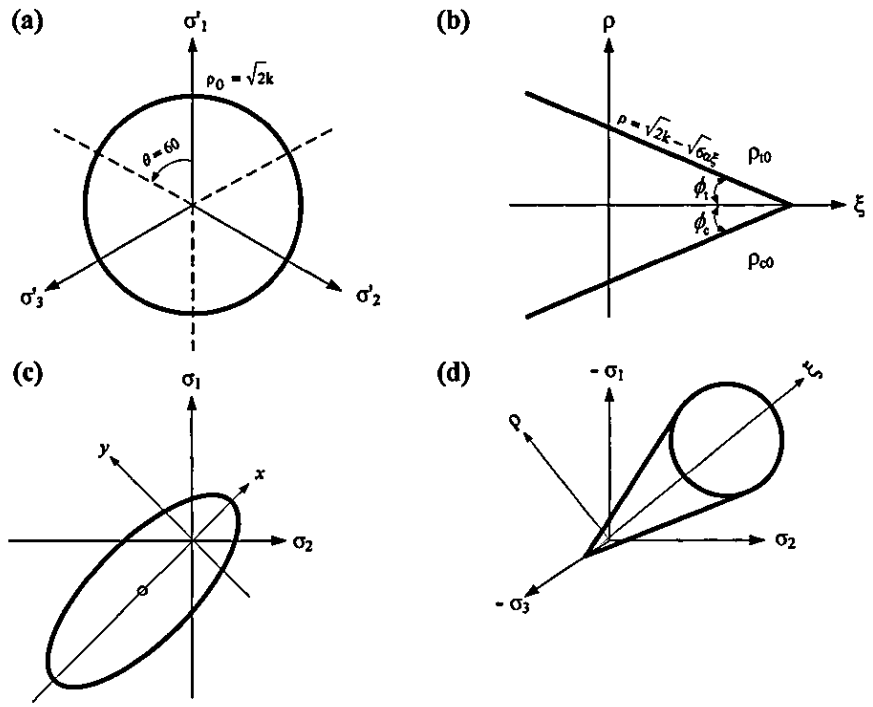

Fig 4 9 Graphical representation of the Drucker-Prager criterion· (a) Deviatoric π-plane; (b) meridian planes, (c) $\sigma_1 - \sigma_2$ plane, (d) yield surface (Chen and Zhang, 1991).

The M-C hexagonal failure surface is mathematically convenient only in problems where one of the six sides is to be used. If this information is not known in advance, the corners of the hexagon can cause considerable difficulty and give rise to complications in obtaining a numerical solution (Chen and Han, 1988). The D-P criterion is a smooth approximation of the M-C criterion, which can be made to match the latter by adjusting the size of the cone. For instance, if the D-P circle in Fig. 4.10 is made to agree with the outer apices of the M-C hexagon (in this case, the two surfaces are made to coincide along the compression meridian ρ_c, where $\theta = 60°$), then constants α and k are related to constants c and φ in equation (14) by

$$\alpha = \frac{2\sin\varphi}{\sqrt{3}(3-\sin\varphi)}, \qquad k = \frac{6c\cos\varphi}{\sqrt{3}(3-\sin\varphi)} \tag{27}$$

The cone corresponding to the constants in equation (27) circumscribed the hexagonal pyramid and represent the outer bound on the M-C failure surface. Conversely, the inner cone passed through the tension meridian ρ_t, where $\theta = 0°$, α and k are written as

$$\alpha = \frac{2\sin\varphi}{\sqrt{3}(3+\sin\varphi)}, \quad k = \frac{6c\cos\varphi}{\sqrt{3}(3+\sin\varphi)} \tag{28}$$

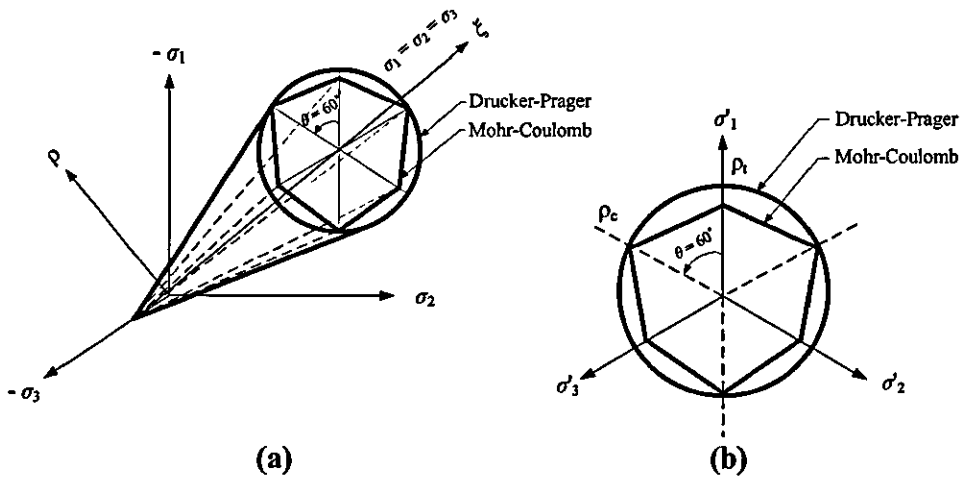

Fig 4 10 Drucker-Prager and Mohr-Coulomb criteria matched along the compressive meridian· (a) Failure surface in principal stress space, (b) in deviatoric plane (Chen and Han, 1988)

4.7 SLS Nylon-12 as a concrete substitute material

From the foregoing topics, it can be deduced that laser sintered SLS Nylon-12 is classed as a consolidated 'granular-solid', with enhanced adhesion forces attributed by sinter bridges developed through partial melting and the recrystallisation of the material. In the process of sintering, high temperature adhesion forces arise from the formation of material bridges, usually through phase change of particle surfaces due to chemical reaction or melting (Simons and Pagliai, 2004). Thin layers of viscous material are developed between the contacts of particles. Upon collision between particles, bonds are formed between them. Solid bridges are formed when particles come into contact, resulting in mutual molecular diffusion at the points of contact to form sintered bridges (see Fig. 4.3a).

In view of the highlighted granular characteristics and the type of structures to be investigated in the upcoming structural layout optimisation chapters, the Drucker-Prager (D-P) yield criterion was determined to be the more appropriate model. In general, The D-P criterion is a pressure-dependent model for determining whether a

material has failed or undergone plastic yielding. Although, the criterion was introduced to model the plastic deformation of soils, it has been widely applied to rock, concrete, polymers, foams and other pressure dependent materials (Tobita and Oda, 1999).

In contrast, the Mohr-Coulomb (M-C) theory is a criterion widely used to model the response of materials such as rubble piles or concrete to shear stress as well as normal stress. In structural engineering, it is used to determine the failure load as well as the displacement fracture (or angle of fracture) of granular materials. The Coulomb's friction hypothesis is applied to determine the combination of shear and normal stress that will cause fracture of the material. For a material failing according to Coulomb's friction hypothesis, the displacement introduced at failure forms an angle to the line of fracture equal to the angle of friction. The strength of the material in this case is determined by comparing the external mechanical work introduced by the displacement and the external load with the internal mechanical work introduced by the strain and stress at the line of failure. Hence, these suggest that the M-C is more suited for pressure-dependent granular materials of brittle nature or under loads that would lead to brittle fracture.

4.8 Research aims and objectives

The principle aim of this thesis was to support the application of a two-stage layout optimisation and thermal discretisation method in the design of a non-convective 'structured insulator'. The first aim was to present a design approach framework where layout optimisation, through use of a growth and degenerative approach, is employed to find an optimal cross-sectional layout for granular-solid structures. The focus was on engineering applications using numerical modelling and experimental investigations to predict the structural responses of scale model structures produced by AMT's.

The second aim was to investigate experimentally the trend of the reduction of heat transfer across a single-material enclosed rectangular structure without the use of secondary insulation materials. This was to be achieved by means of a 'geometry approach', by varying and 'discretising' the internal airspace layout through use of solid conducting partitions. The focus was on whether a geometry layout with limited space would benefit from discretisation or partitioning, to enable the design approach to be extended to cover enclosures with arbitrarily shaped openings or cavities.

The third and final aim was to extend the use of the structural layout optimisation and the thermal discretisation approach to optimally discretise a unit cell structure to satisfy both structural integrity and insulation requirements. The focus was the development of a structurally and thermally optimised/discretised layout, for a modular unit cell non-convective 'structured insulator' with fixed external geometry.

No matter how good the tools employed to aid the design optimisation process, the proposed two-stage optimisation and discretisation process itself had to be managed well and required engineering judgement in selecting the optimal design solutions. Therefore, a further aim is to provide means of a procedure to validate the consistencies of the discretisation method. Within this thesis, a design optimisation approach is presented whereby numerical modelling is employed to predict the performance of the insulator enclosure in the design process.

5

Methodology for Layout Optimisation of Consolidated Granular-solid Structures

5.1 Material and process selection

The selection of SLS Nylon-12 was attributed to the features of the SLS process in producing geometrically and dimensionally accurate structures, with strength that is ideally suited for the load spectrum used in this investigation. Concretes were not favoured, primarily due to the lack of AMT-based processes of comparative features of current additive processes. The focus of this study on SLS Nylon-12 was driven by the requirements to identify an additive manufacturing process which is readily accessible, to produce consolidated granular-solid structures. The selection was attributed to SLS's tight dimensional build tolerances of finished parts (± 0.2 mm), where strength is ideally suited for the load spectrum used in this investigation. Concretes and other mineral based AMT processes (i.e. Z Corp. 3D printing) were not favoured, primarily due to comparably lower build tolerances. In addition, finished parts are not as durable and need to undergo infiltration in which is undesirable for thermal analyses and testing purposes.

5.1.1 Generalities of SLS Nylon-12

Unsintered SLS Nylon-12 is classed as a granular powder, with an average particle size of ~ 58 μm. Consolidated SLS Nylon-12 granular-solids are produced by sintering of Nylon-12 powders at high temperatures (~184 °C). Solid bridges arise when particles come into contact at temperatures high enough to cause the surfaces to melt. This results in mutual molecular diffusion at contact points to form sintered 'bridges'. Two types of bonds can be distinguished; friction and cohesive bonds. Fig. 5.1 shows the

scanning electro microscope (SEM) and micrograph images, distinguishing the physical characteristics in unsintered and sintered form.

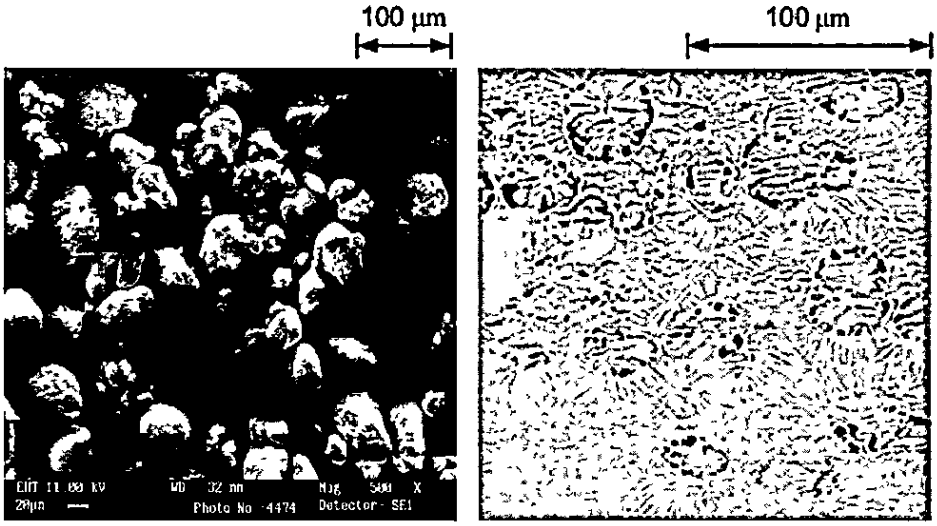

Fig 5 1 Structure of SLS Nylon-12: (a) SEM of unsintered powder Nylon-12, (b) micrograph of sintered or consolidated SLS Nylon-12 granular-solid (images curtesey of M M. Savalini and H. Zaringhalam, Loughborough University, U K.)

From a phenomenological viewpoint, SLS Nylon-12 (powder and sintered) is a material which exhibit dilatancy and sensitivity to hydrostatic stresses. From a structural viewpoint, it is composed of mutually contacting solid particles, within a liquid and/or gaseous phase. In general, it is considered as a two-phase, porous system. Deformation is brought about by mutual sliding of structural units, in contrast to deformation of individual structural units. Hence, its mechanical behaviour is a complex reflection of its structure, which is essentially of the autonomy of motion of the structural units and differs from the mechanical behaviour of a continuum (Feda, 1982).

5.1.2 Mechanical properties of consolidated SLS Nylon-12

Studies on the compressive and tensile behaviours of consolidated SLS Nylon-12 have been reported by Ajoku *et al.*, 2006, Zarringhalam *et al.*, 2006 and Hague *et al.*, 2004. However, these studies have separated compressive and tensile analysis. An investigation on the combined behaviour was presented by Ajoku *et al.* (2006). In all, such investigations are scarce, despite their significance in the design of load bearing structures under combined stress states. A comparative analysis of the experimental results, obtained in accordance to ISO 604 and ISO 527 standards by the above authors,

was performed. Accordingly, a combined stress/strain plot which illustrates the differences in elastic modulus was produced, as Fig. 5.2 shows.

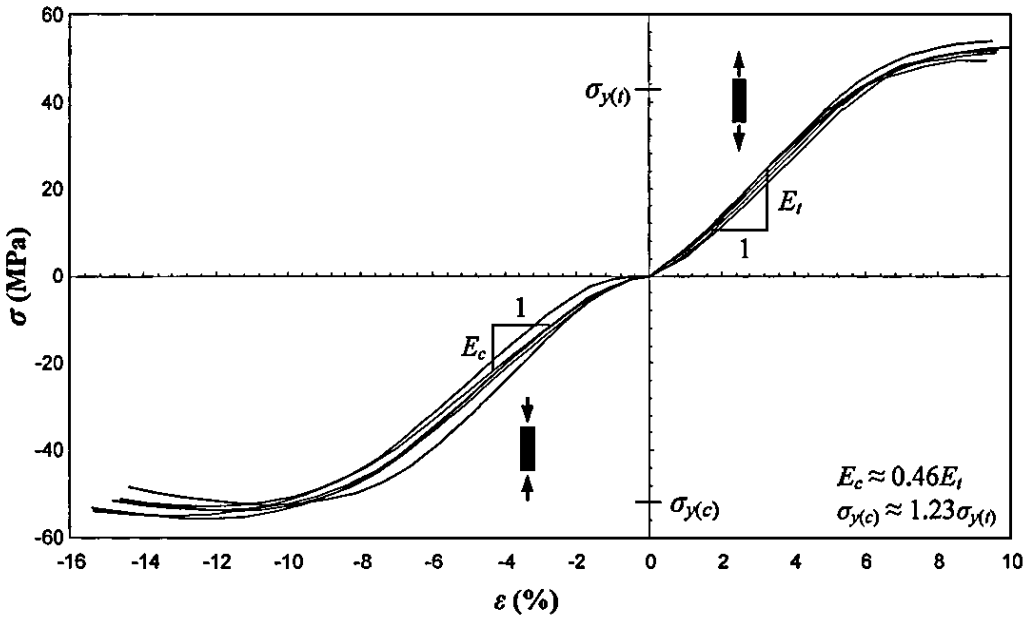

Fig. 5 2 Uniaxial nominal stress/strain curves of consolidated SLS Nylon-12 in compression and tension.

Optimally sintered SLS Nylon-12 granular-solids with $\rho = 0.97$ g/cm^3, in this instance have a tensile yield strength $\sigma_{y(t)} = 44$ MPa, which is about 81% of the compressive yield strength $\sigma_{y(c)} = 54$ MPa. The observed responses are in qualitative agreement with the behaviour normally displayed by concretes and other geomaterials (Tobita and Oda, 1999). The graph shows different elastic stiffness in tension and in compression, indicating the bimodulus characteristics of the material (see Fig. 5.2). The compression Young's modulus $E_c = 741$ MPa is about 46% of that in tension $E_t = 1600$ MPa. Compressive behaviour is ductile, with a softening post-peak branch, which tends to stabilise on a horizontal plateau at residual strength. The response under tension exhibits subtle strain hardening. In post-yield, failure of the brittle cohesive bonds formed during particle sintering was initiated. This is typically associated with the failure of a crystalline cement or material bridge formed by the interaction forces between atoms, ions and molecules of crystal lattices of continuous solids. Failure of the brittle bonds ultimately leads to the formation of friction bonds. At the onset of yield, consolidated SLS Nylon-12 exhibits granular characteristics. The average values of the mechanical properties, reported by reported by Ajoku *et al.* (2006) and Hague *et al.* (2004) are given in Table 5.1.

Table 5.1

Mechanical properties of SLS Nylon-12 granular-solid (uniaxial compression and tension tests)

Properties	Compression	Tension
Young's modulus (E)	E_c = 741 MPa	E_t = 1600 MPa
Poisson's ratio (υ)	υ = 0.3	υ = 0.3
Yield strength (σ_y)	$\sigma_{y(c)}$ = 54 MPa	$\sigma_{y(t)}$ = 44 MPa
Peak strain (ε_p)	$\varepsilon_{p(c)}$ = 15%	$\varepsilon_{p(t)}$ = 9%

5.2 Calibration and modelling of granular material properties

The differences in compressive/tensile responses show that the qualitative features of SLS Nylon-12 are typical of 'frictional' pressure-dependent geomaterials. Hence, the failure criterion chosen must account for yield as a function of hydrostatic pressure. In this study, the Drucker-Prager (D-P) elastoplastic model was calibrated on the basis of the combined experimental data from Ajoku *et al.* (2006) and Hague *et al.* (2004).

To characterise the failure domain in the biaxial stress space (σ_1, σ_2), the yield locus at peak stress contain points ($-\sigma_{y(c)}$, 0) and ($\sigma_{y(t)}$, 0) was obtained from the uniaxial tension/compression tests. Constants α and k are determined from the two characteristic strength values. Here, the compression failure strength ($-\sigma_{y(c)}$) and tensile failure stress ($\sigma_{y(t)}$) are available. Substitution of stress states ($\sigma_1 = \sigma_2 = 0$, $\sigma_3 = -\sigma_{y(c)}$) and ($\sigma_1 = \sigma_{y(t)}$, $\sigma_2 = \sigma_3 = 0$) into (23) gives

$$-\alpha\sigma_{y(c)} + \frac{1}{\sqrt{3}}\sigma_{y(c)} - k = 0, \qquad \alpha\sigma_{y(t)} + \frac{1}{\sqrt{3}}\sigma_{y(t)} - k = 0 \tag{29}$$

Noting that $\sigma_{y(c)} \approx 1.23\sigma_{y(t)}$ and ratio m = $\sigma_{y(c)}/\sigma_{y(t)}$, solving (29) leads to

$$k = \frac{2\sigma_{y(c)}}{(m+1)\sqrt{3}} = \frac{792\sqrt{3}}{49}, \qquad \alpha = \frac{(m-1)}{(m+1)\sqrt{3}} = \frac{5}{49\sqrt{3}} \tag{30}$$

By substituting (30) into (27) and solving for ϕ and c gives

$$\phi = \sin^{-1}\frac{9\alpha}{2\sqrt{3}+3\alpha} = \left(\sin^{-1}\frac{15}{103}\right), \qquad c = \frac{k\sec\phi(\sin\phi - 3)}{2\sqrt{3}} = 54\sqrt{\frac{11}{59}} \tag{31}$$

From the uniaxial tests, $\sigma_{y(t)} = 44$ MPa and $\sigma_{y(c)} = -54$ MPa corresponds to failure points A_1 and A_4, defined by

$$A_1(\sigma_1) = \frac{\sqrt{3}k}{1+\sqrt{3}\alpha}, \qquad A_4(\sigma_2) = \frac{\sqrt{3}k}{1-\sqrt{3}\alpha} \tag{32}$$

Assuming that the failure surface has twofold symmetry along $a-a'$, points A_2 and A_3 also lie on the yield locus using (30). Points C_1 and C_2 are approximated as

$$C_1(\sigma_2) = \frac{\sqrt{3}k}{1+\sqrt{12}\alpha} = 40.271, \qquad C_2(\sigma_1) = \frac{\sqrt{3}k}{1-\sqrt{12}\alpha} = 60.923 \tag{33}$$

Failure points B_2 and B_4 are approximated by substitution of $\sigma_3 = 0$ into (23) and rearranging leads to

$$\sigma_2 = \frac{\left(\sigma_1 - 6k\alpha + 6\sigma_1\alpha^2\right) \pm \left(\sqrt{3}\sqrt{4k - \sigma_1^2 - 12k\sigma_1\alpha + 12\sigma_1^2\alpha^2}\right)}{2\left(1-3\alpha^2\right)} \tag{34}$$

Finding the derivative of σ_2 with respect to σ_1 from (34) gives

$$\frac{d\sigma_2}{d\sigma_1} = \frac{\left(1+6\alpha^2\right) \pm \dfrac{\sqrt{3}\left(24\sigma_1\alpha^2 - 2\sigma_1 - 12k\alpha\right)}{2\sqrt{12\sigma_1^2\alpha^2 - \sigma_1^2 + 4k^2 - 12k\sigma_1\alpha}}}{2\left(1-3\alpha^2\right)} \tag{35}$$

and solving for the maxima and minima of the yield function leads to

$$B_4(\sigma_1, \sigma_2) = (-40.303, -68.445), \quad B_2(\sigma_1, \sigma_2) = (19.651, 47.793) \tag{36}$$

Finally, points B_4 and B_2, like points A_1 and A_4, can generate points B_3 and B_1, lying on the yield locus. A total of ten yield points have been generated on the $\sigma_1 - \sigma_2$ plane from two test points. For the numerical analysis, estimates (30) and (31) have been adopted. Once the failure locus is known, it is possible to locate the failure points along the untested radial paths. The failure locus of the material, characterised by failure points A_1 to A_4, B_1 to B_4, and C_1 and C_2, is plotted in Fig. 5.3.

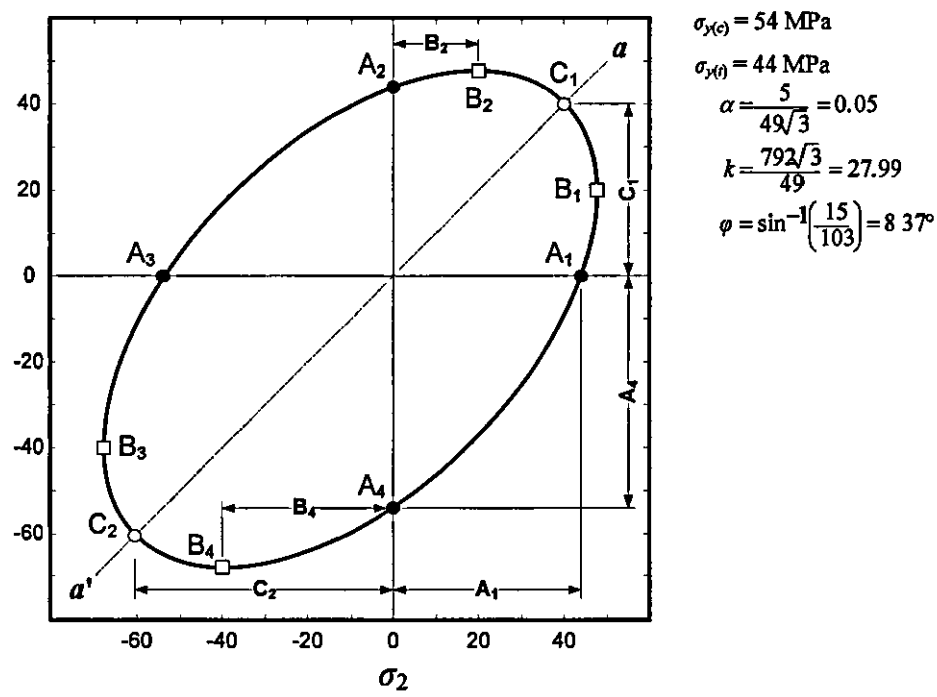

Fig. 5 3 Drucker-Prager (D-P) yield locus of consolidated SLS Nylon-12 in the biaxial stress space (σ_1, σ_2).

The D-P model in ANSYS FEA requires three material constants as inputs; cohesion (where $c > 0$), angle of internal friction (φ), and the dilatancy angle (α), as previously calculated. It should be noted that the cohesion constant c in (27) is not a representation of the true cohesion stemming from a 'physico-chemical' process, but rather a consequence of linear approximation. The amount of dilatancy is controlled by α. If $\alpha = \varphi$, flow rule is assumed to be associative. When $\alpha = 0$ (or $\alpha < \varphi$), there is no or less of an increase in material volume when yielding. In this case, the flow rule is assumed to be nonassociated.

5.3 Validation analysis of optimised structure

5.3.1 Design considerations

In the design of beams with transverse openings, an accurate assessment of the ultimate strength is necessary, to ensure that it does not fail under working loads (Mansur and Tan, 1999). Moreover, deflections produced under working loads should fall within acceptable limits. This is often a subjective judgement that is difficult to quantify and often a perception of application requirements. In this research, the focus is on large

displacement design problems. To design a simply-supported beam to deflect to certain amount is relatively straightforward. For beams with constant cross-section with small openings, the deflections can be approximated by classical beam theory. Due to the provisions of large openings, the indirect way of satisfying the requirements of maximum deflection by ensuring a minimum span to effective depth ratio is not applicable. For statically determinate beams, the bending moment and shear force distributions can be uniquely defined. For statically indeterminate beams with large openings, the distribution of internal forces and moments depend on the relative stiffness of each continuum 'member'. Currently, there are no design standards that apply to non-reinforced consolidated granular-solid beams with openings. The design optimisation implemented here is largely based on the results of the FEA and experience in the application of the MD method.

5.3.2 Design problem

The design of a beam is usually influenced by the maximum absolute bending moment $|M|_{max}$ and shear $|V|_{max}$. For slender beams, this is controlled by the normal stresses (σ_n) at the sections of $|M|_{max}$. The layout must be selected such that σ_n at any cross-sections do not exceed σ_{max}. Since M and V varies along the span, material which undergo stresses relatively lower than σ_{max} can thus be removed. Theoretically, the design of a beam is optimum if the section modulus S at each arbitrary cross-section satisfies

$$S_{min} \geq \frac{|M|_{max}}{\sigma_{max}} \tag{1}$$

where σ_{max} is the maximum allowable stress and S_{min} is the minimum section modulus.

The design task was to find an optimal transverse cross-sectional layout for an elastic beam. This was done using a layout optimisation approach to minimise structural compliance and mass, subject to stress and deflection constraints. A horizontal prismatic beam, under simply-supported bending was considered. The beam was optimised to carry a maximum transverse load of F_y = 500 N, with a targeted vertical deflection of $\delta_{y(max)} \leq 12$ mm at midspan, satisfy a strength criterion of $\sigma_{max} \leq 44$ MPa and built using a single material. The optimisation problem to be solved is written as

Minimise	m
Subject to	$\sigma_{max} \leq \sigma_y$
	$\delta_{max} \leq \delta_y$

where m is mass of a beam, σ_y is the yield stress of the material and δ_y is the vertical deflection at midspan. Due to the bimodulus nature of the material, σ_{max} was based on the lower failure stress, which is the yield stress of the material in uniaxial tension $\sigma_{y(t)}$.

5.3.3 Design domain and constraints, load and boundary conditions

The design domain is the search space where the transverse cross-sectional layout is to be 'metamorphically' developed, by element (or material) growth and degeneration. The schematic diagram in Fig. 5.4 shows the design domains, geometric constraints, load and boundary conditions of the design problem. In this study, the beam is modelled as simply-supported at points A and B, under a concentrated load F_y at midspan C.

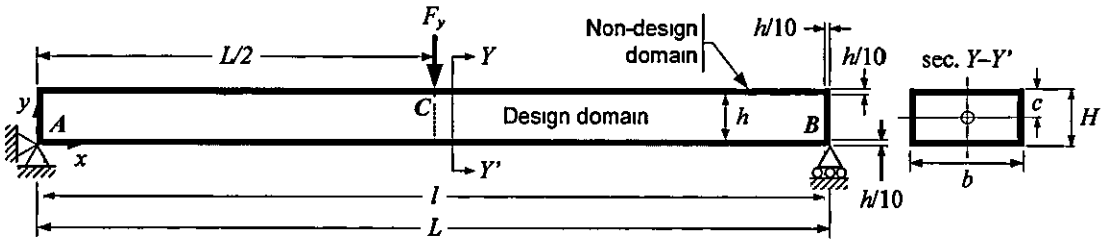

where,
$L \cdot h\,(14:1)$, $l = 69L/70$, $h = 4H/5$

Fig. 5.4 Design domains (Π), shape constraint, loading and boundary conditions of the optimisation model

All elements within the non-design domain are kept 'frozen', where the removal of material was restricted. Growth and degeneration was guided to occur only within the confined rectangular design domain. Hence, only the inner topology was optimised, where a prismatic external geometry with planar surfaces was retained.

5.3.4 FE model of simply-supported beam

The static nonlinear structural response of the beam was modelled using ANSYS Multiphysics™, the FEA package which was used in conjunction with the MD method. In this study, layout optimisation was performed on the x-y plane, where the variation

of stresses is produced predominantly by bending. A 3D model was not required as stresses along the z-axis are symmetrical about the x-y plane. The 'extruded' thickness b (see Fig. 5.4) was defined using a 'real constant' input. To ensure that the mesh density is sufficient, a displacement convergence check was performed by hand using the equation of elastic curve derived from the classical beam bending theory.

Fig. 5.5 shows the discretisation of the initial beam. The FE model consisted of 1400 quadrilateral elements with uniform mesh size of 1 mm^2. The 2D plane stress element PLANE42 used is defined by four corner nodes (i, j, k, l), with displacement δ_x and δ_y at each node, as Fig. 5.6(a) shows. Both the 4-noded and 3-noded types were used in the optimisation model. Although the 'tri' option was generally not recommended, the combinatorial use of both gives a better approximation stresses for curved geometries.

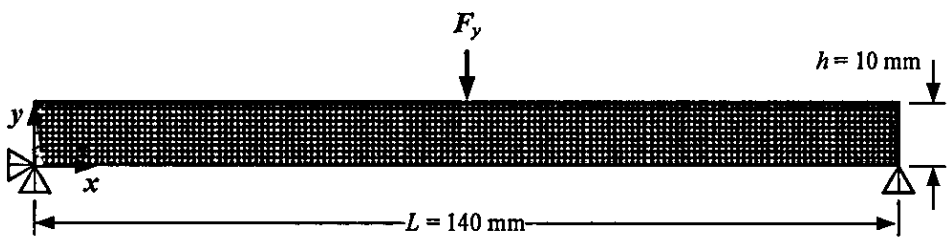

Fig. 5.5 FE discretisation, load and boundary conditions of initial solid beam

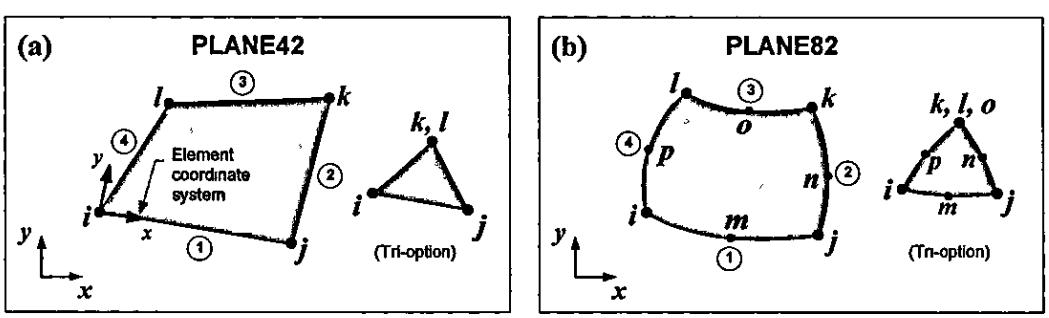

Fig. 5 6 2D solid plane stress elements: (a) PLANE42 quadrilateral element, (b) PLANE82 higher order element with mid-side nodes

PLANE82 element, a higher order version of PLANE42, generated by the addition of mid-side nodes was used to model the optimised beam under large deflection (Fig. 5.6b). Although PLANE42 has large strain/deflection capabilities, PLANE82 provides more accurate results for mixed quadrilateral-triangular meshes. Importantly, it can tolerate irregular shapes without as much loss of accuracy. The element has compatible displacement shapes and is well suited to model the curved boundaries.

5.4 Optimisation methodology – Metamorphic Development

5.4.1 Formulation of optimisation problem

Within the scope of this study, prismatic beam with optimal transverse cross-sectional layout was determined using the MD method. The design problem to minimise structural compliance $f_1(T_i)$ and/or weight $f_2(T_i)$, subject to geometric response constraints, can be formally defined as

$$\min_{T}\left\{f_1(T_i), f_2(T_i) \,|\, T_i = Y_{i1}^1 \oplus Y_{i2}^1 \ldots \oplus Y_{i1}^2 \oplus Y_{i2}^2 \oplus \ldots \oplus Y_{i1}^{\ell} \oplus Y_{i2}^{\ell} \oplus \ldots, T_i \in C_g \cap \Pi,\ Y_{ij}^k \in \Pi_k\right\} \quad (37)$$

$$\Pi = \Pi_1 \cup \Pi_2 \cup \ldots \cup \Pi_{\ell}, \qquad \Pi \subseteq R^2 \qquad (\text{or } R^3) \quad (38)$$

and constraint set C_g in (37), is defined as

$$h_j(T_i) \le 0, \qquad j = 1, 2, \ldots, n, \quad (39)$$

$$\mathbf{K}_i \mathbf{U}_i = \mathbf{P}_i, \qquad \mathbf{U}_i^T \mathbf{K}_i \mathbf{U}_i > 0 \quad (40)$$

$$Y_{ij}^k \in S_k, \qquad S_k = \left(s_{k1}, s_{k2}, \ldots, s_{km_k}\right), \qquad k = 1, 2, \ldots, \ell, \quad (41)$$

where $f_1(T_i) : D \cap \Pi \rightarrow R$ and $f_2(T_i) : D \cap \Pi \rightarrow R$ are real-valued objective functions associated with each topology structure T_i with

$$f_1(T_i) = \int_{\Pi} \mathbf{F}_i \cdot \mathbf{U}_i \, d\Pi + \int_{\tilde{\Gamma}_t} \mathbf{t}_i \cdot \mathbf{U}_i \, d\tilde{\Gamma}_t \,, \quad (42)$$

being the mean structural compliance, which is a positive quantity equal to twice the strain energy of the structure at equilibrium, and $f_2(T_i)$ being the structural weight. The above constraints require that the structure to be generated within a specified series of two or three-dimensional design domains (38), which satisfy structural response constraints (39), meet structural stability equilibrium conditions (40), and are built from specified components (41). The following notations used are

T_i	i-th topology structure
Y_{ij}^k	j-th element in i-th topology structure and an element of Π_k
Π_k	k-th subdomain
$h_j(T_i) \le 0$	structural response constraints
$\mathbf{K}_i \mathbf{U}_i = \mathbf{P}_i$	equilibrium condition

$\mathbf{U}_i^T \mathbf{K}_i \mathbf{U}_i > 0$	immobility condition
$\mathbf{K}_i$	stiffness matrix of T_i
$\mathbf{U}_i$	displacement vector of T_i
$\mathbf{P}_i$	load vector if T_i
$\mathbf{F}_i$	force vector of T_i
$\mathbf{t}_i$	applied traction on boundary $\tilde{F}_t$
S_k	geometry of Π_k

5.4.2 Optimisation methodology

The optimisation problem as previously defined was solved using MD, which is a shape/topology optimisation by material distribution approach with mechanisms for both structural growth and degeneration. Growth is guided to occur at selective locations known as 'growth cones', or a local region of a structural surface with high strain energy, high compliance, and/or high stress (Liu *et al.*, 2000). Growth implemented by the growth cones are based on the following conditions:

- The addition of elements creates new paths for load distributions;
- The addition of elements to these areas can disperse high strain energy and reduce high compliance;
- High stress can be decentralized by addition of elements.

Conversely, elements which carry little or no load are considered to be redundant, and thus removed. The growth cones of MD may be described in terms of the various network topologies, as shown in Fig. 5.7.

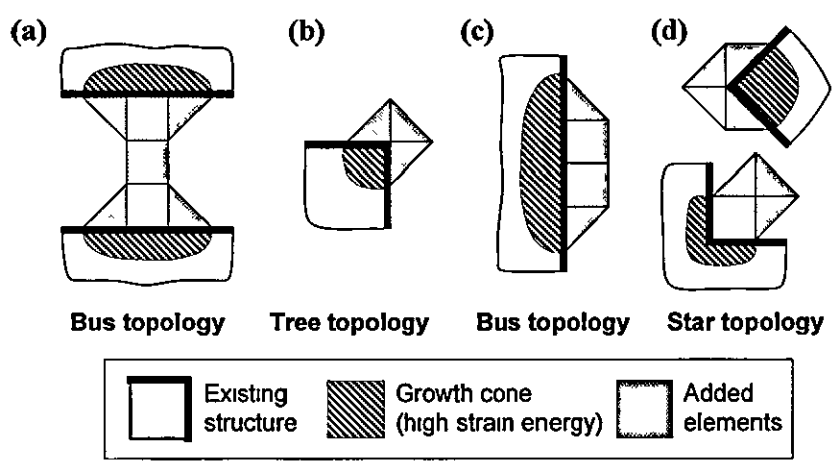

Fig 5.7 Types of growth cone topologies used in the MD method.

Growth and degeneration is controlled by a dynamic growth factor (DGF). A general example of the DGF is shown in Fig. 5.8. The values of *max*(*i*)+, *min*(*i*)+, *min*(*i*)-, and *max*(*i*)- vary throughout the optimisation procedure and depend on factors such as the scale of the structure, size of structural surface, and symmetry in one or more directions. The values and factors which determine the DGF may vary in the recurring iterations. Hence, the DGF is an adaptive function, changing from one structural topology to another. The rate of structural growth and degeneration is dynamically regulated by the DGF and is a function of structural performance, response constraints, and the calculated stress.

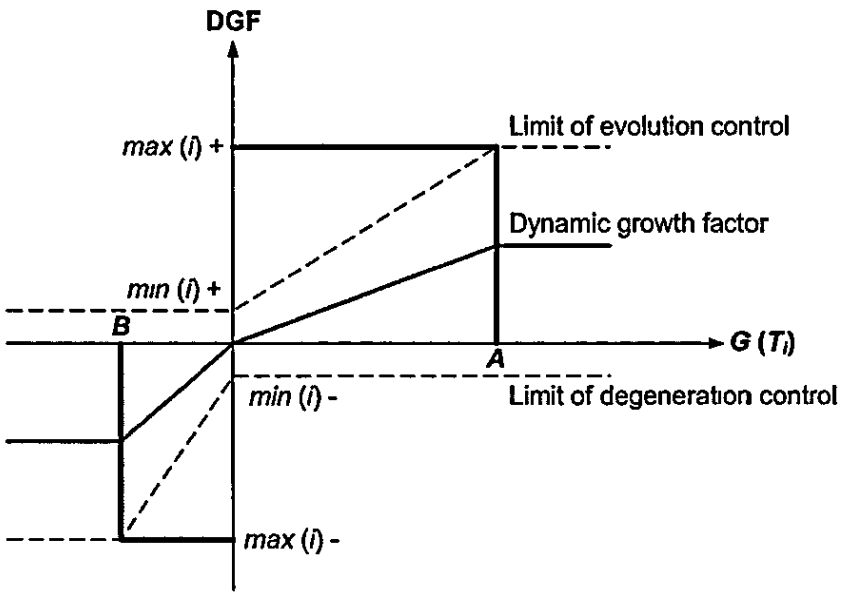

Fig. 5 8 Structural dynamic growth factor/hybrid constraint function

Here, $G(T_i)$ represents a hybrid constraints function and is determined by comparing structural responses within the specified limits defined by

$$G(T_i)=\sum_{j=1}^{n} w_j h_j(T_i)=\sum_{j=1}^{n} w_j\left(\left|R_j(T_i)\right|-\left|R_j^*\right|\right) \tag{43}$$

where $R_j(T_i)$ is the *j-th* structural response, n is the number of the response constraints, R_j^* is a user specified target for the *j-th* response, and w_j is a weighting function. The values of $G(T_i)$ at points A and B are specified as

$$A=\sum_{j=1}^{n} w_j\left|R_j^*\right|, \qquad B=-\frac{A}{2} \tag{44}$$

Thus, the DGF, the value of which depends through simple averaging on the values of the limits $max(i)+$, $min(i)+$, etc., is a piecewise linear function of $G(T_i)$. The adaptive nature of the DGF improves the algorithm's speed of convergence, making MD computationally efficient (Liu *et al.*, 2000).

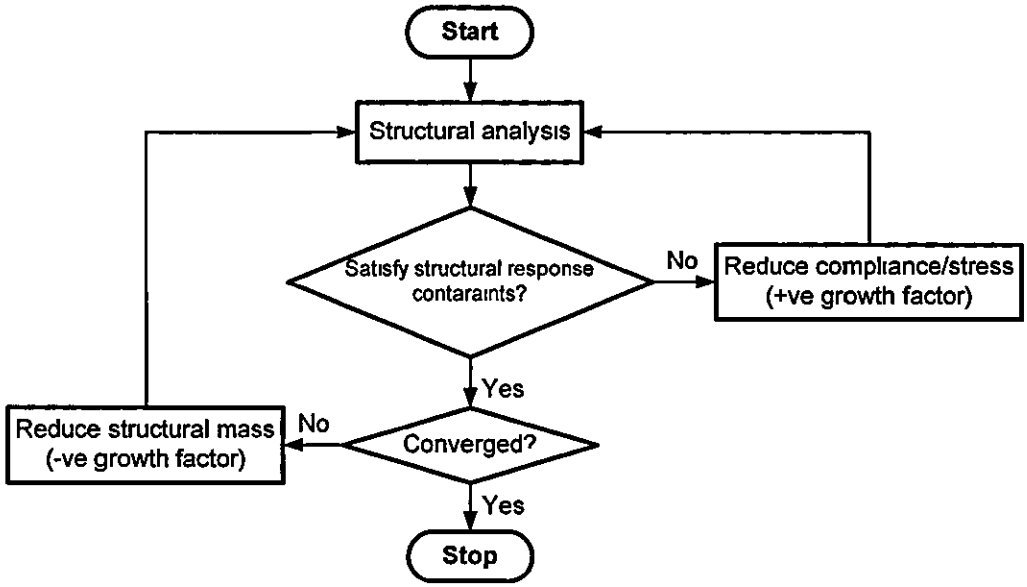

Fig. 5 9 General process flow of the MD optimisation method (Liu *et al*, 2000)

Fig. 5.9 shows the process flow of the MD procedure. The MD algorithm employs a hierarchical optimisation approach. If optimisation is started from an under designed model, initially, the objective function $f_1(T_i)$ for structural compliance is minimised. At this stage, the objective function $f_2(T_i)$ for structural mass was ignored until all structural response constraints are satisfied. In the initial stages, a positive growth factor is employed, where more elements are added than removed. In the later stages, a negative growth factor is employed. Elements which carry no load or undergo relatively low stress are removed. Conversely if the optimisation was started from an over designed model, the opposite design route will be taken, as opposed to the one as mentioned. Convergence is deemed to have occurred when all design criteria and constraints are satisfied, and when structural mass cannot be further reduced.

5.5 Results and discussion

5.5.1 MD layout optimisation

The layout optimisation of the prismatic beam took n_l = 27 recurring iterations to converge, as Fig. 5.10 shows. The von-Mises equivalent stress (σ_{eqv}) contours of both the initial and optimised beams are shown in Fig. 5.11.

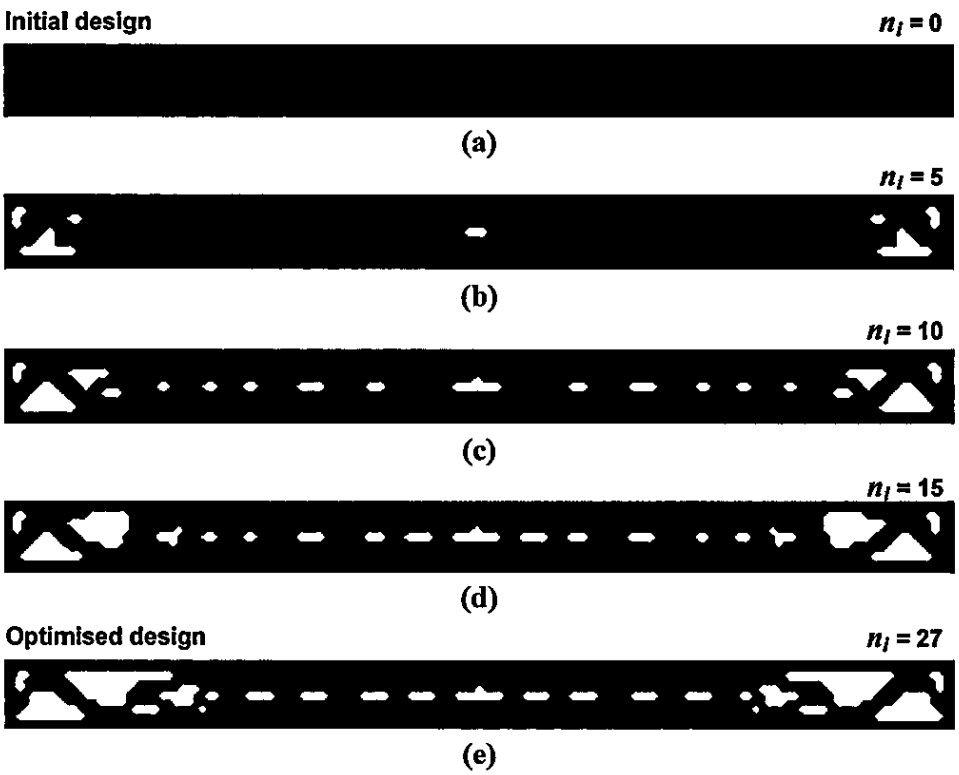

Fig. 5 10MD optimisation history of consolidate Nylon-12 granular solid polymer prismatic beam using the MD method· (a) Initial solid beam, (b) n_l = 5; (c) n_l = 10; (d) n_l =15; (e) optimised design n_l = 27.

Under simply-supported bending, the development of the tension and compression zones was symmetric about the neutral axis. Removal of material was concentrated at the vicinity of the supports and along the neutral axis, where the opening segments were created. This is expected because the level of stress is lower than the compression and tensile faces at the vicinity of the midspan (see Fig. 5.11a). Openings were created in such a way as to not 'cut' material from the compression zones. To maintain an externally flush finish, both 'corner frames' were retained, despite being structurally insignificant (see Fig. 5.11b). The support ends of the optimised layout resembled a continuum 'Vierendeel' truss.

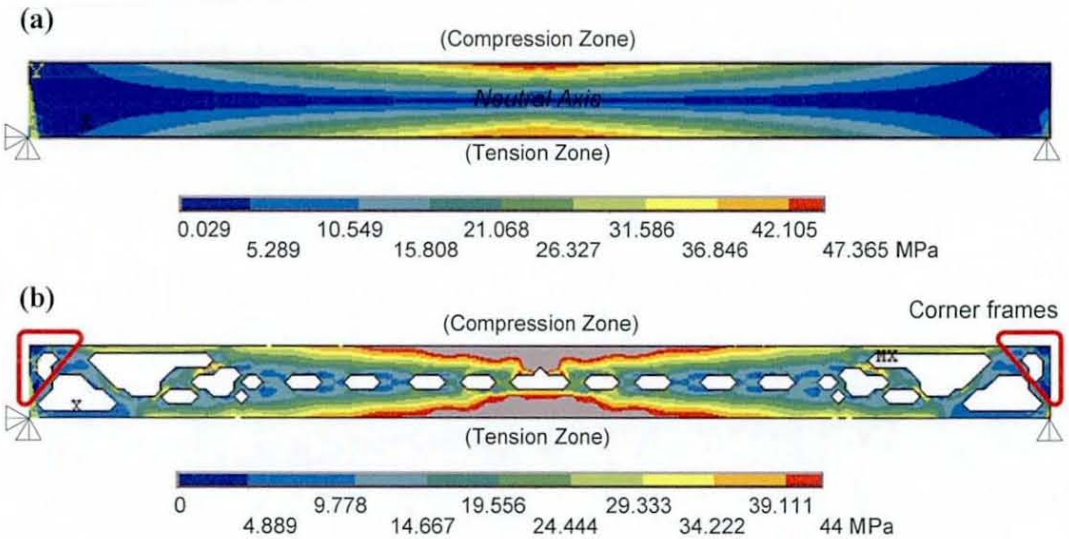

Fig. 5.11 Equivalent stress contours plots of 3PB specimen: (a) initial design; (b) optimised design. Grey regions indicate plastic yield.

5.5.2 MD optimisation history

The convergence and history plot in Fig. 5.12 shows the number of iterations required for the targeted deflection limit under the given transverse load.

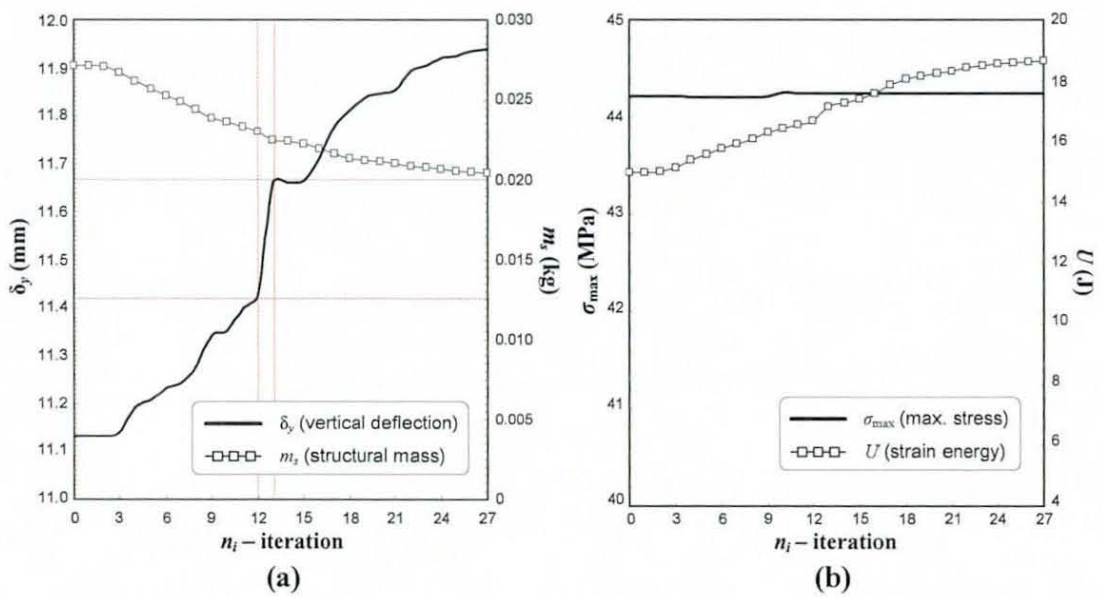

Fig. 5.12 Optimisation convergence and history plot prismatic beam under simply supported bending: (a) deflection convergence plot; (b) U and σ_{max} history plot.

The structure under development shows high sensitivity to the change in layout at n_i = 12, as exhibited by the sudden increase in δ_y indicated by the red markers, as Fig. 5.12(a) shows. With the removal of the relatively unstressed material, δ_y was increased from approximately 11.14 mm to 11.94 mm, hence satisfying the targeted deflection

value. Conversely, m was reduced from approximately 27.16×10^{-3} kg to 20.46×10^{-3} kg., where 25% savings in build material was achieved. Accordingly, strain energy (U) was increased from approximately 14.98 J to 18.85 J. The maximum stress (σ_{max}) was maintained constant, at a value close to the imposed strength criteria of $\sigma_{y(t)} = 44$ MPa throughout the optimisation procedure (Fig. 5.12b). Despite the removal of material, strength was not compromised, under the current loading case. The optimised design satisfies all imposed design constraints and criteria. The design attributes are given in Table 5.2.

Table 5.2

Attributes of the optimised 3PB test specimen

Design attributes	Initial	Optimised
Mass (m)	27.16×10^{-3} kg	20.46×10^{-3} kg
Deflection (δ_y)	11.14 mm	11.94 mm
Maximum stress (σ_{max})	44.21 MPa	44.25 MPa
Mean strain energy (U)	14.98 J	18.65 J

5.5.3 Stress and shear distributions

Fig. 5.13 shows the variation of stresses (σ_{eqv}) and shear (τ_{xy}) on the transverse plane, over length L of the upper planar surfaces of the initial and optimised beams. Material located directly under the load undergoes maximum stress, as Fig. 5.13(a) shows. The variation of σ_{eqv} over L on the initial beam resembled a 'south-opening' hyperbola curve, with a 'vertex' point of $\sigma_{eqv} = 45.88$ MPa. Along $L = 0$ to ¼ L, and ¾ L to L, σ_{eqv} was initially represented by a steep gradient, which then fluctuates along the upper surfaces of the 'truss-supported' horizontal sections, adjacent to the corner frames. Variation of σ_{eqv} over the middle portion, from ¼ L through to ¾ L, where material is removed along the neutral axis, resembled a parabola curve identical to that of the initial beam. Shear (τ_{xy}) is equal to zero under the point load, as Fig. 5.13(b) shows. Here, the variation of τ_{xy} along L on the initial beam is relatively uniform. On the optimised beam, the fluctuations of τ_{xy} somewhat resembled a 'dampened oscillation', with varying 'shear amplitude', found to be most significant at $L = 0$ to ¼ L and ¾ L to L.

Investigations of plane stress and shear variation was made on the upper planar surfaces, because stress concentrations caused by the applied load are comparatively larger than deeper regions in the beam. Ideally, such investigations should be made on the neutral axis. In this case, material along sections on the neutral axis of the optimised beam had been removed, resulting in discontinuous stresses, which in effect, do not provide the basis for any useful comparative analysis.

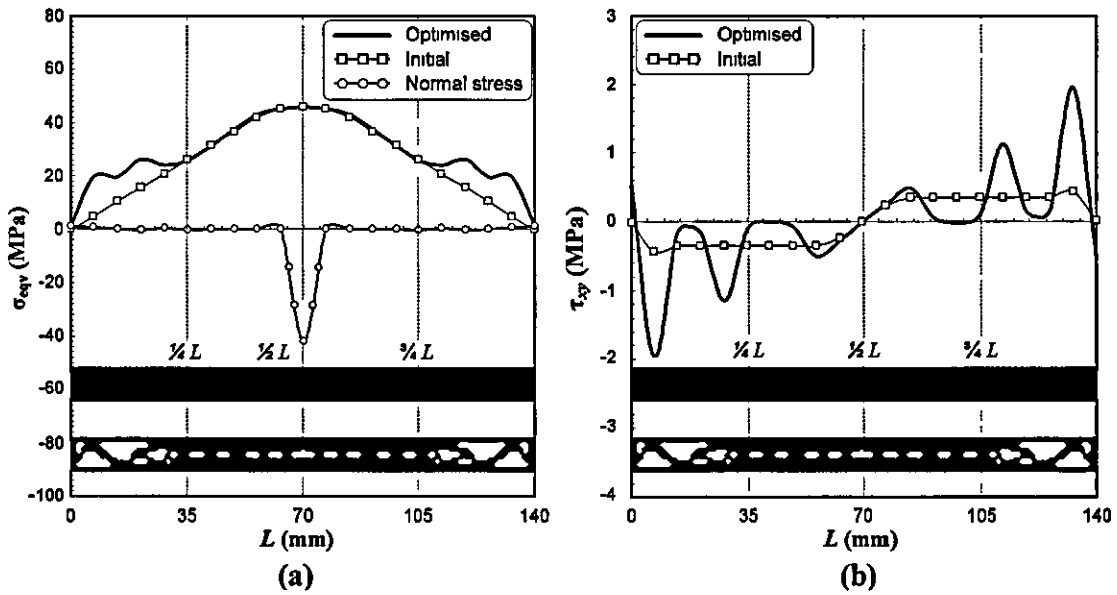

Fig. 5.13 Stress variations of the initial and optimised 3PB test specimens: (a) Variation of plane stress (σ_{eqv}), (b) variation of plane shear stress (τ_{xy})

5.6 Physical experiments

5.6.1 Design of 3PB test specimens

The dimensions of the tests specimen was selected based on the length/height (l/h) and span/height (L/h) ratios, recommended by the ISO 178 standard, where $l/h = 20 \pm 1$ was used. Ratio L/h was selected such that the deflection at rupture $\delta_{y(max)}$ do not exceed the height of the supports (see Fig. 5.17). From several 3PB trials, distance L between the supports was adjusted until a desirable rupture deflection was found at $L/h = 14 \pm 1$. Accordingly, the external dimensions selected for the test specimens was 200 mm × 10 mm × 20 mm, with an effective span L = 140 mm. Fig. 5.14 shows the schematic diagram of the dimensions and test configuration of the 3PB test specimens. For the optimised beams, similar external dimensions were used (Fig. 5.14b).

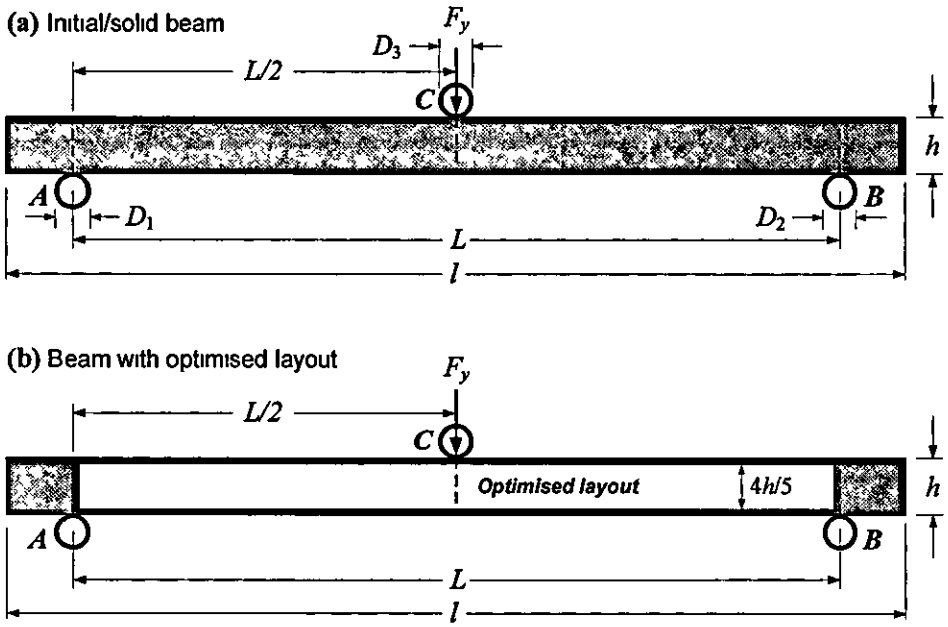

Fig 5 14 Schematic diagrams of the position of the test specimen on the experimental test rig. (a) Initial solid beam, (b) beam with effective span layout optimised using the MD method.

5.6.2 Manufacturing and post-processing of test specimens

Post-processing was required prior to the production of the test specimens. The FE model of the optimised prismatic beam obtained from MD was converted to .STL file, a standard file format in which a structure is described as faceted triangulated surfaces, used widely in AMT's. In this study, post-processing was done manually and involved the following steps as depicted in Fig. 5.15(a) to (f);

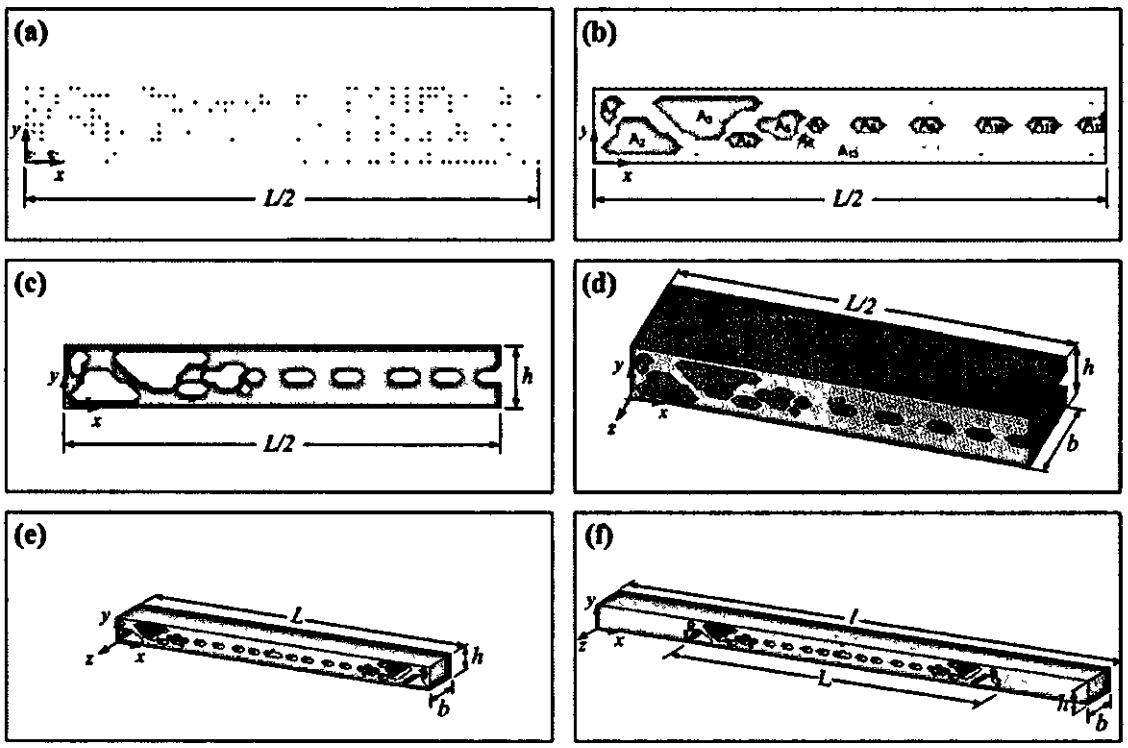

Fig. 5 15 Post-processing of optimised beam: (a) FE nodes; (b) outlining internal and external geometry; (c) subtraction of void geometry to create a 2D cross-section, (d) extrusion of 2D cross-section using CAD, (e) mirror-copy to create effective span; (f) extrusion of edges to create support ends and conversion to .STL.

i) The FE nodes of the optimised layout are read into ANSYS and are converted to 'key points'. Due to symmetry, only a half model was required.

ii) The transverse opening on the beam was highlighted (i.e. A_1, A_2, ..., A_N).

iii) A 2D cross-section of the layout was created using Boolean operation.

iv) A solid model was produced by 'extruding' the 2D cross-section created in Step iii). This was saved as an .IGES file and read by a CAD system.

v) A full model of the effective span was created by 'mirror copy' operation.

vi) Both ends of the beam were extruded to create the support length. The completed solid model was converted to .STL file, ready for manufacturing.

Test specimens were built on a 3D Systems Vanguard-SI SLS machine. The material used was powder Duraform PA^{TM} (Nylon-12), consisting of a manually refreshed standard mix of approximately 70% used and 30% 'virgin' powder. The machine process parameters used to manufacture the test specimens are given in Table 5.3. The

build takes into consideration the orthotropic properties of the parts, based on the isotropy tests by Hague *et al.* (2004). The adopted build configuration is shown in Fig. 5.16.

Table 5.3

Process parameters used for SLS of 3PB test specimens

SLS Manufacturing Parameters	
Feed powder	Heated to > 100 °C
Laser power (fill)	11 W
Laser power (outline)	5 W
Laser scan spacing	0.15 mm
Layer thickness	0.10 mm
Laser scan speed	5000 mm/s
Laser scan direction	*x*-direction only
Temperature of machine room	23 °C

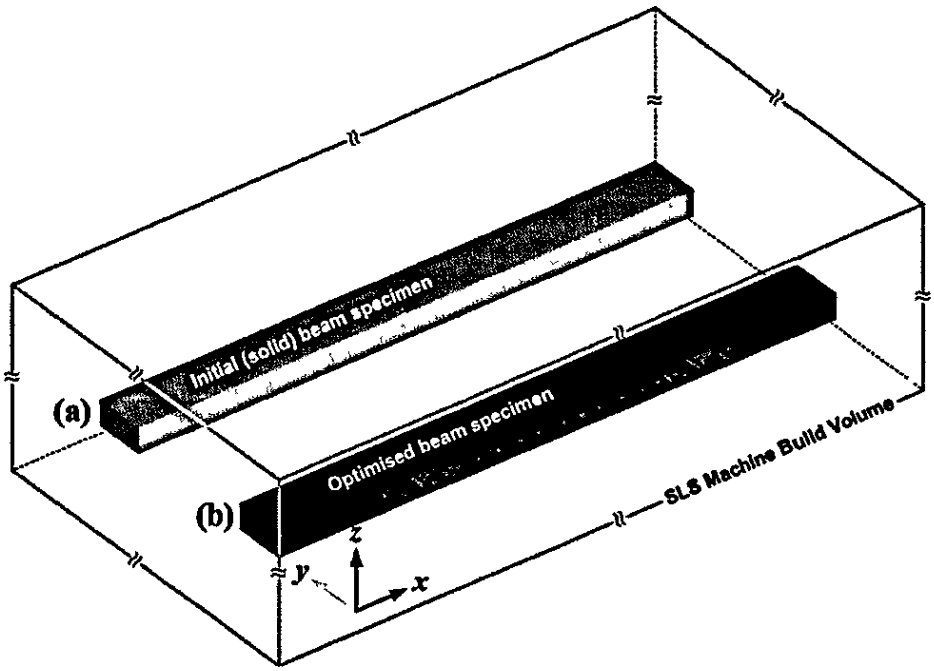

Fig 5.16 Build configuration of SLS Nylon-12 beams for 3PB test in accordance to axis of orthotropic properties (a) initial solid beam specimen; (b) optimised beam specimen.

5.7 3PB test configurations and procedures

The performance assessments of the initial and optimised beams were performed using 3PB tests on a computer controlled Lloyd loading machine (model *LRX*) with maximum bearing capacity of 1 kN. 10 mm diameter supports and loading edges were used. Load was applied at midspan using a cylindrical loading edge, positioned perpendicular to the longitudinal axis. The speed of the vertical displacement load cell used was at a rate of 25 mm/min for all specimens. The chosen specimen dimensions were a compromise between the optimum specimen size for the test rig, and small enough to fail at loads not exceeding the loading limits of the machine. The test configuration and the 3PB apparatus used are shown in Fig. 5.17.

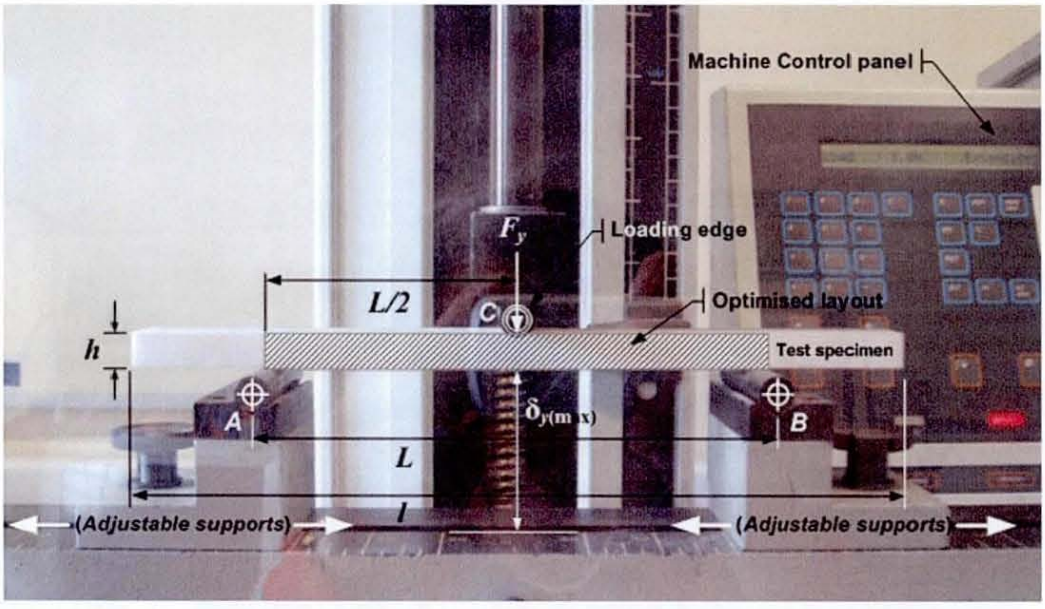

Fig. 5.17 Test configuration of beam specimens on the Lloyd loading machine 3PB rig.

A total of ten specimens, as opposed to five, recommended by the ISO 178 standard were tested for each beam type. With a preload of ~ 1 N, the load/displacement was increased, until the specimens ruptured. The test termination criterion was set to ± 80 % of the peak load. To improve consistency, all specimens were tested within 72 hours of production. The tests were conducted under ambient lab temperature of 20 °C with 40% relative humidity. For each completed test, the F_y/δ_y curves recorded was exported to a spreadsheet. The test data was plotted where the gradient of the linear region was used to determine the flexural stiffness.

5.7.1 Load/deflection plot from experiments and FE models

Fig. 5.18 compares the load/displacement (F_y/δ_y) curves of the 3PB experiments and numerical analysis of the initial and optimised beams. The tests were performed using a quasi-static, vertical displacement control load cell at a rate of 25 mm/min. From Fig. 5.18(a), the initial elastic/linear portions of the F_y/δ_y curves of the initial beams are represented by straight lines with near identical slopes. The beams exhibit strain hardening after yielding, eventually attaining load maximum ($F_y \approx 700$ N), at the onset of plastic deformation. When F_y is increased beyond the load maximum, considerable plastic deformation was observed, prior to rupture at midspan. Specimens were found to give an average rupture load of $F_y \approx 680$ N (at $\delta_y \approx 35$ mm). Importantly, the initial elastic slopes of the F_y/δ_y curves by the bimodulus constitutive approach are in good agreement with the experimental results. The analyses converged smoothly where the qualitative and quantitative features of the responses were reproduced. Load maximum, deflection at rupture and the amount of energy dissipated, were also in good agreement with the experiments.

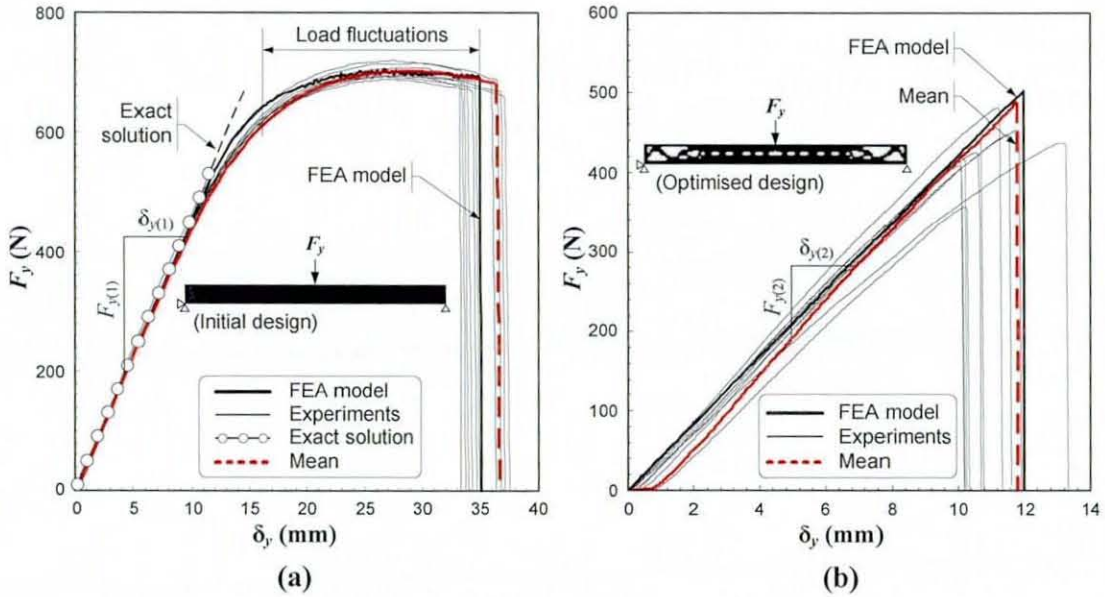

Fig. 5.18 Load/displacement (F_y/δ_y) curves for ultimate strength of 3PB test specimens: (a) F_y/δ_y curves of initial solid beams; (b) F_y/δ_y curves of optimised beams.

The average work done to load maximum and rupture was 13.83 J and 18.59 J, respectively. The F_y/δ_y curves, as computed numerically, revealed that strain hardening is followed by discrete 'load fluctuations', upon load maximum to rupture. Discrete

load fluctuations at the onset of strain hardening to load maximum was caused by the progressive failure of cohesive bonds and formation of friction bonds. This observation was consistent with the experimental findings of Zarringhalam and Hopkinson (2006). This feature, not recorded by the experiments of this current study, was primarily due to the lack of sensitivity of the loading machine load cell used.

For the optimised beams, the initial elastic slopes of the F_y/δ_y curves by the bimodulus approach were in good agreement with the experimental results. From the 3PB test, it was seen that beam-type behaviour of the optimised design was slightly affected, as indicated by the slight differences of the gradients $F_{y(1)}/\delta_{y(2)} \approx F_{y(2)}/\delta_{y(2)}$. From the test, only qualitative features of the responses were reproduced, and quantitative features were not fully reached. The dissimilar gradients and variations in rupture loads recorded could also suggest that mechanical properties among test specimens were somewhat inconsistent. This has been shown by the uneven heat distribution in the build volume, inadequate heat supply from the laser and insufficient process temperatures (Ajoku et al., 2006), and the melt and crystallisation temperature of the material (Zarringhalam and Hopkinson, 2006), by the SLS process, which results in test specimens not achieving optimal mechanical properties. To ensure that optimal mechanical properties are achieved, specimens are to be positioned in the centre of the cubic build volume, where process parameters are near optimal (Hague *et al.*, 2004).

The results of the continuum truss topologies was characterised by load transfer mechanism, which depend on the span to height ratio. Beams with $L/h \geq 3$ generally require inclined tensile ties connecting the horizontal 'compressive struts' to form truss topologies, and shear reinforcements to resist the inclined tensile stresses (Kwak and Noh, 2006). Similar beam-end topologies were obtained in studies conducted on the basis of other optimisation methods (Rozvany and Zhou, 1991; Zhou and Rozvany, 1991; Chu *et al.*, 1996; Kim *et al.*, 2000).

5.7.2 Failure assessment

Yield zone assessment of the FE models confirmed that plastic deformation, as a result of bending, were found on both the compression and tensile faces at the midspan vicinity, as shown in the true scale deformation plot in Fig. 5.19. As expected, stresses at portions between the supports and load point remained elastic, while regions adjacent to the ends and along the neutral bending axis remained relatively unstressed.

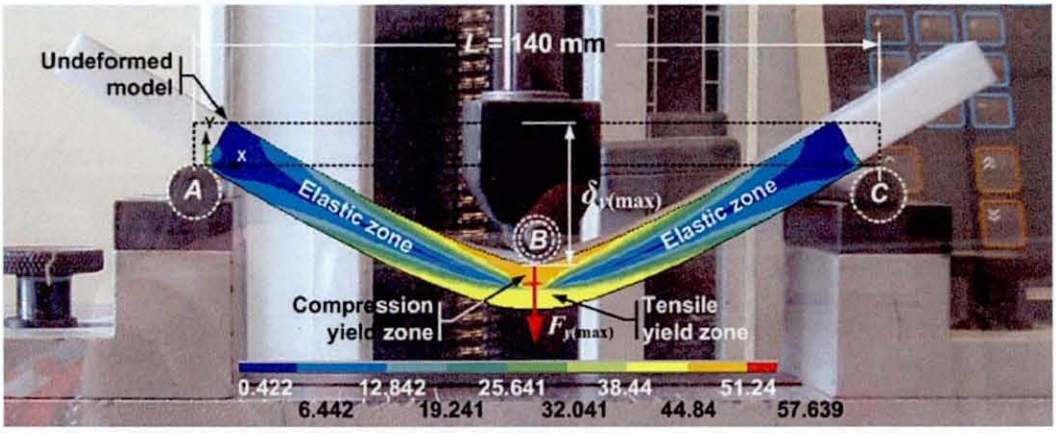

Fig. 5.19 Elastic and yield zone assessment of the initial solid beam under simply-supported bending by 3PB tests and FEA. Units in MPa.

The F_y/δ_y curves of the optimised beams are represented by straight lines of dissimilar gradients (see Fig. 5.18b). In this case, the variation in elastic portion, onset of yielding to load maximum and rupture, do not show marked differences. Specimens were observed to attain an average load maximum $F_y \approx 490$ N (at $\delta_y \approx 11.9$ mm). Plastic deformation was not recorded and the beams were observed to flex elastically. When F_y was increased beyond the load maximum, rupture was observed to be catastrophic. The average work done to load maximum and rupture was recorded as 1.89 J and 2.02 J respectively. The variations in rupture loads among test specimens showed marked differences where most did not achieve the predicted qualitative responses (± 2 mm).

The slight face buckling found experimentally was associated with elastic buckling of the compression 'struts', denoted by ***F*** and ***G***, as Fig. 5.20 shows. This response could not be predicted using the current continuum model without incorporating new features. Specimens were observed to fail catastrophically at points ***D*** and ***E***, indicated by the superimposed τ_{xy} plot from the FEA. The numerical analysis indicated that τ_{xy} peaked at a pair of continuum trusses at ***D*** and ***E***. Failure was associated with brittle shearing at $\tau_{xy} = 20.74$ MPa.

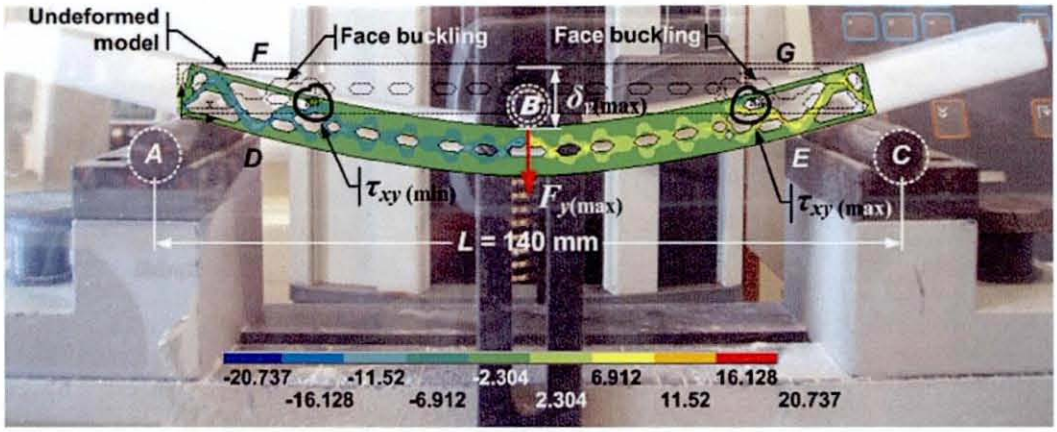

Fig. 5.20 Comparative failure/rupture assessment of optimised 3PB test specimen by plane shear (τ_{xy}) under simply-supported bending by 3PB tests and FEA. Units in MPa.

From the yield zone assessments, the initial beams underwent considerable plastic deformation prior to rupture, while the optimised beams do not. The response under bending was ductile. This is due to the presence of an approximately equal amount of material under compression/tension. However, the removal of material from the compression zone affected the ductile behaviour of the optimised beams. This had lead to failure by shear, a feature typical of geomaterials. Failure/rupture was catastrophic, where 'fail-safe' failure and 'ultimate' failure was somewhat indistinctive. In this study, the consideration of safety factor was not implemented. The fail-safe failure mode was taken to be the ultimate failure criteria and in this case, the optimised structure was considered to have failed, once the elastic limit was exceeded.

5.8 Conclusions and remarks

A design procedure to characterise the optimal structural performance of a granular-solid prismatic beam from an additive manufacturing process has been presented. Savings in build material of 24.7% was achieved, with slight compromise in structural performance. The design procedure comprised of topology (or layout) optimisation, calibration of material parameters, and finite element (FE) modelling. The metamorphic development (MD) method formed the basis of the generalised layout optimisation used. A Drucker-Prager (D-P) model was calibrated on the basis of experimental failure points obtained by Ajoku *et al.* (2006) and Hague *et al.* (2004).

The validity of initial and optimised beam FE models was assessed by simply-supported three-point bending (3PB) experiments. Quantitative and qualitative features of the structural responses of beams investigated experimentally and numerically were reproduced with reasonable error. For the optimised beams, quantitative features of the predicted responses were not fully reproduced by the experiments. 3PB test revealed marked differences in rupture loads and deflections, due to inconsistent mechanical properties among test specimens. In terms of manufacturing considerations, the placement of test specimens within the SLS machine build-volume where process parameters are near optimal, should improve the consistency of mechanical properties of beams produced.

The findings suggested that tensile stresses should ideally be avoided in the design of load bearing granular-solid structures. Although it has been demonstrated that a slight amount of tensile stresses could be accommodated, the material is most durable under compression. Hence, SLS Nylon-12 or plain granular-solid structures alike are ideally suited for structures under compression, which forms the next stage of this research.

6

Investigation of Heat Transfer across Fully Divided Granular-solid Enclosures

6.1 Introduction

The work presented in this chapter attempts to uncover the heat transfer in enclosures fully divided by thin partitions. The types of structures considered were basic rectangular enclosures with fixed external dimensions with shallow rectangular 'subenclosures' of varying width to height (w/h) aspect ratios. Four experimental models were constructed for the purposes of the thermal resistance (R-value) tests performed using the EN 12667 standard. The type of apparatus used was the single specimen guided hot plate method. The overall drop in heat fluxes (q) and increase in R-values were obtained for each layout with varying w/h ratio, due to the increase in N partitions. In addition to the R-value tests, an additional experiment was conducted to determine the effective thermal conductivity (k_{eff}) of the material used. The outcome of the investigation forms the basis of the Discretisation by Partitioning Method (DbPM).

6.2 Correlation of effective thermal conductivity

Due to the physical properties of SLS Nylon-12, additional steps were required to obtain its k_{eff}. As previously noted, SLS Nylon-12 is essentially a solid-fluid composite, with the solid particle phase distributed as the skeleton and the fluid phase filling the remaining space, as Fig. 6.1 shows. If the temperature variation across each solid particle T_s is negligibly small, compared to that across many particles, it could be assumed that the particles and the adjacent fluid temperature T_f are in local thermal equilibrium ($T_f = T_s = T$). Hence, k_{eff} can be used to describe the heat transfer across a

granular-solid medium. If the thermal conductivity (k_s) of the solid matrix and fluid filler medium (k_f) is known, k_{eff} can be obtained empirically (Kaviany, 1999).

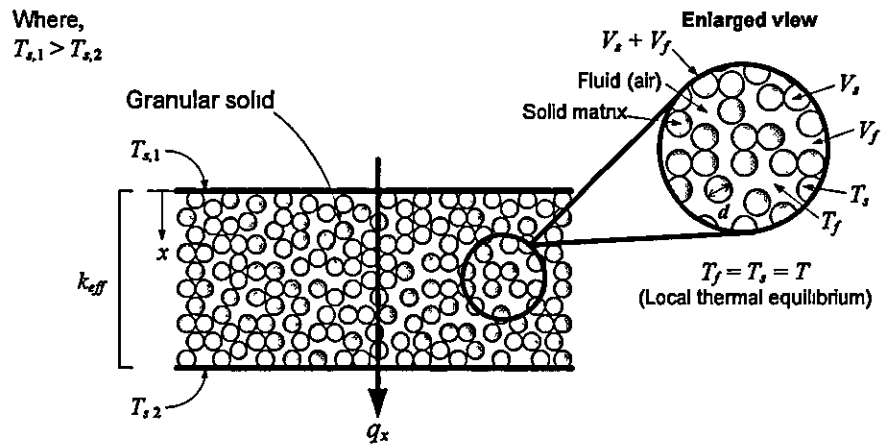

Fig. 6.1 Effective thermal conductivity of randomly arranged granular constituents-air composite showing local temperatures for fluid and solid phase (Kaviany, 2002)

In a porous granular-solid material, besides conduction and convection, heat is also transferred by radiation. However, in this research, due to the low operating temperatures and flow assumed within building structures, radiation is not expected to be significant and neglected significant without loss in accuracy. This assumption is valid, since solid surfaces emit noticeable radiation in excess of 800 K (Çengel, 1998).

In granular materials, k_{eff} may be affected by the arrangements of particles. For granular materials with random solid particles, the k_{eff} may be assumed to be the same in all directions (i.e. isotropic). If particles are not randomly arranged, k_{eff} will be direction dependent (i.e. anisotropic). An example of the k_{eff} of a granular material consisting of randomly packed monosize spherical particles with fluid filled interstitial spaces is shown in Fig. 6.1. Here, the porosity (φ_p) or void ratio is defined as

$$\varphi_p = \frac{V_f}{V_s + V_f} \tag{45}$$

where V denotes volume, and subscripts f and s denotes fluid and solid respectively. k_{eff} is correlated using various related parameters and properties. According to Kaviany (1999), for granular materials with randomly arranged solid particles in fluid phase, the correlation for k_{eff} as a function of φ_p and k_s and k_f is

$$k_{eff} = k_f \left(\frac{k_s}{k_f} \right)^{0.280 - 0.757 \log(\varphi_p) - 0.057 \log\left(\frac{k_s}{k_f}\right)} \quad (46)$$

where $0.2 < \varphi_p < 0.6$. For compacted dense granular solids which $\varphi_p < 0.2$, the material can be treated as a solid substance and k_s is taken to be the thermal conductivity.

Alternatively, the value of k_{eff} could be determined by means of physical experiments in which the apparatus and procedures are presented in the following sections. Due to the low porosity of consolidated Nylon-12 ($\varphi_p \approx 13\%$) based on the maximum density of $\rho \approx 1100$ kg/m^3 (Lombera *et al.*, 1999), k_{eff} should ideally be determined from experiments.

6.3 Experiment apparatus and procedures

The aim was to determine experimentally the value of k_{eff} of consolidated granular-solid SLS Nylon-12, and to establish the trend in the decrease in heat transfer in enclosures due to the presence of parallel partitions. Both these experiments could be performed using the same apparatus. Two sets of experimental apparatus were identified; (i) the hot box (HB) and (ii) guarded hot plate (GHP) method. Due to strict calibration standards and accuracy required, the experiments were outsourced. The details of the test methods are given in Table 6.1.

Table 6.1

Details of test methods of the hotbox (HB) and guarded hot plate (GHP) apparatus

Test method	Hot box (HB)	Guarded hot plate (GHP)
Apparatus standard	BS EN 1934	BS EN 12667
Specimen (orientation)	Vertical (|)	Horizontal (–)
Direction of heat flow	Horizontally left to right (→)	Vertically downwards (↓)
Laboratory (Location)	National Physics Laboratory (NPL, Middlesex)	Thermal Measurement Laboratory (University of Salford, Salford)
Cost per test specimen (£)	£2820[5]	£460[6]

5 Cost per test specimen per experiment of National Physics Laboratory, Middlesex, U K.
6 Cost per test specimen per experiment of Thermal Measurement Laboratory, University of Salford, Salford, U K

In view of the configuration of enclosures, the HB method would be the obvious choice. Due to cost constraints, the method was not feasible. Instead, the experiments were performed using the GHP method. Despite the differences in configuration of the thermal boundary conditions, the predicted outcome of the increasing trend of *Nu* with the increase in Ra is expected to be similar (Nishimura *et al.*, 1989). Hence, the GHP apparatus was seen as a good substitute method. At this stage, optimisation of the partitioning discretisation layout was not performed. Ideally, the test should cover a complete set of enclosure models. Due to the cost of manufacturing and experiments per specimens, test on selective was seen to be sufficient to determine the threshold point of the reduction of the density of heat flow rate.

6.3.1 Guarded hot plate apparatus

Fig. 6.2 shows the schematic diagram of the single specimen GHP apparatus. The main components are the heating unit, metering area, edge insulation, auxiliary guards and cooling unit.

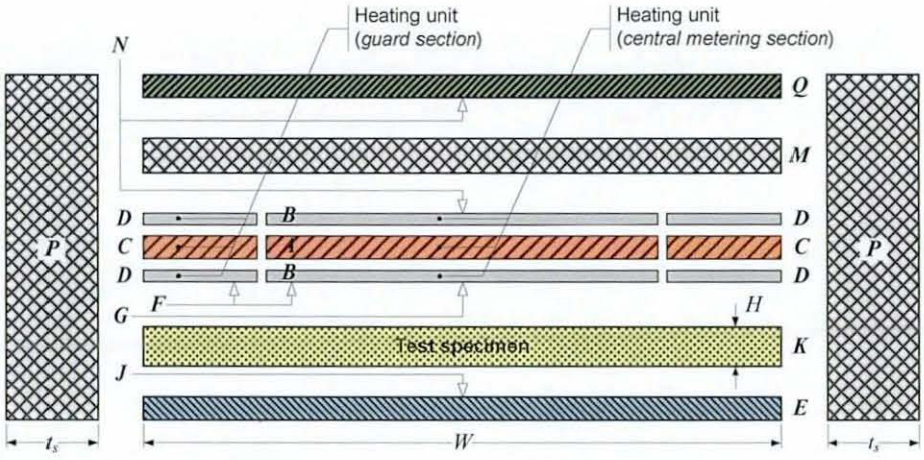

Key

A	Metering section heater	*K*	Test specimen
B	Metering section surface plates	*Q*	Guard plate
C	Guard section heater	*P*	Edge insulation
D	Guard section surface plates	*M*	Guard plate insulation
E	Cooing unit	*N*	Guard plate differential thermocouples
F	Differential thermocouples	*W*	Specimen width
G	Heating unit surface thermocouples	*H*	Specimen height
J	Cooling unit surface thermocouples	t_s	Insulation thickness

Fig. 6.2 Schematic diagram of the single specimen guide hot plate (GHP) experimental apparatus

The heating unit consists of a separate central metering section (*A*), where unidirectional constant and uniform density of heat flow rate (*Q*) is established, which

is surrounded by a guard section. The test specimen is sandwiched in between the heating and cooling units. The temperature sensors used are chromel/alumel (*K*-type) thermocouples mounted in the grooves of the heating and cooling plates. In order to minimise heat loss, the experimental apparatus was covered with edge insulation.

Fig. 6.3(a) shows the experimental test rig used. The edge insulation of 125 mm thickness and auxiliary guards provide additional insulation when operating above or below room temperature. Dots '*F*' and '*G*' indicate the approximate location of the thermocouples on the heating unit. The approximate position on the opposite surface is indicated by the circle. The cooling unit below the test specimen is an aluminium plate which is maintained at a uniform temperature by a liquid circulation duct. The apparatus was contained in an ambient control box which internal air temperature is maintained within ± 2.5 °C. An additional mass weight was used to press the apparatus units against each other to improve the specimen-apparatus contact (Fig. 6.3b).

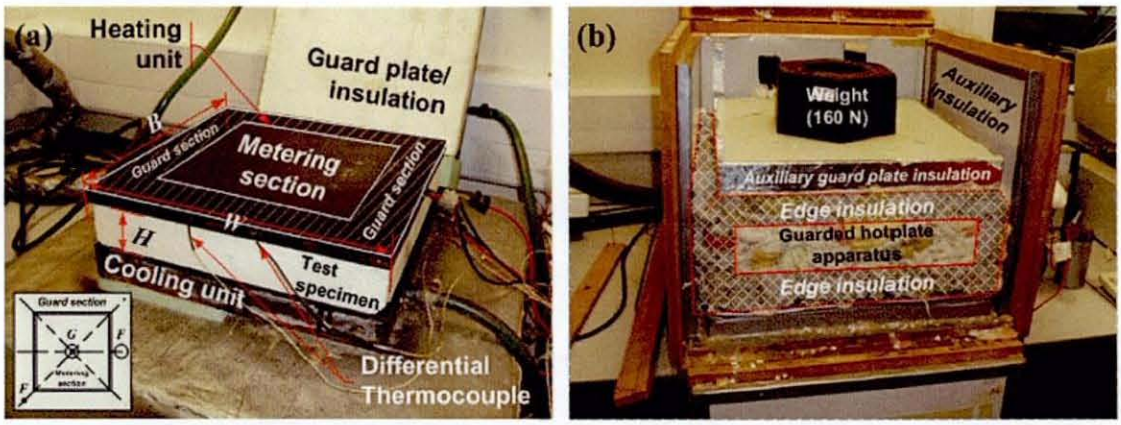

Fig. 6.3 Single specimen guarded hot plate apparatus: (a) Components of the test rig; (b) edge insulation and ambient control box of test rig.

The apparatus was used to establish within specimens with flat parallel edges, in the form of slabs, a unidirectional constant and uniform density of Q at the central metering section. Measurements of q are determined from Q and the metering area (A), perpendicular to the direction of heat flow. The temperature difference (ΔT) across the specimens was measured by the thermocouples. R was calculated from the knowledge of Q, A and ΔT using

$$R = \frac{T_1 - T_2}{Q} A \tag{47}$$

From the additional knowledge of the thickness (H), the specimen thermal conductivity (k) or the apparent thermal conductivity (k_a) and resistance ($1/k$) could be calculated using

$$k = \frac{QH}{A(T_1 - T_2)} \tag{48}$$

6.3.2 Test specimens

The test specimens had contact areas large enough to cover the surfaces of heating and cooling plates. The test specimens were designed to operate in the range of low Nu. They were in the shape of rectangular slabs with external dimensions of 305 mm × 50 mm × 305 mm. The specimens consisted of a main rectangular enclosure with uniform section thicknesses (t) supported by two vertical 'columns', which in this case coincidentally act as thermal bridges. These separated the enclosure into three subenclosures of equidistant width (w). In each subenclosure, the number of partitions (N) was varied from of $N = 0$ to $N = 5$. The thickness of the partitions (t_p) was kept fixed and equidistantly spaced (h_N) parallel to each other. In actual applications, direct thermal bridging should be avoided. Here, the vertical columns provide additional reinforcements and minimise the deflections of the top face shell members, under the loads exerted by the apparatus to less than ± 0.5% of the specimen thickness, such that the good contact specimens/apparatus is achieved. For the case of the experiment to determine the k_{eff}, a solid slab was used. Fig. 6.4 shows the front cross-sectional geometry of the test specimens with dimensions given in Table 6.2.

Table 6.2
Geometric parameters of test specimens

Width	(W, B)	305 mm
Height	(H)	50 mm
Partition length	(w)	92 mm
Enclosure thickness	(t)	7 mm
Partition thickness	(t_p)	2 mm
Subenclosure height	(h_0)	36.8 mm
Subenclosure height	(h_1)	17.42 mm
Subenclosure height	(h_3)	7.72 mm
Subenclosure height	(h_5)	4.48 mm

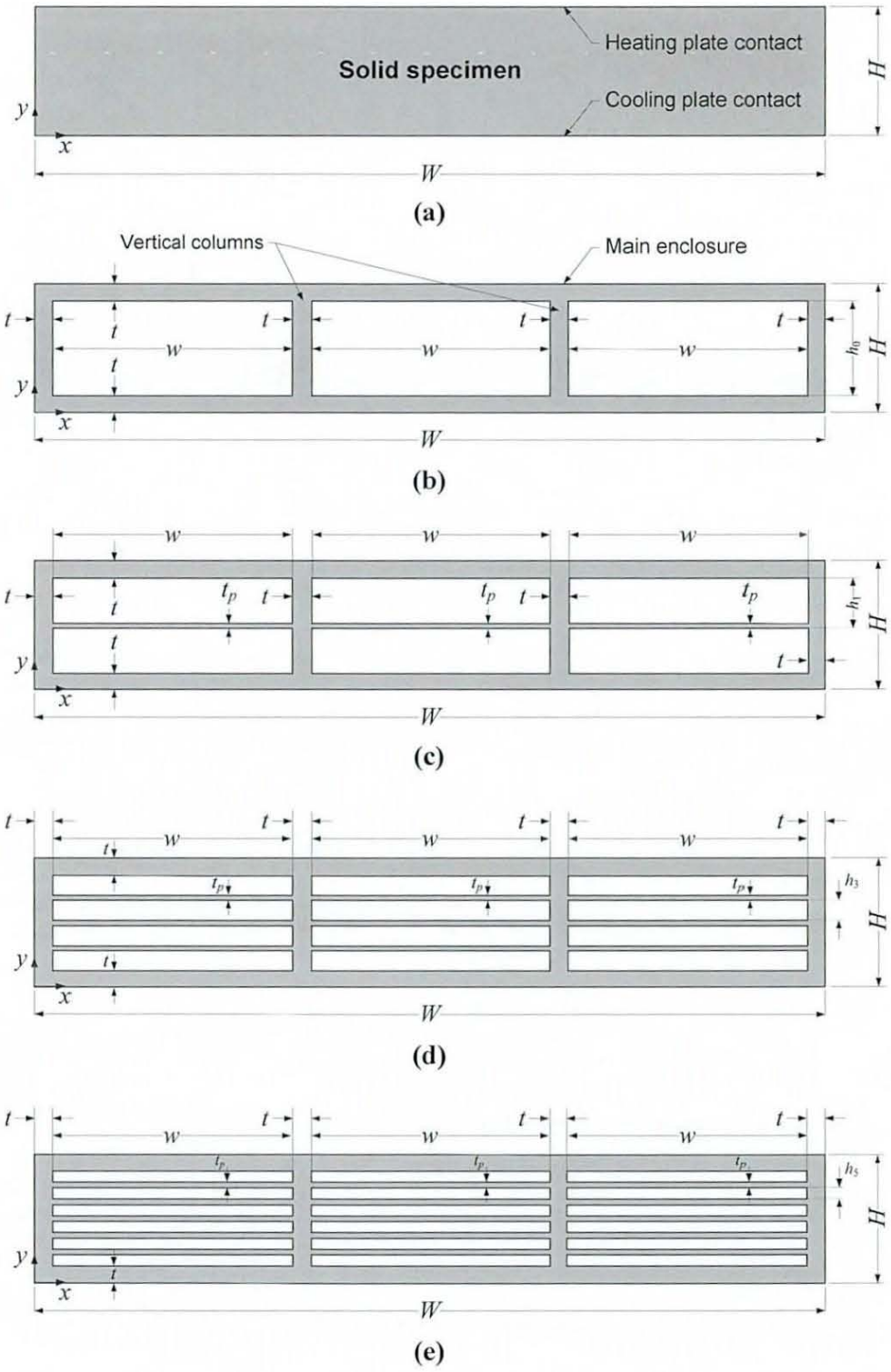

Fig. 6.4 Schematic diagrams of guarded hot plate apparatus test specimens: (a) Solid slab; (b) $N = 0$; (c) $N = 1$; (d) $N = 3$; (e) $N = 5$.

6.3.3 Manufacturing of test specimens

The test specimens, including the solid specimen, were built on a 3D Systems Vanguard-SI LS machine. The material used was powder Duraform PA^{TM} Nylon-12, consisting of a standard refreshed mix of approximately 70% used and 30% virgin powder. The machine process parameters used are given in Section 5.6.2. An example of the SLS build orientation of the test specimens is depicted Fig. 6.5.

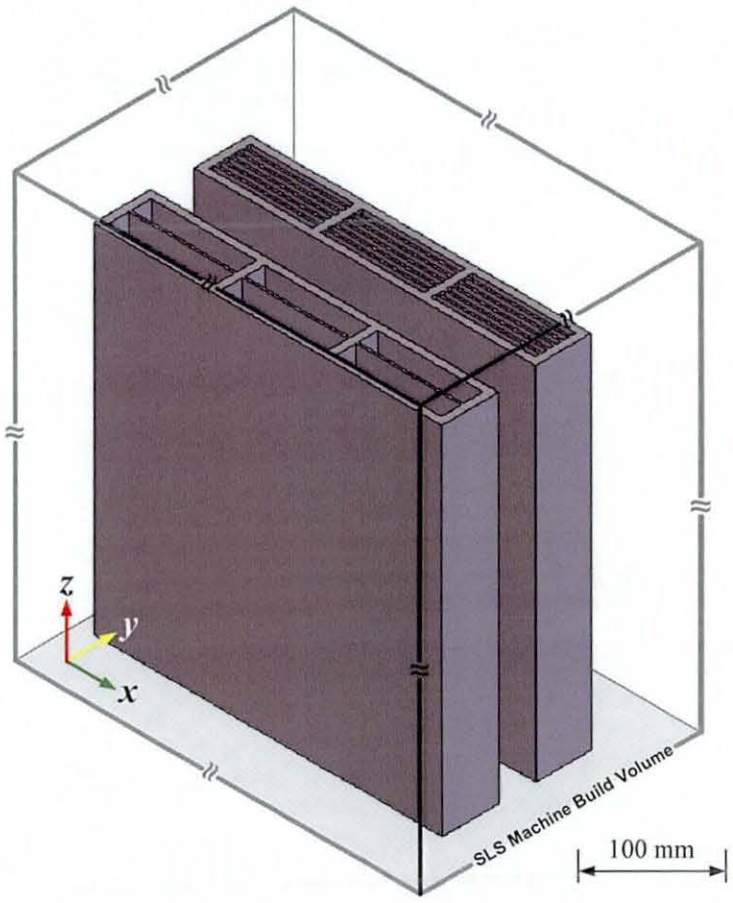

Fig. 6.5 SLS build configuration of partitioned enclosure test specimens (isometric view)

To accommodate for shrinkage during cooling, the specimens were designed and built oversized by 2 mm on the external faces and machined to the recommended dimensions. Due to the large bulk sizes of the specimens, only two could be manufactured in each build. The estimated build time for two specimens per build was approximately 48 hours. Upon the completion of each build, the specimens were allowed to cool at room temperature for approximately 48 hours prior to removal of the unsintered powder.

6.3.4 Post-processing and preparation of test specimens

Face machining was performed using a hardened-steel fly cutter. Due to the low melting point of the material, a low machine spindle speed of 2000 RPM, with a feed rate of 150 mm/min, and depth of cut of 0.5 mm/pass. The use of an end mill was not recommended because heat generated by the tool rotation would cause the sintered layers to delaminate. Due to the high machining times required for each specimen, two milling machines were used. Each was setup to hold the specimens in a horizontal and vertical orientation respectively, so that the contact surfaces and edges could be machined in an alternating fashion, as Fig. 6.6(a) and (b) shows.

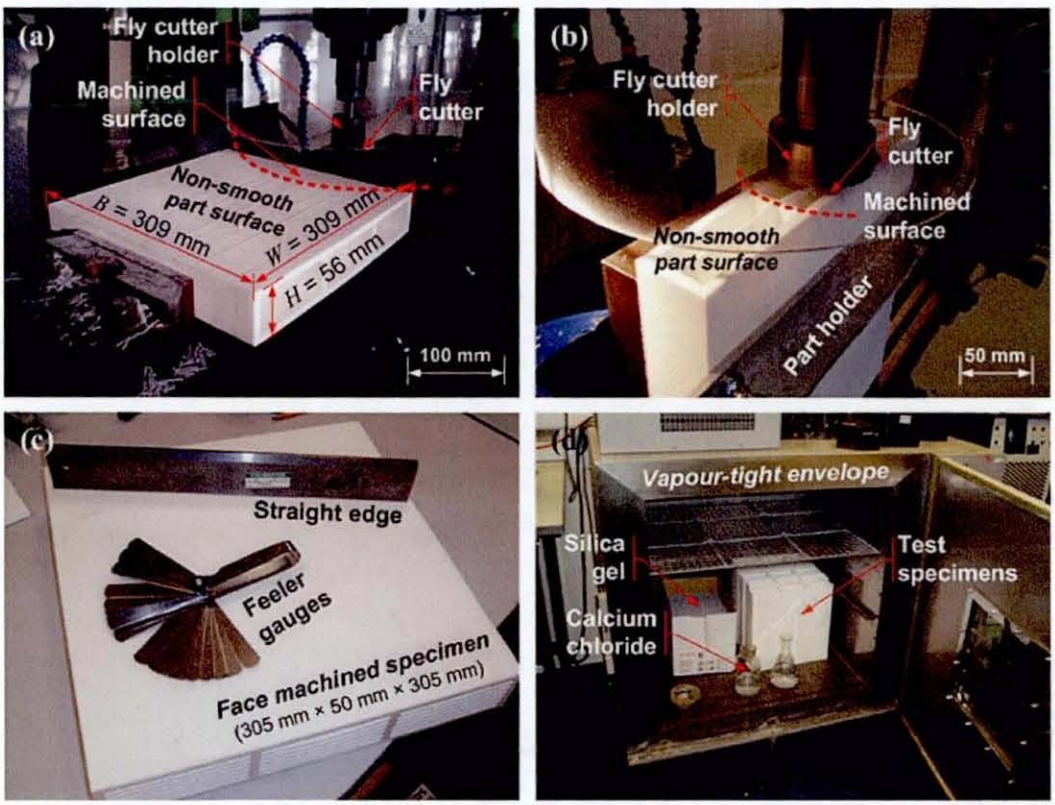

Fig. 6.6 Post-processing and preparation of test specimens: (a) Contact surface machining; (b) opening edge surface machining; (c) surface flatness inspection; (d) specimen conditioning.

All specimens were machined to final dimension of 305 mm × 305 mm × 50 mm, with a minimum flatness tolerance of ± 0.08 mm to minimise contact resistance. Surface flatness was measured using a 'straight-edge' held against the specimen surface (Fig. 6.6c). Surface deviations were determined using 'feeler gauges' along a straight lines of four edges on the contact surface, two diagonal and a centre cross. Prior to the experiments, the specimens were conditioned to a constant mass by drying in a vapour-tight envelope to prevent moisture migration to or from the test specimens during the

tests (see Fig. 6.6d). This is an important procedure because the accuracy may be affected due to the presence of moisture in the specimens. The relative change in mass (Δm) was calculated from the mass determined before and after drying.

$$\Delta m = (m_1 - m_2)/m_2 \tag{49}$$

where m_1 and m_2 are the mass before and after specimen drying, respectively.

6.3.5 Experimental procedures

Before the specimens were mounted in the apparatus, their mass was determined such that the change in mass, due to moisture absorption prior to the tests, was $\pm 0.5\%$. Thickness measurements were taken at gauging points at the outer four corners and the centre of the contact surfaces. The thickness was determined from the average difference in the distance between the gauging points, when the specimens were placed in the apparatus, with the force exerted by the auxiliary weight pressed against the apparatus unit. From the measured thickness and the mass determined from the conditioned specimen, the density (ρ_0) prior to testing can be calculated as

$$\rho_0 = m_2/V \tag{50}$$

where ρ_0 and V are the density and volume of the conditioned specimen as tested.

The temperature drop ΔT across the specimens, corrected for the thermocouple penetration at the contact surfaces of the heating and cooling unit, was set to 10 °C. The average electrical power supplied to the metering area was measured to within 0.1%. Fluctuations or changes in the temperatures of the heating unit surfaces during the test, due to fluctuations or changes in the input power was maintained within 0.3% of the temperature difference between the heating and cooling units. The power input of the guard section was maintained by automatic control, to obtain the degree of temperature balance between the metering and guard suction that is required to keep the sum of imbalance and edge heat loss errors within 0.5%. The average elapsed and settling time for each test was 135 hours, until the values of the thermal resistance of each specimen do not differ by more than 1%.

6.4 Numerical modelling procedures

The computational grids constructed in Gambit™ (see Fig. 6.7) were exported to Fluent™ CFD code, where the steady-state heat transfer and fluid velocity profiles in the partitioned enclosures. 2D steady-state conjugate natural-convection-conduction was considered. The heat transfer in the divided air filled cavities was modelled as 2D steady-state laminar convection. The working fluid was assumed to be incompressible with constant thermal physical properties, except for density which was assumed to be temperature independent, adhering to the Boussinesq approximation. The buoyancy effects on momentum transfer were taken into account through the Boussinesq approximation. Fluid viscous dissipation and compressibility were neglected. In the solid medium, 2D conduction heat transfer was considered. The dimensionless governing assumptions for the conjugate heat transfer problem can be written in terms of vorticity, stream function, and temperature is as follow (Ho and Chang, 1993). In the fluid region;

$$\frac{\partial \psi}{\partial x}\frac{\partial \omega}{\partial y}-\frac{\partial \psi}{\partial y}\frac{\partial \omega}{\partial x}=\mathrm{Pr}\left(\frac{\partial^2 \omega}{\partial y^2}+\frac{\partial^2 \omega}{\partial x^2}\right)+\mathrm{Pr}\,\mathrm{Ra}\frac{\partial \theta}{\partial y} \tag{51}$$

$$\frac{\partial^2 \psi}{\partial y^2}+\frac{\partial^2 \psi}{\partial x^2}=-\omega \tag{52}$$

$$\frac{\partial \psi}{\partial x}\frac{\partial \theta}{\partial y}-\frac{\partial \psi}{\partial y}\frac{\partial \theta}{\partial x}=\frac{\partial^2 \theta}{\partial y^2}+\frac{\partial^2 \theta}{\partial x^2} \tag{53}$$

In the solid partitions/regions;

$$\frac{\partial^2 \theta}{\partial y^2}+\frac{\partial^2 \theta}{\partial x^2}=0 \tag{54}$$

The boundary conditions of the enclosures (see Fig. 6.7), in dimensionless form is

$y=0;\quad \psi=0,\quad \theta=0$

$y=1;\quad \psi=0,\quad \theta=1$

$x=0;\quad \psi=0,\quad \dfrac{\partial \theta}{\partial x}=0$

$$x = 1; \quad \psi = 0, \quad \frac{\partial \theta}{\partial x} = 0 \tag{55}$$

The continuity of the temperature fields and conservation of the energy at the surfaces of the solid partitions/regions exposed to fluid require that

$$(\theta)_f = (\theta)_s; \quad \left(\frac{\partial \theta}{\partial x}\right)_f = \frac{k_s}{k_f}\left(\frac{\partial \theta}{\partial x}\right)_s, \quad \left(\frac{\partial \theta}{\partial y}\right)_f = \frac{k_s}{k_f}\left(\frac{\partial \theta}{\partial y}\right)_s \tag{56}$$

The average heat transfer coefficient of the fluid-wetted partitions/regions of the enclosure is presented as an average Nusselt number in the form of

$$Nu = \frac{q_N}{k_f(\Delta T)} \tag{57}$$

where q is the average heat flux at the fluid-wetted hot wall surfaces. Subscript N denotes the number of number of partitions. In this study, all cases were evaluated for Rayleigh number in the range of $Ra \approx 2000$. The working fluids in the sub-enclosures were air with Prandtl number of 0.71. Table 6.3 shows the thermal physical properties and the initial conditions used in the CFD models.

Table 6.3

Thermal physical properties used in numerical models of enclosures

Thermal conductivity (solid)	(k_s)	0.25 W/m^2
Thermal conductivity (fluid) at T = 300 K	(k_f)	0.0263 W/m^2
Density of (solid)	ρ_s	970 kg/m^3
Density of (fluid)	ρ_f	1.1614 kg/m^3
Specific heat capacity (solid)	c_p	1007 J/kg·K
Specific heat capacity (fluid)	c_p	2350 J/kg K
Dynamic fluid viscosity	μ	1.846 × 10^{-5} kg/m s
Coefficient of thermal expansion	β	0.00344 (1/T)
Gravitational acceleration	g	9 81 m/s^2

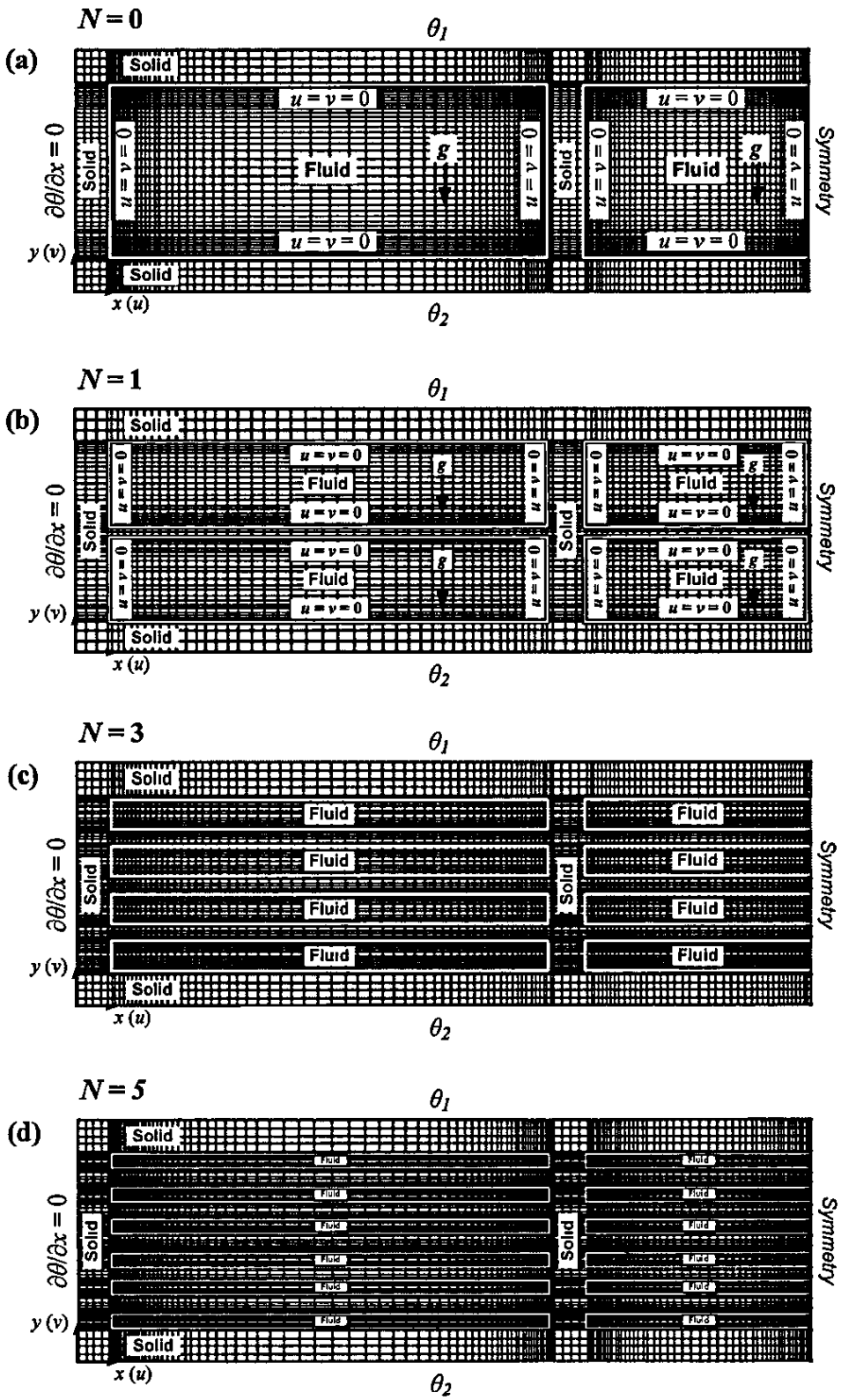

Fig. 6 7 Computational grids of the analysis of the horizontal test specimens· (a) $N = 0$, (b) $N = 1$; (c) $N = 3$; $N = 5$.

6.4.1 Computational procedures

The equations (51) to (54) with the respective boundary conditions (55) and initial conditions as previously stated defined were solved through a control-volume formulation of the finite difference method. The pressure-velocity coupling was handled through the SIMPLE algorithm by Patankar and Spalding (1972). The power-law discretisation scheme recommended by Patankar (1980) was used for the evaluation of the interface convection fluxes. A second order backward scheme was used for time stepping. Starting from the assigned values of the dependent variables (i.e. assigned initial temperature and velocity fields through the enclosure); at each time step the discretised governing equations were solved iteratively through a line-by-line application of the Thomas algorithm. Under relaxation was used to ensure the convergence of the iterative procedure. Time discretisation was chosen to be uniform. Within each time step, the spatial solution was considered to be fully converged when the maximum absolute values of both the mass source and the percent changes of the dependent variables at any grid node from iteration to iteration are smaller than the prescribed values of 10^{-6} and 10^{-5} respectively.

6.5 Results and discussion

6.5.1 Heat and fluid flow fields

The heat transfer rate across the enclosures was measured electronically. The results from the experiments revealed the rate of heat transfer but not their characteristics. This was determined by plotting the steady-state isotherm contours obtained from numerical analyses, as Fig. 6.8 and Fig. 6.9 shows. In all, the isotherms remain almost parallel to the upper and lower walls and the dividing partitions. The isotherms were not affected by the increase in the number of partitions and vary linearly across the solid and fluid regions. The horizontal partitions remained isothermal, indicating a uniform heat flux and that heat transfer is conduction dominated. With the current enclosure configuration, the density of the working fluid does not decrease in the direction of the gravitational force. Therefore, the conditions in the fluid are stable. Only a minute trace of fluid motion at the vicinity of the vertical columns could be observed. The heat transfer of horizontal enclosures has no effect on subenclosure

aspect ratios. The findings were consistent with those found by Nishimura *et al.* (1989).

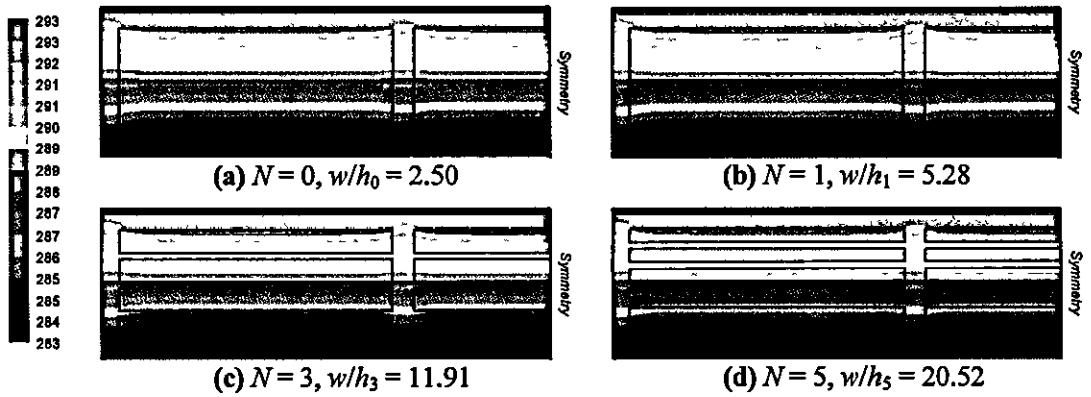

Fig. 6 8 Steady-state isotherms of test specimens from guarded hot plate apparatus: (a) $N = 0$, (b) $N = 1$; (c) $N = 3$; (d) $N = 5$ Dimension in Kelvin (K)

The stream functions (ψ) in the fluid regions are represented by pairs of diagonally symmetric counter-rotating cells at the vicinity of the conducting bridges, where minute traces of fluid motion are present, as Fig. 6.9 shows. The size of the cells and the value of the ψ_{max} are observed to decrease with increasing N. The ψ_{max} decreases by approximately two orders of magnitude. Given that thermal boundary layers are not present and that the fluid remained relatively stagnant, the effects of convection may be negligible. In contrast, the fluid regions in between the middle of the cells remained stagnant and heat is expected to be transferred predominantly by means of conduction.

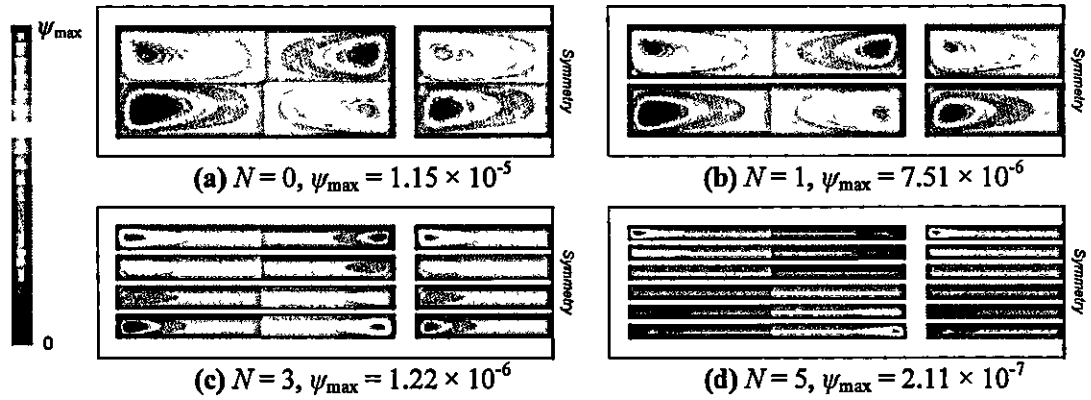

Fig. 6 9 Stream function (ψ) of test specimens from guarded hot plate apparatus (a) $N = 0$, (b) $N = 1$; (c) $N = 3$; (d) $N = 5$. Dimension in m^2/s

6.5.2 Heat transfer results

The heat transfer rate across the enclosures was measured electronically, from the power dissipated by the heating unit (see page 118). The heat transfer quantities of interest, the k_a and R-value, were calculated using equations (47) and (48). Fig. 6.10 conveys the results of k_a and R-value, for $N = 0$ to $N = 5$.

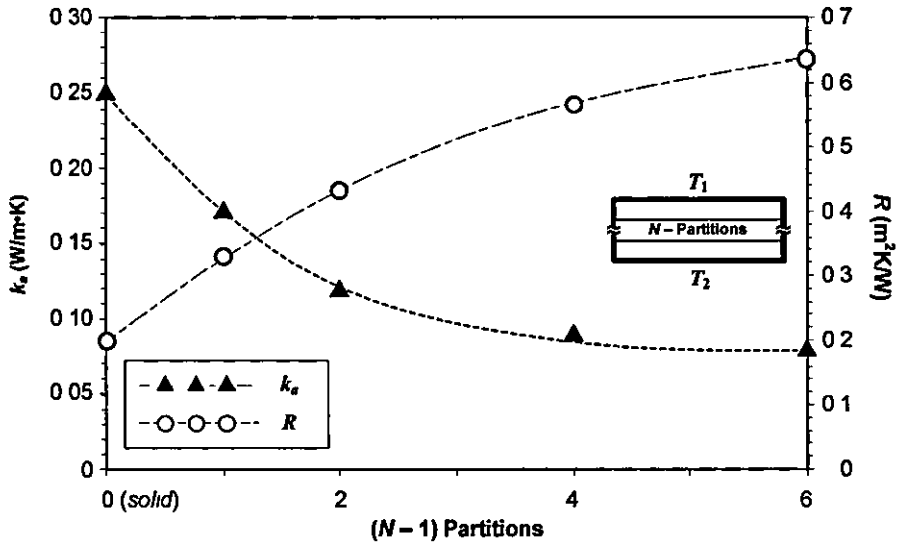

Fig. 6.10 Apparent thermal conductivity (k_a) and thermal resistance (R-value) vs. $N-1$ partition

The R-value of the specimens increases due to the increase in the number of partitions. Despite the orientation of the thermal boundary conditions, the dependence of k_a and R-value on N not proportional and tended to diminish with increasing N. From the experiments, q and R-value was found to vary by approximately 56%, when N number of partitions is increased from 1 to 5.

For the case of the solid slab specimen, the value k_{eff} was found to be approximately 0.25 W/m·K. In contrast, this figure was higher than the thermal conductivity of an equivalent material, sintered PA2200 Nylon-12 ($k = 0.144$ W/m·K measured using DIN 52616 standard), obtained from the material data sheet. In this case, the experimentally measured k_{eff} and data sheet given k differ by approximately 42%. The thermal material properties of solids, particularly those build using AMT's, should ideally be determined through experiments. Parts built on the same machine using different machine settings may have different properties.

Table 6.4 summarises the heat transfer results of the horizontal enclosure obtained from the GHP apparatus.

Table 6.4

Summary of result from guarded hot plate GHP experiments of enclosures with $N = 0$ to $N = 5$

Partitions	w/h ratio	V_s/V_f ratio (φ)	Heat flux, q (W/m^2)	R-value (m^2-K/W)
$N = 0$	2.5	0.328	40.17	0.272 ± 4.1%
$N = 1$	5.28	0 364	30.76	0.421 ± 4.5%
$N = 3$	11.91	0.437	19.85	0 565 ± 4.5%
$N = 5$	20 52	0.509	17.86	0.635 ± 4 5%

To further quantify the effects of the heat transfer of the horizontal partitions, Nu and q is plotted against N (see Fig. 6.11a). The correlation used for the horizontal enclosures is based on the correlation recommended by Nishimura *et al.* (1989).

$$Nu = 0.158\left[\frac{Ra}{(N+1)^4}\right]^{0.283} \tag{58}$$

The results show that Nu for no the enclosure with no partitions ($N = 0$) was in good agreement with heat transfer characteristics expected from the configuration of test specimens. This confirmed that heat transfer across the undivided airspace was conduction dominated. Conversely, the decease in Nu and q with increasing N is not proportional. However, the presence of partitions did not produce a proportional reduction in heat transfer rate. Fig. 6.11(b) shows the effect of the w/h_N ratio of subenclosures on decreasing Nu. Given that conduction is the dominant mode, the reduction of Nu was observed to be most profound for the first two partitions. Accordingly, heat was transferred by means of pure conduction. In all, Nu and q decreases by 85% and 56% respectively, as a result of the increase in N and subenclosure aspect ratio.

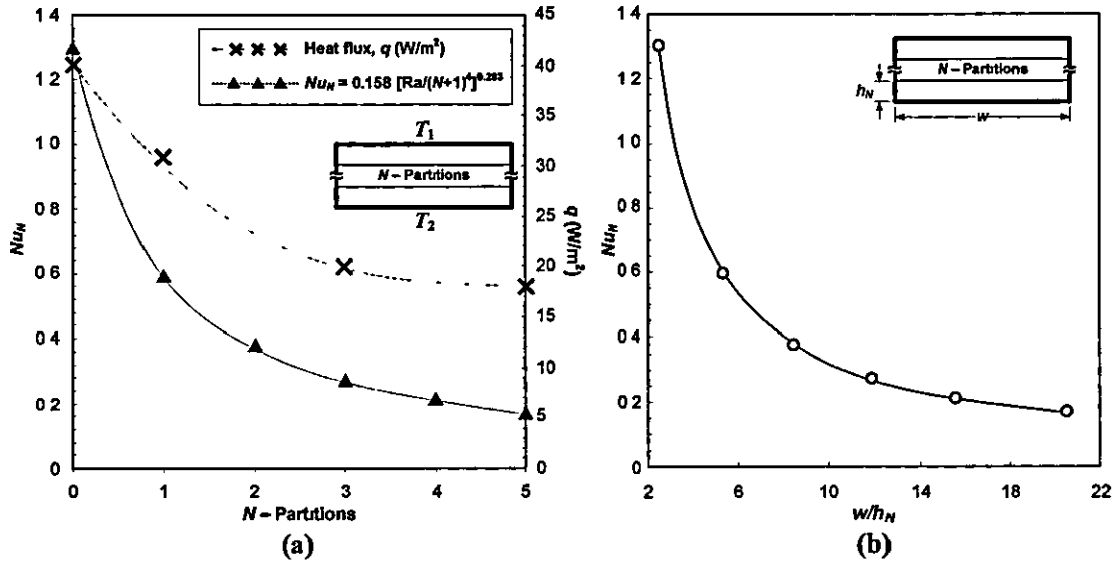

Fig 6 11 Experimental results of horizontal enclosures. (a) Reduction of heat flux q and Nu vs. N, (b) reduction of Nu vs the increase in subenclosure w/h_N ratio

Fig. 6.12(a) shows the relationship of Nu and q in terms of φ. The increase in φ yielded a non-proportional reduction in both Nu and q, but diminishes with increasing N. This is expected as the increase in volume of the solid medium with higher conductivity would lead to increased conduction. Fig. 6.12(b) presents the relationship of the φ and h_N/h in terms of N.

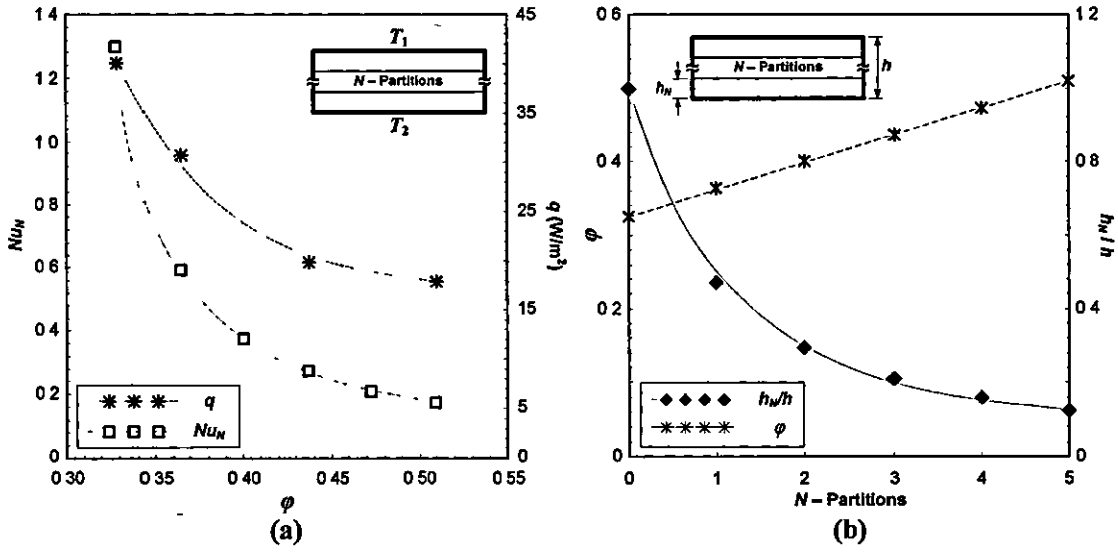

Fig. 6.12 Experimental results of horizontal enclosures. (a) Effect of fluid/solid volume fraction (φ) on Nu_N and q, (b) effect of N on φ and h_N/h

As expected, the introduction of partitions with uniform thicknesses yielded a proportional increase in φ (or mass) and a non-proportional decrease in the

subenclosure h_N/h aspect ratios. In terms of engineering application, the efficiency (η) of the partitions decreases with increasing N. The increase in η was not proportional and decreases with increasing N, as Fig. 6.13 shows.

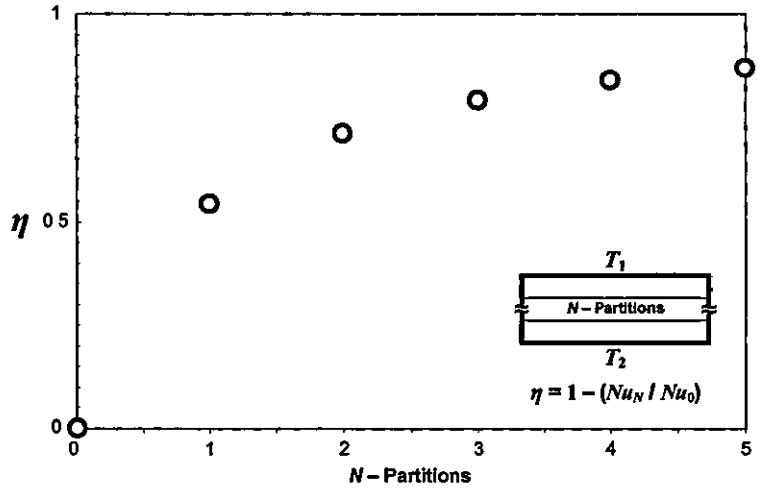

Fig 6 13 Insulation efficiency (η) of vertical parallel partitions as a function of N-partitions

6.6 Conclusions and remarks

From the results, it was deduced that an optimal threshold limit exists, in which the R-value of an enclosure could be maximised by minimising q. This meant that the heat flow rate across enclosures could be controlled and optimally suppressed through use of partitions to discretise the internal airspaces. Theoretically, an optimal thermal solution is one where convection is effectively suppressed. So far, the work focussed on the analysis of heat transfer for a fully divided partitioned enclosure. In Chapter 8, a Discretisation by Partitioning Method (DbPM) is devised and applied to optimise the thermal insulation of a load bearing structure by minimising the heat flow rate across. The trend of the reduction of heat transfer and thermal properties has now been established through the heat transfer experiments, the analyses of the subsequent investigations could be performed using numerical modelling. The upcoming work in Chapter 8 is envisaged to form Stage-2 of the 'two-stage' layout optimisation and discretisation approach for a non-convective structured insulator. The results show a nonproportional reduction in heat transfer. This reduction resembles a polynomial function which suggests that the minima of the curve could give an optimal discretisation, in which formed the basis for the upcoming investigation.

7

Layout Optimisation of Structured Insulator Enclosure

7.1 Introduction

The initial investigation of beam structures demonstrated good correlation between the FEA and physical experiments. The findings formed a basis which paved the way for an investigation on design optimisation of the structural layout of an insulator enclosure. The current study forms Stage-1 of the proposed 'two-stage' design optimisation/discretisation approach for a non-convective 'structured insulator'.

Layout optimisation of the insulator enclosures was performed using the MD method. The objective was to find a continuum structural layout with maximum possible stiffness and minimal volume. The granular material properties calibrated for consolidated SLS Nylon-12 have been used for the FEA of the optimisation models. The type of structure and load cases to be considered was intended to take advantage of the attributes of the material in compression where they are most durable. Accordingly, the optimum structural layout to be sought should ideally produce a 'compressive structure'.

In the 'two-stage' approach, structural integrity was considered as the primary requirement. This had to be addressed before a thermal solution could be determined. The structural layout optimisation covers two loading cases. In this chapter, the basic design considerations are highlighted, along with the design optimisation problems, meshing strategy and post-processing procedures. Results of the layout optimisation of

both the investigated loading cases and the post-processed layout are evaluated. The optimised layout would therefore form the basis of the initial design for the thermal discretisation/optimisation problem, to be addressed in the upcoming chapter.

7.2 Key design considerations

7.2.1 Build/Construction material

A notable characteristic of consolidated SLS Nylon-12 is its apparent brittleness in direct tension. In layout optimisation, the use of the material for structural members subjected to this type of loading should be avoided. From the salient features observed in the initial investigations covered in Chapter 5, SLS Nylon-12 parts share similar characteristics to that of plain concretes, which are best suited for structures under compression with light transverse loads. In addition, tensile failures could be compensated if members are preloaded in compression. The layout to be determined from the optimisation should ideally produce members in direct compression.

7.2.2 Modular construction

The optimisation study of Stage-1 considers a 'modular structure'. A good example is the concrete masonry units (CMU's) used widely in construction, as Fig. 7.1 shows. In application, the units could be bonded to form a wide variety of 'bulk' assemblies (e.g. walls, etc.). In the case of building walls, these are predominantly subject to downward and horizontal loads. This specific case was chosen, as it demonstrates the design problem of a structure with strength and insulation requirements, in its most basic configuration. The problem considered here is a generic one, in the sense that the optimisation approach is applicable in many cases, even for complex loading conditions.

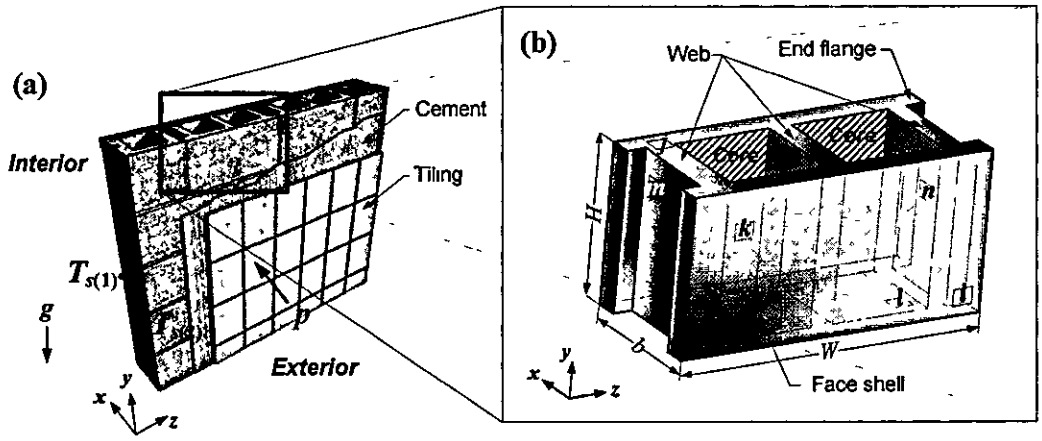

Fig. 7.1 Typical example of modular concrete masonry unit (CMU) load bearing wall: (a) Rectangular 'split-core' CMU wall structure, (b) enlarged view of split-core modular CMU. (*P* denotes pressure loads)

7.2.3 Design and application versatility

CMU's are one of the most versatile building materials used in both structural and non-structural components. Current load bearing versions come under the ASTM C90 Grades 'N' and 'S' (Spence, 1998). Their designs are emphasised on application flexibility, aimed at covering a wide range of generic building applications. As a result, the layout tended to be conservative where the basic design had remained relatively unchanged. Current load bearing CMU's were seen to lack the flexibility in terms of addressing specific building needs. This creates the provision for the design optimisation of such structures.

7.2.4 Integration of functionality

Standard CMU's emphasise on strength requirements and application versatility. As a result, the degree of 'primary insulation' which could potentially be gained from geometric features was often overlooked. In construction, the common approach to increase thermal resistance was to fill up the cores with insulation material. In contrast to a 'multiple material' construction, structural and thermal functionality could alternatively be achieved by means of geometric features. Currently, there are no design standards that apply to the design of modular structures with strength and insulation requirements. The current design approach is largely based on experience and expetimental data from the initial investigations.

7.2.5 Design for AMT's

The drawback of layout optimisation is that the design solutions tended to be 'geometrically' complex. This inhibits conventional means of manufacture. Given the gradual 'shift' of AMT's, from lab and shop floor-based manufacturing towards construction application, the on/offsite fabrication of large scale structures could be made possible though FC in the near future. Using the layer by layer build approach, metre-scale building structures consisting of arrays of optimised modular units could be 'printed', negating the need for secondary bonding material. Some of the potential advantages of this approach include reduced material construction, integration of geometric form and function, savings in build material and freedom of build geometry.

7.2.6 Modular configuration

The layout optimisation focussed on a modular unit structure with width to height aspect ratio of 1:1 (see Fig. 7.2). The split-core configuration with open cores on faces '*j*' and '*l*' of the standard CMU was not adopted. This was because desirable insulation could not be gained. Instead, a cubic structure with open cores on faces '*m*' and '*n*' was used. In contrast, this particular configuration is expected to give better insulation against the internal convective flows. Although lateral stiffness is generally higher with a webbed layout, thermal insulation is severely hampered. To address the structural design problem, an alternative layout was determined using the MD method.

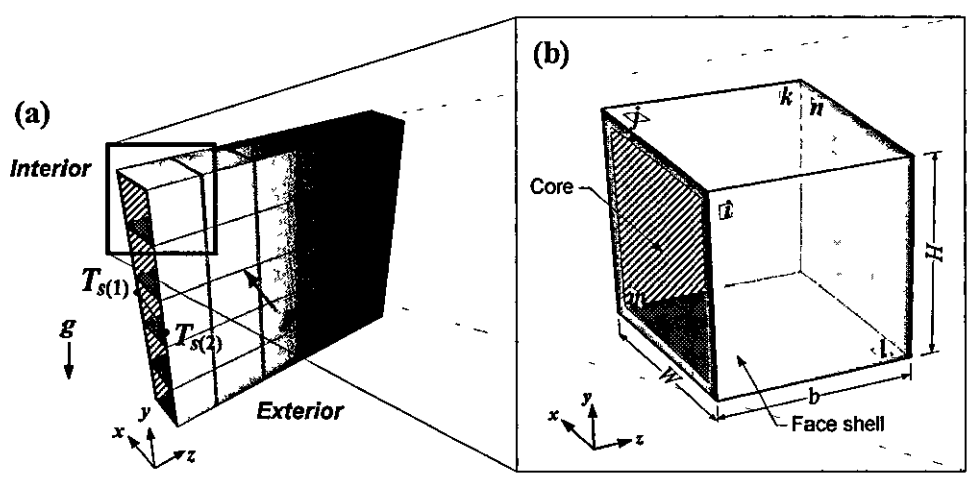

Fig 7.2 Idealised unit cell CMU wall structure. (a) Wall structure consisting of an assembly of discrete cubic structures, (b) enlarged view of a unit cell cube. (*P* denotes pressure loads)

7.2.7 Design constraints

In most design problem, there are bound to be design constraints in order for the design to be feasible. For building structures, such as the case of the walls and floors, the external surfaces were often maintained 'planar'. In most cases, it would be of no useful purpose if a wall or floor were to have non-planer surfaces. In this case, the design constraints 'indirectly' provide means as an 'interface' for other structural members, which may come in contact to form an assembly or as load transfer mechanism. In most building structures however, such geometric design constraints are seldom required by internal layout, in which forms the design domains of the structural layout optimisation.

7.3 Design optimisation problem

The design task is to optimise the cross-sectional layout of an insulator enclosure. The aim was to find a maximum static stiffness design of least weight by minimising compliance, subject to stress and deflection constraints. Fig. 7.3 depicts the schematic diagram of the optimisation problem. In cross-sectional view, the enclosure resembles a 'box' structure with W/H ratio of $S = 1$, void w/h ratio of $s = 1$ and uniform section thicknesses t. The top and bottom face shells are assumed to be bonded to form a wall structure, under loads F acting vertically downwards on face-j, and surface loads P acting horizontally on face-k. In addition, the inner and outer surfaces are subjected to a temperature drop of 10°C across the cross-sectional width, as Fig. 7.3(a) shows.

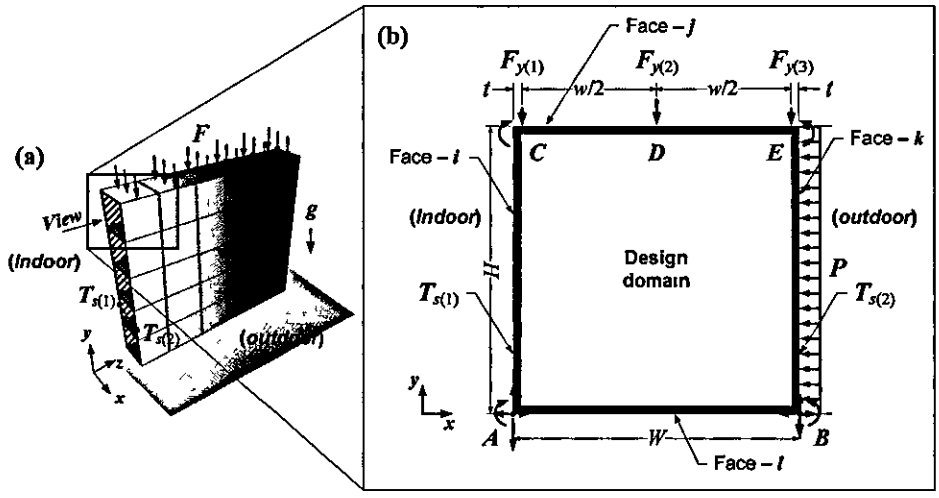

Fig 7.3 Schematic diagram of design optimisation problem (a) applied loads on the bulk assembly, (b) Free body diagram denoting the force and moment reactions (P denotes pressure loads)

The free body diagram depicting the force and moment reactions, which forms the basis of the current design problem, is shown in Fig. 7.3(b). The investigated loading condition is a generic one, analogous to the loads exerted by a 'floor joist' or beam resting on top of a load bearing wall, as Fig. 7.4 shows. If the total deflection is assumed to be small and that the stresses would remain planar. Hence, only a plane strain model was considered. The effects of stresses in the third dimension are negligible. The extruded length b could be defied using a 'real constant' thickness.

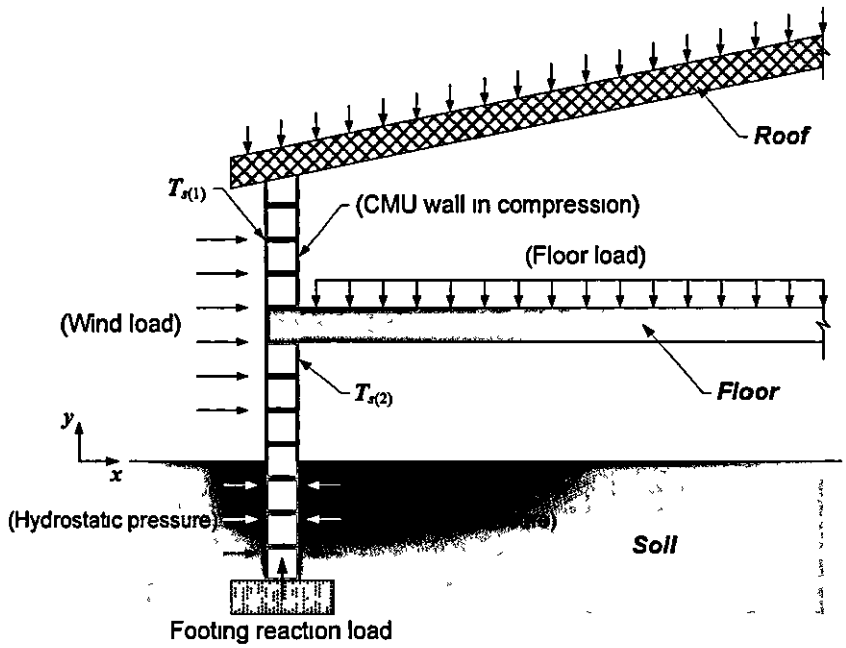

Fig. 7.4 Typical loading condition of a load bearing CMU wall (cross-sectional view)

In this current investigation, the design optimisation covers two loading cases; 'static mechanical load' only and 'coupled-field static mechanical and steady state thermal' loads. The static mechanical load case serves as a basis for results comparison, as well as to demonstrate the significance of the thermal loads on the design outcome.

The design optimisation problem to be solved may be formally stated as

Minimise	m
Subject to	$\sigma_{\max} \leq \sigma_y$
	$\delta_{\max} \leq 0$

where m is the structural mass. In this study, the modular units were designed to support loads $F_{y(1)} = F_{y(3)} = 600$ N and $F_{y(2)} = 1200$ N, at points ***C***, ***D*** and ***E*** respectively, on the top face shell. The corner vertices ***A*** and ***B***, at the bottom face shell, were fixed in the x and y-direction (see Fig. 7.3b). Due to the bimodulus nature of the material, the strength limit σ_{max} for members under bending and tension was $\sigma_{y(t)} = 44$ MPa. For members under compression, $\sigma_{y(c)} = 54$ MPa was used. In the initial investigation, a value was given to δ_{max}. In this particular study however, to find a layout with maximum stiffness using MD, δ_{max} has to be set to zero.

7.3.1 Design optimisation model

Fig. 7.5 shows the schematic diagram of the MD optimisation model. The dimensions of the enclosure are $W = H = 150$ mm, $w = h = 130$ mm, and thickness $t = 10$ mm.

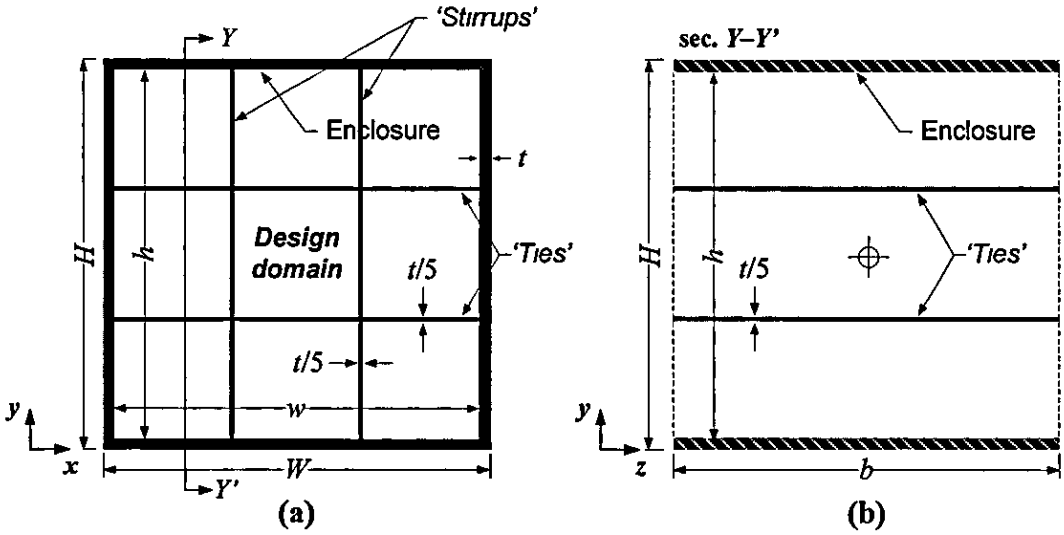

Fig. 7 5 Design domains, shape constraint, loading and boundary conditions of the optimisation model.

The third dimension was not modelled. A thickness constant of $b = 150$ mm was given to account for the extruded length in the z-axis. Growth and degeneration was guided to occur within the 2D rectangular design domain on the x-y plane. A shape constraint was defined, whereby the removal and addition of elements in the non-design domain was restricted. This was to ensure that the external surfaces of the face shells remained planar. Within the design domain, additional elements were used to horizontally and vertically 'tie' the face shells. These elements provide means for initial growth to form initial load paths, but not as additional supports structures. Design constraints was not applied to the 'ties' and 'stirrups'. During the optimisation, these may be removed if

they do not contribute to the static stiffness. For the generalised layout methods, the definition of explicit optimisation parameters was not required; the material distribution function over the design domain serves as the optimisation parameter.

7.3.2 FE modelling of optimisation model

Fig. 7.6 shows the FE discretisation, loads and boundary conditions of the optimisation model. The main enclosure, 'stirrups' and cross 'ties' consists of 5620 and 1028 quadrilateral elements respectively, with element size of 1 mm by 1 mm.

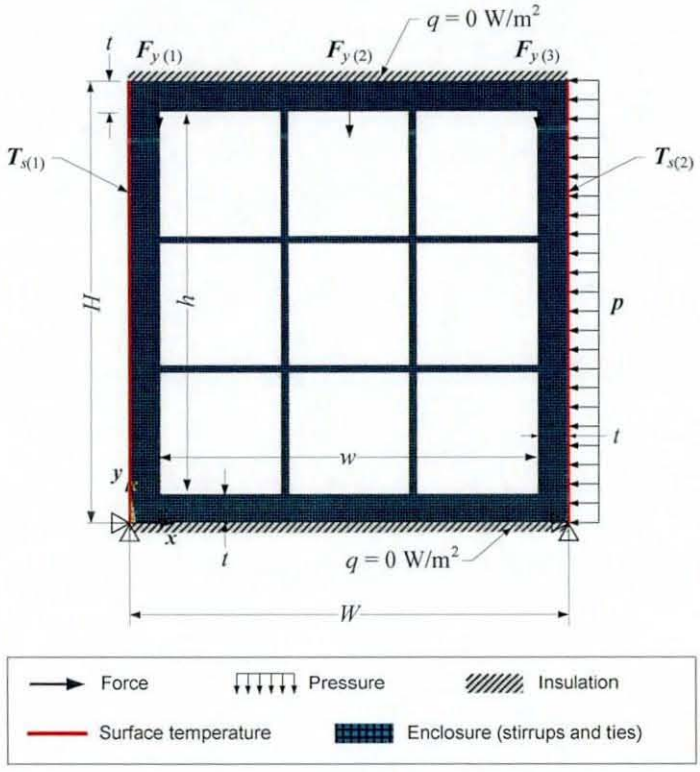

Fig. 7.6 FE discretisation, load and boundary conditions optimisation model.

The MD optimisation model of the structured insulator enclosure was constructed manually using the 'input file' text input approach in ANSYS. First, the FE nodes of the cross-sectional layout of the enclosure were generated. This was followed by the definition of the sequence order of the nodal positions, to form the quadrilateral elements. In the MD method, only the FE model is required but not the geometric features. These procedures were done using the ANSYS commands, instead of the graphical user interface (GUI) method. The 'input file' contains the information of the optimisation model, to be read by the FE code prior to the layout optimisation.

7.3.3 Coupled field analysis

In this current investigation, both the PLANE42 and PLANE55 (the equivalent elements for thermal analysis) elements were used in the optimisation model. To account for the effects of thermal stress, the 'indirect' sequential 'coupled-field' thermal-structural analysis was performed. This involved a combination of analysis from a structural and thermal physics field which interact to solve a global analysis problem. In this method, different databases and results files are maintained, as Fig. 7.7 shows.

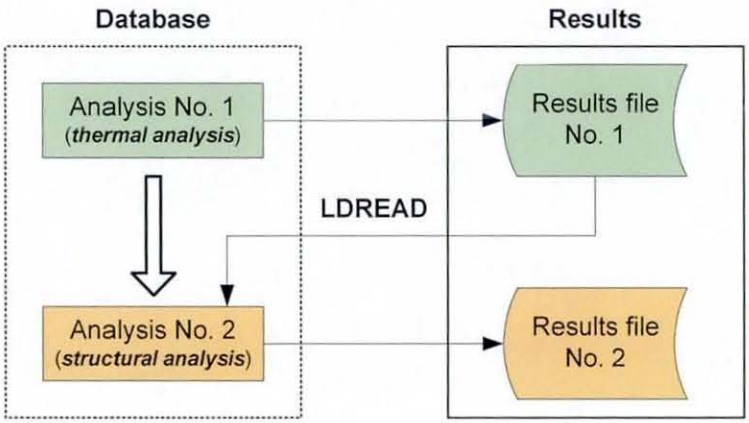

Fig. 7.7 Data flow diagram of indirect sequential coupled-field thermal-structural analysis.

The thermal (*Analysis No. 1*) and structural analyses (*Analysis No. 2*) databases contain the appropriate solid models, nodes, elements, applied loads and boundary conditions. Initially, the model was meshed using the PLANE55 elements and thermal analysis was performed. 'Coupling' was then performed using the 'LDREAD' ANSYS command. The model was then re-meshed the using PLANE42 elements to be structurally analysed. Following that, the results file of the thermal analysis was then transferred, to be applied as body loads in the structural analysis. In this approach, the nodes and elements of the FE models must be consistent between both the analyses databases.

7.3.4 FE discretisation of optimisation model

Within the MD method, two meshing strategies apply in the discretisation of the MD optimisation models. As a standard practice, a finer mesh should be used in the design domains, but not for the whole model. St. Venant's Principle implies that local stresses in one region of a structure do not affect the stresses elsewhere. Hence, a considerably courser mesh can used be in the region of the structure which lie in the non-design domains, subject to permitting a reasonable quality of transition while minimising the number of 'badly shaped' elements. In a FE-based layout optimisation, the discretisation scheme greatly influences the results. As the optimisation could start from either an under-designed or over-designed layout, the ideal discretisation is one in which the final optimised design could achieve mesh convergence. Alternatively, a reasonably finer mesh could be used for regions in the design and non-design domains, the only drawback being the lengthy solution timeline. This was a straightforward approach since and use of a transition mesh was not required, which may have been difficult to construct for large complex models. A good example can be found in Liu *et al.* (2001).

No strict guidelines apply to the type and size of mesh required for the optimisation models. However, the FE discretisation used in each design domain must be consistent (i.e. element type, size, etc.). As each optimisation problem may be somewhat unique, the suitable discretisation may have to be determined by performing an initial investigative analysis prior to excuting the optimisation run. In most optimisation problems, the second approach would be used due to simplicity. If the section thicknesses of the constrained geometries and design domains vary greatly in the design domains, the first approach would be more computationally efficient. In general, the selection of an appropriate or resonable FE discretisation scheme depends on the user's experience in the MD method.

7.4 Results

7.4.1 Structural layout optimisation

Layout optimisation was performed on insulator enclosures under *i*) static mechanical and *ii*) coupled-field static mechanical and steady state thermal loads. The optimisation histories of both design cases are shown in Fig. 7.8 and Fig. 7.9 respectively.

i) *Static mechanical loads only*

The optimisation took 160 recurring MD iterations (n_i) to converge, as Fig. 7.8 (a) to (o) shows. Layout optimisation was initiated from an 'underdesigned' rectangular enclosure with horizontal and vertical face shells connected by vertical stirrups and horizontal ties. From $n_i = 0$ to $n_i = 10$, growth was concentrated at regions of high stress, at the vicinity of the intersections of the stirrups and ties. From $n_i = 10$ to $n_i = 23$, new load paths are created with the relatively 'unstressed' elements removed. From $n_i = 23$ to $n_i = 44$, the formation of the primary 'struts', which resembled an 'A-arm', began to take place. From $n_i = 44$ to $n_i = 73$, a conceptual layout of the optimised design was established. Hereafter, the design 'refinement' was primarily centred on the further removal of material, before an optimal solution with externally flush finish was found at $n_i = 160$.

ii) *Coupled-field static mechanical and steady state thermal loads*

Layout optimisation of the insulator enclosure under coupled mechanical-thermal loads took $n_i = 148$ iterations to converge, as Fig. 7.9(a) to (o) shows. The optimisation began from an identical initial model used in the optimisation study of case (*i*). Initially, from $n_i = 0$ to $n_i = 30$, growth was concentrated at intersections of the stirrups and ties. At $n_i = 40$ to $n_i = 70$, the formation of the newly created load paths leading a conceptual optimised layout began to take place. At this stage, the main strut members were 'held' by slender 'shear ties' to the main enclosure. These shear ties were gradually removed as the A-arm layout began to take shape. From $n_i = 70$, the optimisation was centred on further volume reduction through removal of the relatively unstressed material. An optimal solution found at $n_i = 148$.

(a) $n_i = 0$, $\varphi = 0.295$

(b) $n_i = 10$, $\varphi = 0.477$

(c) $n_i = 23$, $\varphi = 0.624$

(d) $n_i = 30$, $\varphi = 0.675$

(e) $n_i = 40$, $\varphi = 0.694$

(f) $n_i = 44$, $\varphi = 0.593$

(g) $n_i = 48$, $\varphi = 0.598$

(h) $n_i = 73$, $\varphi = 0.528$

(i) $n_i = 89$, $\varphi = 0.515$

(j) $n_i = 100$, $\varphi = 0.503$

(k) $n_i = 120$, $\varphi = 0.472$

(l) $n_i = 144$, $\varphi = 0.458$

(m) $n_i = 150$, $\varphi = 0.461$

(n) $n_i = 152$, $\varphi = 0.459$

(o) $n_i = 160$, $\varphi = 0.458$

Fig. 7.8 MD optimisation history of consolidated Nylon-12 granular-solid polymer insulator enclosure under static mechanical loads: (a) Iteration $n_i = 0$ to (o) iteration $n_i = 160$.

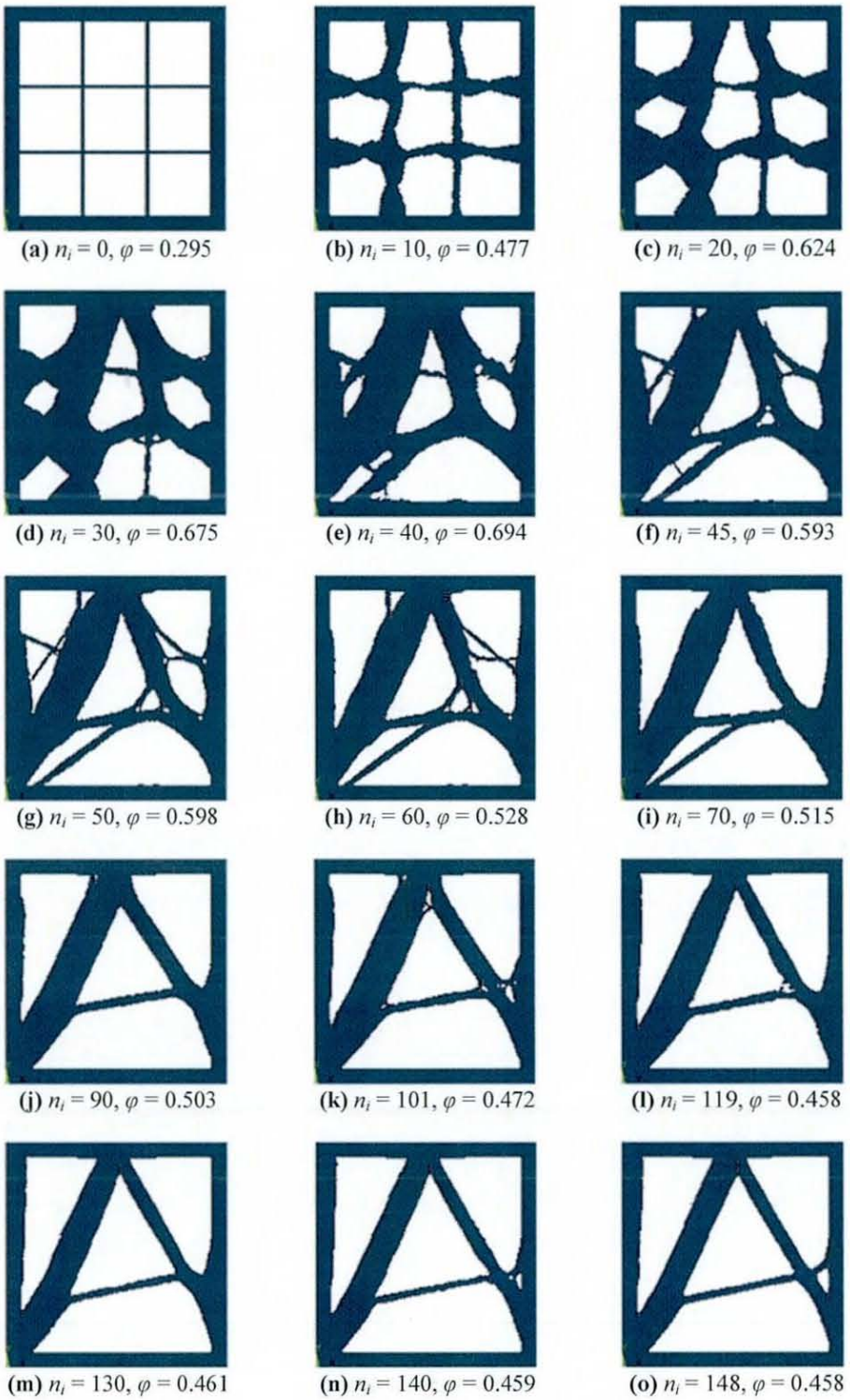

Fig. 7.9 MD optimisation of history of consolidated Nylon-12 granular-solid polymer insulator enclosure under coupled steady state thermal and static mechanical loads: (a) Iteration $n_i = 0$ to (o) iteration $n_i = 148$.

7.4.2 Stress distributions

Fig. 7.10 and Fig. 7.11 show the equavalent stress (σ_{eqv}), plane shear stress (τ_{xy}), maximum ($\sigma_{(t)}$) and minimum principal stresses ($\sigma_{(c)}$) contour plots of the optimised insulator enclosures, respectively. The FE models of the design solutions given by the MD method consisted of 11056 and 11072 nodes, respectively.

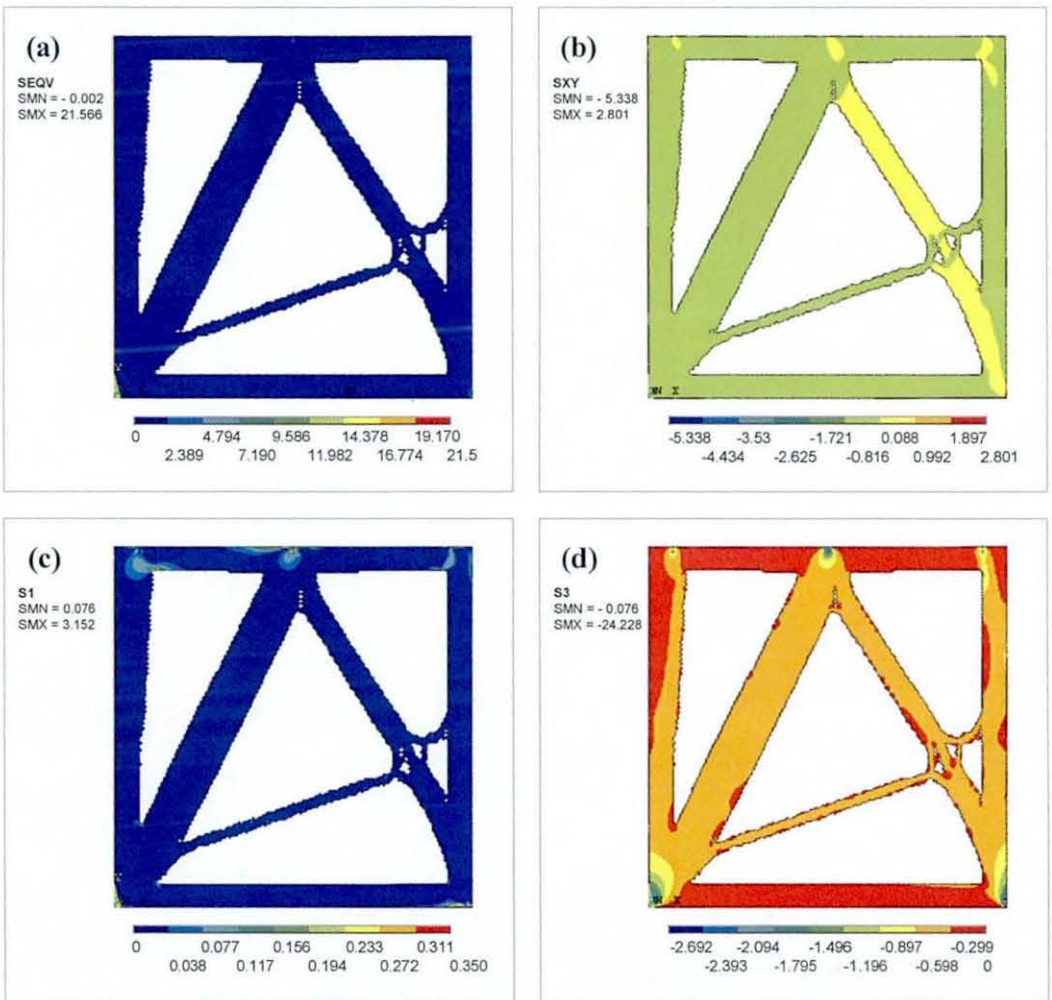

Fig. 7.10 Stress contour plots of structurally optimised insulator enclosure under static mechanical loads: (a) σ_{eqv} equivalent stress; (b) τ_{xy} plane shear; (c) direct tensile; (d) direct compression. (in units MPa)

The results showed that σ_{eqv} of both the optimised enclosures range from 0 to ~ 21.6 MPa. This indicated that the continuum truss members remained elastic, as Fig. 7.10(a) and Fig. 7.11(a) show. The τ_{xy} plots in Fig. 7.10(b) and Fig. 7.11(b) revealed that shear stress was in the range of ~ -5 MPa to ~ 3 MPa. These figures were below the shear limit (k) of the material, in which was determined to be less than the uniaxial yield strengths. Although the maximum stresses were observed to be below the strength criteria, the computed values were unreliable, given that support and loading points

would usually generate stress concentrations. In all, the stresses away from the loading points and constraints were below the allowable strength criteria of the material.

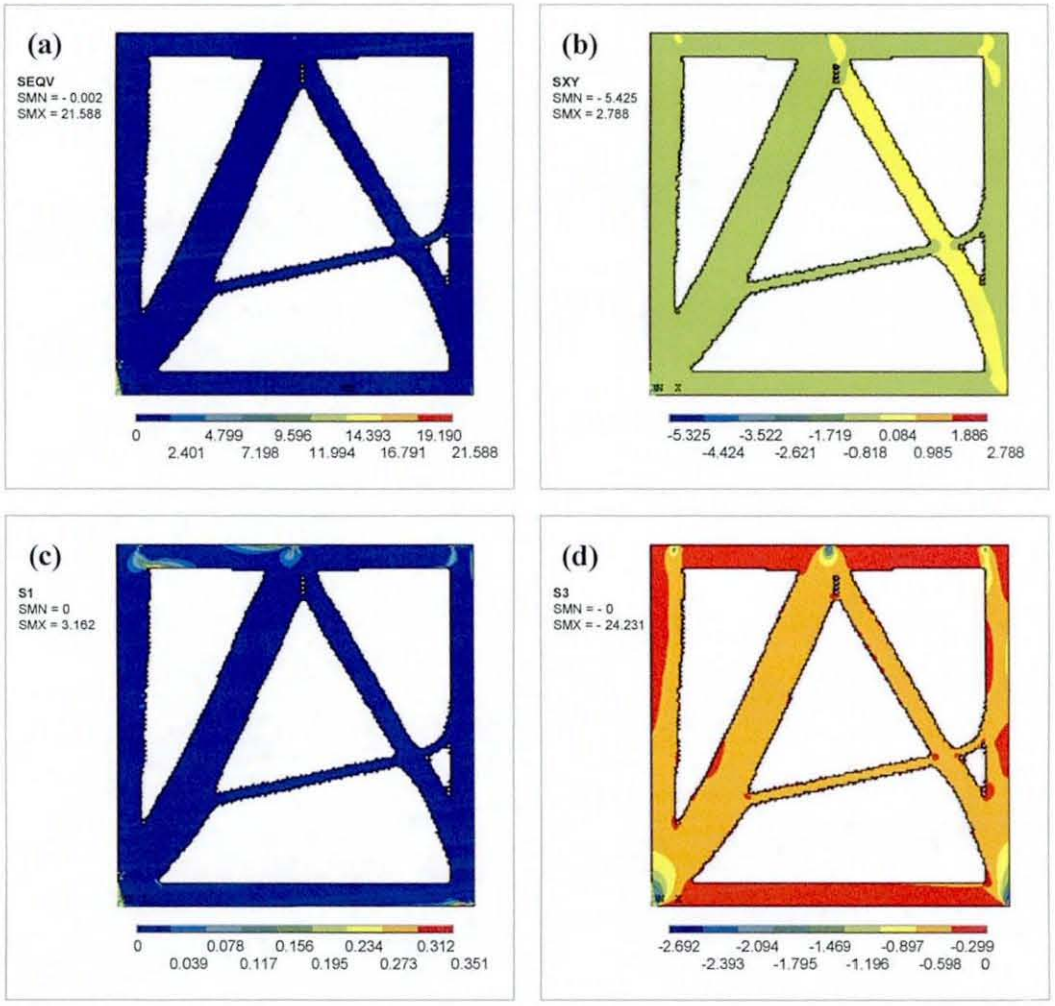

Fig. 7.11 Stress contour plots of insulator enclosure under coupled-field static mechanical and steady state thermal loads: (a) σ_{eqv} equivalent stress; (b) τ_{xy} plane shear; (c) direct tensile; (d) direct compression. (in units MPa)

The stress contours depicting the tensile and compressive stresses are shown in Fig. 7.10(c and d) and Fig. 7.11(c and d), respectively. Tensile stresses developed on the top, bottom and outer face shells. This was expected because these members undergo bending due to the transverse loads. The tensile stresses were found to be in the range of ~ 0.32 MPa to ~ 3.16 MPa. In contrast, the vertical face shells and A-arm structures remained predominantly under compression. The compressive stresses range of approximate -3 MPa to -24 MPa. Hence, the structure should remain safe under the applied loads.

7.4.3 Optimisation history and convergence

Fig. 7.12 and Fig. 7.13 show the variation of the objective functions and optimisation history, in terms of n_i recurring iterations. The curve in Fig. 7.12(a) indicates a steady increase in mass (m_s) objective function, as a result of growth, up to $n_i = 36$. Hereafter, the m_s objective function shows a steady and gradual decreasing trend, with slight fluctuations up to the $n_i = 130$. Prior to approaching an optimal solution, the objective function shows higher sensitivity with respect to the change in layout, due to the removal of structurally 'inefficient' material. The total deflection (δ_{total}) convergence curve shows a steep decreasing trend up to $n_i = 12$. After which, the δ_{total} objective function shows a flat decrease. Strain energy (U) decreases steeply up to $n_i = 30$, as Fig. 7.12(b) shows. Subsequently, a flat increasing trend is observed up to the region of optimal solution. Conversely, an opposite trend was observed for the maximum stress.

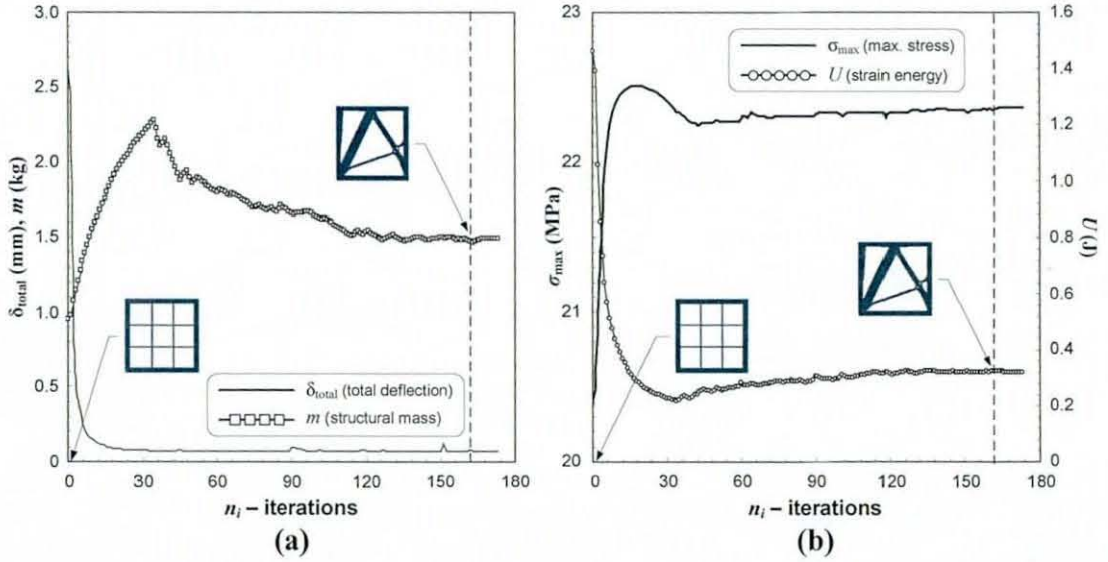

Fig. 7.12 Optimisation convergence and history plot of insulator enclosure under static mechanical loads: (a) deflection convergence plot; (b) U and σ_{max} history plot.

Fig. 7.13(a) shows the variation of the m and δ_{total} objective functions of the layout optimisation of the insulator enclosure under coupled mechanical-thermal loads. The m_s convergence curve indicates a steady increase in the objective function value up to $n_i = 40$. After this, the curve shows a decreasing trend up to $n_i = 72$. This is followed by a sharp decrease at $n_i = 74$ and $n_i = 77$, due to the higher sensitivity of the layout with respect to the change in layout. Hereafter, the m objective function shows a steady increase up to $n_i = 97$. The curve decreases gradually before converging to an optimal solution at $n_i = 148$. The δ_{total} objective function however, shows a steep decrease up to

n_i = 12. This is followed by a flat decreasing trend up to n_i = 71. The δ_{total} objective function increased rapidly at n_i = 72 and n_i = 77, corresponding to the higher sensitivity to the change in layout. After this, the curve remains flat before converging to an optimal solution at n_i = 148.

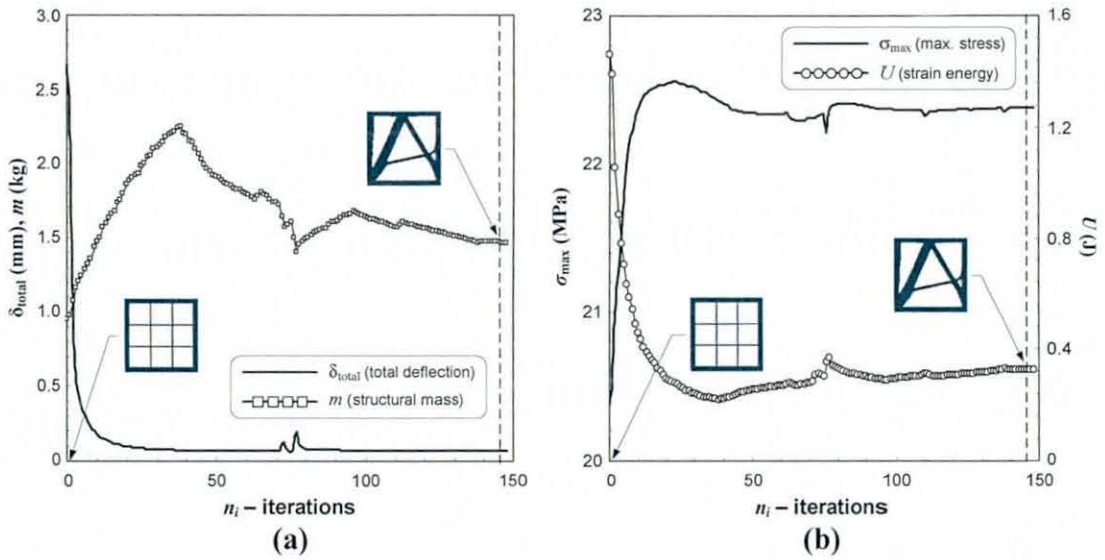

Fig. 7.13 Optimisation convergence plot for insulator enclosure under coupled-field static mechanical and steady state thermal loads: (a) deflection convergence plot; (b) U and σ_{max} history plot.

In Fig. 7.13(b), the U curve shows a steep decrease up to n_i = 38. This is followed by a gradual increase up to n_i = 76. The U curve shows a steep at n_i = 77 corresponding to the higher sensitivity to the change in layout observed in Fig. 7.13(a). On the contrary, the inverse is observed for the σ_{max} curve. Despite the fact that $\sigma_{max} < \sigma_y$, these values were somewhat 'unrelistic' as they were the nodal stresses at the support point vertices. Incorporating new features in the FE models would decrease the effects of these localised stresses. Importantly, even though the values of stresses showed by the curves are 'local', the values of σ_{max} were found to be significantly less after the optimisation.

In the optimisation of the insulator enclosure under static mechanical loads, a series of apparently 'local optimum' solutions can be observed, as Fig. 7.12(a) shows. Here, it was assumed that the minimum of all local optimums gives the 'near global' optimum solution. In this study, at n_i = 160 the m and δ_{total} objective functions attain minimum values of 1.487 kg and 0.074 mm respectively. Hence, the layout corresponding to n_i = 160 was considered as the near optimal design solution.

The convergence curves of insulator enclosure under coupled mechanical-thermal loads showed less local optimas. In this case, only one minimum point, where the objective functions is least sensitive to layout change could be identified. Accordingly, the layout at n_i = 148 is considered the near optimal solution, with m and δ_{total} attaining values of 1.464 kg and 0.075 mm, respectively.

7.5 Post-processing optimised result

Although both quadrilateral and triangular plane elements were used by the MD method to approximate 'smooth' surface boundaries, the given optimised layouts may not be suitable for manufacturing. This was largely due to the relatively 'jagged' surface boundaries of the transition between quadrilateral and triangular elements. In some designs, the associated local stress intensity factors may be severely influenced by the local stress field induced by these irregular boundaries. In most cases, optimised layouts without post-processing are not realisable in practice. Hence, post-processing is seen as an essential step in the design procedure to improve the objective functions, as well as to yield a practical design fit for manufacturing and application.

The optimised layout was post-processed manually in two stages. Initially, the nodes of the external boundaries were identified from the FE models. Spline curves were fitted through to approximate a smooth profile, as Fig. 7.14 shows.

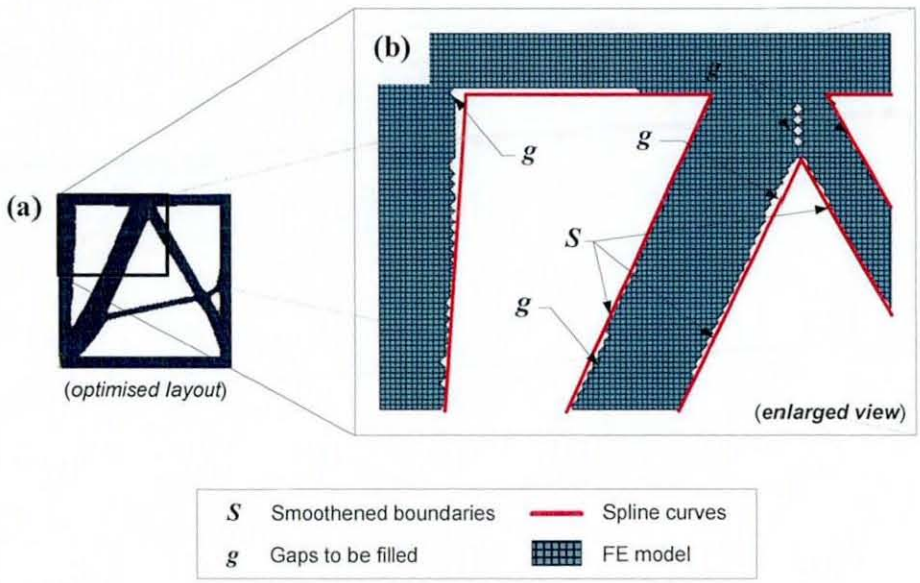

Fig. 7.14 Post-processing of MD optimised insulator enclosure layout: (a) Optimised cross-sectional layout; (b) smoothened optimised internal boundaries.

The gaps in between the optimised layout and spline curves were 'filled' to give a smooth finish. However, this resulted in a slight increase in mass. The alternative approach of fitting spline curves to create smoothened surfaces that would result in the removal of material is not recommended, as doing so would ultimately affect the global stiffness of the optimised structure. In the next step, a cross-sectional layout of the smoothened geometry was generated by means of a simple Boolean operation, followed by a 3D model. This was converted into a neutral data format (i.e. IGES, Parasolid, etc.) which could be read by a commercial CAD system.

The abrupt edges of the continuum members were 'rounded' by means of the 'fillet' option through use of a CAD package. This secondary smoothing procedure eliminated the geometric features which may potentially cause high stress concentration (i.e. notch effect). The model with smoothened edges was converted to a neutral format to be read by the FEA code. At this stage, higher order elements, PLANE82, with mid-side nodes were used to discretise the post-processed enclosure models, as Fig. 7.16 shows. The post-processed models were then re-analysed using the loading and boundary conditions as mentioned in Section 7.3.2. Fig. 7.15 shows an example of the process flow of the post-processing procedures implemented here.

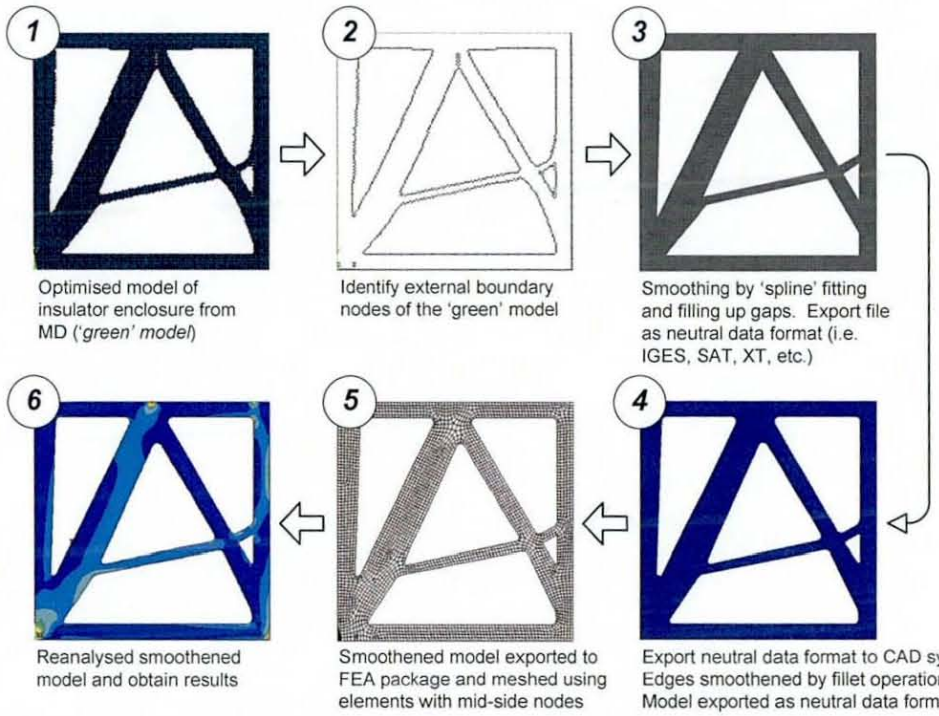

Fig. 7.15 Process flow of the post-processing of MD optimised insulator enclosure

7.5.1 Stress distributions

Fig. 7.16(a) and (b) shows the FE discretisation of the post-processed insulator enclosures. The FE models were meshed using higher order (2^{nd} degee) quadrilateral PLANE82 elements and consisted of 9093 and 9151 nodes, respectively. A mesh size of 2 mm was used. The post-processed models were re-analysed and the resultant stress fields are presented in Fig. 7.17 and Fig. 7.18, respectively.

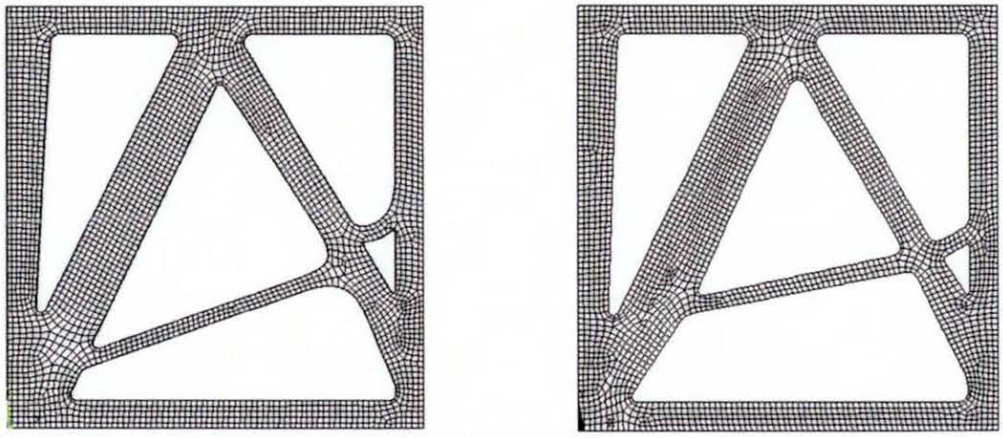

(a) (b)

Fig. 7.16 FE Discretisation of post-processed insulator enclosures: (a) enclosure under static mechanical loads with 9093 nodes; (b) enclosure under coupled mechanical and thermal loads with 9151 nodes.

From the stress contour plots, it was observed that post-processing had resulted in a more uniform stress distribution, notably along the smoothened boundaries and filleted profiles. The 'jagged' boundaries were eliminated by the spline curve smoothened boundaries. The σ_{eqv} contour plots, in Fig. 7.17(a) and Fig. 7.18(a), indicated a peak stress of 30 MPa at the point supports. Fig. 7.17(b) and Fig. 7.18(b) shows the τ_{xy} contour plots of the post-processed enclosures. The results revealed that shear stress peaked at 3 MPa. The magnitude of τ_{xy} was found to be greater at lower portion of the 'legs' and 'angular cross ties' of the A-arm structure.

Fig. 7.17(c and d) and Fig. 7.18(c and d) depict the $\sigma_{(t)}$ and $\sigma_{(c)}$ components of the post-processed enclosures. The development of $\sigma_{(t)}$ is more pronounced at the top, bottom and outer face shells. This was primarily due to bending of these face shells produced by the applied loads. The results indicated that $\sigma_{(t)}$ was in the range of 0 to 6 MPa. Conversely, the vertical inner face shells and the A-arm layouts were largely under

compression. Here, the compressive stresses range from 0 to 30 MPa. As a general observation, the magnitudes of $\sigma_{(t)}$ were found to be higher in the continuum inclined members of the A-arm and inclines cross ties.

It can be seen that the σ_{eqv} along the surfaces of the post-processed layouts have a near constant stress distribution. This means that the current design layout will have considerably increased fatigue endurance. The level of stresses at the point supports was considerably greater than the stresses at other locations. Stresses at these regions are unrealistic due to stress concentration at a single node. A similar trend was observed for the loading points on the top horizontal face shell. In all, the stresses in the continuum members were below the allowable limits. This indicates that the structure would remain elastic under the applied loads.

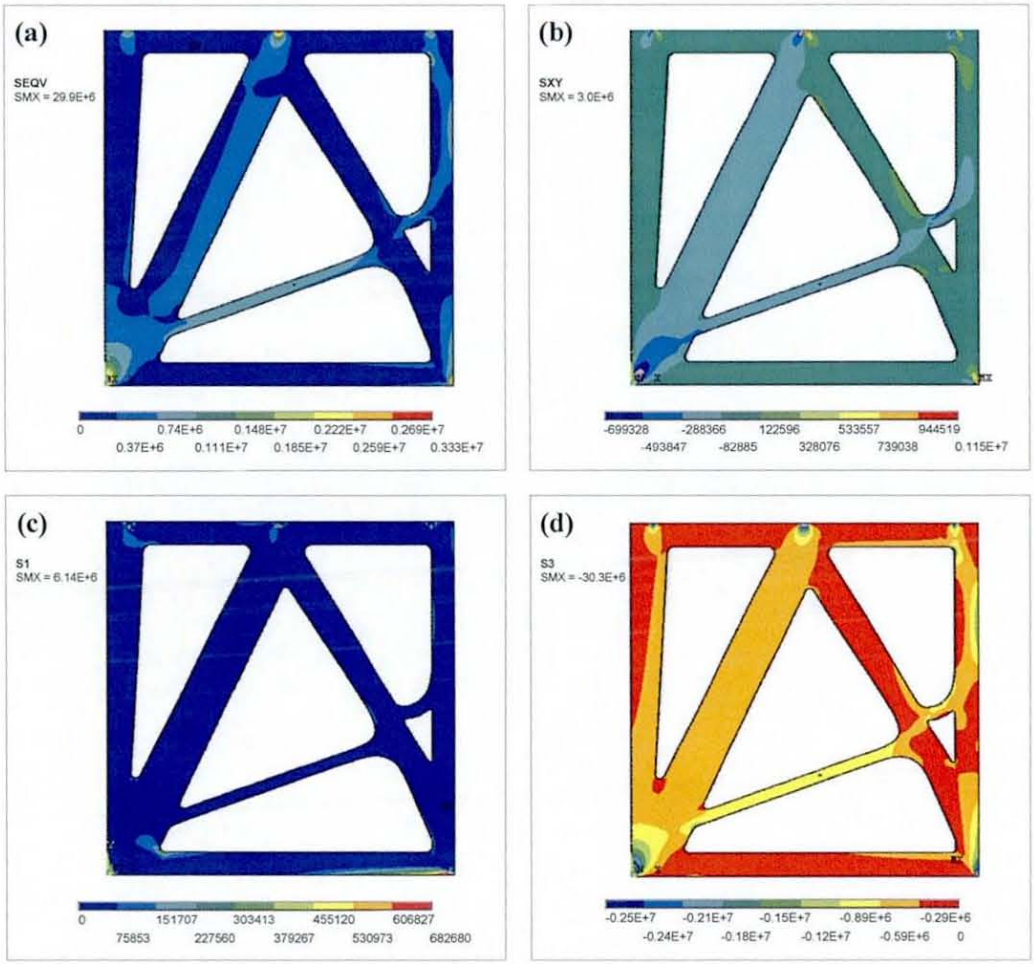

Fig. 7.17 Stress contour plots of post-processed insulator enclosure under static mechanical loads only: (a) σ_{eqv} equivalent stress; (b) τ_{xy} plane shear; (c) $\sigma_{(t)}$ direct tensile; (d) $\sigma_{(c)}$ direct compression. (in units MPa)

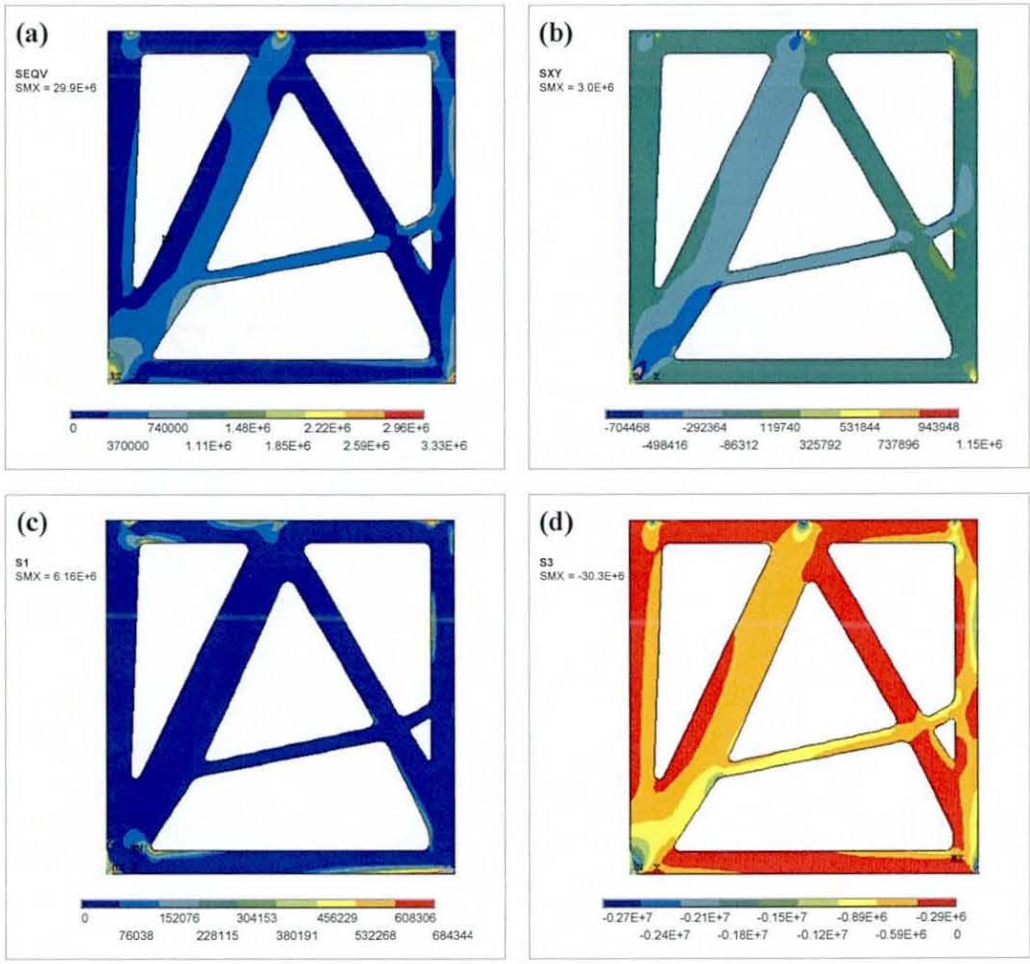

Fig. 7.18 Stress contour plots of post-processed insulator enclosure under coupled-field static mechanical and steady state thermal loads: (a) σ_{eqv} equivalent stress; (b) τ_{xy} plane shear; (c) $\sigma_{(t)}$ direct tensile; (d) $\sigma_{(c)}$ direct compression. (in units MPa)

7.6 Discussions

7.6.1 Growth cone development

During the layout optimisation, structural growth was guided to occur at regions of high stress in the structure within the defined design domains. With the introduction of material by means of the various growth cones, regions of high stress are 'decentralised' with the formation of load paths to 'redistribute' the load. Conversely, material which carry virtually no load or undergo relatively low stress were identified and removed, because they do not contribute to the overall stiffness. In context to other generalised methods, MD's approach closely resembles that of the adaptive growth employed by load bearing biological structures. The approach employed by MD uses a fundamentally different approach compared to SBG methods by Baumgartner *et al.* (1992) and Mattheck and Burkhardt (1990).

In general, the growth/degenerative optimisation procedures of the MD method could be categorised as the *initial*, *intermediate* and *refinement* development stages. Such distinctive optimisation stages could also be observed from the convergence plots of ESO methods (Querin *et al.*, 1998; Das *et al.*, 2005). The discussions of the optimised layouts by the MD method are based on that of Case (*ii*).

7.6.2 Initial stages

At the initial stages, growth was mainly aimed at reducing the level of stresses of the chosen under-designed initial structure. Growth at this stage did not produce a layout that differs much from the initial layout and occurs primarily by means of the 'bus' and 'star' topologies, as Fig. 7.19(a) shows. Despite the reduced level of stresses, the resultant layout still resembles that of the initial layout. However, the two vertical members, at the top quadrants, began to tilt towards the middle, as exemplified by angles Θ_1 and Θ_2 (Fig. 7.19b). If the additional stirrups and ties were not included, growth would therefore take the form of the 'ring' topology, towards the development of the inclined primary strut members of the 'A-arm' layout. Optimisation had resulted an increase in mass (or volume) of 48%. This is a substantial increase for the initial development stages alone. In terms of convergence, the structure is highly sensitive to

changes in layout. Hence, the current layout was still somewhat 'unstable' and could be further improved.

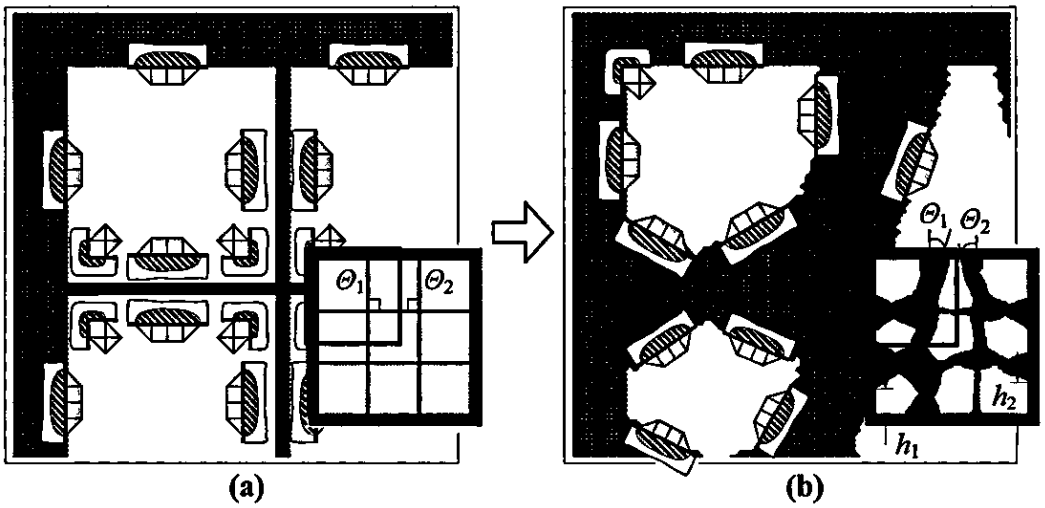

Fig 7 19 *Initial* development stages of Case (*ii*) (a) Initial layout of structure, (b) layout at $n_l = 20$.

7.6.3 Intermediate stages

At the intermediate stages, the resultant layout differs significantly and bears no resemblance to that of the initial structure, as Fig. 7.20(a) shows.

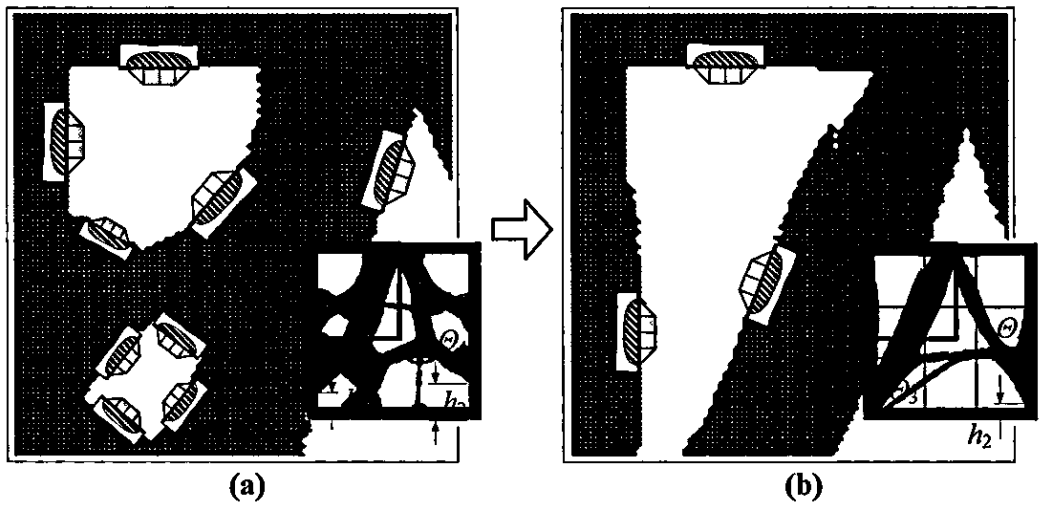

Fig. 7 20 *Intermediate* development stages of Case (*ii*)· (a) Layout at $n_l = 30$; (b) layout at $n_l = 70$

In contrast, growth/degeneration was concentrated on the development of new load paths to transfer the dominant loads. The initial members, notably those that do not fall in the path of the 'force flow', were identified and removed. The horizontal members at the lower quadrants were retained, due to the surface loads on the outer face shell. The horizontal members gradually 'moved' downwards as the development progressed,

as h_1 and h_2 in Fig. 7.19(b) and Fig. 7.20(a) compares. These members would eventually develop to form the lower portions of the inclined struts, as angle Θ_3 and Θ_4 decreases (Fig. 7.20b)

The current layout somewhat violated the basic assumptions required for a continuum truss layout, because two load paths should ideally not overlap (Schlaich *et al.*, 1987). At this stage, more elements were removed than being added. This had resulted in a reduction mass of approximately 18%. At this stage, all the basic continuum members were seen to have fully developed. The sensitivity of the objective functions to the change in layout was comparably less than that of the initial stages, indicating a more stable layout.

7.6.4 Refinement stage

At this stage, growth/degeneration was merely centred on the refinement of the load carrying members, as Fig. 7.21 shows.

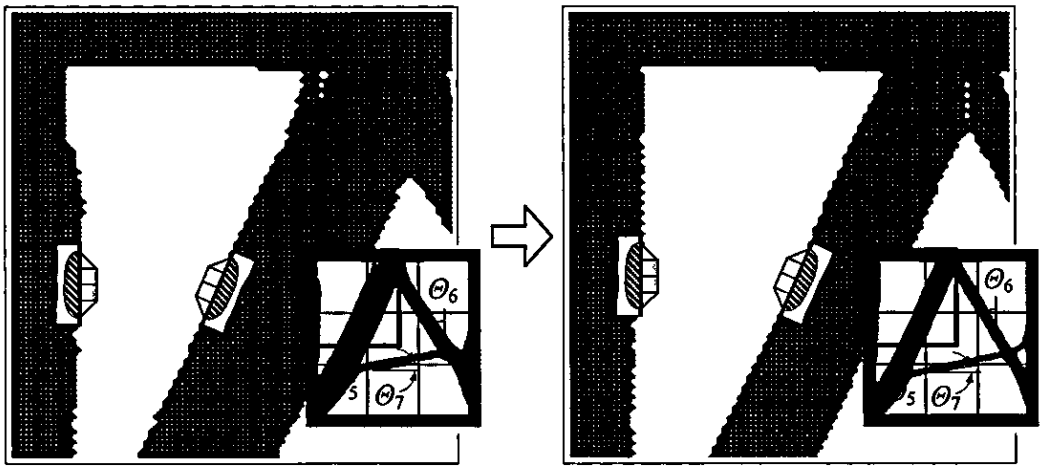

Fig. 7 21 Refinement development stages. (a) Layout at $n_i = 90$, (b) layout at $n_i = 148$

Here, the section thicknesses of the continuum members were reduced, while Θ_5, Θ_6 and Θ_7 remained relatively unchanged. In most design cases, layout development at the refinement stages would not result in any significant changes. A similar trend could be observed in most optimisation studies demonstrated by FE-based generalised layout methods.

In general, the compressive members of continuum truss structures with $L/D \leq 3$ do not require additional inclined tensile ties (Kwak and Noh, 2006). However, this is not the case if the applied transverse or bending loads are dominant, as exemplified by studies given by Liang *et al.* (1999; 2003) and Kim *et al.* (2000; 2003).

In contrast to the previous development stages, the rate of growth/degeneration at the refinement stages was comparably less. In fact, more elements were being removed than added. At this stage, the mass of the insulator enclosure was reduced by approximately 9%. However, the total net gain was estimated to be 35%. From a convergence point of view, the sensitivity of the objective functions with respect to the addition and removal of material was also significantly reduced, indicating that an optimum solution has been found.

For most generalised layout methods, the chosen initial layout would not, in anyway, affect the outcome of the final solution. However, this is not the case for ground mesh methods. In the MD method, this has been proven through the various optimisation studies. However, this does not mean that any randomly shaped layout could be used as a starting layout. The efficiency of the optimisation run towards convergence may be hampered if a severely underdesigned or overdesigned initial structure is to be used. Hence, the selection of a starting layout could be seen as an important consideration prior to the optimisation, as exemplified by Liu *et al.* (2001).

In the MD method, there are no fixed rules which determine the type of layout to be used as the starting design. Each design optimisation problem is unique in certain respects. The selection if a layout considered to be appropriate for a particular design problem is largely based on the user's experience in the MD method and the understanding of the mechanics of the design optimisation problem. In general, for continuum problems, the initial layout must be a continuous, with all loading points/surfaces connected. Based on the author's experience, the use of 'additional' elements in place of the apparent paths of the dominant loads would help improve the efficiency of the solution, thereby reducing the number of recurring iterations needed to obtain a solution.

7.6.5 Stress distributions

Due to the relatively large differences between the peak and minimum stresses, the range of stresses of interest could not be clearly interpreted. Most FEA packages, by default, would employ what is known as a 'contour washout' to even out the contour bands. The default stress plots, indicating a decievingly uniformly stressed structure, does not give a clear picture of the stresses (see Fig. 7.22a). To plot the σ_{eqv} within the range of interest, the stress scale was capped at maximum equivalent stress obtained from the analysis. The new contour plot in Fig. 7.22(b) shows that σ_{eqv} range from ~ 0.37 MPa to ~ 3.33 MPa, indicating that stresses was in fact not uniform. The results agree well with design examples given by Mattheck (1998), which also demonstrated that stresses continuum members are unlikely to achieve uniformity, if mass reduction is taken into consideration.

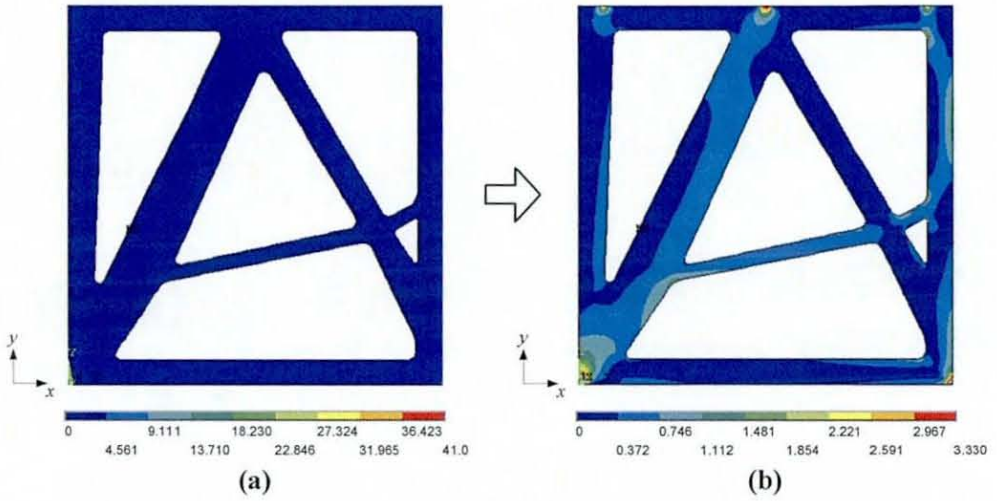

Fig. 7.22 Differences in the σ_{eqv} contour plots of optimised insulator enclosure of Case (*ii*): (a) Default stress contour plot with peak stress figure; (b) stress contour plot disregarding peak stress values. (in units MPa)

From the σ_{eqv} contour plots, it can be seen that no yielding or stress concentrations were developed in the continuum members. Values of the peak stresses, at the supports and loading points, can be disregarded because loads and supports applied to a node would usually produce stress singularity that lead to infinitely high stresses. This can be improved through use of surface or pressure loads. Instead of point loads, forces can be applied such that they are evenly distributed over an area. Despite the high stress concentration, the σ_{eqv} of the optimised layouts still remained below that of the constrained value.

The first (S_1) and third principal stress (S_3) plots depicts the tensile and compressive stress components. It is evident that the inclined strut and tie members developed by MD were predominantly put under compression. In contrast, the horizontal face shells undergo tension as a result of bending. In this case, the purpose of the principle stress plots was to give a visual comparison of the type of loads each continuum members undergo. The maximum principle stress criterion (i.e. Tresca creterion) is rarely suitable for design purposes for the type of material used in this study.

7.6.6 Problematic geometries

In MD, the procedures of growth/degeneration were executed automatically. In this study, manual involvement was required due to 'problematic geometries'. Problematic geometries may arise due to the nature of the removal of relatively unstressed elements. In MD, this was done based on the level of stresses developed over the structure. In some cases, portions of the structure may undergo rigid body motion when low stress elements are removed at certain regions. This would result in problematic geometries and affect the automated process of the optimisation. Although the occurrences of problematic geometries may seem to be initially somewhat random, they can be predicted and prevented from arising by monitoring the progress of the optimisation run. Problematic geometries are usually caused by 'bending' or 'buckling' effects, at regions where stresses are expected to be comparably higher at the intermediate lengths (Fig. 7.23 and Fig. 7.24), largely due to the removal of relatively low stress elements adjacent to those that undergo comparably high stresses.

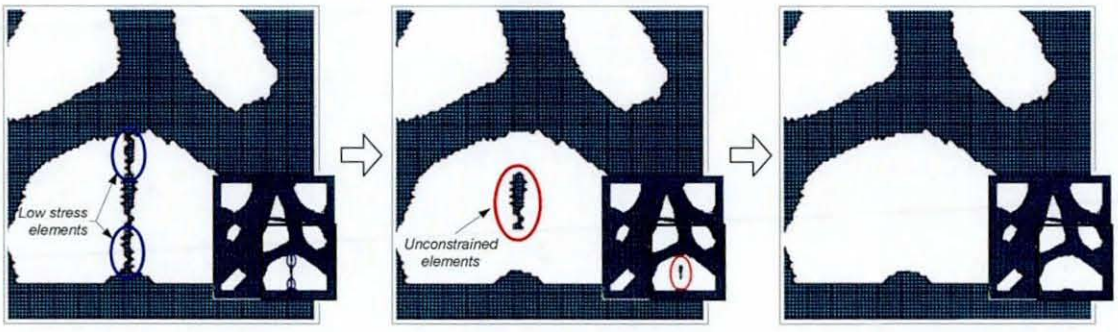

Fig. 7.23 'Buckling effect' problematic geometries: (a) buckling of a slender member; (b) removal of relatively low stress elements unconstrained elements; (c) deletion of unconstrained elements.

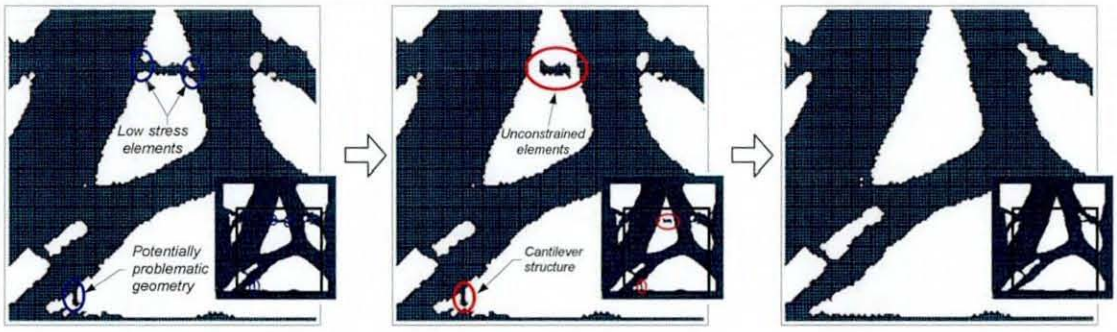

Fig. 7.24 'Bending effect' problematic geometries; (a) Problematic geometry; (b) unconstrained elements resulted from degeneration; (c) repaired model.

The removal these elements would lead to insufficiently constrained elements. Unsupported elements would result in a singular stiffness matrix and the FE code is unable to solve the stiffness equation for the nodal degrees of freedom. Because of the iterative approach of the MD method, where the optimisation cycle forms a closed-loop consisting of a layout optimisation and FE analysis, the continuity of this process would be interrupted. Until the problematic geometries are eliminated, the optimisation would be 'interrupted'. With MD, the optimisation can not be restarted from the stage to when it was interrupted, but had to be 'restarted' from the beginning.

However, the development of problematic geometries could be predicted and prevented. From observations, they are most likely to occur on slender geometries, particularly at the initial and intermediate optimisation stages. The development of such geometries into problematic geometries may be identified from the 'real time' progress layout optimisation run, particularly during the stage where slender members start to develop. Slender members with section thicknesses less than ~ 1/10 of the thickest primary members were identified and deleted from the input files of the optimisation model. This is repeated at the intervals of the iterations by temporarily suspending the optimisation. Once this is completed, the optimisation is continued using the updated model (see Fig. 7.23c and Fig. 7.24c). In this study, the problems cause by problematic geometries is a recurring one. The aforementioned process is repeated, until the primary load carrying members have been fully developed.

Although the above solution is a rather straightforward one, the only drawback is that it is time consuming. From the optimisation trial runs conducted in this study, problematic geometries was found to be a recurring problem, notably at initial and intermediate stages. This problem could be solved efficiently through use of a subroutine which could automatically identify and remove unconstrained elements within the optimisation model. However, the limitation of the FEA code used was seen as the barrier to realising this. Although ANSYS FEA is capable of identifying insufficiently constrained elements, it could only identify the first among the many unsupported elements. For instance, if the optimisation model has N unsupported elements, ANSYS is only capable of identifying the first node based on chronological numbering order. Although the manual approach may not be ideal, it is still manageable for most 2D layout problems.

7.6.7 Differences in continuum layout of optimised enclosures

Fig. 7.25 highlights the differences in layout of the insulator enclosures derived from MD. In all, the resultant layouts consisted of four primary continuum members (E, F, G, and H) enclosed within a rectangular enclosure. Although the optimised layouts appear to be somewhat similar, their configurations differ in some respects. For this comparative discussion, the post-processed optimised layouts would be used.

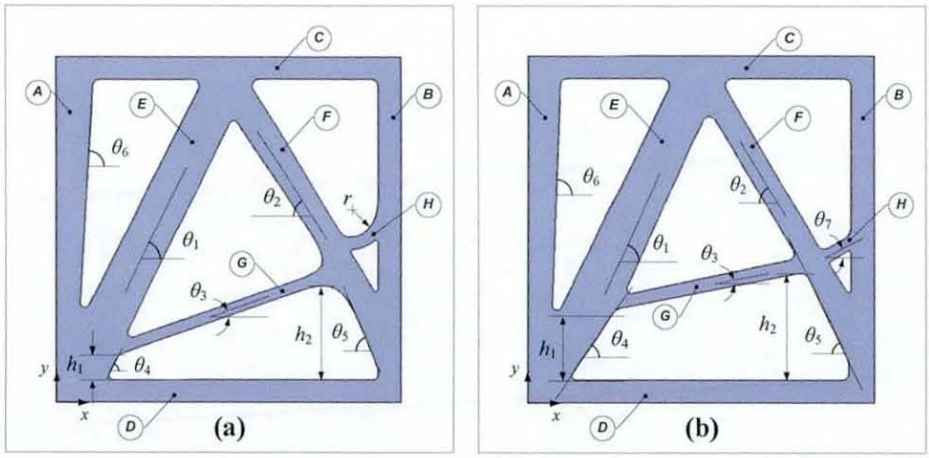

Fig. 7.25 Differences in continuum layout of optimised insulator enclosure: (a) Case (*i*) under static mechanical loads; (b) Case (*ii*) under coupled static mechanical and steady state thermal loads.

The angle of inclination of the primary struts E and F (θ_1 and θ_2) differ by only 1.1° and 1.6°, respectively. However, this is not the case with the inclined slender ties member

G, developed across the lower portion of the primary struts. In Case (*i*), the angle of inclination (θ_3) of the slender tie, from the horizontal axis, was 19.4°. In contrast, θ_3 of Case (*ii*) remained relatively flat at 11.5°. The differences in slope of these members differ by 42%. In addition, the locations of the development of these slender ties are noticeably different. In Case (*i*), the height of the left portion where it intersected strut member E, denoted by h_1, was relatively close to the bottom face shell member D. In Case (*ii*) however, h_1 was comparably higher. In both layouts, height h_2 differs by approximately 6 mm. A layout optimisation study conducted by Kwak and Noh (2006) demonstrated that the angle of inclination of continuum member is not greatly influenced by the FE discretisation of the optimisation model.

The differences in angle of the continuum inclined tie members, developed across the primary struts, suggested that the layout of Case (*ii*) undergo an additional horizontal force component. This can be explained using the displacement vector sum (δ_{Total}) plots shown in Fig. 7.26. To get a better understanding of the deformation, the δ_{Total} plots are rescaled and the outlines of the un-deformed edges are shown. Under vertical and horizontal loads, the enclosure compresses and distorts to the left (Fig. 7.26a). With thermal loads, the enclosure expands and the 'distorts' to the right (Fig. 7.26b).

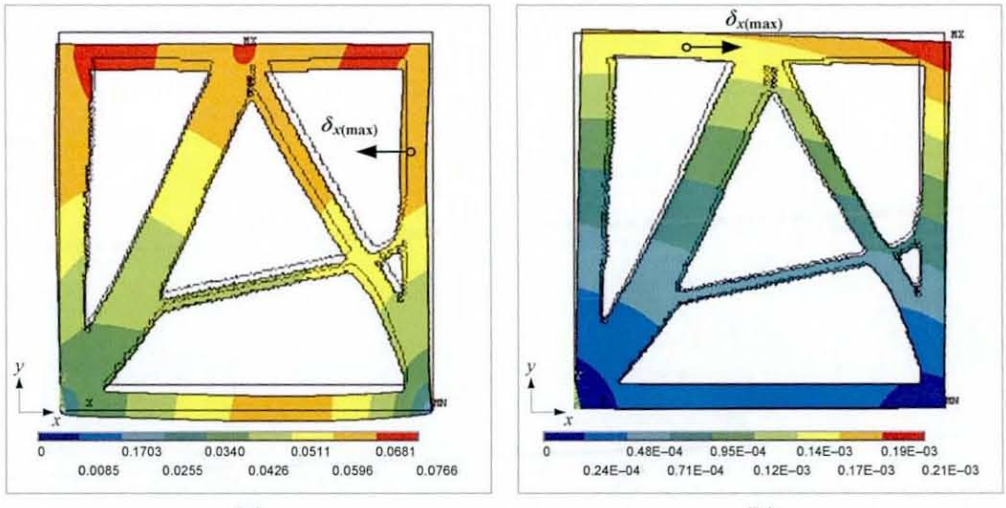

(a) **(b)**

Fig. 7.26 Scaled total deflection (δ_{Total}) plot of Case (*ii*) with undeformed edge: (a) δ_{Total} under static loads only; (b) δ_{Total} due to thermal loads. (Dimensions in unit mm, $\delta_{x(\max)}$ indicates maximum lateral deflection)

The sum of the lateral forces produces a net resultant force acting towards the left, hence the slightly lower rise of the slender tie. In contrast, the optimised layout of Case

(*i*) is not subjected to this additional lateral force component, resulting in a steeper angle.

Another distinctive difference was the layout of the short inclined tie *H*, adjacent to the vertical face shell *B*. In Case (*ii*), this is located slightly higher than the inclined slender tie member *G*, with $\theta_7 = 29.6°$. It forms a load path to transfer the horizontal loads from the vertical face shell to *G*. In Case (*i*) however, *H* resembles a rotated 'rampant round arch' with radius of ~ 6 mm, which 'in-posts' are connected to the intermediate length of the vertical face shell where *G* and *F* intersects. This feature violates the basic requirement of a truss layout because it does not form triangulated or rectangular openings. In continuum layout design, this feature is acceptable. Table 7.1 compares the differences.

Table 7.1

Differences in configuration of the continuum members of Case (*i*) and Case (*ii*)

Angle (θ) and height (h)	**Case (*i*)**	**Case (*ii*)**
θ_1	63.6°	64.7°
θ_2	57.7°	59.3°
θ_3	19.4°	11.5°
θ_4	63.9°	55.9°
θ_5	67.1°	64.0°
θ_6	86.8°	87.9°
h_1	10.7 mm	29.3 mm
h_2	40.5 mm	46.4 mm

The weight of the optimised enclosures increased slightly due to the amount of material being added in the post-optimisation stage. As a result of post-processing, the increase in weight was estimated to be ~ 5.1 % and ~ 4.6%, for Case (*i*) and Case (*ii*) respectively. In Case (*i*), the gaps to be filled in the optimised model obtained from MD was comparably more those of Case (*ii*), hence the slight increase in mass. Interesting, in Case (*ii*), despite the additional thermal loads on the vertical enclosure face shells, its weight was found to be less than that of the layout developed in Case (*i*). In layout optimisation, the development of the optimised layout largely depends on the magnitude and direction of externally applied loads. In this case, the total deformation due to thermal expansion and the externally applied forces somewhat opposes each

other. This produces net resultant total deformation which is comparably less than that of the total deformation the enclosure in Case (*i*) undergo, hence the lighter structure. The figures of the increase in mass as a result of post-processing are given in Table 7.2.

Table 7.2

Differences in weight of optimised (*green model*) and *post-processed* insulator enclosures

Design optimisation cases	**Mass (kg)**	**Increase in Weight (%)**
Case (*i*) *post-processed*	1.567	5.105
Case (*i*) *green model*	1.487	
Case (*ii*) *post-processed*	1.535	4.625
Case (*ii*) *green model*	1.464	

7.7 Conclusions and remarks

A design solution of least weight and maximum stiffness was determined for a modular structured insulator enclosure through use of the MD method. Of the two design cases considered here, it was shown that the addition of thermal loads to the analysis/optimisation model resulted a slight change in the configuration of the developed members. The design solutions obtained by the MD method were simple and realistic. A design layout with maximum possible stiffness was achieved with savings in build material of 40%. The results from the analysis show that the structural members of the optimised layout will remain safe under the applied loads. The interesting finding was the fact that the members generated by MD were predominantly compressive dominant. This type of layout, where members are aligned to the third principal axis, favours granular-solid material which is comparably more durable in compression. The members in tensile should not be of concerned. In application, CMU's are predominantly put under compression. It is this compression 'preload' that gives the apparent ductile behaviour of most granular materials. The optimal structural layout would form the basis of the starting layout for the optimal discretisation problem towards achieving a non-convective structured insulator.

Now that a design solution for strength requirements has been found, the upcoming chapter focuses on the optimal discretisation of the insulator enclosure towards a design solution to satisfy both strength and insulation requirements.

8

Optimal Discretisation/Partitioning of Structured Insulator Enclosures

8.1 Introduction

The dependence of the global heat flux (q) on the number of partitions within an enclosed airspace was revealed from the initial investigations of horizontal enclosures. This confirmed that the heat flow rate across a structure decreases due to the presence of equidistantly spaced parallel partitions. In the initial investigations, the interest was to establish a trend of reduction due to the presence of low partition count. The initial findings show that the trend of reduction resembles a polynomial curve. This indicates that the minimum of the function could potentially give an optimal discretisation. In the initial investigations, no attempt was made to optimise the discretisation layout. The current investigation involved devising a modified DbPM to optimally discretise of structures with heated and cooled side walls. In addition, a validation study was performed, whereby the effectiveness of the modified DbPM was tested on forty rectangular enclosures with randomly selected internal layouts.

The modified DbPM could be extended to cover 3D structures and non-cubic structures. In this study, equidistantly spaced partitions were used and were found to yield positive results. However, non-equidistantly spaced partitions may be useful, as highlited in the future works in Chapter 9. Based on the discretisation/partioning analogy, the contours of partitions for non-uniformly shaped airspaces should ideally form an 'offset' and 'blend-in' with the inner faces of a structure. This approach is

straightforward and does not differ much from the original concept, of which is the focussed of the current study.

8.2 Optimal discretisation of a 'basic' enclosure

8.2.1 Analysis model

The analysis model of the design problem under consideration was a 2D rectangular enclosure with external width/height ratio of $S = W/H$. It was bounded by two vertical isothermal walls at temperatures T_1 and T_2, and two horizontal adiabatic walls with uniform section thicknesses t_e. The inner airspace was a rectangular cavity fully divided by N vertical partitions of uniform thicknesses t_p. These form a series of equidistantly spaced fluid-filled subenclosures (or cells) with aspect ratio of $s_N = h/w_N$. The enclosure and partitions are modelled as consolidated granular-solid Nylon-12 with a constant thermal conductivity of k_s. The working fluid is atmospheric air, with constant thermal conductivity of k_f. Fig. 8.1 shows the schematic diagrams of a basic 'undivided' and 'fully divided' enclosure which formed the basis of the investigations of the optimal 'discretisation' for suppression of heat transfer of single cell structures.

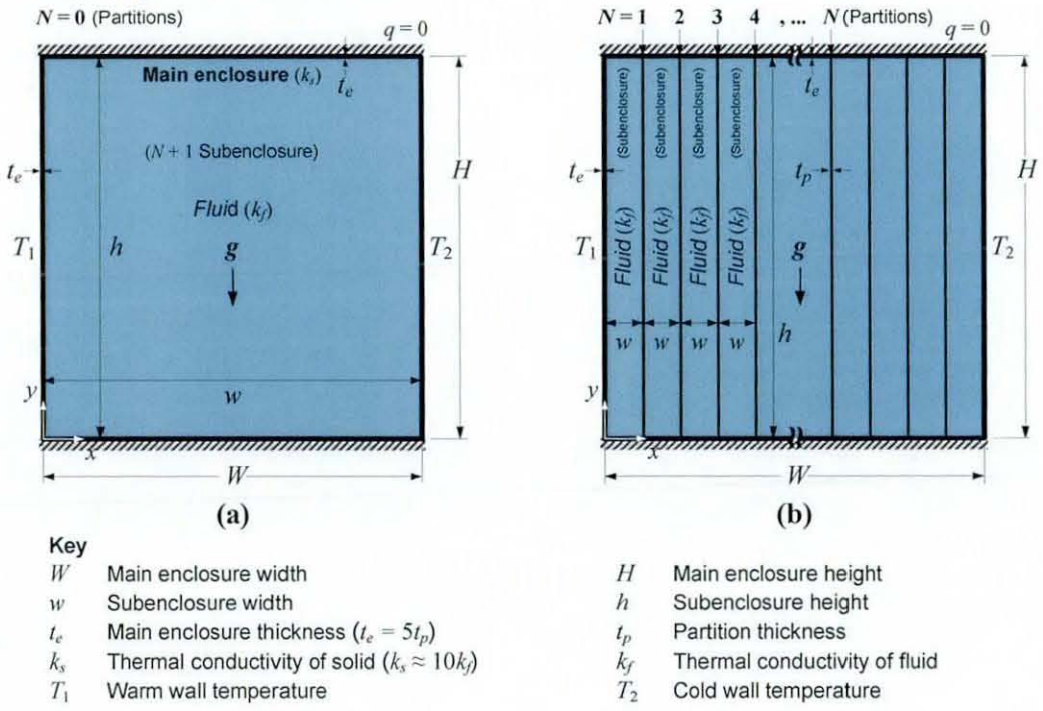

Key

W	Main enclosure width	H	Main enclosure height
w	Subenclosure width	h	Subenclosure height
t_e	Main enclosure thickness ($t_e = 5t_p$)	t_p	Partition thickness
k_s	Thermal conductivity of solid ($k_s \approx 10k_f$)	k_f	Thermal conductivity of fluid
T_1	Warm wall temperature	T_2	Cold wall temperature

Fig. 8.1 Schematic diagram of 2D single cell rectangular enclosures: (a) Basic enclosure with $N = 0$ partitions; (b) partitioned or discretised enclosure with N-partitions.

8.2.2 The discretisation by partitioning method (DbPM)

The requirements for thermally insulating 'single-material' structures in this study have motivated the development of the Discretisation by Partitioning Method (DbPM). This design approach is used for finding optimum enclosure partitioning layouts by discretisation of enclosed airspaces to form a series of fully divided closed cells. The fundamental question to be addressed was how to select a 'global' partitioning layout, such that the thermal resistance of a conjugate natural-convection-conduction system is optimally maximised. The discretisation was done based on these following reasons;

i) The degree to which natural convective flow is minimised
ii) The degree to which the thermal insulator is appropriate
iii) The amount of solid material enclosing the fluid

A working hypothesis was drawn, whereby the global heat transfer could be suppressed when a closed cavity is discretised using vertical equidistantly spaced parallel partition, as opposed to filling it with insulation material. An optimal threshold discretisation could be determined when the effective thermal conductivity k_{eff} of air is effectively maximised, by suppressing convection. By analysing the performance models of enclosures with varying partition layouts, the effects of the discretisation on the global heat transfer could be drawn. Here, the associated design variables were identified as;

i) The number of vertical partitions (N)
ii) The equidistance widths (w_N)
iii) The solid/fluid volume ratio (φ)
iv) The width/height ratio of the subenclosure ($s_N = h/w_N$)

The DbPM is an iterative approach consisting of two key stages; *i*) design/redesign and *ii*) analysis. The method incorporates the use of a commercial CAD and a CFD package. These formed the basis of the partition layout design and the numerical analysis. The idea is to introduce one vertical partition, at recurring n_i iteration, such that the heat transfer of the enclosure is progressively modified. In this study, procedures of the DbPM were not automated but performed manually. The scenario envisioned in Fig. 8.2(a) to (d) illustrates the iterative discretisation procedures of the DbPM.

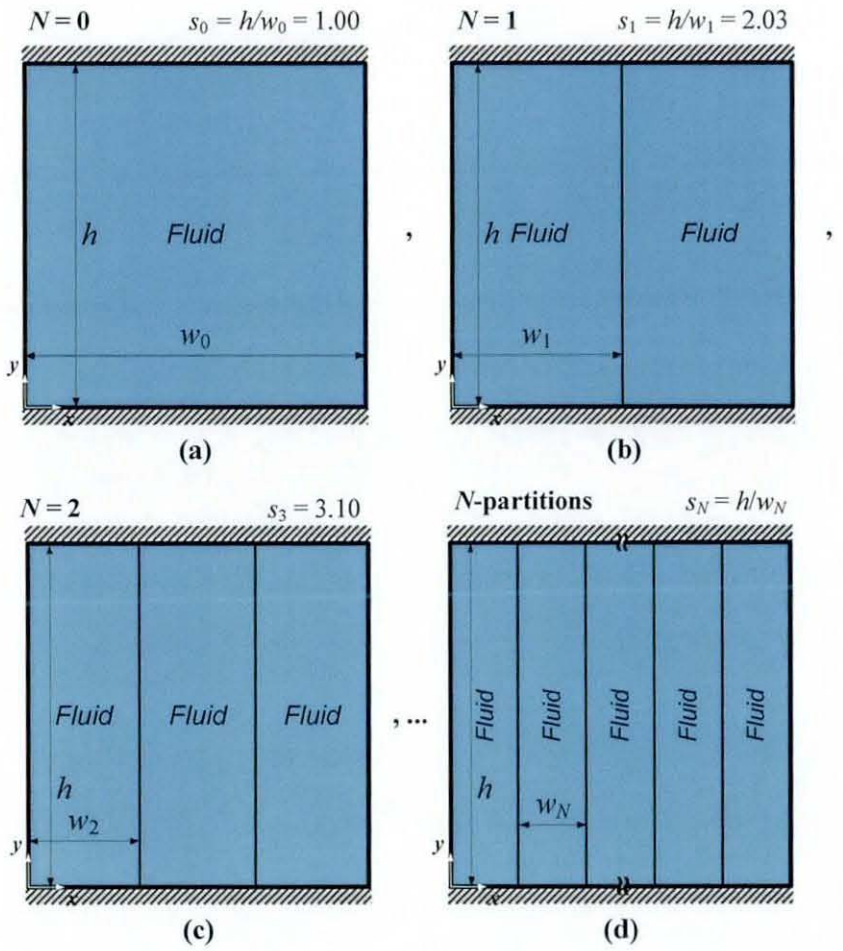

Fig. 8.2 Discretisation of single cell rectangular enclosure by the Discretisation by Partitioning Method (DbPM): (a) $N = 0$; (b) $N = 1$; (c) $N = 2$; (d) N-partitions.

The discretisation is based on a basic enclosure ($N = 0$) with subenclosure widths $w_N = w_0$ and $s_0 = h/w_0$ (Fig. 8.2a). At the first iteration, a vertical partition was inserted in the middle of the internal airspace to form an enclosure of $N = 1$, with equidistance widths of $w_N = w_1$ and $s_1 = h/w_1$ (Fig. 8.2b). The relationship of w_N in terms of N is

$$w_N = \frac{W - 2t_e - Nt_p}{N+1} \tag{59}$$

Here, the partitions do not act as structural elements, but as solid matrices to impede the bulk fluid motion within the subenclosures. However, their presence varies the solid/fluid volume fraction (φ). This would alter the heat transfer characteristics, from a natural-convective to conductive dominant. Both these extreme cases were seen as detrimental. Hence, a balance between both had to be sought. The relationship of φ, in terms of the geometric parameters of the enclosure model can written as

$$\varphi = \frac{[(HW) - h(W - 2t_e)] + N(t_p h)}{HW} \tag{60}$$

where both (59) and (60) are valid for $0 \leq N \leq w_0/t_p$.

To determine the effectiveness of the partitions in suppressing heat transfer, both the average heat flux (q) and correlated Nusselt number (Nu_N) are considered. For each increment of N, a 2D grid of the analysis model was constructed. This was done using Fluent™ CFD pre-processor known as Gambit™. Subsequently, the heat and flow fields were solved using Fluent CFD code. The reduction of q with respect to N was computed from the numerical analysis. A convergence plot was generated manually by plotting q vs. N. The above procedures were repeated iteratively, until an optimal discretisation (N_O) was obtained, when q could be reduced through further discretisation. The process flow of the basic DbPM is depicted by the flowchart in Fig. 8.3.

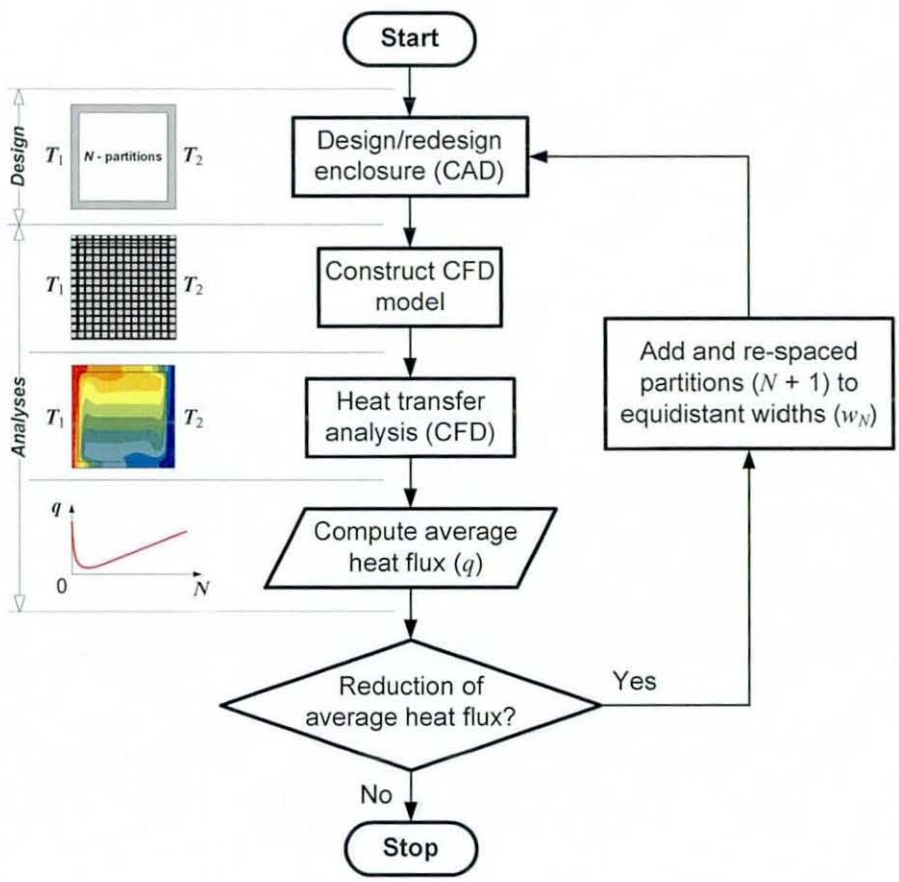

Fig. 8.3 General process flow of the Discretisation by Partition Method (DbPM) of single cell enclosures.

8.3 DPbM for enclosure with 'multiple' cavities

The outcome of the previous investigation suggested that the DbPM could be extended to enclosures with arbitrarily shaped cells. It was theorised that the effectiveness of the parallel partitions in suppressing heat transfer across enclosures of arbitrarily shaped cells with fixed external geometries would exhibit a rather similar trend. Based on the outcome of the previous investigations, a modified DbPM was devised. This technique was envisaged to form the Stage-2 of the proposed 'two-stage' optimisation/discretisation method for structures with strength and insulation requirements.

8.3.1 Discretisation of arbitrarily shaped cavities

Fig. 8.4 shows an example enclosure with an arbitrarily shaped closed cavity. Assuming that layout is an optimal structural solution given by the layout optimisation, the fundamental question to be address is the approach to discretise such a layout.

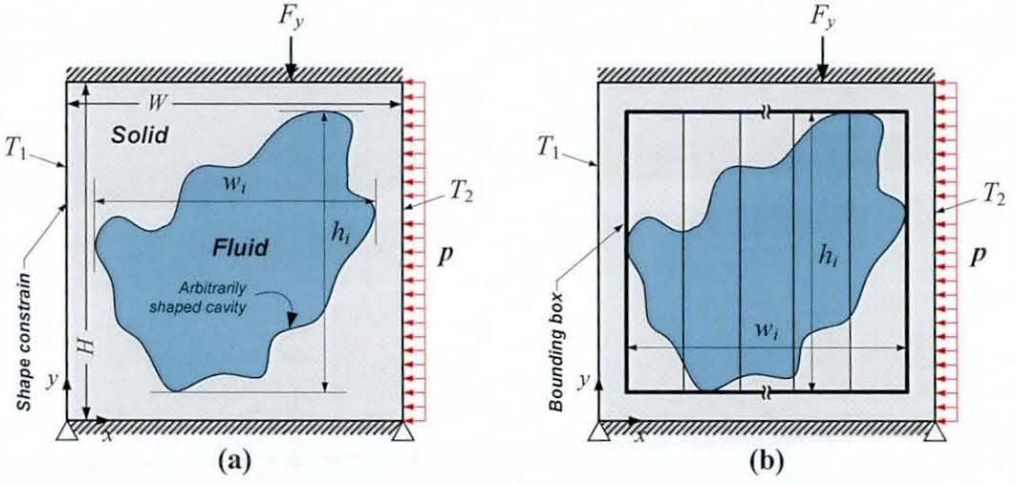

Fig. 8.4 Discretisation of enclosure with arbitrarily shaped cavity: (a) Geometric approximation of arbitrarily shaped cavity; (b) discretisation of arbitrarily shaped cavity.

Despite the reduced mass, any voids created internally if left 'untreated' would enhance convection. In this case, the DbPM may be used to discretise the voids to impede the convective flows, as opposed to insulation filling.

However, the internal airspaces within building structures do not exhibit geometric uniformity. In general, most design problems exhibit geometric non-uniformity. In order to address such problems, the discretisation approach has to be able to

accommodate such geometries. Arbitrarily shaped cells may be discretised such that the *R*-value of a structurally optimised enclosure is optimally maximised. The method works by 'approximating' an arbitrarily shaped void as a rectangular cavity, as Fig. 8.4a shows. Subsequently, a rectangular 'bounding box' is 'mapped' onto the cavity. This is then discretised, through introduction of solid partitions, until an optimal suppression is obtained (Fig. 8.4b). This approach can be extended to cover enclosures with multiple arbitrarily shaped cavities.

8.3.2 Discretisation of multiple non-uniformly shaped cavities

Fig. 8.5 shows an example of the procedures involved with the approximation and discretisation of an enclosure with multiple arbitrarily shaped cavities.

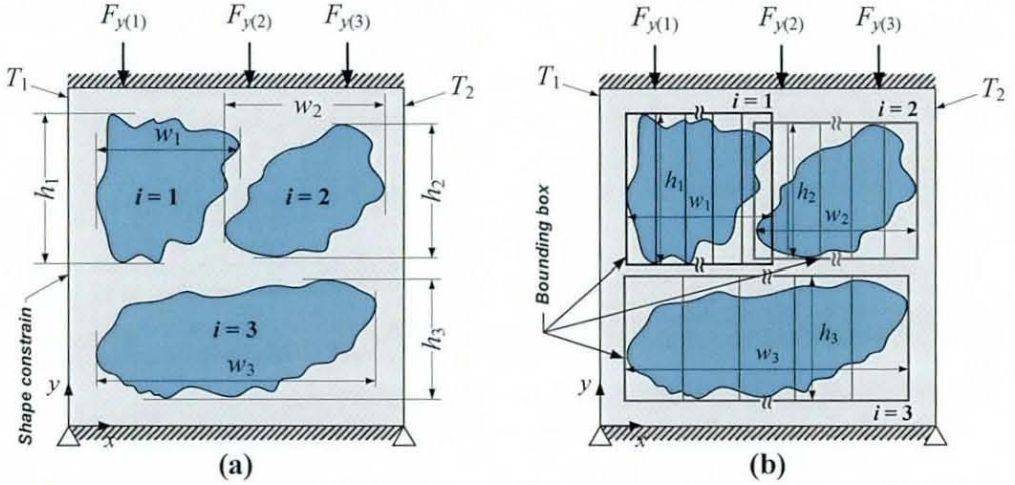

Fig. 8.5 Example of structurally optimised enclosure with multiple arbitrarily shaped cells: (a) Geometric approximation of *i*-cells; (b) discretisation of enclosure with *i*-cells.

In this case, the discretisation was made complicated, due to the differences in aspect ratios of the cells/cavities (Fig. 8.5a). Therefore, a discretisation layout obtained by using a 'global' discretisation approach would not necessarily yield an optimal suppression. In order to achieve an optimal suppression, each of the approximated cells had to be considered separately and discretised 'locally' (Fig. 8.5b). In addition to the design criteria highlighted in Section 8.2.2, the additional considerations for the discretisation of enclosure with multiple cells are;

i) The local thermal boundary conditions of the cell

ii) The 'approximated' aspect ratios of the local cell

iii) The range of the average *Nu* and operating *Ra*

8.4 Optimal discretisation of structured insulator enclosures

If the initial hypothesis was correct, the rate of suppression of q across enclosures with multiple arbitrarily shaped cells is a function of N_i within each cell. This is valid up to a threshold discretisation limit, whereby further discretisation would not yield increased insulation. Fig. 8.6 depicts the discretisation approach of the modified DbPM on the layout optimised insulator enclosure.

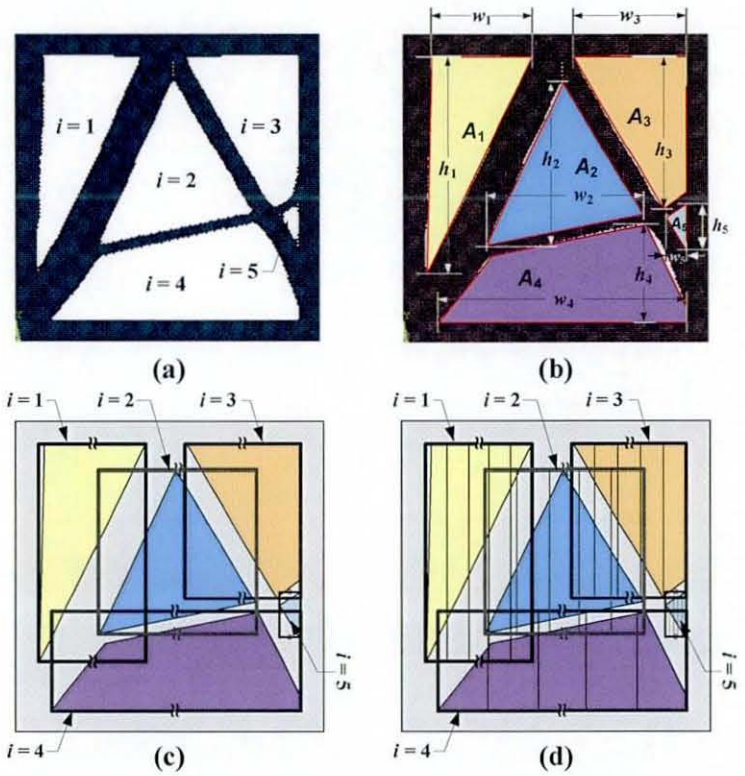

Fig. 8.6 Geometric approximation and discretisation of multiple cells: (a) FE-model of optimised enclosure by MD; (b) 'defeaturing' of cell geometry; (c) discretisation of i-cells.

In this study, the outcome of the optimisation resembled a 2D continuum 'plane truss' with $i = 5$ cells (Fig. 8.6a). To facilitate the creation of the CFD analysis models, the geometric features incorporated at the post-processing stage of are removed. The maximum height and width of each cell was identified (Fig. 8.6b). Subsequently, a rectangular bounding box was 'circumscribed' onto each of the cells to approximate them as rectangular cavities (Fig. 8.6c). The approximated cells are then discretised 'locally', using an iterative approach with an increment of $N_i + 1$ partition.

Fig. 8.7 depicts the iterative discretisation procedure of the modified DbPM for n_i-iterations. The discretisation was started from an enclosure of N_i = 0, with cell widths $w_{N_i} = w_0$ and approximated aspect ratios of $s_{N_i} = h_{N_i} / w_{N_i}$ (Fig. 8.7a).

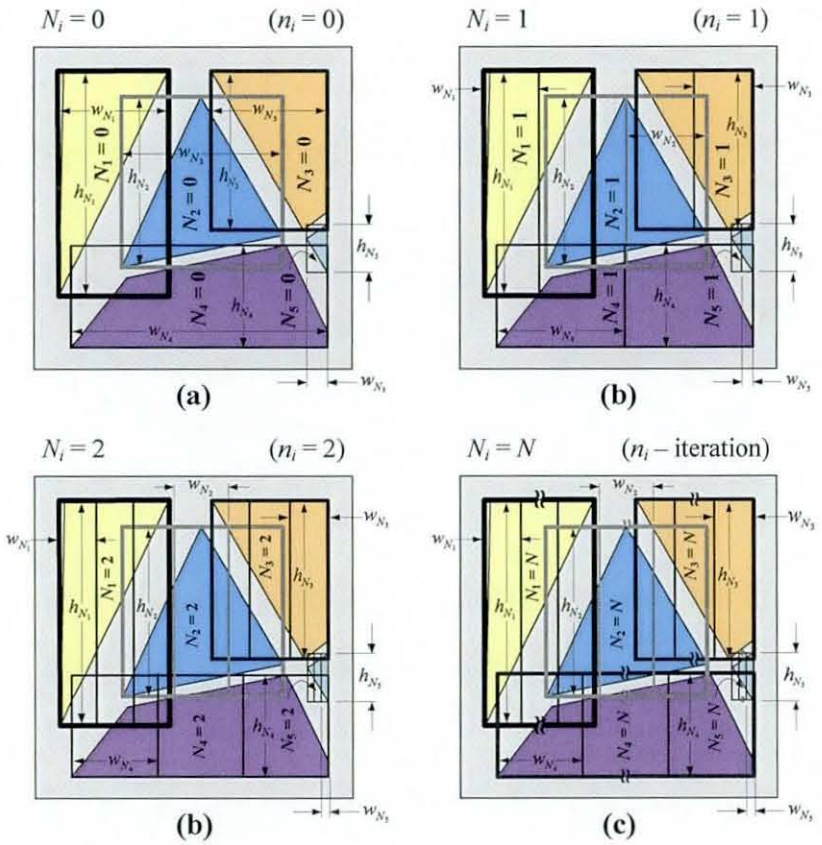

Fig. 8.7 'Local' discretisation of enclosures with multiple cells by the modified DbPM: (a) Iteration-0 initial design with $N_i = 0$; (b) iteration-2 with $N_i = 1$; (c) iteration-n with $N_i = N$.

At the first iteration (Fig. 8.7b), a vertical partition was inserted to bisect the approximated cells to form an enclosure consisting of N_i local partitions with a total number of partitions

$$N_T = \sum_{i=N_{i\min}}^{N_{i\max}} N_i \tag{61}$$

The relationship of the width w_{N_i} in terms of N_i of the i-th discretised cell is written as

$$w_{N_i} = \frac{w_i - N_i t_p}{N_i + 1} \tag{62}$$

where w_i is the width of the approximated i-th cells. In addition to seeking an optimal discretisation, a balance between convection-conduction was sought, in which is controlled by the 'macro' solid volume fraction of the discretised enclosure, given by

$$\varphi = \frac{V_d}{V_s} \tag{63}$$

where V_d and V_s are the volume of the enclosure with optimal discretisation and solid enclosure respectively. Fig. 8.8 shows the general process flow of the DbPM for an enclosure with multiple cells.

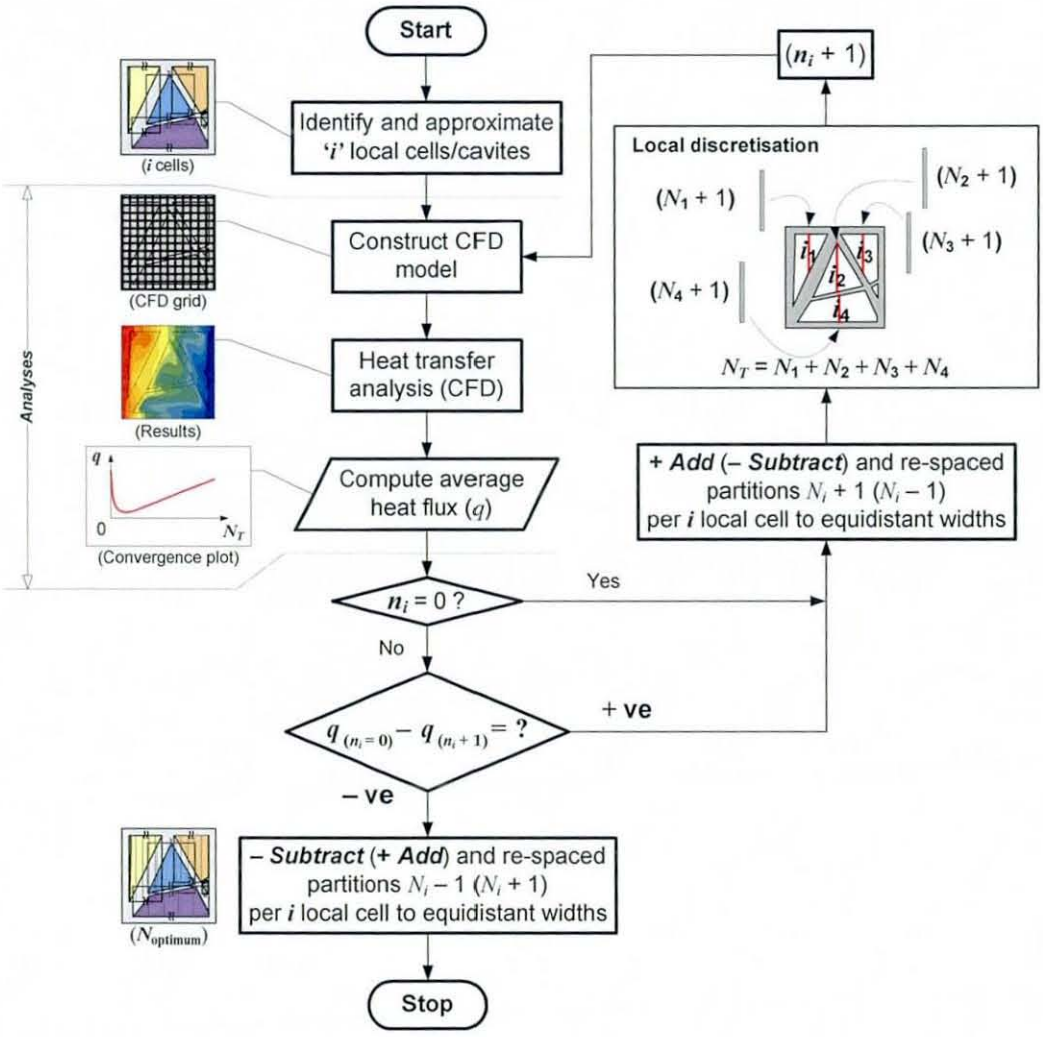

Fig. 8.8 General process flow of the modified DbPM for enclosure with multiple cells

In the DbPM, it is not the design objective for the introduced partitions do not act as additional structural supports. Instead, they act as solid matrices to suppress the natural convective flows within the discretised cells. Ideally, the thicknesses of the partitions

should be considerably thinner than the section thicknesses of the structural members of the enclosure. When manufacturing by AMT is taken into consideration, the minimum thickness is limited to the minimum section build thickness of the manufacturing process used.

8.5 Mathematical model of the DbPM

The discretisation problem of the insulator enclosure to be solved can be formally stated as

Minimise $q(N_1, N_2, ..., N_i)$ (64)

.

subject to $N_{i_{\min}} \le N_i \le N_{i_{\max}}$ (65)

$$Nu = \frac{1}{h/w_N}\left[\frac{\left\{\int_0^{h/w_N}\left(\frac{\partial \mathrm{T}}{\partial X}\right)\partial Y\right\}_{conv.}}{\left\{\int_0^{h/w_N}\left(\frac{\partial \mathrm{T}}{\partial X}\right)\partial Y\right\}_{cond.}}\right] \quad , \quad Nu \approx 1 \tag{66}$$

with $a_l \le m/m_0 \le a_u$ (67)

$\sigma \le \sigma_0$, $\delta \le \delta_0$ (68)

where q is the average heat flux, which is a function of N vertical partitions. Subscript 'i' denotes the local cell within an enclosure. $N_{i_{\min}}$ and $N_{i_{\max}}$ are the minimum and maximum number of 'local' partitions within an enclosure. The average Nusselt number Nu, which is a ratio of the convective to conductive heat transfers, is used as a measure to quantify effectiveness of the discretisation layout. The aim of the discretisation is to produce a value of Nu close to unity, indicating a conductive dominant state.

Despite the gain in thermal insulation, the introduction of partitions would affect the reduced mass brought about by the structural optimisation performed in Stage-1. In the two-stage approach, this slight increase in mass caused by the increase in volume of the introduced partitions is unavoidable. In this study, the increase in mass can be estimated from a secondary validation analysis used to determine the mass ratios (m/m_0) of the optimally discretised enclosures. Subscript '0' denotes the mass of the insulator

prior to discretisation. By taking into consideration the imposed design constraints, the analysis is valid for enclosures with volume ratio φ of ~ 0.25 to 1, with the latter indicating a solid volume. For this particular design problem, 'a' is an empirical constant to be determined by a regression analysis. Here, subscripts 'l' and 'u' denotes the lower and upper bound of the mass ratio. Here, a_l and a_u is determined to be ~1.002 to ~ 1.371. In general, the a constant depends on;

i) Volume ratio φ

ii) Thermal boundary conditions

iii) Thermal physical properties

iv) Solid/fluid thermal conductivity ratio

In this study, the analysis to determine the mass ratio is performed manually, with the use of the modified DbPM to determine the optimal discretisation for a total of forty enclosure models with randomly selected cell layouts. In addition, the analysis also serves as a validation study to check for consistency of the discretisation results.

8.6 Validation procedure of DbPM

The aim of the secondary analysis is to determine an optimal discretisation layout for a range of cell geometries using the modified DbPM. The validity of the method was tested to establish the trend of the mass ratio m/m_0 terms of the solid/fluid volume fraction (φ) and the percentage (%) suppression of the global heat flux q. A total of forty enclosure models of fixed external dimensions with various cell layouts, were designed, as Fig. 8.9 shows. These initially non-discretised enclosure models can be categorised as; (a) variable size single continuum cavity, (b) randomly shaped multiply cavity, and (c) rotated continuum single branching cavity. For the results to be comparable, the thermal boundary conditions and design constraints used were similar to that of the analysis covered in the previous section.

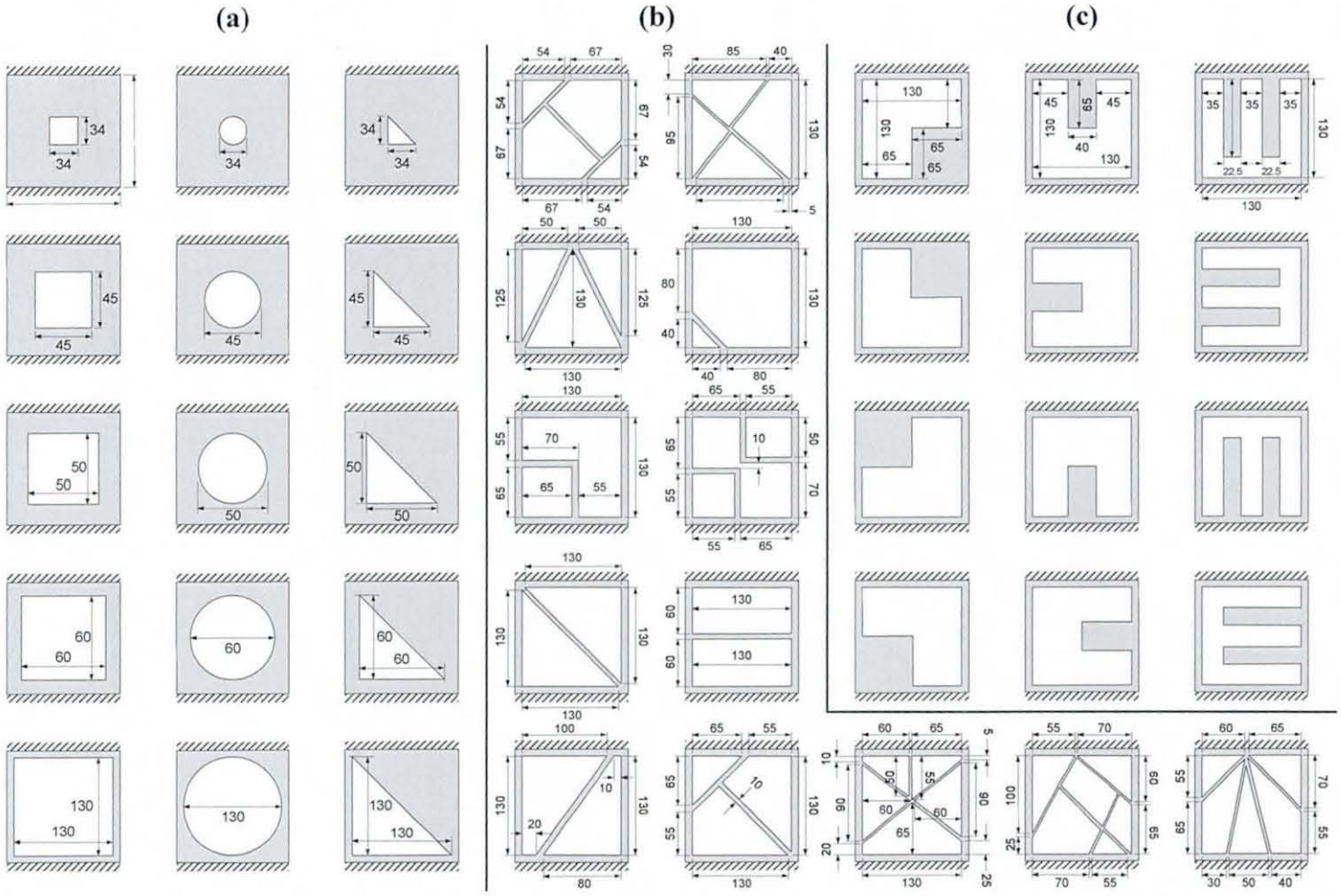

Fig. 8.9 Enclosure models used in the validation study of the DbPM: (a) single closed cavity; (b) multiple closed cavity; (c) single 'branching' cavity.

Using the modified DbPM, equidistantly spaced vertical parallel partitions were introduced in an iterative fashion to the each i-th local cells. This was process was repeated until the global heat flux q across the enclosure could not be further reduced. For example, if the value of q for an enclosure with i cells and N_i partitions decreases when the number of partitions is increased by $N_i + 1$, this would indicate that the current layout is not the optimum and could be improved. Thus, the number of partitions needed to be increased by $N_i + 1$, to the point where the onset of increase in q is observed. Due to the fact that each of the geometries of the i-th cells may have different approximated aspect ratios, the discretisation may involve trial and error before an optimal discretisation layout could be found. In this validation study, the aforementioned procedures were repeated until an optimal discretisation was obtained for each of the selected enclosure models. The results are presented by means of graphical form in Section 8.10, in which the empirical constant 'a' was determined from the validation analysis.

8.7 Computational models

The computational grids of the analysis models were constructed using the CFD pre-processor Gambit™. Fig. 8.10 shows the first three iterations of the solution domains, discretised using the four-node quadrilateral grids. A higher grid concentration was distributed at the solid-fluid interfaces, where variations in fluid velocities were expected to be more significant, particularly for subenclosures with lower aspect ratios. A uniform spacing ratio is used, where relatively stagnant cores are predicted. A relatively course mesh is used in the solid regions. Fig. 8.11 shows the solution domains of the insulator enclosure models discretised using the modified DbPM. A three-node triangular mesh with global mesh size of 2 mm was used. For simplicity, a uniform grid was sufficient because the effects of the boundary layers are expected to diminish with a discretised layout.

For both sets of analysis models, steady-state temperatures of T_1 = 298.15 K and T_2 = 283.15 K was applied to the left (at $x = 0$, $0 \leq y \leq H$) and right walls (at $x = W$, $0 \leq y \leq H$) respectively. The upper (at $y = H$, $0 \leq x \leq W$) and lower horizontal walls (at $y = 0$, $0 \leq x \leq W$) were assumed to be perfectly insulated, with $\partial T/\partial y = 0$. Nonslip boundary conditions were assumed for velocities at all solid-fluid interfaces with $u = 0$ and $v = 0$. The analysis models were designed to simulate high Rayleigh number in the range of $Ra \approx 10^7$, the operating range encountered in most engineering applications. The thermal physical properties of the working fluid used in the numerical analysis were based on those of atmospheric air at 300 K, as given in Table 8.1. The computational method used is previously covered in Section 6.4.

Table 8.1

Thermal physical properties of atmospheric air (evaluated at 300K, 1atm)

Thermal conductivity (k_f)	0.0263 W/m•K
Specific heat capacity (c_p)	1007 J/kg•K
Density (ρ)	1.1614 kg/m^3
Kinematic viscosity (v)	1.655×10^{-5} m^2/s
Dynamic viscosity (μ)	1.846×10^{-5} kg/m•s
Prandtl number (Pr)	0.71
Thermal expansion coefficient ($1/T_\infty$)	0.00344

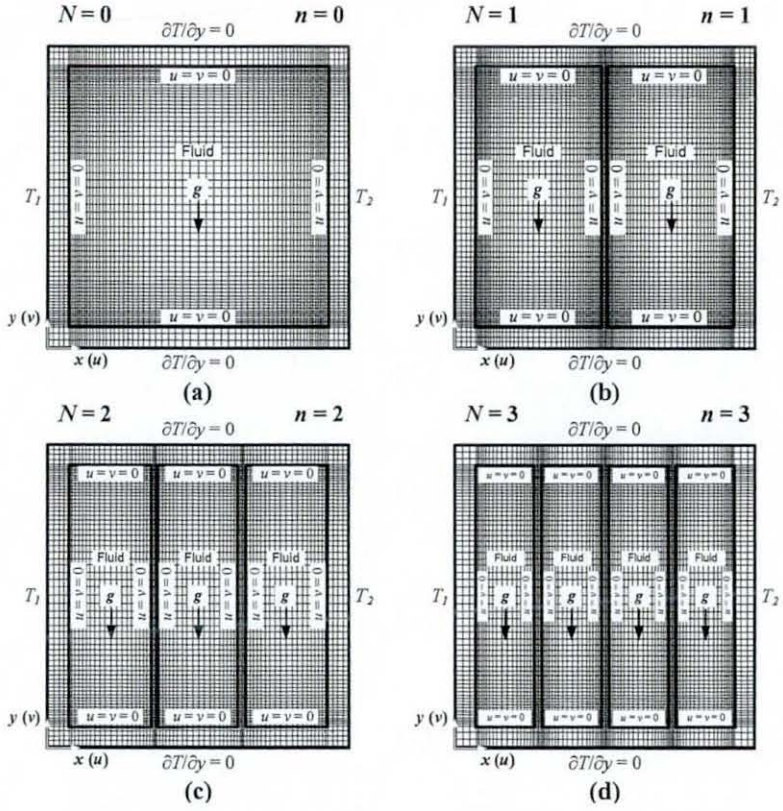

Fig. 8.10 Computational grids and boundary conditions of basic vertical enclosure: (a) $N = 0$; (b) $N = 1$; (c) $N = 2$; (d) $N = 3$.

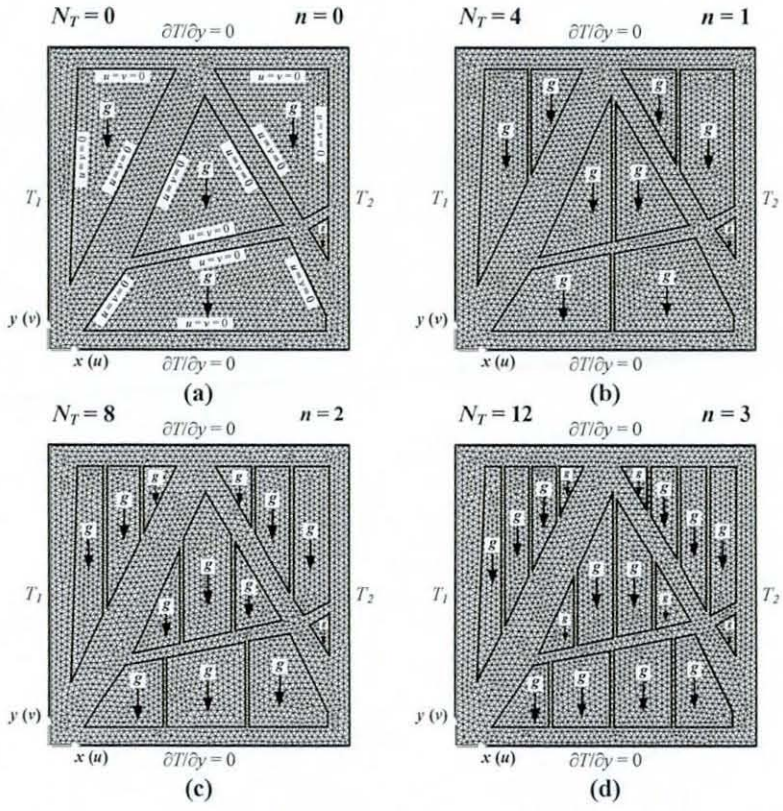

Fig. 8.11 Computational grid and boundary conditions of partitioned structured insulator: (a) $N_T = 0$; (b) $N_T = 4$; (c) $N_T = 8$, $N_T = 12$.

8.8 Results for 'basic' enclosure

8.8.1 Isotherm and stream function

Fig. 8.12 and Fig. 8.13 show the steady-state isotherms and stream functions of the basic enclosures with $N = 1$ to $N = 14$ partitions, evaluated at $Ra = 10^7$.

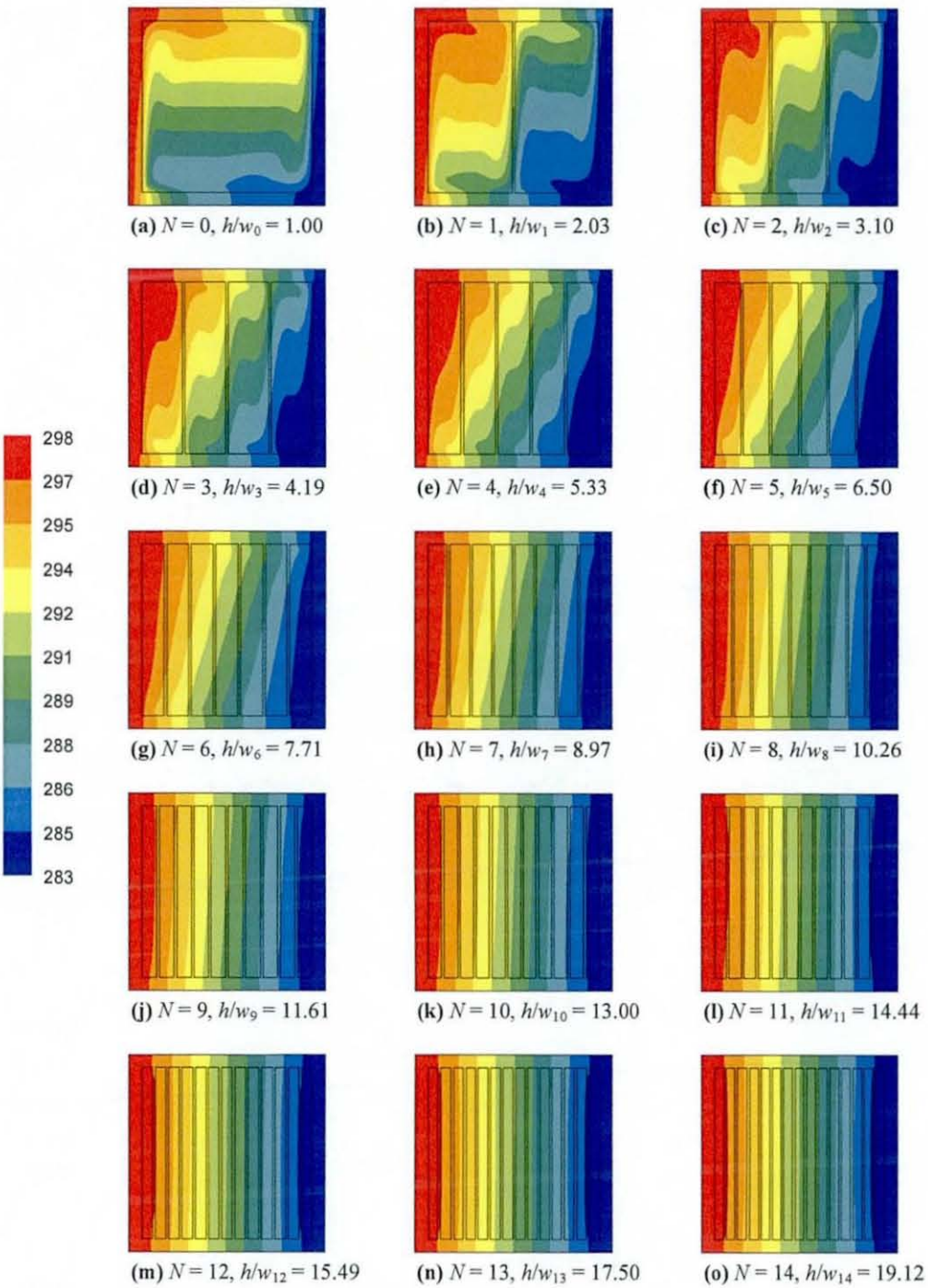

Fig. 8.12 Steady-state isotherms of partitioned enclosures for $N = 1$ to $N = 14$. Dimensions in Kelvin (K).

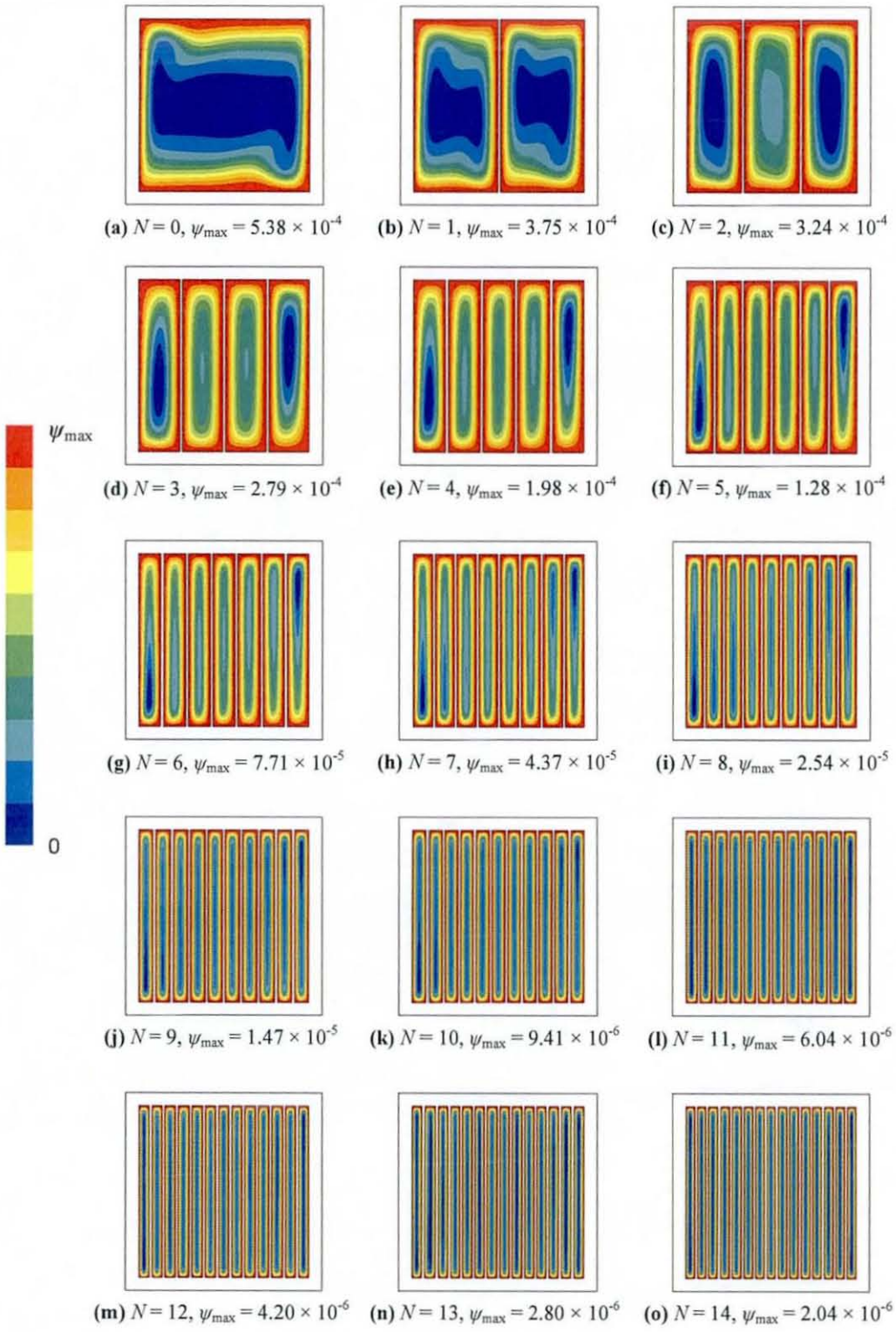

Fig. 8.13 Stream function of partitioned enclosures for $N = 1$ to $N = 14$ partitions. Dimensions in m^2/s.

For $N = 0$ to $N = 4$, the density of isotherms is more intense near the side walls and the partitions, but is less profound in the middle of each cell. The warmer fluid occupies the upper quadrants and the isotherms are compressed towards the solid-fluid interfaces.

From $N = 1$ to $N = 4$, the isotherms undulate remarkably, but diminished from $N = 5$ to $N = 8$. From $N = 9$ to $N = 14$, the isotherms become almost parallel to the side walls and partitions.

At $N = 0$, single cellular flows with a relatively stagnant core are formed and the streamlines are diagonally symmetrical. At $N = 1$, these were represented by a pair of diagonally symmetrical clockwise cellular flows. Hereafter, the development of the core region, which resembled offcentred ellipses, is more pronounced in the cells adjacent to the side walls. From $N = 3$ to $N = 9$, the circulating cells shifted away from the middle. From $N = 10$ to $N = 14$, the streamlines become crowded into the vicinity of the fluid-solid interfaces. As a general observation, the maximum stream functions (ψ_{max}) reduce with increasing N and h/w_N.

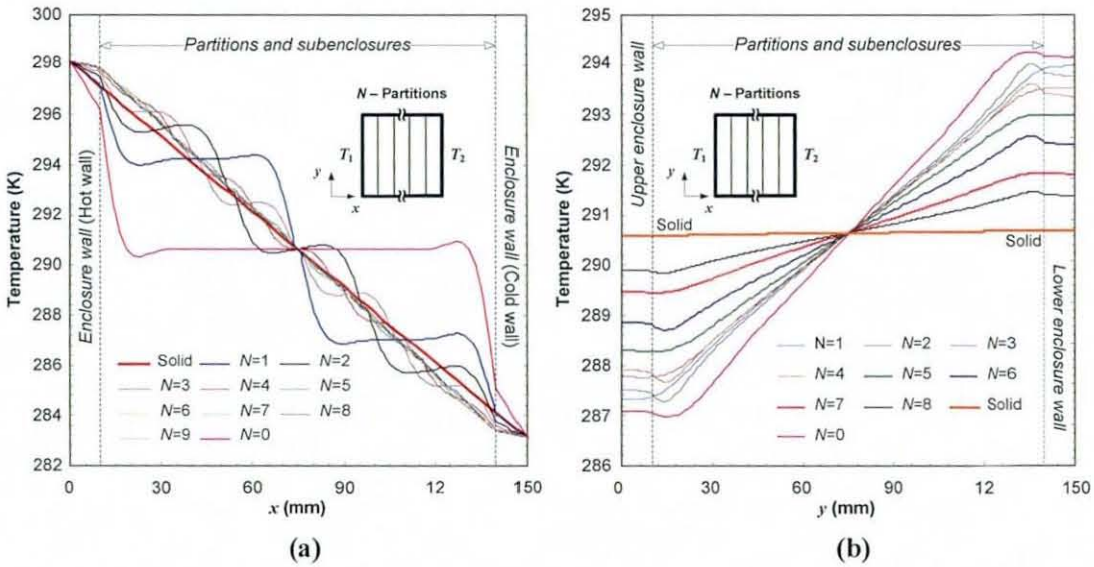

Fig. 8.14 Temperature profiles at the horizontal section for enclosures with $N = 0$ to $N = 8$.

Fig. 8.14(a) shows the temperature profiles of $N = 0$ to $N = 8$ plotted across the horizontal section at $y = H/2$. The temperature was observed to vary linearly across the solid regions of the enclosure walls. For $N = 0$ to $N = 4$, the temperature at the solid-fluid interfaces are initially represented by steep gradients, which is then maintained uniform at the core regions. Fig. 8.14(b) shows the temperature variation of $N = 0$ to $N = 8$ plotted vertically, at $x = W/2$. The temperature in the fluid region varies linearly, except near the lower and upper walls. When N is further increased, the variations approach a straight line.

8.8.2 Heat transfer results

The quantity of practical interest is the rate of suppression of q. The performance of the discretised enclosure is assessed by plotting q versus N, as Fig. 8.15(a) shows.

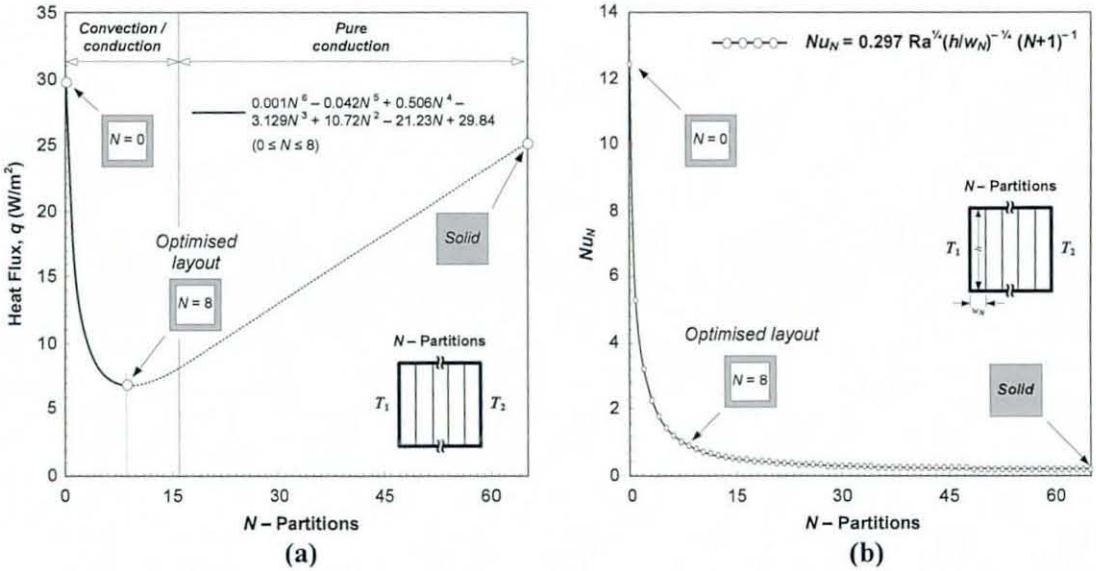

Fig. 8.15 Heat transfer results: (a) Global heat flux (q) vs. N-partitions; (b) correlation of Nusselt number (Nu_N) for partitioned enclosures.

Results from the numerical computations, show that the partitions have profound effects on q. The value of q decreases drastically with increasing N, but the introduction of partitions did not produce a proportional reduction. From a basic enclosure of $N = 0$, the reduction was found to be most significant from $N = 1$ to $N = 3$, but gradually diminished when N is increased from $N = 4$ to $N = 8$. For this current investigation, an optimum discretisation layout of $N_o = 8$, where q is optimally suppressed, was determined. Subsequent introduction of partitions, from $N = 8$ to $N = 16$, yielded a nonproportional increase in heat transfer. From $N > 16$, q increases linearly with N. The enclosure essentially becomes a solid when the upper limit of $N = 65$ is reached.

In order to elucidate the effects of partitions, additional calculations are performed for enclosures with $N = 0$ to $N = 64$. Fig. 8.15(b) shows the correlated Nusselt number (Nu_N) based on the correlation of recommended by Nishimura *et al.* (1988),

$$Nu_N = 0.297 Ra^{1/4} (h/w_N)^{-1/4} (N+1)^{-1} \tag{69}$$

where Nu_N is a function of h/w_N ratio and N. The introduction of equidistantly spaced vertical partitions resulted in a substantial reduction in Nu_N. However, the progressive introduction of partitions did not produce a proportional reduction. This reduction was found to be most significant for $N = 1$ to $N = 8$, but diminished when additional partitions are introduced. At $N_o = 8$, the correlation shows that $Nu_N \approx 0.78$, a close to unity. The effectiveness of N on Nu_N is greatly reduced when $N > 8$, where the curve shows a significant decline upon reaching a minimum at $N = 64$.

Fig. 8.16(a) presents the influence of the h/w_N on the heat transfer effectiveness across the partitioned enclosure. Nu_N is markedly reduced in subenclosures with $h/w_1 = 1.00$ to $h/w_3 = 4.19$, or as the slenderness is increased. However, the reduction is nonproportional and tended to diminish with increasing h/w_N. The results shows that at $N_o = 8$, the layout for which heat transfer is optimally suppressed, has $h/w_8 = 10.26$. Hereafter, the effectiveness of h/w_N on Nu_N exhibits a significant decline and gives way to a decreasing trend.

Fig. 8.16(b) shows the discretisation of enclosures as a function of N. From $N = 0$, φ increases proportionally with the increase in N, but this was not case for w_N/w. The reduction of w_N/w is most profound from $N = 0$ to $N = 8$ and diminishes with increasing N. The results show that the optimum partition layout with $N_O = 8$, as previously determined, has a volume fraction of $\varphi = 0.34$ and width ratio of $w_N/w = 0.097$.

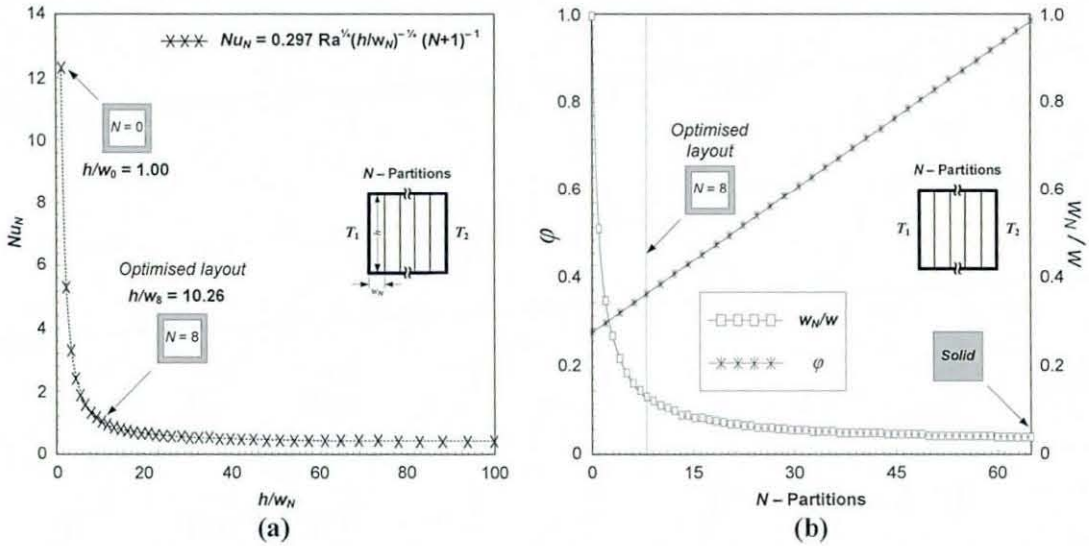

Fig. 8.16 (a) Subenclosure height/width ratio (h/w_N) vs. correlated Nusselt number (Nu_N), (b) solid/fluid volume ratio (φ) and subenclosure width ratio (w_N/w) vs. N-partitions

8.9 Results for structured insulator

8.9.1 Steady state isotherm, stream function and flow velocity

Fig. 8.17 through to Fig. 8.19 shows the steady-state isotherms, streamlines and velocity (v) contours plots of the discretisation history of the structured insulators with $N_T = 0$ to $N_T = 28$, evaluated at $Ra = 10^7$.

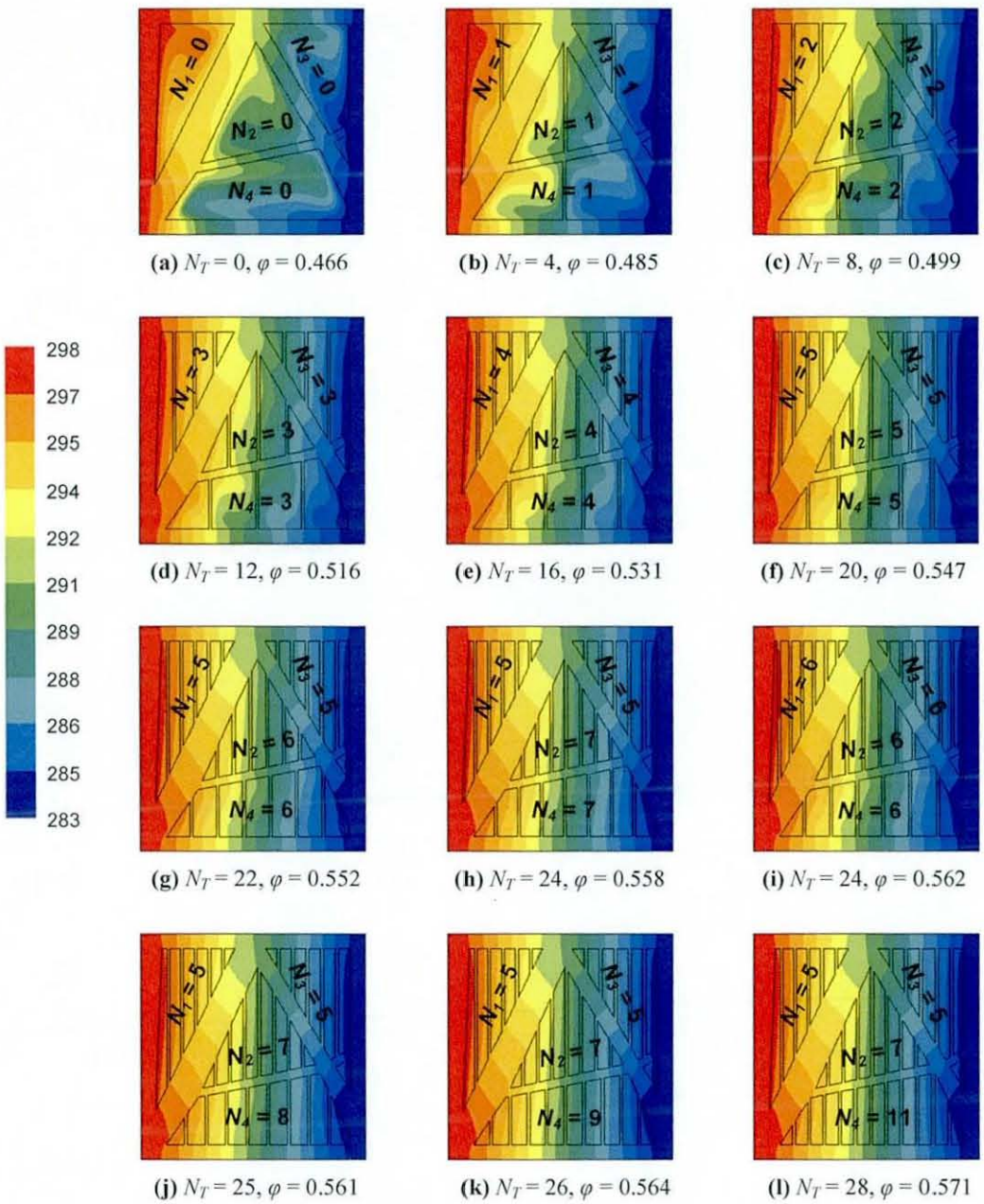

(a) $N_T = 0$, $\varphi = 0.466$ **(b)** $N_T = 4$, $\varphi = 0.485$ **(c)** $N_T = 8$, $\varphi = 0.499$

(d) $N_T = 12$, $\varphi = 0.516$ **(e)** $N_T = 16$, $\varphi = 0.531$ **(f)** $N_T = 20$, $\varphi = 0.547$

(g) $N_T = 22$, $\varphi = 0.552$ **(h)** $N_T = 24$, $\varphi = 0.558$ **(i)** $N_T = 24$, $\varphi = 0.562$

(j) $N_T = 25$, $\varphi = 0.561$ **(k)** $N_T = 26$, $\varphi = 0.564$ **(l)** $N_T = 28$, $\varphi = 0.571$

Fig. 8.17 Steady-state isotherms of structurally optimised partitioned enclosure of with multiple cells with $N_T = 0$ to $N_T = 28$ vertical partitions. Dimensions in Kelvin (K).

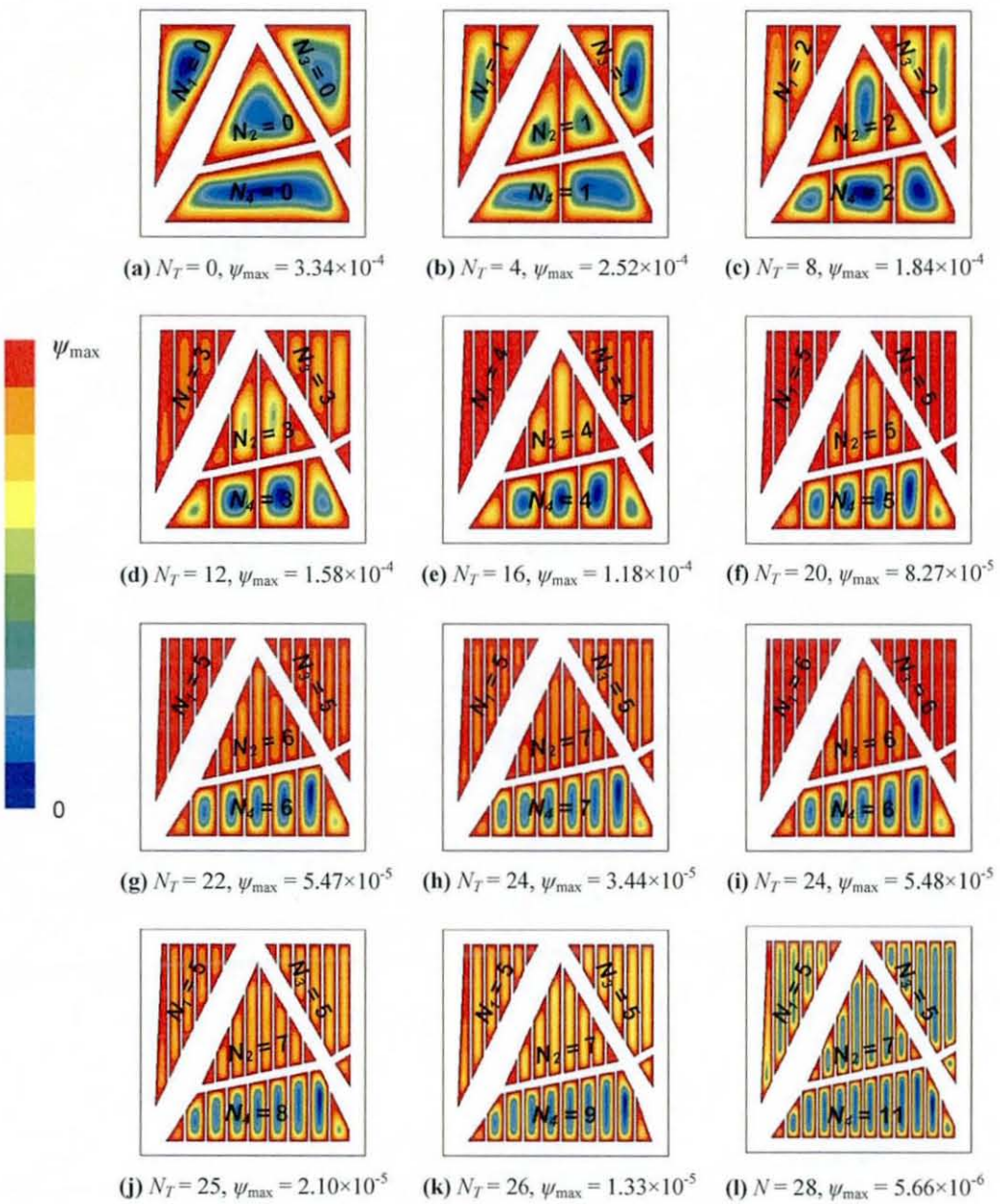

(a) $N_T = 0$, $\psi_{max} = 3.34\times10^{-4}$ **(b)** $N_T = 4$, $\psi_{max} = 2.52\times10^{-4}$ **(c)** $N_T = 8$, $\psi_{max} = 1.84\times10^{-4}$

(d) $N_T = 12$, $\psi_{max} = 1.58\times10^{-4}$ **(e)** $N_T = 16$, $\psi_{max} = 1.18\times10^{-4}$ **(f)** $N_T = 20$, $\psi_{max} = 8.27\times10^{-5}$

(g) $N_T = 22$, $\psi_{max} = 5.47\times10^{-5}$ **(h)** $N_T = 24$, $\psi_{max} = 3.44\times10^{-5}$ **(i)** $N_T = 24$, $\psi_{max} = 5.48\times10^{-5}$

(j) $N_T = 25$, $\psi_{max} = 2.10\times10^{-5}$ **(k)** $N_T = 26$, $\psi_{max} = 1.33\times10^{-5}$ **(l)** $N = 28$, $\psi_{max} = 5.66\times10^{-6}$

Fig. 8.18 Stream function (ψ) of structurally optimised partitioned enclosure with $N_T = 0$ to $N_T = 28$ vertical partitions. Dimensions in m^2/s.

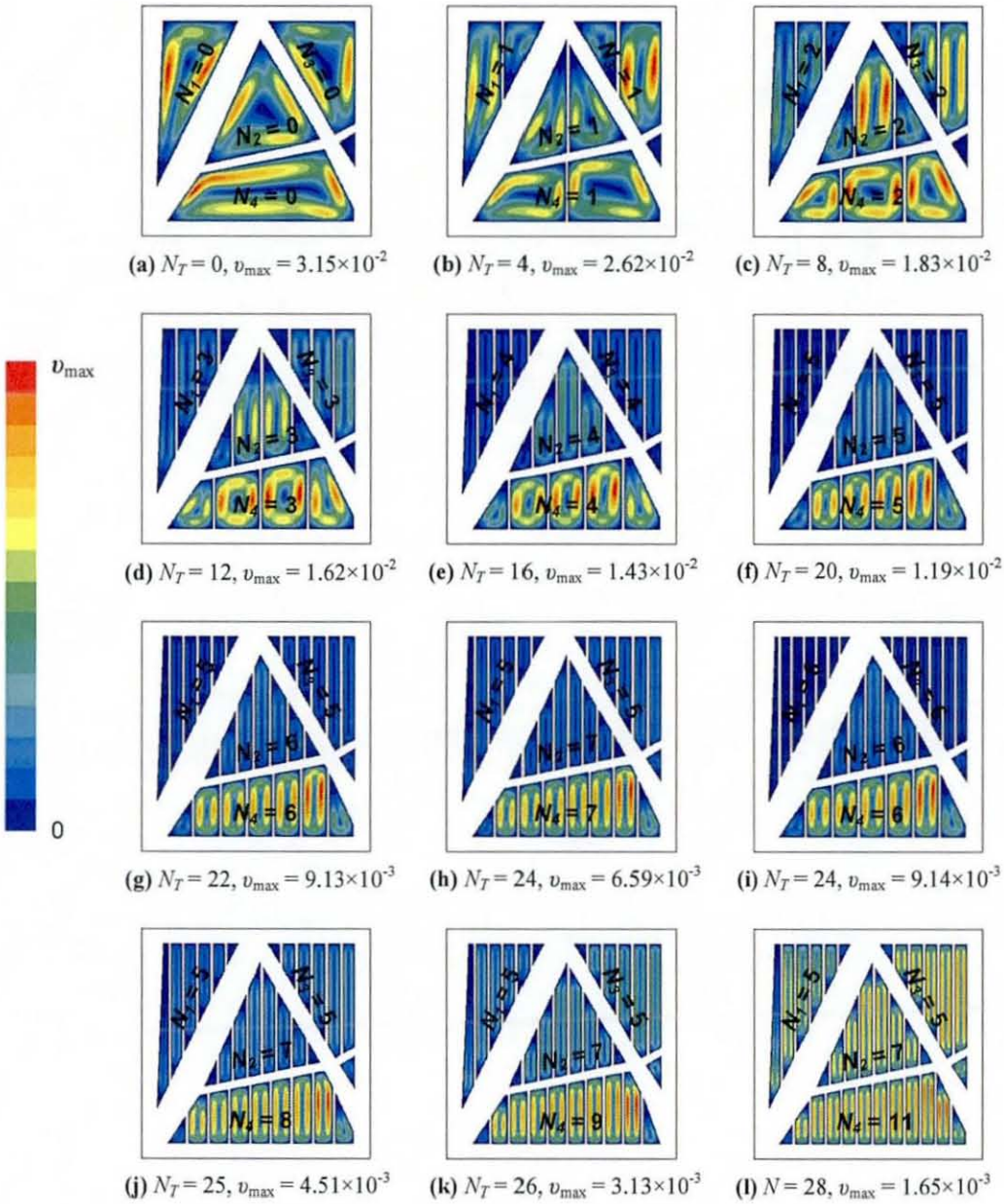

(a) $N_T = 0$, $v_{max} = 3.15\times10^{-2}$ **(b)** $N_T = 4$, $v_{max} = 2.62\times10^{-2}$ **(c)** $N_T = 8$, $v_{max} = 1.83\times10^{-2}$

(d) $N_T = 12$, $v_{max} = 1.62\times10^{-2}$ **(e)** $N_T = 16$, $v_{max} = 1.43\times10^{-2}$ **(f)** $N_T = 20$, $v_{max} = 1.19\times10^{-2}$

(g) $N_T = 22$, $v_{max} = 9.13\times10^{-3}$ **(h)** $N_T = 24$, $v_{max} = 6.59\times10^{-3}$ **(i)** $N_T = 24$, $v_{max} = 9.14\times10^{-3}$

(j) $N_T = 25$, $v_{max} = 4.51\times10^{-3}$ **(k)** $N_T = 26$, $v_{max} = 3.13\times10^{-3}$ **(l)** $N = 28$, $v_{max} = 1.65\times10^{-3}$

Fig. 8.19 Velocity magnitude (v) of structurally optimised partitioned enclosure with $N_T = 0$ to $N_T = 28$. Dimensions in m/s.

Fig. 8.17 shows the changes in the heat transfer characteristics due to the progressive introduction of equidistantly spaced parallel partitions in the cavities. In all, twelve design iterations are required before an optimal discretisation is determined. From $N_T = 0$

to $N_T = 8$, the isotherms are compressed to the solid-fluid interfaces and undulated within core regions. This indicated that the density of the isotherms is more intense at these regions. In addition, the upper quadrants are occupied by the warmer fluid. From $N_T = 12$ to $N_T = 24$, the undulations diminished with the increase in N_i. For $N_T > 25$, they become almost parallel to the partitions and sidewalls. In contrast, the isotherms at the solid regions remained relatively unchanged with the increase in the number of partitions.

Examination of the stream functions for enclosure with $N_T = 0$ to $N_T = 8$ (see Fig. 8.18), indicates that the flow structure within the cells are asymmetric. These are represented by the clockwise cellular flows with relatively stagnant cores, impinged by the inclined continuum structural members. From $N_T = 12$ to $N_T = 24$, the flow in cells i_1 to i_3 gradually diminish with increasing N_i. Hereafter, the recirculation was found to be noticeable only in cell i_4. For $N_T > 25$, the fluid remained almost stationary. Inspection of the figures revealed that the increase in the approximated subenclosure aspect ratio had resulted in weaker fluid flows. This is indicated by the decreasing values of ψ_{max}. In all, the optimal discretisation effectively decreases the ψ_{max} by two orders of magnitude.

Fig. 8.19 shows the influence of the total number partitions N_T on the velocity magnitude v_{max} of the convective flows in the discretised cells. From $N_T = 0$ to $N_T = 8$, the uprising and descending flows exhibit higher velocities, notably along the vertical and inclined surfaces. The same trend is observed for the horizontal flows at cell i_4. For $N_T = 12$ to $N_T = 28$, v_{max} decreases gradually with the increase of subenclosure slenderness. As a general observation, figures of the v_{max} showed that the increase in the number of partitions have effectively reduced the bulk fluid velocity by an order of magnitude.

Fig. 8.20 shows the horizontal and vertical temperature of the discretised enclosures with $N_T = 0$ to $N_T = 28$. The horizontal temperature profiles within the conducting solids exhibit a linear variation, as Fig. 8.20(a) shows. The temperature profiles at the solid-fluid interfaces are initially represented by a series of steep gradients. These are later maintained relatively uniform at the core regions in each cell. With further discretisation, the uniform temperature regions at the cores gradually diminish. This gives way to an almost linear temperature drop across each cell, indicated by the difference in gradients of the curves.

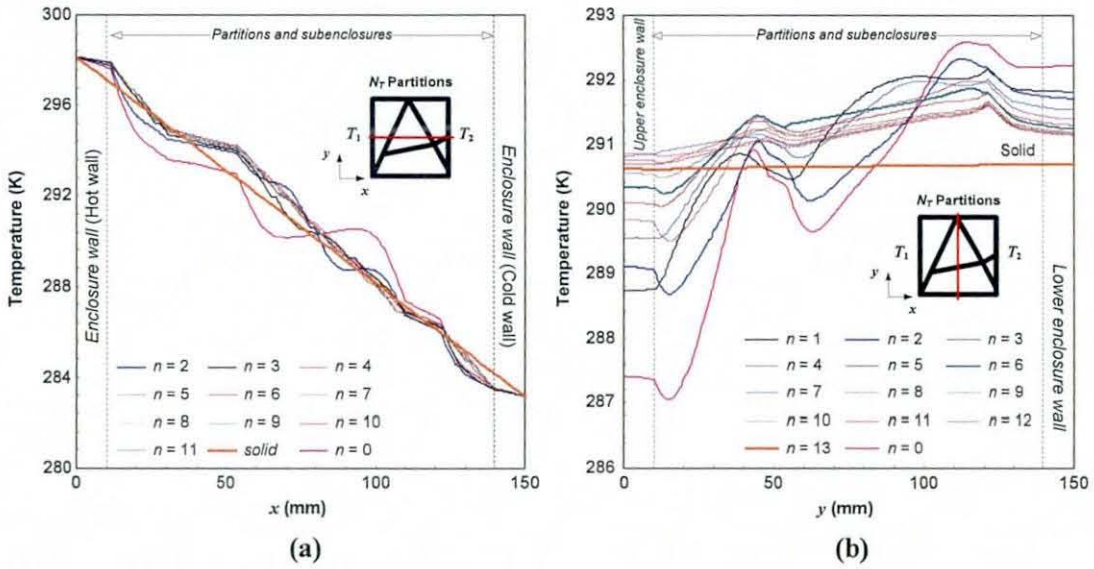

Fig. 8.20 Temperature profiles structured insulators with $N_T = 0$ to $N_T = 28$: (a) Horizontal section at $y/2$; (b) vertical section at $x/2$.

From Fig. 8.20(b), the vertical temperature variation is highly nonlinear, with significant fluctuations within the fluid regions. From $N_T = 0$ to $N_T = 24$, the temperature at the lower portion varies steeply, where a maximum temperature drop of ~ 5 °C is initially recorded. These fluctuations are observed to gradually diminish through further introduction of parallel vertical partitions. A near uniform vertical temperature distribution could not be achieved by the optimally discretised structured insulator. With close examination, it is revealed that the temperature variation along the vertical height is nearly isothermal which remained relatively uniform to within 1°C.

8.9.2 Heat transfer results

Fig. 8.21(a) shows the discretisation history plot of the structured insulators when q is plotted against n_i-iterations. In general, the q-n curve consist two distinct regions; a nonproportional reduction and linear increase of q with increasing N_i.

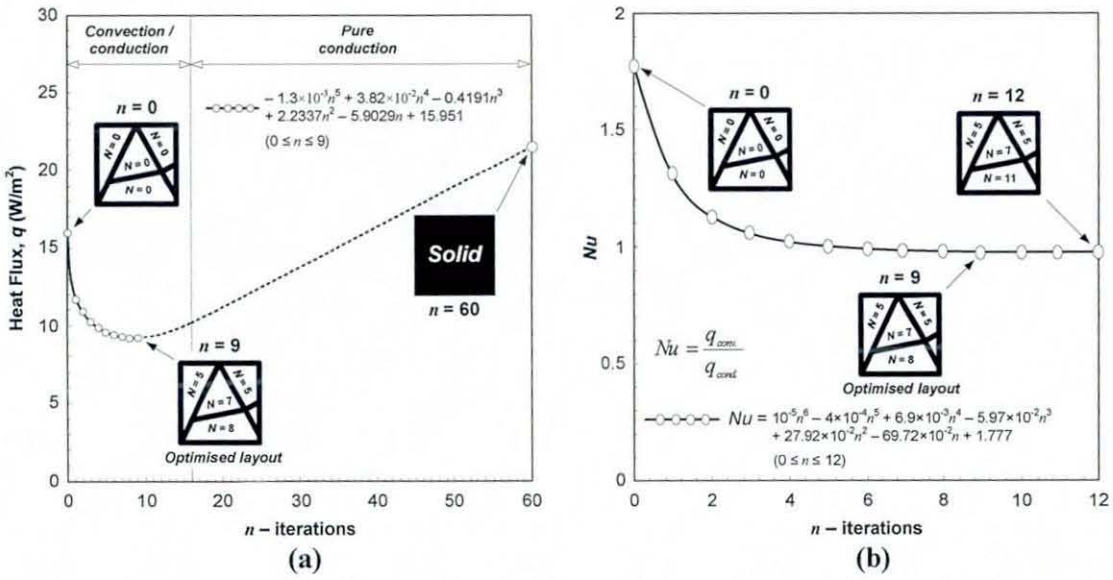

Fig. 8.21 Heat transfer results of discretised structured insulator: (a) Global heat flux vs. N_T for n-iterations; (b) average Nusselt number (Nu) vs. N_T for n-iterations.

The trend of the suppression is obtained using the least square fit to plot the best-fit curve to a fifth order polynomial. The global heat flux prior to discretisation was 15 W/m^2. Initially, q reduces considerably with increasing N_i. The introduction of parallel partition produces a nonproportional heat transfer reduction. At n = 9, the curve reaches a minimum, with global heat flux value of q = 8 W/m^2. This suggests that a maximum suppression has been achieved. In this study, this particular layout is regarded as the optimal design (where N_1 = 5, N_2 = 7, N_3 = 5, N_4 = 8, N_5 = 0). Based on the given design constraints, the subsequent introduction of partitions would not yield further suppression. Instead, a linear increasing trend is observed. This is valid up to the threshold limit where the structure essentially becomes a solid body.

Fig. 8.21(b) shows the relationship of the average Nu in terms of N_T, for n_i-iterations. Due to the complex internal layout of the enclosures, the heat transfer rate as a result of the discretisation could not be predicted by empirical correlation. Instead, the average Nu was determined from the ratio of the average convective to conductive heat transfer rate,

from the left to right bounding walls of the insulator enclosure. In this case, the relationship of Nu in terms of N_T was obtained using the least squares fit to plot a best-fit curve to a sixth order polynomial trend line. The average Nu prior to discretisation was computed as approximately 1.6. The results indicated that Nu was markedly reduced as the number of parallel partitions in the cells increases. With further increase in N_T, this deceasing trend diminishes and gives way to a flat decrease. The optimal discretisation layout obtained at $n_i = 9$ (where $N_T = 25$) corresponds to an average Nu of approximately 1.1. It was observed that a slight decrease in Nu could be gain through further discretisation. In fact, subsequent introduction of solid partitions beyond the point of the optimal solution would not yield further suppression of heat transfer. Table 8.2 summarises the design attributes of the discretised insulator enclosure.

Table 8.2

Design attributes of the non-convective structured insulator using DbPM

Attributes		**Initial design**	**Optimally discretised**
Mass	(m)	1.53 kg	1.84 kg
Global heat flux	(q)	15.97 W/m^2	9.39 W/m^2
Average Nusselt number	(Nu)	1.78	0.98
Maximum stream function	(ψ_{max})	3.34×10^{-4} m^2/s	2.10×10^{-5} m^2/s
Maximum velocity	(v_{max})	3.15×10^{-2} m/s	4.51×10^{-3} m/s
Number of partitions (local)	(N_i)	$N_1 = 0, N_2 = 0, N_3 = 0,$ $N_4 = 0, N_5 = 0$	$N_1 = 5, N_2 = 7, N_3 = 5,$ $N_4 = 8, N_5 = 0$
Number of partitions (total)	(N_T)	$N_T = 0$	$N_T = 28$

8.10 Results for validation analysis of DbPM

Fig. 8.22 shows the results of the validation analysis of the DbPM in finding the optimal discretisation for a total of forty rectangular enclosures with various cell layouts.

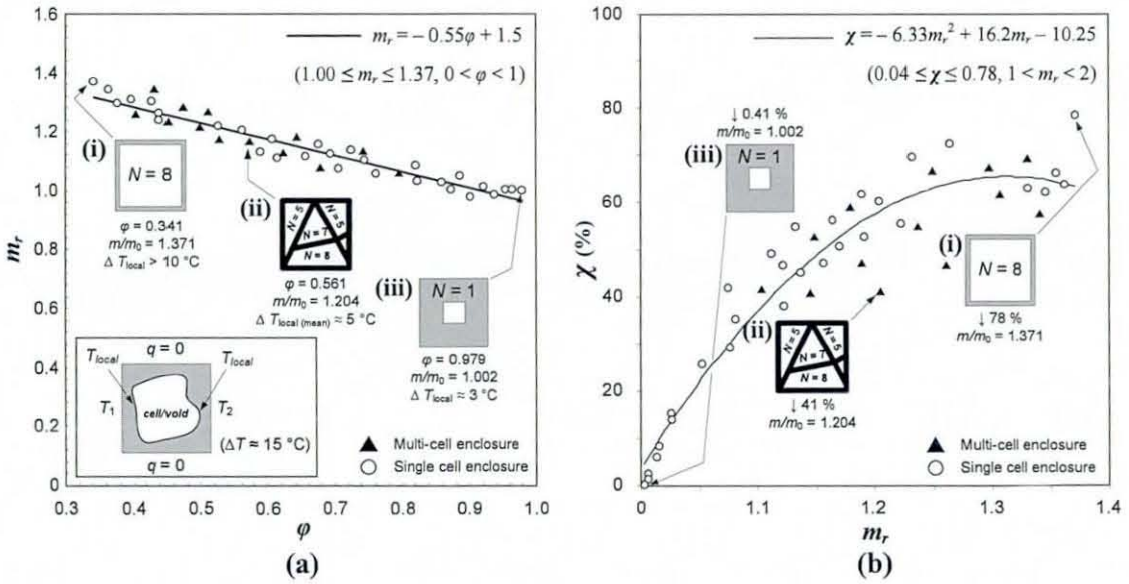

Fig. 8.22 Validation analysis of DbPM on enclosures with various cell layouts: (a) mass ratio m/m_0 vs. solid/fluid volume fraction φ regression plot; (b) percentage gain in suppression χ (%) vs. mass ratios.

The obtained data points, each representing an enclosure with optimally discretised layout, show a decreasing trend. The least squares fit was use to approximate the best-fit linear trend line, as Fig. 8.22(a) shows. The decreasing trend of the various optimal discretised layouts was observed to be fairly consistent, regardless of the geometry of the cell layout. In general, enclosures with low cell aspect ratios (i.e. rectangular and circular cells) would require more partitions to achieve an optimal suppression. In fact, the number of N local or global partitions required to achieve an optimal suppression depended not only on cell geometries and aspect ratios, but also the 'local' thermal boundary conditions. This effect is illustrated by the upper and lower limits of the m/m_0 for the investigated enclosure models, as (**i**) and (**iii**) highlights. For the case of the structured insulator (**ii**), the increase in m/m_0 discretised using the modified DbPM, falls within the estimated range.

Fig. 8.22(b) shows the curve obtained when the maximum percentage (%) suppression of q is plotted against m/m_0. Although the data points were fairly dispersed, an increasing trend could still be observed. Initially, the data points fall close to the mean, but deviate

with increasing m/m_0. The least square fit is use to approximate the best-fit curve to a second order polynomial trend line. The curve indicated that the maximum percentage increase in suppression is not proportional, and tended to decrease with increase m/m_0. In this study, the minimum and maximum percentage gain in suppression of q was recorded as 0.41% to 78% respectively, as indicated by (**i**) and (**iii**). Enclosure (**iii**) could be seen as a threshold limit whereby the introduction of parallel vertical partitions would actually benefit the suppression of heat transfer. With $\Delta T_{local} \approx 3$ °C ($\varphi \approx 0.95$), just 0.41 % suppression could be achieved. Therefore, this indicated that cells with local temperature drop of approximately $\Delta T_{local} < 3$ °C, regardless of geometry or aspect ratio would not benefit from the introduction partitions of similar material to the main enclosure. As a general observation, the number of partitions required for optimal suppression, in relation to the range of ΔT_{local} are summarised in Table 8.3.

Table 8.3

Range of ΔT_{local} and number of optimal partitions (N_o)

Temperature drop across cell (ΔT_{local})	**Number of optimal partitions (N_o)**
$\Delta T_{local} > 10$	$5 < N_o < 8$
$3 < \Delta T_{local} < 10$	$1 < N_o < 5$
$\Delta T_{local} \approx 3$	$N_o = 1$
$\Delta T_{local} < 3$	$N_o = 0$

These figures only serve as a general design guideline in the selection of the number of useful partitions for this particular design problem. An iterative discretisation approach is to be performed in order to determine N_O.

8.11 Discussions

8.11.1 Effects of discretisation on heat and fluid flow fields

Prior to discretisation, thermal boundary layers (TBL) developed at the solid-fluid interfaces, due to the differences of the far-field and surface temperatures. The rate of heat transfer across the TBL is determined by the thickness δ_t adjoining the sidewalls. The transport of heat is primarily provided by buoyancy-driven convective circulation, caused by the fluid density gradient and gravitational force. This motion, which is confined to the region affected by heat transfer, is known as the heat transfer-controlled buoyant motion (Kaviany, 2002). As the TBL developed along the surfaces, the effects of heat transfer penetrated into the 'far-fields' (Fig. 8.23). The general characteristics of the isotherms for a single rectangular cavity is consistent with findings of Kaminski and Prakash (1986), Acharya and Jetli (1990), Misra and Sarkar (1997), Chang and Tsai (1997) and Cianfrini et al. (2005), to name a few relevant ones.

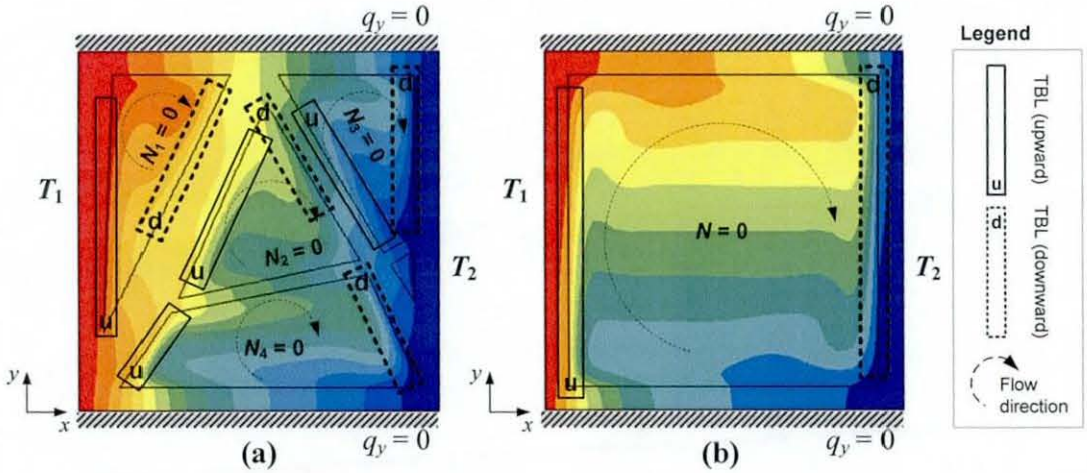

Fig. 8.23 Development of the 'upward' and 'downward' thermal boundary layer (TBL) in non-discretised enclosures: (a) Structured insulator; (b) basic rectangular enclosure.

The structural layout produced by the MD method consisted of inclined surfaces which are not aligned with the gravitational vector g. Hence, buoyancy forces are subjected to normal and parallel force components. Since the y-component is reduced to $g \cos \theta$, fluid velocities along the inclined surfaces are reduced, with an attendant reduction in convection (Rohsenow *et al.*, 1998) depicted in Fig. 8.24(a). Moreover, the distance y needed for the TBL to fully develop and for the heat transfer to penetrate the far-field is comparably less. Therefore, it is expected that an attendant reduction in convection could

be gained from cells with opposing inclined surfaces. This observation agrees well with the findings presented by Varol *et al.* (2006), Basak *et al.* (2007) and Natarajan *et al.* (2007) on the analysis of enclosures with inclined roofs. In contrast, buoyancy forces act only in the vertical direction to induce fluid motion within enclosures with partitions parallel to the sidewalls. In this case, the TBL would remain flat over the vertical surfaces; a typical feature which indicate the dominance of the thermobuoyant heat transport mechanism, depicted in Fig. 8.24(b).

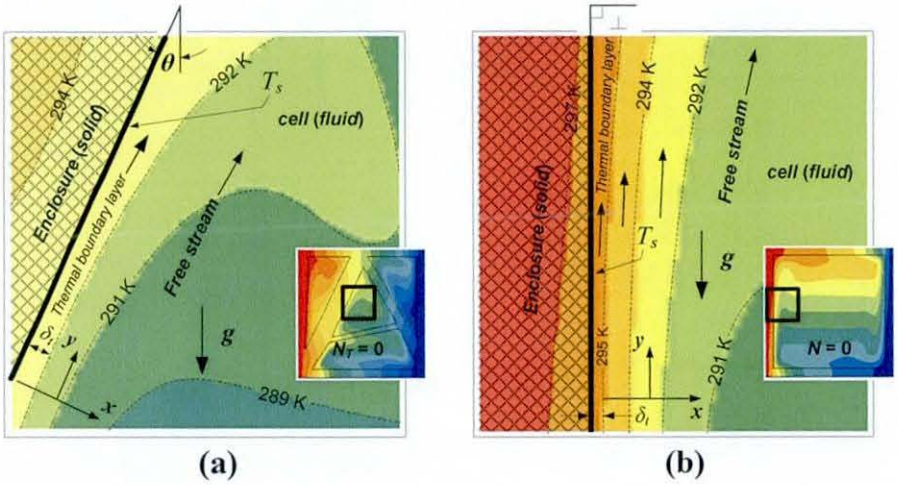

Fig. 8.24 Development of thermal boundary layers (TBL) in fluid-filled cells: (a) Upward flow on inclined surface of the structured insulator; (b) upward flow on a vertical surface of the initial investigative model.

The inclusions of thin parallel vertical partitions have profound effects on the flow and heat transfer characteristics (see Fig. 8.25). At the upper quadrants, the upstream flow 'detached' and penetrates the free stream. This observation is consistent with the findings by Ho and Chang (1993). Although the magnitude of the convective flows are markedly reduced, as indicated by the ψ_{max} and v_{max} plots, the undulations of isotherms indicated that heat transfer in the fluid region was still primarily provided by convection (Fig. 8.25b). In contrast, the TBL appeared to be more developed on the inclined surfaces. Despite the comparably weaker flow, the dominance of convection was still evidently visible at this stage (see Fig. 8.25a). This observation is rather similar to the findings given by Kangni *et al.* (1991).

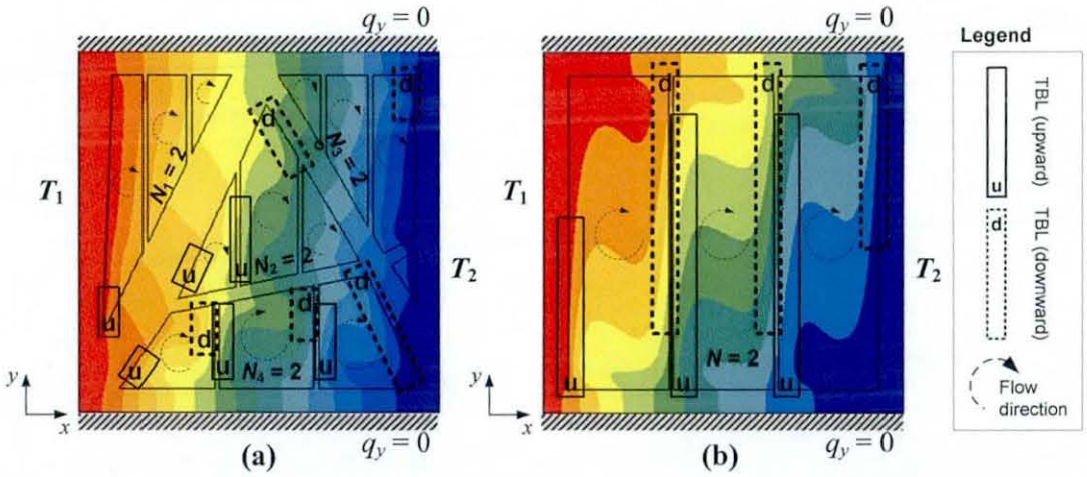

Fig. 8.25 Effects of vertical partitions on thermal boundary layers in discretised enclosures: (a) Structured insulator; (b) enclosure model from initial investigation.

The conditions in the TBL, as a result of the discretisation, strongly influence the surface temperature gradients, and heat transfer rate. This is evident on the inclined surfaces, where the isotherm penetrates directly into the far-fields, indicating conduction. Accordingly, the developments of the TBL on the inclined surfaces are inhibited, as Fig. 8.26(a) shows. On the adjacent partitions, TBL's developed but the distance required to fully develop is seen to be comparably less. Despite the slight growth in thickness, the TBL's on the vertical surfaces of the basic enclosure remained relatively flat. The slight undulation, at the middle of each cell, indicated the presence of a relatively stagnant core and that the transport of heat was primarily provided by the weakened boundary layer flows.

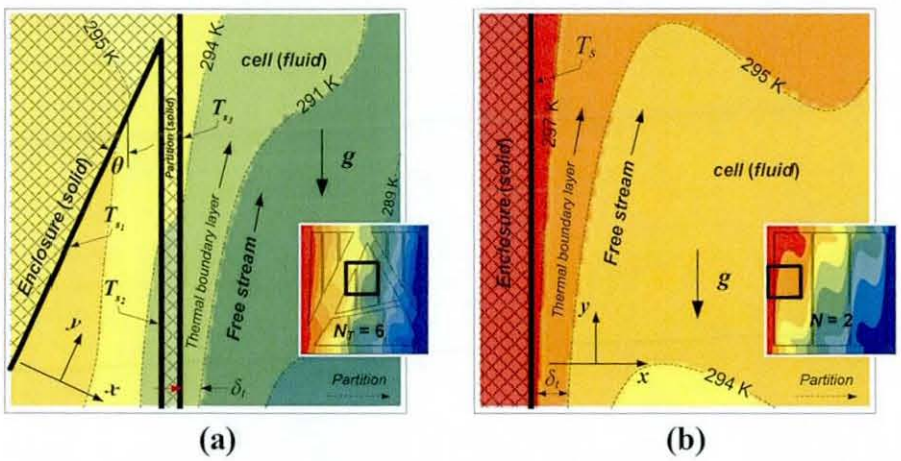

Fig. 8.26 Effects of discretisation on the development of TBL's: (a) Upward flow on an inclined surface of the structured insulator; (b) upward flow on a vertical surface of initial investigative model.

With further discretisation, the deformation of isotherms was markedly decreased, as exemplified by the 'non-development' of the TBL. The temperature in the vertical direction of both enclosure models is nearly isothermal, as Fig. 8.27 shows. Despite the presence of slight convection, the local heat flux along each partition was relatively uniform. The slight inclined isotherms indicated that heat transfer across the subenclosures was 'pseudoconduction'. Relatively similar characteristics were seen on the optimally discretised structured insulator shown in Fig. 8.27(a). In contrast, the isotherms appear to be affected by the inclined members, which clearly demonstrated the heat transfer interaction between the adjoining subenclosures through the structural members. Unlike the thin partitions, which are 'passive' in the sense that neither their temperature nor heat flux was prescribed (Rohsenow *et al.*, 1998). Depending on orientation, multiple parallel partitions could have profound effects on heat transfer.

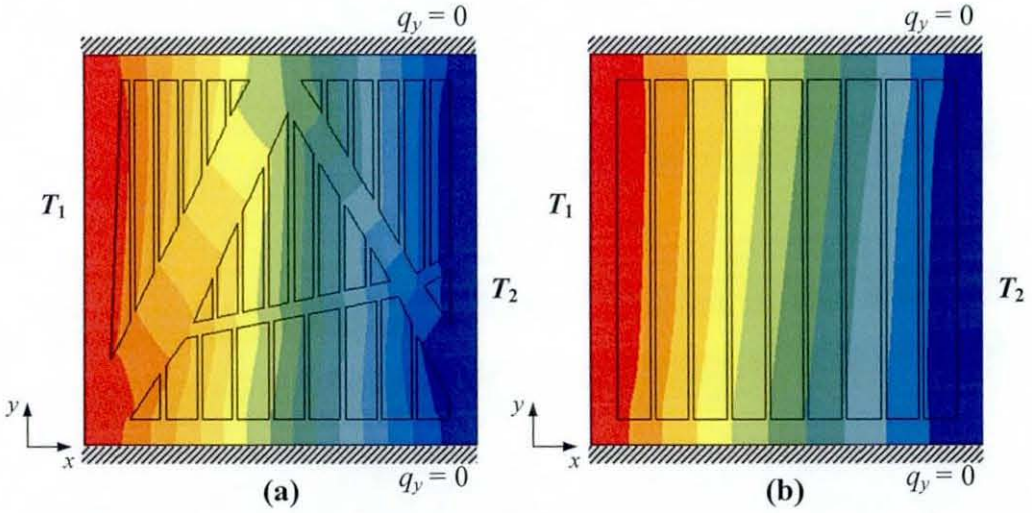

Fig. 8.27 Effect of vertical partitions on heat transfer of enclosures: (a) Structured insulator with optimal discretisation layout; (b) vertical enclosure with optimal discretisation layout.

Fig. 8.28(a) and (b) illustrates the influence of the optimal discretisation layout on the global heat transfer across the structured insulator and basic enclosure. The non-development of the TBL indicates that the buoyancy-driven flow is weak and that the working fluid is relatively 'stagnant'. With the suppression of the thermobuoyant flows, the effective thermal conductivity k_{eff} of the working fluid is reduced, thereby increasing the global thermal resistance. The outcomes show that the increase in subenclosure aspect ratio s_N, as a result of the discretisation, yielded an increase of the global thermal resistance. Fig. 8.28(a) compares the heat transfer interaction between the adjoining

subenclosures through the conducting enclosure and partitions where the isotherms emanating from the fluid wetted wall, penetrated the dividing partitions.

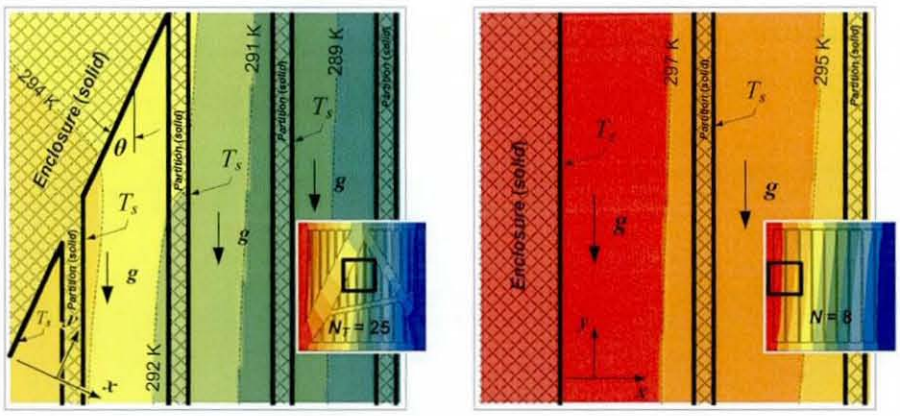

Fig. 8.28 Effect of optimal discretisation on the flow characteristics of subenclosures: (a) structured insulator with optimal discretisation; (b) vertical rectangular enclosure with optimal discretisation.

8.11.2 Heat flux distribution

The heat flux (q) is an important heat transfer quantity which depicts the heat transfer per unit area normal to the direction of heat transfer across the enclosure. Shown in Fig. 8.29 is the direction and magnitude of q across the non-discretised and optimally discretised structured insulator.

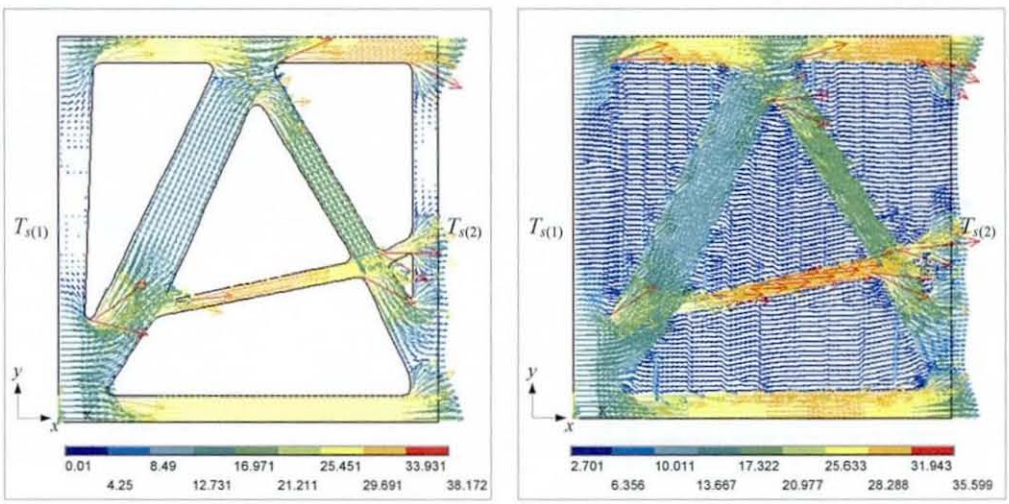

Fig. 8.29 Heat flux vector of insulator enclosures: (a) non-discretised enclosure with $N_T = 0$ partitions; (b) structurally optimised enclosure with optimal discretisation of $N_T = 25$ partitions.

It should be noted that the q plots obtained from the numerical model were based on $k_s/k_f \approx 10$, with $T_{s(1)} > T_{s(2)}$. The q across the structure appears to be a strong function of the

number of partitions and layout. The heat flux was found to be higher in members normal to the direction of heat flow (i.e. the horizontal face shells and the inclined ties) and varied with position along the continuum members. The maximum heat flux is found in members forming a direct 'thermal bridge' linking the heated and cooled faces posing the least thermal resistance. In contrast, q in the inclined members and the vertical face shells are found to be comparatively less. Although the introduction of parallel vertical partitions to the openings has profound effect on the average heat flux, the local heat flux distribution of the solid enclosures remained relatively unchanged.

8.11.3 Effects of discretisation on global heat transfer

The general characteristic of heat transfer, as a result of the discretisation, was observed to have undergone changes, from a convective to a conductive dominant system. This change is clearly distinguishable from the discretisation history plots, in which could generally be classified into three stages, as shown in Fig. 8.30.

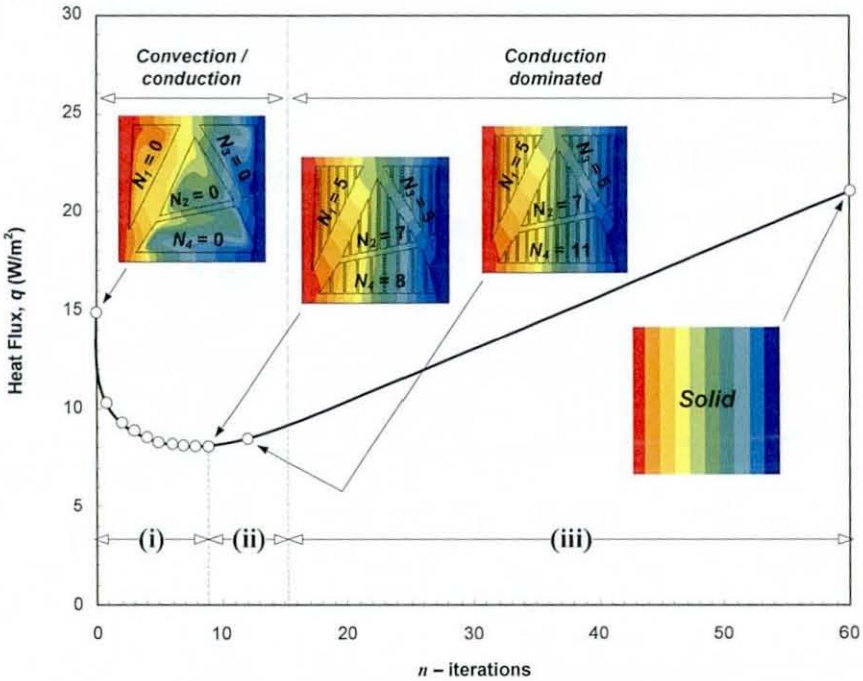

Fig. 8.30 Characteristics of heat transfer due to discretisation of cells using vertical parallel partitions: (i) Nonproportional reduction; (ii) nonproportional increase; (iii) linear increase in heat transfer/flux.

i) Nonproportional reduction – The inclusion of partitions reduces the convective heat transport mechanism, as exemplified by gradual 'detachment' of the thermal boundary layers along the height of the enclosure walls.

ii) Nonproportional increase – 'Pseudoconduction' gradually giving way to conduction. The undulations of isotherms diminishes, but still remained at an angle, indicating that the heat flux along the partitions are not uniform.

iii) Linear increase – At this final stage, q increases linearly with N. Heat transfer is conductive dominant, in which the isotherms are almost parallel to the sidewalls and vertical partitions, indicating a more uniform heat flux distribution.

The features highlighted above corresponded well with the calculated dimensionless parameter Nu of both the discretised basic enclosure and structured insulator. Although convection was observed to be significant at the initial stages, the thermo buoyant flows within the cells were well within the laminar region. This is attributed to the low recirculation rate of a natural convective system, which usually is several orders of magnitude lower than forced convection systems. In addition, both minima of the q-N curves agree well to a value of Nu which indicated 'slug flow' or laminar flow. Importantly, the decreasing trend of convection, as given by the correlated Nu_N and calculated Nu is in good agreement. For the structured insulator, the reduction of the average Nu due to the introduction of $N_i = 1$ partition at $n_i = 1$, is approximately 27 %. In contrast, the introduction of $N = 1$ partition at $n_i = 1$ in the basic enclosure yielded approximately 58 % reduction. For the range of $Ra = 10^7$, the velocity of recirculation is expected to be comparably higher for cells with low aspect ratios, as opposed to cells with higher aspect ratios. In all, the observed characteristics of heat transfer are consistent with the flow regimes in enclosures given by Mac Gregor and Emerry (1969).

8.12 Efficiency of partitions

In relation to the engineering application of this study, the thermal insulation of multiple parallel vertical partitions for the basic enclosures and structured insulators are assessed. According to Nishimura *et al.* (1988), the reducing rate of the insulation efficiency η in terms of N-partitions can be written as

$$\eta = 1 - (Nu_N / Nu_0) \tag{70}$$

where Nu_0 is the average Nusselt number of enclosures with no partitions and Nu_N or Nu is the Nusselt number of the enclosure with partitions, respectively.

Fig. 8.31 compares η vs. N-partitions, evaluated at $Ra = 10^7$, for both the discretised basic enclosures and structured insulators respectively.

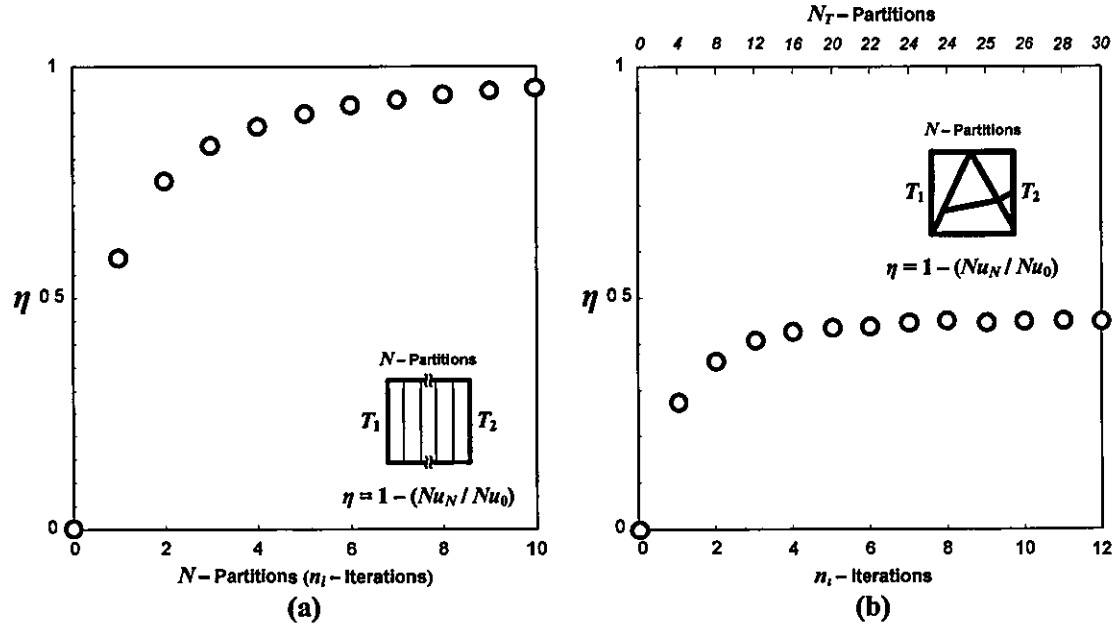

Fig 8.31 Insulation efficiency (η) of vertical parallel partitions as a function of N-partitions (or n_i-iteration) (a) basic vertical enclosure, (b) structured insulator.

For single cell enclosures with low aspect ratios, bisecting the internal air space would yield ~ 58 % reduction in convection. This observation agrees well with the findings obtained by Ho and Yih (1987). Based on the design constraints imposed in this study, the maximum gain in efficiency is ~ 94 %. This is a substantial amount considering the effect of heat transfer alone. This example serves only as a benchmark for comparison purposes. In contrast, the bisection of air-filled cells of the structure optimised using MD would yield approximately 27 % gain in efficiency. This initial gain is expected to be lower because the continuum truss layout with inclined cell walls had initially attributed to 47 % decrease in heat flux. In this case, the maximum efficiency gained from the discretisation is approximately 45 %.

From an engineering standpoint, the useful number of partitions is determine to be approximately five to eight per cell, with an attendant reduction of global heat transfer by ~ 40 % to ~ 78 %, respectively. Table 8.4 summarises the η of the partitions within the discretised structured insulator.

Table 8 4

Summary of the efficiency (η) of partitions in the reduction of heat transfer

	Basic rectangular enclosure		**Layout optimised structured insulator**	
n_I-iterations	N_T-partitions	Efficiency (η)	N_T-partitions	Efficiency (η)
1	0	0	0	0 %
2	1	58.1 %	4	27.3 %
3	2	74.9 %	8	36 2 %
4	3	82.5 %	12	40.7 %
5	4	86 8 %	16	42.7 %
6	5	89.6 %	20	43.6 %
7	6	91.4 %	22	43.9 %
8	7	92.8 %	24	44.6 %
9	8	93.8 %	24	45.0 %
10	9	94.6 %	25	44.8 %

8.13 Concluding remarks

An optimal discretisation layout with maximised thermal resistance (R-value) or minimised hear flux (q) was obtained using the discretisation by partitioning method (DbPM), for a structurally optimised granular-solid modular unit load bearing structure. The discretisation approach of the proposed DbPM was initially demonstrated through 88% reduction of heat flow for an idealised unit cell enclosure. The method was then modified and extended to cover the discretisation problem of structures with nonuniform internal layout, typically expected from a layout optimisation. In the case of the structured insulator under consideration, a gain in insulation performance of 41% was achieved, considering that the structurally optimised layout had initially yielded 47% reduction in heat transfer. The result of the optimal discretisation by the proposed DbPM was validated by an additional study. The gain in thermal insulation, at the expense of slight increase in structural mass, was demonstrated to be somewhat consistent for the forty randomly selected enclosure layouts. From the validation study, the range of thermal boundary conditions in which the DbPM would produce the most desirable gain in insulation is highlighted.

The results obtained using the two-stage optimisation and discretisation method is different to designs solutions proposed by Gu *et al.* (2001), Lorente and Bejan (2002) and Gosselin *et al.* (2004), in that the current method combines the attributes of layout and sizing/configuration optimisation. Design solutions obtained through use of sizing methods may in overall, be stiffer and lighter, but insulation performance will be affected due to amount of thermal bridging present. In this study, a modular unit cell structure optimised for load and heat transfer is produced using the proposed design two-stage layout optimisation and discretisation method. The results indicated gains in material savings and insulation is substantial for a single material structure and that the results were positive. Importantly, the research paves the way for future work to similar class of design optimisation problems.

9

Conclusions and Further Work

9.1 Summary of research findings

The key findings of this research from the foregoing chapters are summarised below;

i. A systematic design procedure for characterising strength and insulation requirements of a modular unit structure from additive manufacturing has been presented. The proposed two-stage method consisted of structural optimisation and thermal discretisation, through use of the Metamorphic Development (MD) and a specifically devised Discretisation by Partitioning Methods (DbPM), respectively.

ii. Layout optimisation of a consolidated granular-solid structure, initially considering only strength requirements is demonstrated. A bimodulus constitutive Drucker-Prager (D-P) material model was calibrated to accurately model the responses of the material used. The reliability of the optimised design solution, tested using physical experiments and finite element (FE) modelling, are reproduced with reasonable accuracy. The attributes of the design approach yielded 40% savings in build material whilst satisfying the targeted deflection.

iii. It was established that heat transfer across a differentially heated and cooled structure could be controlled and optimally discretised through use of the proposed DbPM. The attributes of the approach have been demonstrated through 88% reduction in heat transfer for an idealised analysis model and 40% for the

investigated design study. The reliability and consistency of the design solutions have been validated through an additional validation precedure.

iv. The research demonstrated that the attributes of layout and configuration/sizing optimisation methods can be combined to produce conceptual design solutions to engineering design problems which encompasses more than one domain.

v. It was demonstrated that strength and insulation requirements of load bearing structures could be achieved through use of single bulk material by means of varying geometry to produce the required functions.

The research demonstrated and introduced the notion of design optimisation for Freeform Construction (FC) which has not previously been considered for a load bearing thermal insulation granular-solid structure. The outcome of the research lays the foundations for the design optimisation of full scale concrete structures.

9.2 Conclusions

This research is of importance to construction and manufacturing engineering applications, with the search for a design optimisation approach for load bearing structures with thermal insulation requirements. Of key importance is that most current design studies only consider mechanical strength and heat transfer requirements alone. The research presented in this thesis demonstrated the design approach for a new class of design problems, where the system architecture is derived from a combination of mechanical strength and thermal insulation requirements, aimed at the design optimisation of building components or similar structures. In this study, a 'two-stage' structural optimisation and thermal discretisation method was presented. The method utilised the combinatorial techniques derived from layout and sizing methods, respectively. In the proposed method, the structural requirements were initially addressed prior to finding a thermal solution. The method was tested and shown to be effective in maximising the static stiffness and minimising heat loss of a conceptual design build using consolidated granular-solid SLS Nylon-12.

The proposed method is envisaged to benefit design engineers with a systematic approach in the design of load bearing structures with insulation requirements. The outcome of the shapes produced compares well with known analytically obtained solutions. The method is ideally suited for establishing first design estimates. However, post-processing of the design boundaries in the intermediate and final stages is necessary and important for optimisation procedure and real life applications. In all, the attributes of the two-stage approach had been demonstrated through savings in build material of 44% and with increased thermal resistance of 62%, with the used of a single build material. The current research lays down the initial investigative principles for that of a two-stage strength and insulation layout design optimisation approach.

9.2.1 Layout optimisation of consolidated granular-solid structures

A procedure for the design optimisation of a granular-solid prismatic beam has been demonstrated through use and substitution of consolidated Nylon-12 granular-solid as the build material. The metamorphic development (MD) method formed the basis of the generalised layout optimisation used to yield a lightweight design. The attributes of the approach have been demonstrated through savings in build material of 24.7%, without compromising the targeted displacement and strength requirements. Two types of prismatic beams were considered, an initially solid and layout optimised beam. The design procedures comprised of layout optimisation, modelling and calibration of material parameters, and finite element analysis (FEA). A nonlinear analysis was performed to simulate the material nonlinearity and large displacement characteristics, which is typical of most polymer materials. A bimodulus constitutive Drucker-Prager (D-P) model was calibrated on the basis of experimental and calculated failure points of the material used. The calibrated material model was used for the MD optimisation model of the prismatic beam structure. The reliability of the results of the initial and optimised beams was assessed by simply-supported three-point bending (3PB) tests. The quantitative and qualitative features of the structural responses of the beams were investigated experimentally and numerically, and reproduced with reasonable error. For the case of the optimised beams, quantitative features of the predicted responses were not fully reproduced by the experiments. The 3PB tests revealed a slight difference in rupture loads and deflections. This was largely due to inconsistent mechanical properties among test specimens. In terms of manufacturing considerations, the placement of the

test specimens within the SLS machine build-volume, with near optimal process parameters should improve the consistency of mechanical properties. From the initial investigation, the validity of an MD optimised structure and calibrated yield criteria were established for consolidated SLS granular-solid Nylon-12. This paved the way for the application of the MD method in the generalised structural layout design optimisation of the enclosure of an insulator enclosure which makes up the proposed Stage-1 of the two-stage design approach.

9.2.2 Optimal discretisation of structured insulators

The initial investigation of the discretisation of heat insulating structures was aimed at exploring the effects of heat transfer due to the presence of solid partitions. A feasibility study was performed to explore the decreasing trend of q due to the introduction of partitions. This was done by means of physical experiments of consolidated granular-solid test specimens through use of the horizontal guided hot plate (GHP) apparatus. Also obtained from the experiment was the effective thermal conductivity k_{eff} of solid material, which was a primary thermal property required for the numerical modelling of heat transfer across the enclosures. For the case of a granular material, k_{eff} could alternatively be obtained through empirical correlation. A total of five test specimens, each with varying internal layout, was manufactured and tested. The test specimens were post-processed and conditioned prior to the tests. The experimental analyses consider the effects of the conjugate natural-convection-conduction heat transfer across horizontally orientated rectangular enclosures of low aspect ratios. The enclosures considered were bounded by isothermal horizontally heated and cooled walls with adiabatic edges. In the discretisation, horizontal partitions were introduced in an $N + 1$ fashion to equidistantly discretise the internal airspace, where the number of partitions N was varied from 1 to 5. In the experiments, each enclosure specimen was tested until a measurement repeatability of thermal equilibrium of $< 0.2\%$ was achieved. The conditions of the experiments were modelled using computational fluid dynamics (CFD) to visualise the steady-state isotherms, in which could not be obtained from the experiments. The GHP test results revealed a nonproportional decreasing trend head flux, despite the fact that conduction wais dominant and confirmed by the isotherm plots. The nonproportional decrease of q in terms of N resembled a polynomial function. This indicated that the minimum of the function would give an optimal solution. The initial characterisation of the effects of the

Discretisation by Partitioning Method (DbPM) in suppressing the heat transfer across granular-solid enclosures had allowed the research to be extended to Stage-2.

9.2.3 Two-stage structural optimisation thermal discretisation approach

This research demonstrated the design optimisation and discretisation of the internal layout of a structured insulator to meet strength and insulation requirements. Due to the competition between structural and thermal requirements, a two-stage layout optimisation and partitioning discretisation approach is carried out to identify the optimal layout for a unit cell structure. The concrete masonry unit (CMU) was chosen because it demonstrated this particular design problem in its simplest configuration. In the first stage, the strength requirements were addressed using the MD method to find a design of maximum stiffness of least material. In the second stage, a shape constraint was imposed on the optimal structural layout. The airspaces within the openings were subsequently discretised until a minimum heat flux design was determined.

Most of the thermal design work was based on the maximisation of heat and fluid flow performance, without addressing mechanical strength. Similarly, considerable examples of structural design are focussed on the maximisation of strength, without referencing the need for insulation requirements. The competition between structural and thermal functions of the structure represents a challenge to the design optimisation. From a material distribution point of view, the addition of structural material to form new load paths could affect thermal insulation performance. Conversely, the removal of material could increase thermal resistance, at the same time this may affect stiffness or strength. In this research, the strength of the enclosure was considered as the integral requirement. An enclosure optimised based purely on thermal requirements would be unfeasible if it do not meet strength requirements. Based on this consideration, the proposed method was shown to address the global problem.

The two-stage consideration of the strength and thermal requirements of a complex structure is a defining feature of the design optimisation problem proposed in this thesis. The number of partitions and subenclosures built into the unit cell structure can be optimised when the static stiffness was optimised. The optimal number of N-partitions increases when the effect of natural convection increases, when the specified stiffness of

the enclosure increases. Thermal resistance was larger when natural convection in the subenclosures was weaker, when the enclosure stiffness was higher. The optimum solid/fluid volume fraction of the structured insulator decreases when the natural convection effects became stronger and when the enclosure stiffness is low. The conceptual design of the unit cell structure considered here is shown in Fig. 9.1

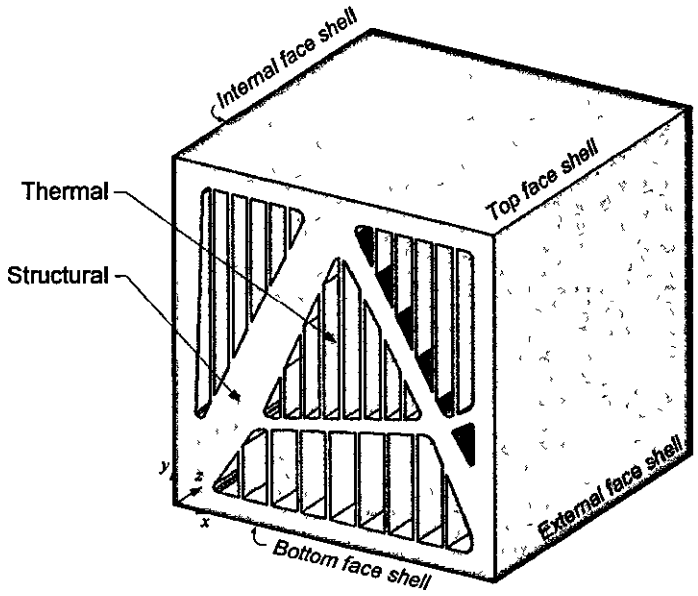

Fig 9 1 Optimised internal layout of unit cell structure that meets structural and thermal insulation requirements

The 'two-stage' structural optimisation and thermal discretisation method presented in this thesis was not only limited to building applications. It can be applied to other fields where structures must carry loads while posing most resistance to heat flow. Examples of application include aircraft, ships, automobiles and other mobile structures. Instead of utilising different material to form composites, insulation could be increased by varying the internal layout of the load carrying members utilising a single build material. One of the cited benefits was the opportunity to recycle used build materials at the 'end of life'. The design approach could be carried further where a design could be conceptualised and 'morphed' into geometric forms with more than one function, whilst retaining the single material construction.

9.2.4 Recommendations for further work

In this research, three areas of further work were identified. These were primarily centred on the development of an improved discretisation by partitioning method (DbPM) and metamorphic development (MD) method, and the type of analysis used for the optimisation model. The differences in the physics of the respective analyses of the design problem require different means of numerical methods. For instance, finite element analysis (FEA) is required for structural optimisation and computational fluid dynamics (CFD) for thermal discretisation. With a 'multiphysics' simulation, both these analyses could be coupled in one environment. In that, the results of the thermal analysis can be read and used as body loads in the structural analysis, providing the flow of information between the two different analyses. Due to the fact that both structural and fluid mesh may be simultaneously required in the optimisation model, advanced mesh morphing and multi-field solvers may be required. Assuming that the physics of the problem could be modelled, the next challenge lies in the nature of the optimisation approaches used. Due to the competition between structural and thermal requirements, a material distribution approach would not be practical for the optimisation of the heat flow problem. With a multiphysics simulation, it is hoped that an improved DbPM and MD method would enable the procedures of structural and discretisation optimisation to be performed in an automated fashion.

9.2.5 Areas of further work

In this study, the Discretisation by Partitioning Method (DbPM) was implemented manually. Although a desirable gain in thermal insulation was achieved for a single material structure, the process largely consisted of manual work. Similarly, the MD method used for the layout optimisation involved model updating by means of manual approach. This was largely due the development of problematic geometries during the course of the layout optimisation. Despite producing a solution which meets the design criteria, the proposed method would benefit if these highlighted areas are addressed;

i. Due to the repetitive nature of the process, procedures of the DbPM could be automated. This would allow structures with complex internal opening layouts to

be optimally discretised in a more efficient manner. This could prove to be a highly useful tool for evaluating design changes of complex shape structures.

ii. The current DbPM is limited to the optimal discretisation of differentially structures with uniform external geometries. It would be beneficial if the method could be used to solve design problems with multiple heat sources of structures with arbitrarily shaped internal and external geometries (i.e. multiple arbitrary heat sources, etc.).

iii. Alternative, structures could be designed with 'selective thermal resistances' which could be 'tuned' to meet certain thermal requirements. In addition, the thermal discretisation could consider the optimal discretisation which would produce a near uniform heat flux structure (i.e. selective thermal resistance and uniform heat flux).

iv. The thickness t_p of the vertical partitions used this is study is not a design variable, where t_p may be used as a design variable. The value of t_p may be determined by the geometry of the openings. This feature may be useful when differences in sizes of the openings are considerable, allowing relatively smaller openings to be effectively discretised (i.e. variable thicknesses t_p).

v. The thickness t_p of the partitions should ideally be kept as thin as possible. Such geometries should be modelled using shell or plate elements, if bending is the dominant behaviour. Hence, the use of solid elements may not be appropriate because stresses do not vary greatly across the thickness (i.e. the use of multiple element types).

vi. Currently, the two-stage layout optimisation and discretisation method was used to optimise 2D plane models. Ideally, it would be beneficial if the method could be extended 3D design problems (i.e. 3D design problems).

vii. Due to the use of a single bulk material, structures optimised for least build material using AMT would be ideal for recycling or reuse of materials. Build

materials may be reused though sizing bulk structures. The technologies of material sizing are readily available and they could be seen as a complementary technology to Freeform Construction (FC) (i.e. environmental considerations).

viii. Ideally, a connection could be made between optimised structures build using concretes to the current granular-solid RP material used in this current research. In addition, layout optimised reinforced structures could be considered. This would benefit and offer an alternative design approach to structural engineers (i.e. optimisation of reinforced concrete structures).

ix. Improvements could be made to the FE models used in the MD layout optimisation. The 'locally' high stress regions caused by point loads could be eliminated by applying 'surface loads'. Alternatively, the loading edges could be explicitly modelled using contact analysis.

x. It would be beneficial if the DbPM could consider 'non-equidistantly' spaced parallel partitions within artbitrarilly shaped enclosure voids. Such partitioning configuration may be useful for structures that require 'selective insulation'.

xi. The proposed 'two-stage' method could be improved if a 'combined' or 'one-stage' approach could be deviced. Before it could be realised, the physics of the optimisation problem, which is a multiphysics problem, had to be modelled using fluid structure interation (FSI) analysis. The challenge lies in how design optimisation could be performed, in which is a topic for future investigation.

References

Adeli, H , Kamal, O , 1992 Concurrent analysis of large structures – I. algorithms Computers and Structures 42, 413-424

Ajoku, U , Hopkinson, N , Caine, M , 2006 Experimental measurement and finite element modelling of the compressive properties of laser sintered Nylon-12. Materials science and engineering A 428, 211-216

Ajoku, U , Saleh, N , Hopkinson, N , Hague, R J M and Erasenthiran, P E , 2006 Investigating Mechanical Anisotropy and End of Vector Effect in Laser Sintered Nylon Parts, Proceedings of the Institute of Mechanical Engineers (Part B), Journal of Engineering Manufacture 220, 1077-1086

Al-Homoud, M S , 2005 Performance characteristics and practical application of common building thermal insulation materials Building and Environment 40, 353-366

Allaire, G , Jouve, F , Toader, A M , 2004 Structural optimisation using sensitivity analysis and a level-set method Journal of Computational Physics 194, 363-393

Anagnostou, G , Rønquist, E M , Patera, A T , 1992 A computational procedure for part design Computer Methods in Applied Mechanics and Engineering 97, 33-48

Anderson, R , Bejan, A , 1981. Heat transfer through single and double vertical walls in natural convection theory and experiment International journal of heat and mass transfer 24, 1611-1620

Ansola, R , Canales, J , Tárrago, J A , Rasmussen, J , 2002 An integrated approach for shape and topology optimisation of shell structures Computers and Structures 80, 449-458

ANSYS, 2004 ANSYS Multiphysics Release 9 0 help files ANSYS Ltd

Archarya, S , Jethi, R , 1990 Heat transfer due to buoyancy in a partially divided square box International Journal of Heat and Mass Transfer 33, 931-942

Archarya, S , Mehrotra, A , 1991 Natural convection in smooth and ribbed vertical channels International Journal of Heat and Mass Transfer 36, 236-241

Augusto, P A , Castelo-Grande, T , Augusto, P , Barbosa, D , 2006 Optimisation of refrigerated shields using multilayer thermal insulations Cryostats design – analytical solution Cyrogenics 46, 449-457

Bajorek, S M , Lloyd, J R , 1982 Experimental investigation of natural convection in partitioned enclosures Journal of Heat Transfer 104, 527-532

Balaguer, C , Abderrahim, M , Navarro, J M , Boudjabeur, S , Aromaa, P , Kahkonen, K , Slavenburg, S , Seward, D , Bock, T , Wing, R & Atkin, B , 2002 FutureHome An integrated construction automation approach

Balling, R J , 1991. Optimal steel frame design by simulated annealing Journal for Structural Engineering 117, 1780-1795

Bardet, J P , 1998 Introduction to computational granular mechanics In Cambou, B , ed Behaviour of Granular Materials International Centre for Mechanical Sciences, CISM Courses and Lectures (385) Springer-Verlag Wien New York, 1998, 99-170

Basak, T , Roy, S , Thirumalesha, Ch , 2007 Finite element analysis of natural convection in triangular enclosure effects of various thermal boundary conditions Chemical engineering science 62, 2623-1640

Baumann, B , Kost, B , 2005 Structure assembling by stochastic topology optimisation Computers and Structures 83, 2175-2184

Baumgartner, A , Harzheim, L , Mattheck, C , 1992 SKO (soft kill option) the biological way to find an optimum structure topology International Journal of Fatigue 14, 387-393

Bejan, A , 1985 Mass and heat transfer by natural convection in a vertical cavity International Journal of Heat and Fluid Flow 6, 149-159

Bejan, A , 2002 Dendritic constructal heat exchanger with small-scale crossflows and larger-scales counterflows International Journal of Heat and Mass Transfer 45, 4607-4620

Bendsøe, M P , Kikuchi, N , 1988 Generating optimal topologies in structural design using a homogenisation method Computer Methods in Applied Mechanics and Engineering 71, 197-224

Bennage, W A , Dhingra, A K , 1995. Single and multiobjective structural optimisation in discrete-continuous variables using simulated annealing International Journal for Numerical Methods in Engineering 38, 2753-2773

Bethge, K , Mattheck, C , 1990 Fatigue testing of a shape-optimised circular hole in a plate under tensile and bending loads International Journal of Fatigue 12, 489-492

Biserni, C , Rocha, L A O , Bejan, A , 2004 Inverted fins geometric optimisation of the intrusion into a conducting wall International Journal of Heat and Mass Transfer 47, 2577-2586

Bishop, A W , 1954 Correspondence on shear characteristics of a saturated silt measured in triaxial compression Geotechnique 4, 43-45

Bochenek, B , Foryś, 2006 Structural optimisation for post-buckling behavior using particle swarms Struc Multidisc Optim 32, 521-531.

Brown, R L., Richards, J C , 1970 Principles of powder mechanics Pergamon Press, London

Buswell, R A , Soar, R C , Gibb, A G F., Thorpe, A., 2007 Freeform Construction Mega-scale Rapid Manufacturing for construction Automation in Construction 16, 224-231

Cambou, B , 1999 Fundamental concepts in homogenization process In Satake, M , *et al* , eds Fundamentals for Mechanics of Granular Materials In. Oda, M , Iwashita, K , eds Mechanics of Granular Materials An Introduction Balkema, Rotterdam, 35-39

Capello, F , Mancuso, A , 2003 A genetic algorithm for combined topology and shape optimisations Computer-Aided Design 35, 761-769

Chang, K -H , Tang, P -S , 2001. Integration of design and manufacturing for structural shape optimisation Advances in Engineering Software 32, 555-567.

Chang, L C , Lloyd, J R , Yang, K T , 1982. A finite difference study of natural convection in complex enclosures. Heat transfer 1982, Proceedings of Seventh International Heat Transfer Conference, Munich 1, 183-188

Change, Y P , Tsai, R , 1997 Natural convection in a square enclosure with a cold source International communication in heat and mass transfer 24, 1019-1027

Chapman, C D , Saitou, K , Jakiela, M J , 1994 Genetic algorithms as an approach to configuration and topology design Journal of Mechanical Design, Transactions of ASME 116, 1005-1012

Chen, K S , Ko, P W , 1991 Natural convection in a partially divided rectangular enclosure with an opening in the partition plate and isoflux side walls International Journal of Heat and Mass Transfer 34, 237-246

Chen, T Y , Lin, C Y , 2000 Determination of optimum design spaces for topology optimisation Finite Elements in Analysis and Design 36, 1-16

Chen, T -Y , Su, J -J , 2002 Efficiency improvement of simulated annealing in optimal structural designs Advances in engineering software 33, 675-680

Chen, W F , Han, D J , 1988 Plasticity for structural engineers Springer-Verlag, New York.

Chen, W F , Zhang, H , 1991 Structural plasticity theory, problems, and CAE software Springer-Verlag, New York

Cheng, C -H , Wu, C -Y , 2000 An approach combining body-fitted grid generation and conjugate gradient methods for shape design in heat conduction problems Numerical Heat Transfer Part B 37, 69-83

Chirehdast, M , Papalambros, P Y , 1992 A note on automated detection of mobility of skeletal structures Computers and Structures 45, 197-207

Chu, D N , Xie, Y M , Hira, A , Steven, G P , 1996 Evolutionary structural optimisation for problems with stiffness constraints Finite Elements in Analysis and Design 21, 239-251

Cianfrini, C , Corcione, M , Dell'Omo, P P , 2005 Natural convection in tilted square cavities with differentially heated opposite walls International journal of thermal sciences 44, 441-451.

Cooper, K G , 2001 Rapid prototyping technology, Mercel Dekker, Inc , USA

Corcione, M , 2003. Effects of the thermal boundary condition at the sidewalls upon natural convection in rectangular enclosures heated from below and cooled from above International journal of thermal sciences 42, 199-208

Cousineau, L , and M Nobuyasu, 1998 Construction Robotics The Search for New Building Technology in Japan Reston, VA ASCE press

Cousineau, L , Nobuyasu, M , 1998 Construction Robotics The search for new building technology in Japan, American Society of Civil Engineers (ASCE), USA

da Silva, A K., Lorente, S , Bejan, A , 2006 Constructal multi-scale structures for maximal heat transfer density Energy 31, 620-635

Dagtekin, I , Oztop, H F , 2001 Natural convection heat transfer by heated partitions within enclosure International Communications in Heat and Mass Transfer 28, 823-834

Das, R , Jones, R., Xie, Y M , 2005 Design of structures for optimal static strength using ESO Engineering Failure Analysis 12, 61-80

Du, Z -G , Bilgen, E , 1992 Coupling of wall conduction with natural convection in a rectangular enclosure Internal Journal of Heat and Mass Transfer 35, 1969-1975

Eberhart, R C , Kennedy, J , 1995 A new optimiser using particles swarm theory In· 6th Int. Symp Micro Machine and Human Science (held in Nagoya, Japan), 39–43

Elperin, T , 1988 Monte Carlo structural optimisation in discrete variables with annealing algorithm. International Journal for Numerical Methods in Engineering 26, 815-821

Feda, J , 1982 Mechanics of particulate materials Developments in Geotechnical engineering 30 Elsevier Scientific Publishing Company

Fernandes, P , Guedes, J M , Rodrigues, H , 1999 Topology optimisation of three-dimensional linear elastic structures with a constraint on "perimeter" Computers and Structures 73, 583-594

Fourie, P C , Groenwold, A A , 2002 The particle swarm optimisation algorithm in size and shape optimisation Struc. Multidisc Optim 23, 259-267

Fowler, A J , Ledezma, G A , Bejan, A , 1997 Optimal geometric arrangement of staggered plates in forced convection International Journal of Heat and Mass Transfer 40, 1795-1805

Frederick, R L , 1999 On the aspect ratio for which the heat transfer in differentially heated cavities is maximum International communication in heat and mass transfer 26, 549-558

Ganzarolli, M M , Milanez, L F , 1995 Natural convection in rectangular enclosures heated from below and symmetrically cooled from the sides International journal of Heat and mass transfer 38, 1063-1073.

Goldberg, D E , 1989 Genetic algorithms in search, optimization, and machine learning Addison-Wesley Publishing Company.

Gosselin, L , Bejan, A , Lorente, S , 2004 Combined 'heat flow and strength' optimisation of geometry mechanical structures most resistant to thermal attack International journal of heat and mass transfer 47, 3477-3489

Gu, S , Lu, T J , Evans, A G , 2001. On the design of two-dimensional cellular metal for combined heat dissipation and structural load capacity International journal of heat and mass transfer 44, 2163-2175

Guan, H , Chen, Y J , Loo, Y C , Xie, Y M , 2003 Bridge topology optimisation with stress, displacement and frequency constraints Computers and Structures 81, 131-145

Haftka, R.T., 1981 Techniques for thermal sensitivity analysis International Journal of Numerical Methods in Engineering 17, 71–80

Hague, R., Mansour, S , Saleh, N , 2003. Design opportunities with rapid manufacturing Assembly automation 23, 346-356

Hague, R , Mansour, S , Saleh, N , 2004 Material and design considerations for rapid manufacturing International journal of production eesearch 42, 4691-4708

Haiba, M , Barton, D C , Brooks, P C , Levesley, M C , 2005 Evolutionary structural optimisation of dynamically loaded components in consideration of fatigue life Advances in Engineering Software 36, 49-57

Hajela, P , 1999 Nongradient Methods in Multidisciplinary Design Optimisation—Status and Potential. Journal of aircraft 36, 255–265.

Hansel, W , Treptow, A , Becker, W , Freisleben, B , 2002 A heuristic and a genetic topology optimisation algorithm for weight-minimal laminate structures Composite Structures 58, 287-294

Hansen, S R , Vanderplaats, G N , 1988 An approximation method for configuration optimisation of trusses, AIAA Paper No 88-2432, AIAA/ASME/ASCE/AHS Structures, Structural Dynamics and Materials Conf

Hasançebi, O , Erbatur, F , 2002. Layout optimisation of trusses using simulated annealing, Advances in engineering software 33, 681-696

Hicher, P Y , 1998 Experimental behaviour of Granular Materials In Cambou, B , ed Behaviour of Granular Materials International Centre for Mechanical Sciences, CISM Courses and Lectures (385) Springer-Verlag Wien New York, 1998, 1-98

Ho, C J , Chang, J Y ,1993 Conjugate natural-convection-conduction heat transfer in enclosures divided by horizontal fins International journal of heat and fluid flow 14, 177-184

Ho, C J , Yih, Y L., 1987. Conjugate natural convection heat transfer in an air-filled rectangular cavity International communication in heat and mass transfer 14, 91-100

Hoppe, R H W , Petrova, S I , 2004 Optimal shape design in biomemetics based on homogenisation and adaptivity Mathematics and Computers in Simulation 65, 257-272

Howe S , 2005, Personal correspondence by Rupert Soar

J J. Broek, I Horváth, B Smit, A F Lennings, Z Rusák, J S M. Vergeest, 2002. Free-form thick layer object manufacturing technology for large-sized physical models Automation in Construction 11, 335–347.

Jacobsen, J B , Olhoff, N , Rønholt, E , 1998 Generalised shape optimisation of three-dimensional structures using material with optimum microstructures Mechanics of Materials 28, 207 225

Jakiela, M J , Chapman, C , Duda, J , Adewuya, A , Saitou, K , 2000 Continuum structural topology design with genetic algorithms Computer Methods in Applied Mechanics and Engineering 186, 339-356

Jármai, K , Snyman, J A , Farkas, J , 2006 Minimum cost design of a welded orthogonally stiffened cylindrical shell Computers and structures 84, 787-797

Jenkins, W M , 1991 Towards structural optimisation via the genetic algorithm Computers and Structures 40, 1321-1327.

Kajima, 1997. Kajima News and Notes· Next Generation Broadcasting Centre Kajima Corporation, Japan

Kaminski, D A , Prakash, C , 1986 Conjugate natural convection in a square enclosure effect of conduction in one of the vertical walls Internal Journal of Heat and Mass Transfer 29, 1979-1988

Kane, C , Schoenauer, M , 1996 Topological optimum design using genetic algorithms Journal of Control Cybernetics 25, 1059-1088

Kangni, A , Yedder, R B , Bilgen, E , 1991 Natural convection and conduction in enclosures with multiple vertical partitions International journal of heat and mass transfer 34, 2819-2825

Karayiannis, T G , Ciofalo, M , Barbaro, G , 1992 On natural convection in a single and two zone rectangular enclosure International journal of heat and mass transfer 35, 1645-1657

Karthiravan, R , Ganguli, R , 2007 Strength design of composite beam using gradient and particle swarm optimisation Composite structures 81, 471-479

Kennedy, J , Eberhart, R C , 1995 Particle swarm optimisation In Proc 1995 IEEE Int Conf Neural Networks, Perth, Australia, 1942–1948

Khoshnevis, B , 2004 Automated construction by contour crafting - Related robotics and information technologies Automation in Construction - Special issue The best of ISARC 2002, 5-19

Kim, H , Querin, O M , Steven, G P , 2002 On the development of structural optimisation and its relevance in engineering design Design Studdies 23, 85-102

Kim, Y Y , Kim, T S , 2000 Topology optimisation of beam cross sections International Journal of solids and structures 37, 477-493.

Kirkpatrick, S , Gelatt, C D , Vecchi, M P , 1983 Optimisation by simulated annealing Science 220, 671-680

Kishino, Y , Thornton, C , 1999 Discrete element approaches. In Oda, M , Iwashita, K , eds Mechanics of Granular Materials An Introduction Balkema, Rotterdam, 147-219

Kitayama, S , Arakawa, M , Yamazaki, K , 2006 Penalty function approach for the mixed discrete nonlinear problems by particle swarm optimisation Struc Multidisc. Optim 32, 191-202

Krog, L.A , Olhoff, N , 1999 Optimum topology and reinforcement design of disk and plate structures with multiple stiffness and eigenfrequency objectives Computers and Structures 72, 535-563

Kwak, B M , 1994. A review on shape optimal design and sensitivity analysis. Structural Engineering/Earthquake Engineering 10, 159–174.

Kwak, H G , Noh, S H , 2006 Determination of strut and tie models using evolutionary structural optimisation Engineering Structures 28, 1440-1449

Lan, C H , Cheng, C H , Wu, C.Y , 2001 Shape design for heat conduction problems using curvilinear grid generation, conjugate gradient, and redistribution methods Numerical Heat Transfer Part· A 39, 487-510

Ledezma, G , Bejan, A , 1996 Heat sinks with sloped plate find in natural and forced convection International Journal of Heat and Mass Transfer 39, 1773-1783

Lee, B.Y., 1993 Shape sensitivity formulation for an axisymmetric thermal conducting solid. Proceedings of The Institution of Mechanical Engineering Part C· Journal of Mechanical Engineering Science 207 (C3), 209–216

Lee, C -D , Lee, W D , 1992 Optimal truss design by stochastic simulated annealing Proceedings of the Korea-Japan Joint Seminar on Structural Engineering Seoul, 191-200

Leite, J P B , Topping, B H ,V., 1999 Parallel simulated annealing for structural optimisation Computers and structures 73, 545-564

Levi, C G , 2004 Emerging materials and processes for thermal barrier systems Current Opinion in Solid State and Material Science 8, 77-91

Li, L J , Huang, Z B , Liu, F , Wu, Q H , 2007 A heuristic particle swarm optimiser for optimisation of pin connected structures Computers and structures 85, 340-349.

Li, Q , Steven, G P , Querin, O M , Xie, Y M , 2001 Stress based optimisation of torsional shafts using an evolutionary procedure International Journal of Solids and Structures 38, 56661-5677.

Li, Q , Steven, G P , Xie, Y M , 2000 Evolutionary structural optimisation for stress minimisation problems by discrete thickness design Computers and Structures 78, 769-780

Li, Q , Steven, G P , Xie, Y M , Querin, O M , 2004 Evolutionary topology optimisation for temperature reduction of heat conducting fields International journal of heat and mass transfer 47, 5071-5083

Li, W , Li, Q , Steven, G P , Xie, Y M , 2003 An evolutionary approach to elastic contact optimisation of frame structures Finite Elements in Analysis and Design 40, 61-81.

Liaqat, A , Baytas, A C , 2001 Conjugate natural convection in a square enclosure containing volumetric sources International journal of heat and mass transfer 44, 3273-3280

Lin, N N , Bejan, A , 1983 Natural convection in a partially divided enclosure International Journal of Heat and Mass Transfer 26, 1867-1878

Lipton, R , 2002 Design of functionally graded composite structures in the presence of stress constraints International Journal of Solids and Structures 39, 2575-2586

Liu, J -S , 1996 PhD Thesis

Liu, J -S , Lu, T J , 2001. Optimal design of optical fibre-holding microclips with metamorphic development Journal of Micromechanics and Microengineering 11, 195-201

Liu, J -S , Parks, G T , Clarkson, P J , 1999 Can a structure grow towards an optimum?

Liu, J -S , Parks, G T , Clarkson, P J , 2000 Metamorphic development a new topology optimization method for continuum structures Structural and Multidisciplinary Optimization 20, 288-300

Liu, J -S , Parks, G T , Clarkson, P J , 2001 Shape optimisation of axisymmetric cylindrical nozzles in spherical pressure vessels subject to stress constraints International Journal of Pressure Vessels and Piping 78, 1-9

Liu, T., Deng, Z C , Lu, T J , 2006 Design optimisation of truss-cored sandwiches with homogenisation International Journal of Solids and Structures 43, 7891-7918

Lorente, S , Bejan, A , 2002 Combined 'flow and strength' geometric optimisation· internal structure in a vertical insulating wall with air cavities and prescribed strength International journal of heat and mass transfer 45, 3313-3320

M Kaviany, 1999 Principles of Heat Transfer in Porous Media, Second Edition (Second Printing), Springer-Verlag, New York

Ma, Z -D , Kikuchi, N , Cheng, H -C , 1995 Topological design for vibrating structures Computer Methods in Applied Mechanics and Engineering 121, 259-280

Macgregor, R K , Emery, A F , 1969 Free convection through vertical plane layers – moderate and high Prandtl number fluids Journal of heat transfer 91, 391-403

Machado, G , Trabucho, L , 2004 Some results in topology optimisation applied to biomechanics Computers and Structures 82, 1389-1397

Madeira, J F A , Rodrigues, H , Pina, H , 2005 Multi-objective optimisation of structures topology by genetic algorithms Advances in Engineering Software 36, 21-28

Manickarajah, D , Xie, Y M , Steven, G P , 2000 Optimum design of frames with multiple constraints using and evolutionary method Computers and Structures 74, 731-741

Manoharan, S , Shanmuganathan, S , 1999. A comparison of search mechanisms for structural optimisation Computers and Structures 73, 363-372

Mansur, M A , Tan, K -H , 1999 Concrete beans with openings Analysis and design CRC Press LLC, USA

Massoudi, M , 2004 Constitutive modeling of flowing granular materials a continuum approach In Antony, S J *et al* , eds Granular Materials Fundamentals and Applications The Royal Society of Chemistry, 63-107

Mattheck, C , 1998 Design in nature – learning from trees Springer Verlag, Heidelberg, Berlin, New York.

Mattheck, C , 2006 Teacher tree The evolution of notch shape optimization from complex to simple Engineering Fracture Mechanics 73, 1732-1742

Mattheck, C , Baumgartner, A , Kriechbaum, R , Walther, F , 1993 Computational methods for the understanding of biological optimization mechanisms Computational Materials Science 1, 302-312

Mattheck, C., Burkhardt, S , 1990 A new method of structural shape optimisation based on biological growth International Journal of Fatigue 12, 185-190

Mattheck, C , Erb, D , 1991. Shape optimisation of rubber bearing International Journal of Fatigue 13, 206-208

Meric, R A , 1988 Shape design sensitivity analysis for nonlinear anisotropic heat conducting solids and shape optimisation by the BEM Int. J numer meth eng 26, 109–120

Michell, A G M , 1904 The limits of economy of material in frame-structures Phil Mag 8, 589-597

Min, S , Nishiwaki, S , Kikuchi, N , 2000 Unified topology design of static and vibrating structures using multiobjective optimisation Computers and Structures 75, 93-116

Misra, D , Sarkar, A , 1997 Finite element analysis of conjugate natural convection in a square enclosure with a conducting vertical wall Computer Methods in Applied Mechanics and Engineering 141, 205-219

Nansteel, M.W , Greif, R , 1984 An investigation of natural convection in enclosures with two- and three-dimensional partitions International Journal of Heat and Mass Transfer 27, 561-571.

Natarajan, E , Basak, T , Roy, S , 2007. Natural convection flows in a trapezoidal enclosure with uniform and non-uniform hearing of bottom wall International journal of heat and mass transfer Article in press

Ngim, D B , Liu, J -S , Soar, R C , 2007 Design Optimization for Manufacturability of Axisymmetric Structures using Metamorphic Development International Journal of Solids and Structures 44, 685-704

Ngim, D B , Liu, J -S , Soar, R C , 2009 Design optimisation of consolidated granular-solid prismatic beam using metamorphic development International Journal of Solids and Structures 46, 726-740

Nishimura, T , Nagasawa, F , Kawamura, Y , 1989 Natural convection in horizontal enclosures with multiple vertical partitions International journal of heat and mass transfer 32, 1641-1647

Nishimura, T , Shiraishi, F , Kawamura, Y , 1987 Natural convection heat transfer in enclosures with an off-center partition International journal of heat and mass transfer 30, 1756-1758

Nishimura, T., Shiraishi, M , Nagasawa, F , Kawamura, Y , 1988 Natural convection heat transfer in enclosures with multiple vertical partitions International journal of heat and mass transfer 31, 1679-1686

Nishiwaki, S , Min, S , Yoo, J , Kikuchi, N , 2001. Optimal structural design considering flexibility Computer Methods in Applied Mechanics and Engineering 190, 4457-4504

Obayashi, 2004 Obayashi Annual Report 2004 Obayashi Corporation, Japan

Oda, M , Iwashita, K , 1999. Mechanics of granular materials an introduction Balkema, Rotterdam

Oda, M , Iwashita, K., eds Mechanics of Granular Materials An Introduction Balkema, Rotterdam, 50-55.

Oka, F , Tamura, T , 1999 Continuum theory of granular materials In Oda, M , Iwashita, K , eds Mechanics of Granular Materials An Introduction Balkema, Rotterdam, 86-142

Omkar, S N , Mudigere, D , Naik , N , Gopalakrishnan, S , 2008 Vector evaluated particle swarm optimisation (VEPSO) for multi-objective design optimisation of composite structures, Computers and structures 86, 1-14

Oshaki, M , 1995 Genetic algorithm for topology optimisation of trusses Computers and Structures 57, 219-225.

Park, C W , Yoo, Y M , 1988 Share design sensitivity analysis of a two-dimensional heat transfer system using the boundary element method Computers and Structures 17, 543-550

Park, H Y , Sung, C W , 2002 Optimisation of steel structures using distributed simulated annealing algorithm on a cluster of personal computers Computers and structures 80, 1309-1316

Patankar, S V , 1980 Numerical Heat Transfer and Fluid Flow McGraw-Hill, New York

Patankar, S V , Spalding, D B , 1972 A calculation procedure for heat, mass and momentum transfer in three-dimensional parabolic flows International journal of heat and mass transfer 15, 1787- 1806

Pauwels, F , 1965 Gesammelte Abhandlungen zur funktionellen Anatomie des Bewegungsapparates Springer Verlag, Berlin

Pegna, J , 1997 Exploratory investigation of solid freeform construction Automation in Construction 5, 427-437

Perez, R E , Behdinan, K , 2007. Particle swarm approach for structural design optimisation Computers and structures 85, 1579-1588

Q Li, G P Steven, O M Querin, Y M Xie, 1999 Shape and topology design for heat conduction by evolutionary structural optimisation International journal of heat and mass transfer 42, 3361–3371

Q Li, G P Steven, O M. Querin, Y M Xie, 2000 Structural topology design with multiple thermal criteria Engng comput. 17, 715–734

Querin, O M , Steven, G P , 1998 Evolutionary structural optimisation (ESO) using a bidirectional algorithm Engineering Computations 15, 1031-1048

Querin, O M , Steven, G P , Xie, Y M , 2000a Evolutionary structural optimisation using an additive algorithm Finite Elements in Analysis and Design 34, 291-308

Querin, O M , Young, V , Steven, G P , Xie, Y M , 2000b Computational efficiency and validation of bi-directional evolutionary structural optimisation Computer Methods in Applied Mechanics and Engineering 189, 559-573

Rapid Design and Manufacture (RDM) Centre Rapid Prototyping Group, Ryder, G , Ion, B , Green, G , Harrison, D , Wood, B , 2002 Rapid design and manufacture tools in architecture Automation in Construction 11, 279-290

Rocha, L A O , Lorente, S , Bejan, A , 2002 Constructal design for cooling a disc-shaped area by conduction International Journal of Heat and Mass Transfer 45, 1643-1652

Rong, J H , Xie, Y M , Yang, X Y , 2001 An improved method for evolutionary structural optimisation against buckling Computers and Structures 79, 253-263

Rowe, P.W , Barden, L , Lee, I K , 1964 Energy component components during the triaxial cell and direct shear test Geotechnique 14, 245-261.

Rozvany, G I N , Zhou, M., 1991 The COC algorithm, Part I Cross-section optimisation or sizing Computer methods in applied mechanics and engineering 89, 281-308

Salama, M , Bruno, R , Chen, G -S , Garba, J , 1990 Optimal placement of excitation and sensors by simulated annealing Recent Advances in Multidisciplinary Analysis and Optimisation NASA CP-3031, 1441-1458

Schlaich, J , Schafer, K , Jennewein, M , 1987 Toward a consistent design of structural concrete PCI Journal 32, 74-147 (special report)

Schutte, J F , Groenwold, A A , 2003 Sizing design of truss structures using particle swarms Struc Multidisc Optim 25, 261-269

Scott Howe, A 2000 Designing for automated construction Automation in Construction 9, 259-276

Scott, R F , 1963 Principles of soil mechanics Addison – Wesley Publishing Company

Shalaby, M M , Saitou, K , 2004 Topology optimisation of structural supports for MEMS switches using discrete simulated annealing, MDP-8 Cairo University Conference Proceesings of MDP-9, Cairo University Conference of Mechanical Design and Production, Cairo, Eqypt, January 4-6

Shim, P Y , Manoochehri, S , 1997 Generating optimal configurations in structural design using simulated annealing International Journal For Numerical Methods in Engineering 40, 1053-1069

Sigmund, O , 2000 A new class of extremal composites Journal of the Mechanics and Physics of Solids 48, 397-428

Simons, S J R , Pagliai, P , 2004 High temperature particle interactions. In Antony, S J *et al* , eds Granular Materials Fundamentals and Applications The Royal Society of Chemistry, 108-134

Soar, R C , 2006 Additive manufacturing technologies for the construction industry In Hopkinson, N , Hague, R J M , Dickens P M , eds Rapid Manufacturing Wiley and Sons, 249-273

Spence, W , 1998 Construction materials, methods and techniques Albany, N Y , London Delmar Publishers

Steven, G , Querin, O , Xie, M , 2000 Evolutionary structural optimisation (ESO) for combined topology and size optimisation of discrete structures Computer Methods in Applied Mechanics and Engineering 188, 743-754

Steven, G P , Li, Q , Xie, Y M , 2000 Evolutionary topology and shape design for mathematical physical problems Computational Mechanics 26, 129-139

Steven, G P , Li, Q , Xie, Y M , 2002 Multicriteria optimisation that minimises maximum stress and maximises stiffness Computers and Structures 80, 2433-2448

Sun, Y S , Emery, A F , 1997 Effects of wall conduction, internal heat sources and an internal baffle on natural convection heat transfer in a rectangular enclosure. International Journal of Heat and Mass Transfer 40, 915-929

Suresh, S , Sujit, P B , Rao, A K , 2007 Particle swarm optimisation approach for multi-objective composite box-beam design Composite structures 81, 598-605

Suzuki, K., Kikuchi, N , 1991 A homogenisation method for shape and topology optimisation Computer Methods in Applied Mechanics and Engineering 93, 291-318

Swan, C C , Kosaka, I , 1997 Homogenisation-based analysis and design of composites Computers and Structures 64, 603-621

Taisei, 1995 Taisei Corporation Annual Report 1995 Taisei Corporation, Japan

Takenaka, 2000 Takenaka e-Report 2000 Takenaka Corporation's Fiscal 1999 Environmental Conservation Activities Report Takenaka Corporation, Japan

Tanijiri, H , Ishiguro, B , Arai, T , Yoshitake, R , Kato, M , Morishima, Y & Takasaki, N , 1997 Development of automated weather-unaffected building construction system Automation in Construction 6, 215-227

Taylor, D W , 1948 Fundamentals of soil mechanics John Wiley and Sons

Tenek, L H , Hagiwara, I , 1993 Static and vibrational shape and topology optimisation using homogenisation and mathematical programming Computer Methods in Applied Mechanics and Engineering 109, 142-154

Tenek, L H , Hagiwara, I , 1994 Optimal rectangular plate and shallow shell topologies using thickness distribution or homogenisation Computer Methods in Applied Mechanics and Engineering 115, 111-124

Tobita, Y , Oda, M , 1999 Friction based deformation and strength behaviours of granular soils In Satake, M , *et al* , eds Fundamentals for Mechanics of Granular Materials In. Oda, M , Iwashita, K , eds Mechanics of Granular Materials An Introduction Balkema, Rotterdam, 50-55

Tong, T W , Gerner, F M , 1986 Natural convection in portioned air-filled rectangular enclosures International communication in heat and mass transfer 13, 99-108

Tontowi, A E , Childs, T H C , 2001 Density prediction of crystalline polymer sintered parts at various bed temperatures Rapid Prototyping Journal 7, 180-184

Topology layout? – Metamorphic development a new topology optimization method Proceedings of the Third World Congress of Structural and Multidisciplinary Optimization (WCSMO-3) CD-ROM

Tottorelli, D A , Haber, R B , Lu, S C -Y , 1989 Design sensitivity analysis for nonlinear thermal systems Computer methods in applied mechanics and engineering 77, 61-77.

Varol, Y , Koca, A , Oztop , H F , 2006 Natural convection in a triangle enclosure with flush mounted heater on the wall International journal of heat and mass transfer 33, 951-958.

Venter, G , Sobieszczanski-Sobieski, J , 2004 Multidisciplinary optimisation of a transport aircraft wing using particle swarm optimisation Struc Multidisc Optim 26, 121-131

Viswatmula, P , Amin, M R , 1995 Effects of multiple obstructions on natural convection heat transfer in vertical channels International Journal of Heat and Mass Transfer 38, 2039-2046

Wakisaka, T , Furuya, N , Inoue, Y , Shiokawa, T 2000 Automated construction system for high-rise reinforced concrete buildings Automation in Construction 9, 229-250

Wang, S Y , Tai, K , 2004. Graph representation for structural topology optimisation using genetic algorithms Computers and Structures 82, 1609-1622

Wang, S Y , Tai, K , 2005 Structural topology design optimisation using genetic algorithms with a bit-array representation Computer Methods in Applied Mechanics and Engineering 194, 3749-3770

Wechsatol, W , Lorente, S , Bejan, A , 2003 Dendritic heat convection on a disc International Journal of Heat and Mass Transfer 46, 4381-4391

Wing, R , Atkin, B , 2001 FutureHome - A prototype for factory housing 19th International symposium on automation and robotics in construction (ISARC)

Wohlers, T T , 2004 Wohlers Report 2004 Rapid prototyping, tooling and manufacturing state of the industry annual world progress report, Wohlers Associates, USA

Woon, S Y , Tong, L , Querin, O M , Steven, G P , 2005 Effective optimisation of continuum topologies through a multi-GA system Computer Methods in Applied Mechanics and Engineering 194, 3416-3437.

Xie, Y M & Steven, G P 1997, Evolutionary structural optimisation, Springer, London

Xie, Y M , Felicetti, P , Tang, J W , 2005 Form finding for complex structures using evolutionary structural optimisation method Design Studdies 26, 55-72

Xie, Y M , Steven, G P , 1993. A simple evolutionary procedure for structural optimisation Computers and structures 49, 885-896

Xie, Y M , Steven, G P , 1995 Evolutionary structural optimisation for dynamic problems Computers and Structures 58, 1067-1073

Yamazaki, Y , Maeda, J , 1998 The SMART system an integrated application of automation and information technology in production process Computers in Industry 35, 87-99

Yang, X Y , Xie, Y M , Steven, G P , 2005. Evolutionary methods for topology optimisation of continuous structures with design dependent loads Computers and Structures 83, 956-963

Zarringhalam, H , Hopkinson, N , Kamperman, N F , de Vliger, J J , 2006 Effects of processing on microstructure properties of SLS Nylon 12 Materials science and engineering A 435-436, 172-180

Zhou, M , Rozvany, G I N , 1991 The COC algorithm, Part II Topological, geometrical and generalized shape optimisation Computer methods in applied mechanics and engineering 89, 309-336

Zhuang, C G , Xiong, Z H , Ding, H , 2007. A level set method for topology optimisation of heat conduction problem under multiple load cases Computer methods in applied mechanics and engineering 196, 1074-1084

Zimmerman, E , Acharya, S , 1987 Free convection heat transfer in a partially divided vertical enclosure with conducting end walls. International Journal of Heat and Mass Transfer 30, 319-331.